AD-A158 005 USE OF HINGED STRAKES FOR LATERAL CONTROL AT HIGH ANGLES OF ATTACK(U) AIR FORCE INST OF TECH WRIGHT-PATTERSON AFB OH R E ERB MAY 85 1/1

UNCLASSIFIED AFIT/CI/NR-85-61T F/G 20/4 NL

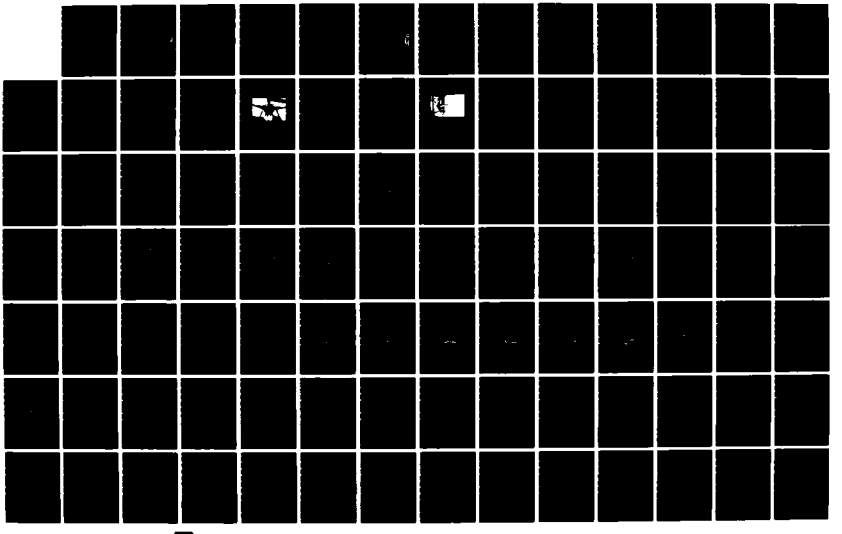

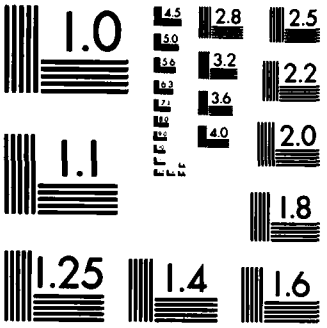

MICROCOPY RESOLUTION TEST CHART
NATIONAL BUREAU OF STANDARDS-1963-A

REPORT DOCUMENTATION PAGE

READ INSTRUCTIONS BEFORE COMPLETING FORM

1. REPORT NUMBER: AFIT/CI/NR 85-61T	2. GOVT ACCESSION NO.
3. RECIPIENT'S CATALOG NUMBER	
4. TITLE (and Subtitle): Use of Hinged Strakes for Lateral Control at High Angles of Attack	5. TYPE OF REPORT & PERIOD COVERED: THESIS/DISSERTATION
6. PERFORMING ORG. REPORT NUMBER	
7. AUTHOR(s): Russell Earl Erb	8. CONTRACT OR GRANT NUMBER(s)
9. PERFORMING ORGANIZATION NAME AND ADDRESS: AFIT STUDENT AT: Texas A&M	10. PROGRAM ELEMENT, PROJECT, TASK AREA & WORK UNIT NUMBERS
11. CONTROLLING OFFICE NAME AND ADDRESS: AFIT/NR, WPAFB OH 45433	12. REPORT DATE: May 85
	13. NUMBER OF PAGES: 151
14. MONITORING AGENCY NAME & ADDRESS (if different from Controlling Office)	15. SECURITY CLASS. (of this report): UNCLASS
	15a. DECLASSIFICATION/DOWNGRADING SCHEDULE

16. DISTRIBUTION STATEMENT (of this Report)

APPROVED FOR PUBLIC RELEASE; DISTRIBUTION UNLIMITED

17. DISTRIBUTION STATEMENT (of the abstract entered in Block 20, if different from Report)

18. SUPPLEMENTARY NOTES

APPROVED FOR PUBLIC RELEASE: IAW AFR 190-1

J AUG 1985

LYNN E. WOLAVER
Dean for Research and
Professional Development
AFIT, Wright-Patterson AFB OH

19. KEY WORDS (Continue on reverse side if necessary and identify by block number)

20. ABSTRACT (Continue on reverse side if necessary and identify by block number)

ATTACHED

DD FORM 1 JAN 73 1473 EDITION OF 1 NOV 65 IS OBSOLETE

USE OF HINGED STRAKES FOR LATERAL CONTROL AT HIGH ANGLES OF ATTACK

A Thesis

by

RUSSELL EARL ERB

Approved as to style and content by:

Donald T. Ward
(Chairman of Committee)

Stan J. Miley
(Member)

Peter F. Stiller
(Member)

Cyrus Ostowari
(Member)

Walter E. Haisler, Jr.
(Head of Department)

May 1985

USE OF HINGED STRAKES FOR LATERAL CONTROL AT HIGH ANGLES OF ATTACK

A Thesis

by

RUSSELL EARL ERB

Submitted to the Graduate College of
Texas A&M University
in partial fulfillment of the requirements for the degree of

MASTER OF SCIENCE

May 1985

Major Subject: Aerospace Engineering

AFIT RESEARCH ASSESSMENT

The purpose of this questionnaire is to ascertain the value and/or contribution of research accomplished by students or faculty of the Air Force Institute of Technology (AU). It would be greatly appreciated if you would complete the following questionnaire and return it to:

AFIT/NR
Wright-Patterson AFB OH 45433

RESEARCH TITLE: Use of Hinged Strakes for Lateral Control at High Angles of Attack

AUTHOR: Russell Earl Erb

RESEARCH ASSESSMENT QUESTIONS:

1. Did this research contribute to a current Air Force project?

( ) a. YES ( ) b. NO

2. Do you believe this research topic is significant enough that it would have been researched (or contracted) by your organization or another agency if AFIT had not?

( ) a. YES ( ) b. NO

3. The benefits of AFIT research can often be expressed by the equivalent value that your agency achieved/received by virtue of AFIT performing the research. Can you estimate what this research would have cost if it had been accomplished under contract or if it had been done in-house in terms of manpower and/or dollars?

( ) a. MAN-YEARS _____ ( ) b. $_____

4. Often it is not possible to attach equivalent dollar values to research, although the results of the research may, in fact, be important. Whether or not you were able to establish an equivalent value for this research (3. above), what is your estimate of its significance?

( ) a. HIGHLY SIGNIFICANT ( ) b. SIGNIFICANT ( ) c. SLIGHTLY SIGNIFICANT ( ) d. OF NO SIGNIFICANCE

5. AFIT welcomes any further comments you may have on the above questions, or any additional details concerning the current application, future potential, or other value of this research. Please use the bottom part of this questionnaire for your statement(s).

NAME GRADE POSITION

ORGANIZATION LOCATION

STATEMENT(s):

FOLD DOWN ON OUTSIDE - SEAL WITH TAPE

AFIT/NR
WRIGHT-PATTERSON AFB OH 45433

OFFICIAL BUSINESS
PENALTY FOR PRIVATE USE. $300

NO POSTAGE
NECESSARY
IF MAILED
IN THE
UNITED STATES

BUSINESS REPLY MAIL
FIRST CLASS PERMIT NO. 73236 WASHINGTON D.C.

POSTAGE WILL BE PAID BY ADDRESSEE

AFIT/ DAA
Wright-Patterson AFB OH 45433

FOLD IN

ABSTRACT

Use of Hinged Strakes For Lateral Control at High Angles of Attack

(May 1985)

Russell Earl Erb, B.S., United States Air Force Academy

Chairman of Advisory Committee: Dr. Donald T. Ward

An investigation was conducted to study using a portion of the leading edge strake hinged along the longitudinal axis as a roll control device for a high performance aircraft at high angles of attack (AOA). A wind tunnel test was conducted to gather static force and moment data for use in a six degree of freedom (DOF) computer simulation. Asymmetric strake deflections, both dihedral and anhedral, were investigated. The longitudinal coefficients were little affected by strake deflection, but the lateral-directional coefficients showed a nonlinear, but repeatable, behavior with strake deflection. Comparisons to published data indicate that the strakes produce similar behavior for different aircraft designs. Simulations of the aircraft response to the strakes showed that an improvement over current rolling performance could be obtained by combining the positive strake deflection with the ailerons up to 38 deg AOA, after which the strakes alone produced the best roll performance. Sideslip and AOA must be closely controlled or the aircraft will either not roll, or will depart during the roll. The rolling performance using the hinged strakes at high AOA is compared to rolling performance using differential leading edge flaps. The differential leading edge flaps produce comparable roll rates with less sideslip than produced by the hinged strakes. However, the possibility exists of combining hinged strakes with differential leading edge flaps for improved roll performance.

TABLE OF CONTENTS

LIST OF SYMBOLS

A_c	Fuselage cavity area
A_e	Duct exit area
A_i	Reference inlet area
b	Reference wing span
$\bar{c}$	Reference wing mean aerodynamic chord
C_L	Lift coefficient
C_Y	Side force coefficient
C_D	Drag coefficient
C_m	Pitching moment coefficient
C_n	Yawing moment coefficient
C_ℓ	Rolling moment coefficient
C_T	Cross sectional area of the wind tunnel test section, 68 ft^2
F_A	Force in the axial direction, internal balance axes
F_ℓ	Rolling moment in balance axes
F_n	Yawing moment in balance axes
F_N	Force in the normal direction, internal balance axes
i_b	Balance incidence angle
i_t	Incidence angle of the horizontal tail
M	Mach number
P_s	Static pressure in the model cavity
q_c	Dynamic pressure corrected for blockage
q_u	Dynamic pressure uncorrected for blockage
S	Wing reference area
α ,AOA	Angle of attack
β	Sideslip
β_s	Sting angle
β_{actual}	Actual sideslip angle
DOF	Degrees of Freedom
LEF	Leading edge flaps
DLEF	Differential Leading Edge Flaps
LEX	Leading edge extensions
δ_{LS},DLS	Deflection of the left strake (positive upward)
δ_{RS},DRS	Deflection of the right strake (positive upward)

p	Body axes roll rate
q	Body axes pitch rate
r	Body axes yaw rate
SA	Stability Axes
BA	Body Axes
C_{ℓ_β}	Dihedral Effect, $\frac{\partial C_\ell}{\partial \beta}$
C_{n_β}	Directional Stability, $\frac{\partial C_n}{\partial \beta}$

LIST OF FIGURES

LIST OF TABLES

INTRODUCTION

A common feature of contemporary fighter aircraft is a trapezoidal wing with a highly swept leading edge extension, or strake. Examples of this configuration can be seen on the F-16 and the F-18. This design is used extensively due to its ability to maintain a high lift coefficient at angles well beyond the traditional stall angle of attack. This ability is derived from a phenomenon known as vortex lift, in which the separation and subsequent reattachment of the flow over the sharp leading edge of the strakes produces a strong vortex over the leading edge of the strake. This vortex produces lift on the strake surface, and also provides a favorable interference lift on the wing through its interaction with the wing flow field. The phenomenon of vortex lift has been studied and explained by Polhamus[1], and has been quantified by Luckring[2] and Frink and Lamar[3].

This ability to fly at high angles of attack (AOA), made possible by the strake-wing configuration, leads to advantages in aerial combat. The most important advantage is additional capability for offensive and defensive maneuvering. Other capabilities include nose pointing to track an enemy without actually following him, and the use of high drag for aerodynamic braking.

One major problem currently limits the usefulness of high AOA flight. At high angles of attack the traditional control surfaces, the elevator, the ailerons, and the rudder, begin to lose their effectiveness. For instance, the ailerons must operate in the separated flow about the wing, and the rudder becomes submerged in the wake of the fuselage. Under the same conditions where control effectiveness is marginal, the longitudinal and directional stability of many aircraft is greatly reduced. This combination of factors often leads to a departure prone airplane at high AOA, especially in aircraft which depend on active controls for stability.

Rao and Huffman[4] have suggested a "hinged strake" concept as a possible means of longitudinal and lateral control at high AOA. The

---

This thesis follows the style and format of Journal of Aircraft.

hinged strake is a portion of the leading edge extension which is hinged along its root chord (or longitudinal axis). The result of deflecting the strake downward (anhedral) is twofold. First, the projected area of the strake is reduced. Second the strake vortex is weakened. Both effects lead to reduced lift on the corresponding wing panel. Rao and Huffman discussed both symmetrical deflections of the strakes for longitudinal control and asymmetric deflections for lateral-directional control. One of their conclusions was that differential strake anhedral may be a powerful roll and yaw control at high AOA, and that further research was needed on more realistic configurations to answer questions concerning configurational effects.

The objective of this study was to investigate the feasibility of using hinged strakes for high angle of attack controllability of a realistic configuration fighter. In particular, this study considered the feasibility of using hinged strakes for roll control at angles of attack (AOA) between 30 and 40 degrees. These rolls were done about the velocity vector, or the stability X-axis, rather than the body X-axis for departure resistance.[5] This results in the airplane appearing to move around the surface of a cone as it rolls. In addition to looking at the effectiveness of hinged strakes on a realistic configuration, this study also considered at the effects of deflecting the strakes upward (dihedral) as well as downward (anhedral). The model used by Rao and Huffman[4] had no leading edge flaps, and the tip of the strake went below the wing when deflected downward. The configuration used in this test has leading edge flaps which are deflected downward as a function of AOA, and at high AOA the leading edge of the flap lines up with the tip of the anhedral strake at maximum deflection, as shown in Figure 1. Therefore, it would be possible that this would change the way that the strake vortex flows across the wing. By deflecting the strake upward, the strake vortex would be moved away from the upper surface of the wing, and perhaps a different behavior would result. Additionally, the strakes might have different yaw characteristics, since on the strakes with anhedral the normal force (or lift) is tilted outward, away from the fuselage, but on the strakes with dihedral, the normal force would be tilted inward, toward the fuselage.

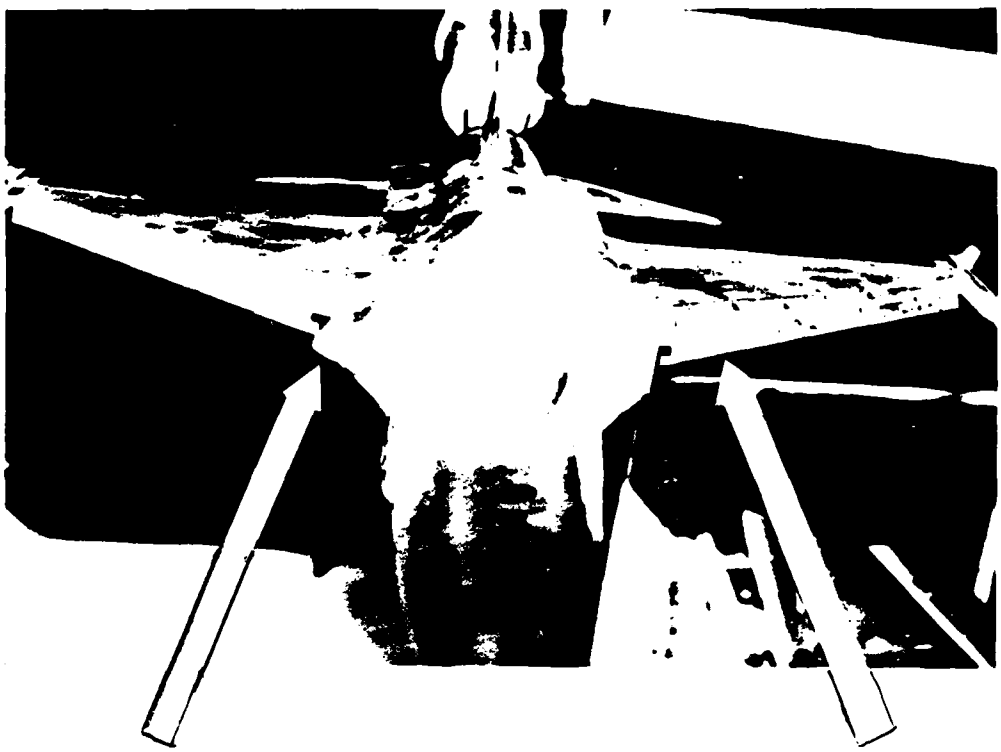

Figure 1. Photograph Showing Deflected Strakes and Leading Edge Flaps.

The approach used in this study consisted of three parts. The first part was a wind tunnel test of a high performance aircraft model fitted with hinged strakes. The wind tunnel test was used to gather static coefficient data including changes in forces and moments due to the deflection of the hinged strakes. The second part of the study analyzed the resulting aerodynamic data. Since the aerodynamic forces and moments are highly coupled in high angle of attack flight, it is impossible to gain an appreciation for the reactions of the aircraft just by looking at the static aerodynamic data. Therefore, for the third part of this study, the wind tunnel data was used in a mathematical model in a six degree of freedom (DOF) simulation to predict the behavior of a full size aircraft fitted with hinged strakes. This simulation used only the static data for the strakes, since no dynamic derivatives for the strakes were available from this test. The lack of dynamic derivatives was partially compensated for by considering the aircraft to be static for each time step.

WIND TUNNEL TEST

In the summer of 1984, a model of a high performance fighter was tested in the Texas A&M Low Speed Wind Tunnel (LSWT)[6]. The model provided by General Dynamics/Fort Worth (GD/FW) is shown in Figure 2. As the picture shows, the sting support was a special offset one, designed to minimize flow interference with the model at high angles of attack.

The purpose of the test was to collect static force and moment data to study the lateral control effectiveness of the hinged strakes at high angles of attack (AOA). The data were reduced according to standard wind tunnel procedures[7], with additional corrections applied for internal drag and model cavity static pressure. These data were then incorporated in the six DOF computer simulation.

Model Description

The model tested was that of a high performance fighter aircraft resembling the YF-16. The model differs from the YF-16 in the shape and size of the leading edge extensions (or strakes); a silhouette of the leading edge wing extension is shown in Figure 3. A summary of the model constants is shown in Appendix A.

The portion of the strake that could be deflected is also shown in Figure 3. Three major factors were considered in deciding how much of the strake to deflect. The first two concerned the design of the full scale aircraft. In order to test a realistic configuration, as had been suggested by Rao and Huffman, it was desired to have a minimal impact on the existing structure of the full scale aircraft. The section of strake deflected in this study is virtually empty internally on the full size aircraft. The second factor was the placement of the existing gun on the full size aircraft. By placing the hinge line of the strake at the location shown, there is no interference with the existing gun. If the strake had been any larger, the gun placement would have to be moved. The third factor deals with the construction of the wind tunnel model. Due to the construction of the cheek which contained the strake, the strake shown was the largest strake that could be made without excessive modification to the model supporting structure.

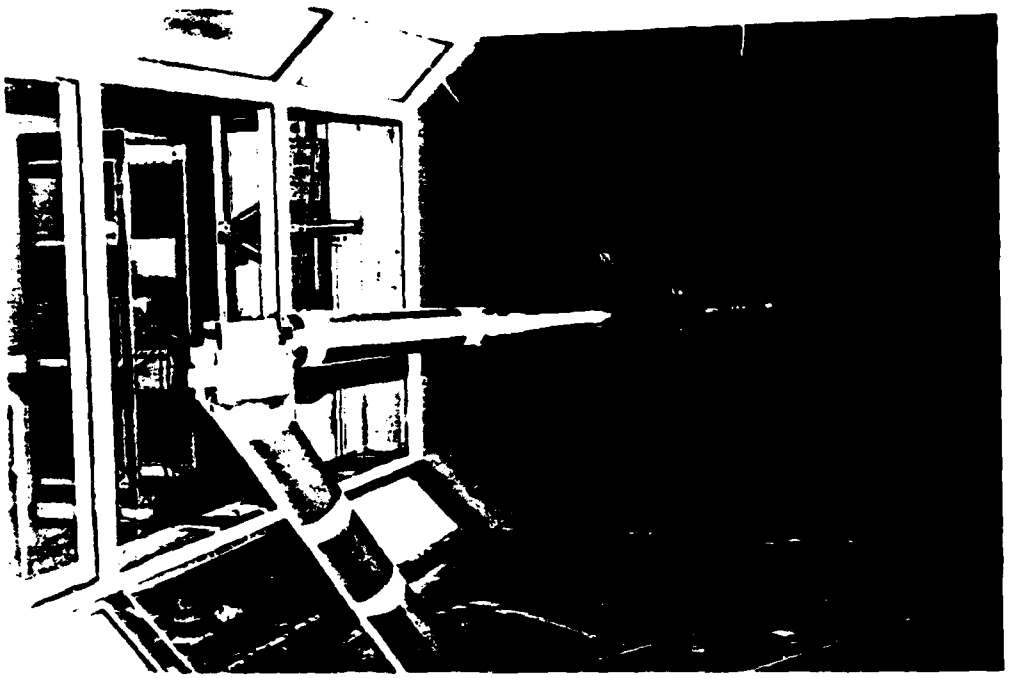

Figure 2. Photograph of Model Mounted in TAMU 7' X 10' LSWT.

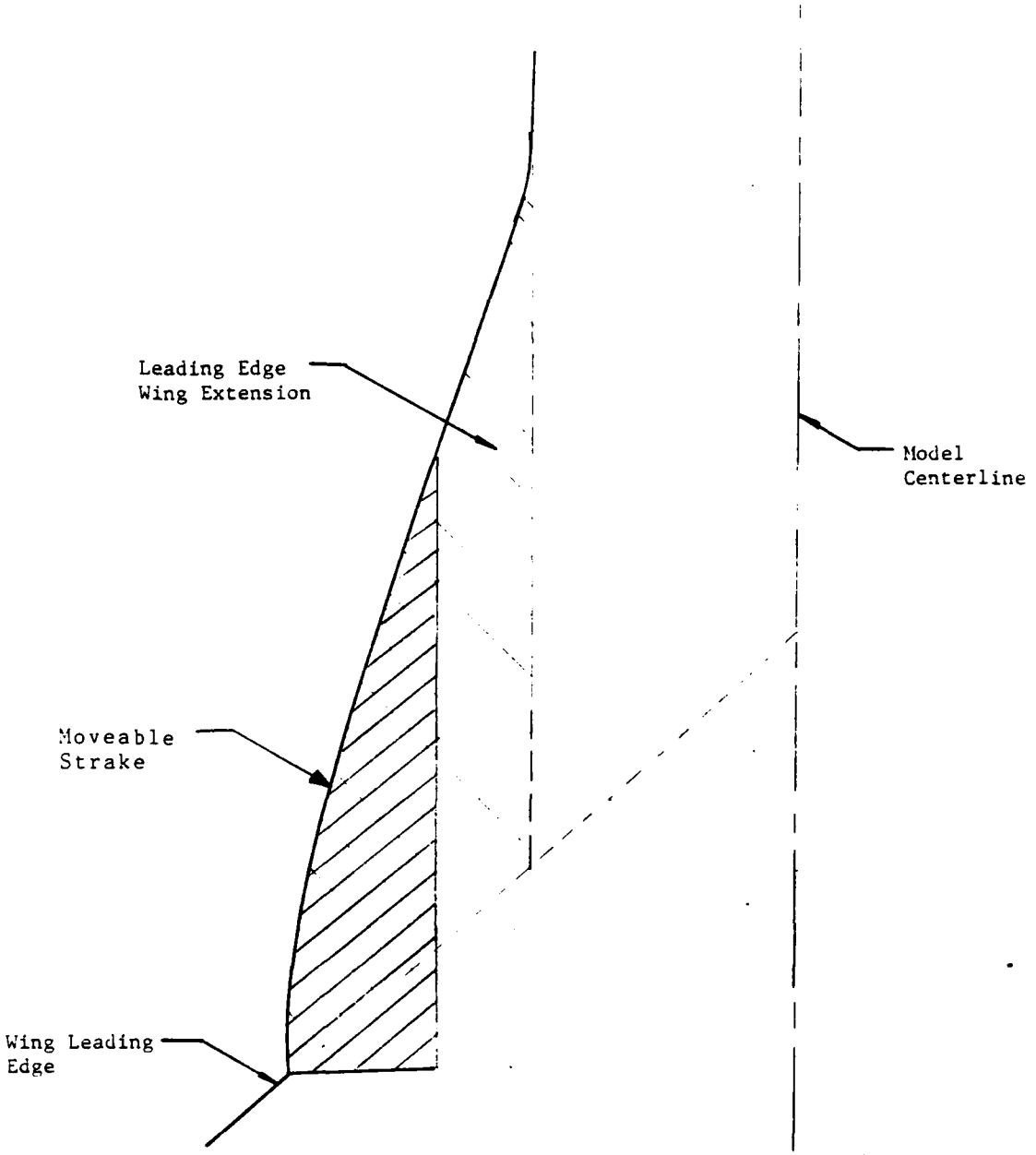

Figure 3. Silhouette of Leading Edge Extension and Moveable Strake.

This strake design was proposed to the sponsor and approved. The model was then modified by the Texas A&M Research and Instrumentation Division. The hinged strakes for the wind tunnel model were made with deflections from $+45^{o}$ to -45^{o} in increments of 15^{o}. The original strake provided with the model was used for the 0^{o} deflection case. Figure 1 shows the deflected strakes on the model. The deflected strakes were made with flat lower surfaces and modeling clay was used to fair in the sharp breaks in the LEX curvature. Figure 1 also shows the leading edge flaps (LEF) deflected to 30^{o}. All runs were made with the LEF in this position, since it was the most representative of their position in high AOA flight.

Tunnel Installation

The model was mounted in the tunnel on a sting with the wings vertical, as shown in Figure 4. The sting was fitted into a manually adjustable knuckle which was used to change the yaw orientation of the model with respect to the wind tunnel in order to test different side-slip angles. Angle of attack variations were obtained by rotating the turntable to the desired angles. The knuckle could be set at yaw angles of 0^{o}, 5^{o}, 10^{o}, and 15^{o}. Since the knuckle could only be rotated upward, positive or negative yaw orientations were obtained by rotating the sting 180^{o} at the center joint.

Instrumentation

Force and moment data were collected with a Task Mark XIII six component internal balance. The frequency spectrum of one of the balance outputs was recorded during Runs 1-3 to check for the resonant frequencies of the model/sting system and to compare them with the data sampling frequencies since previous tests had shown considerable vibration of the model and sting support. The balance resolution in terms of coefficients is shown in Table 1.

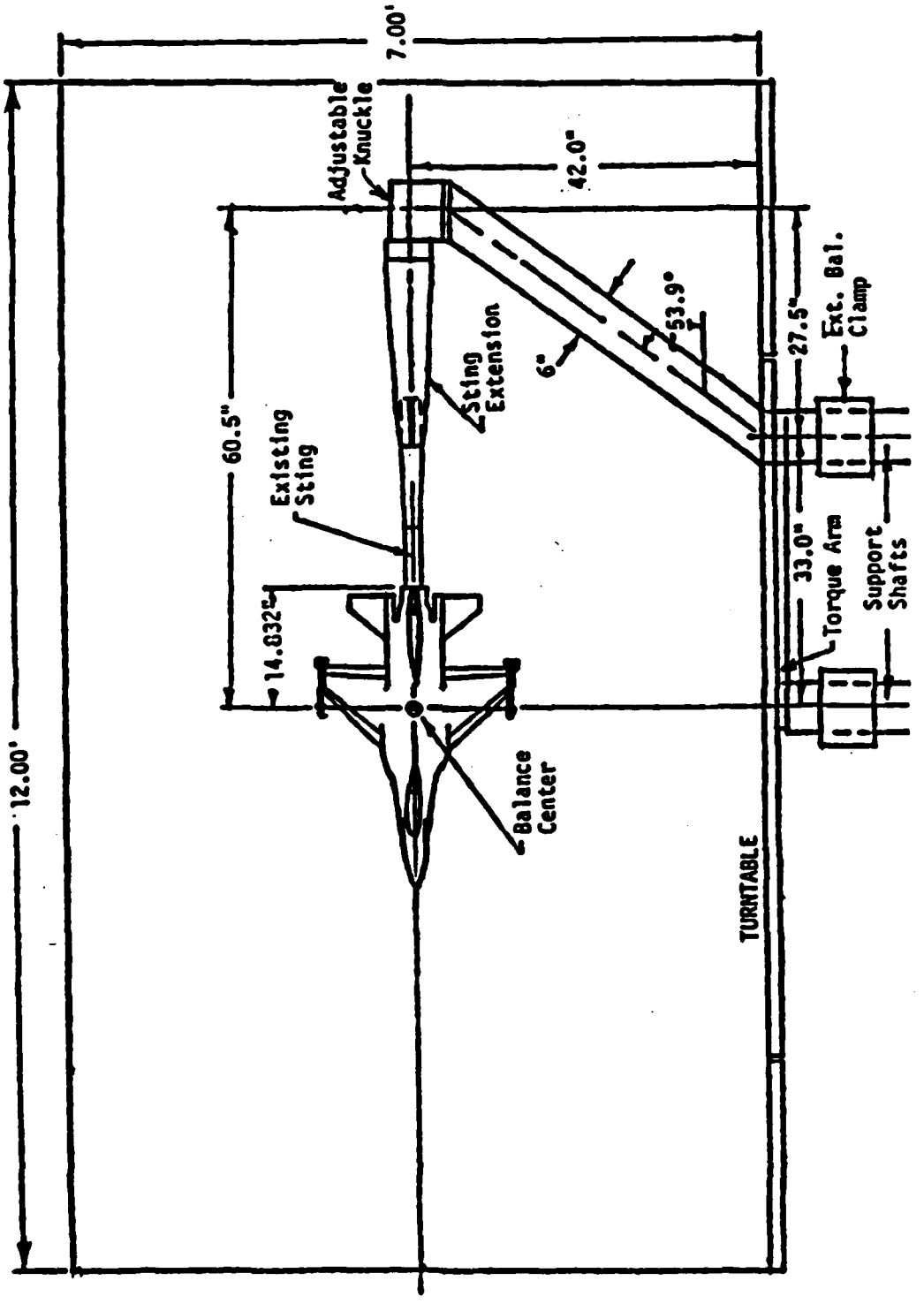

Figure 4. Diagram of Model and Extended Sting Mount in TAMU 7' X 10' LSWT.

TABLE 1

Internal Balance Resolution

C_L	$\pm$ 0.00670
C_Y	$\pm$ 0.00670
C_D	$\pm$ 0.00670
C_m	$\pm$ 0.00551
C_n	$\pm$ 0.00208
C_ℓ	$\pm$ 0.00208

Base pressure corrections were calculated using pressures obtained from a pressure manifold located in the model cavity immediately behind the balance. The manifold was simply a ring of tubing around the sting support with pressure orifices at four points 90° apart. This arrangement provided an average pressure in the cavity.

Test Procedures

The calibration of the internal balance was checked each morning during the test by applying known loads to the model and comparing these values with the balance output. This procedure is standard LSWT practice, but it proved to be very useful because it revealed that approximately halfway through the first half of the testing one of the redundant axial force gages on the internal balance had failed. The data from this gage were not included in the data reduction.

All runs were made with the wings vertical in the tunnel. The run schedule for this test is shown in Appendix B. The sideslip angle of the model was varied using the knuckle adjustment of the sting. In all cases, the model was run at a given strake deflection through all positive or negative sideslip angles, using the turntable to sweep through angle of attack from -4° to 68°. During the first half of the testing, the model was then rotated 180° and the remaining sideslip angles were run. After all sideslip angles were completed, the strakes were changed and the process repeated. However, at the conclusion of Run 40, the center joint of the sting seized and the model

had to be removed from the tunnel to repair the sting. When the tests were completed, the strakes were changed and the same sideslip angles were run to minimize the number of times the model had to be rotated 180°. After all strake deflections were run, the model was rotated 180° and the same strake deflections were run for the remaining sideslip angles. Sideslip angles ranged from -15° to 15° for asymmetric cases, and from -10° to 10° for anhedral-dihedral cases.

Data Reduction Methods

The data were reduced using standard procedures as described by Pope[7]. The sponsor requested that several corrections be made to the data in addition to the standard data reduction procedures. These corrections are summarized as follows.

The model was constructed with a 57 minute difference between the model longitudinal axis and the internal balance longitudinal axis. To account for this difference, the forces and moments were rotated from balance axes, balance center to body axes, balance center using the following equations:

$$F_N = F_N \cos 57' + F_A \sin 57'$$
$$F_A = -F_N \sin 57' + F_A \cos 57'$$
$$F_\ell = F_\ell \cos 57' - F_n \sin 57'$$
$$F_n = F_\ell \sin 57' + F_n \cos 57'$$

Static base pressure was measured in the model cavity at each data point and the correction was applied in balance axes to the coefficients during data reduction by the formula:

$$\Delta C_D = \frac{(P_\infty - P_s)\, A_c}{q_c\, S}$$

$$C_{D_{total}} = C_{D_{measured}} - \Delta C_D$$

Since the model was a flow through model, being open from the inlet to the base of the model, the drag due to flow through the model was accounted for. This internal drag was subtracted from the drag coefficient as determined from Table 2.

TABLE 2

C_D Corrections ($M < 0.3$)

α	ΔC_D	α	ΔC_D
-5	.0025	20	.0038
0	.0023	25	.0049
5	.0023	30	.0062
10	.0025	32	.0068
15	.0030	90	.0068

The usual blockage and wall corrections[2] were made for an AOA below 32°. For any AOA above 32°, wall corrections were not applied and the following Maskell correction was used:

$$q_c = q_u[1 + 2.5(C_D S/C_T)]$$

In addition to these deviations from the standard data reduction procedures, moments were resolved about the 35% mean aerodynamic chord at the request of the sponsor. This change from resolving moments about the 25% mean aerodynamic chord was requested because of the relaxed static stability of the design.

Due to the geometry of the sting support, the sting angle, listed as β in the run schedule, is not the actual sideslip angle of the model. Since the model was rotated about the wind Y-axis in the tunnel rather than about the body Y-axis, the actual sideslip is a function of angle of attack. Stability axes sideslip was calculated according to the formula:

$$\beta_{actual} = \sin^{-1} (\cos \alpha \ \sin \beta_s)$$

This formula is derived in Appendix C.

Highly separated, vortical flows like those encountered in this test, present problems that are difficult to address in the data reduction process. Even though the blockage correction was changed and the wall corrections were discontinued at high AOA, discrepancies such as model movement off of the tunnel center, model oscillations, and asymmetric flows are known to exist, but no corrections were made since no adequate basis for correcting such conditions is known.

DISCUSSION OF RESULTS

Runs 1, 2, and 3 were run with the baseline configuration at dynamic pressures of 40, 60, and 80 psf respectively with corresponding Reynolds Numbers of 846,000, 1,025,000, and 1,161,000. This check looked at variations due to Reynolds number and also to insure that the steel sleeve would reduce the vibrations seen previously[8]. In addition, a spectral analyzer was attached to the side force channel to check for the dominant frequencies to compare against the sampling rate. These vibrations had their largest amplitudes at 50^{o} AOA. The frequency spectrum of the forward side force channel at 50^{o} AOA is shown in Figure 5. The side force channel was chosen since the amplitude of the oscillations was greatest in the lateral direction. This spectrum shows that the model was oscillating with a fundamental frequency of 11 Hz. The balance output was sampled once every 4.5 milliseconds, or at a frequency of 222 Hz. The measured value of the balance output was the average value of 100 of these samples. Therefore, at least one complete period of an oscillation would be measured for frequencies up to 22.2 Hz. In this case, the data were sampled over two fundamental periods. If the sample size and sampling rate were to cause an error, this error would be seen as non-repeatability in the data points.

In Run 3 data were taken with both increasing and with decreasing angles of attack. As can be seen in Figure 6, the data points were repeatable and no hysteresis is apparent. Runs 2 and 3 at dynamic pressures of 60 and 80 psf gave almost identical results at low angles of attack and were still in fairly close agreement at very high angles of attack. The rolling moment was the parameter of primary interest, and this agreement is shown in Figure 6. Note that these data and all other plotted data are plotted in stability axes. Run 1 is far removed from Runs 2 and 3 in this region. Based on this information, following runs were made at a dynamic pressure of 80 psf.

On Run 8, LSWT personnel noticed that the rolling moment produced by the model was exceeding the limits of the internal balance. Referencing the previous figure, the Principal Investigator decided to reduce the dynamic pressure to 60 psf. Run 9 was run with the

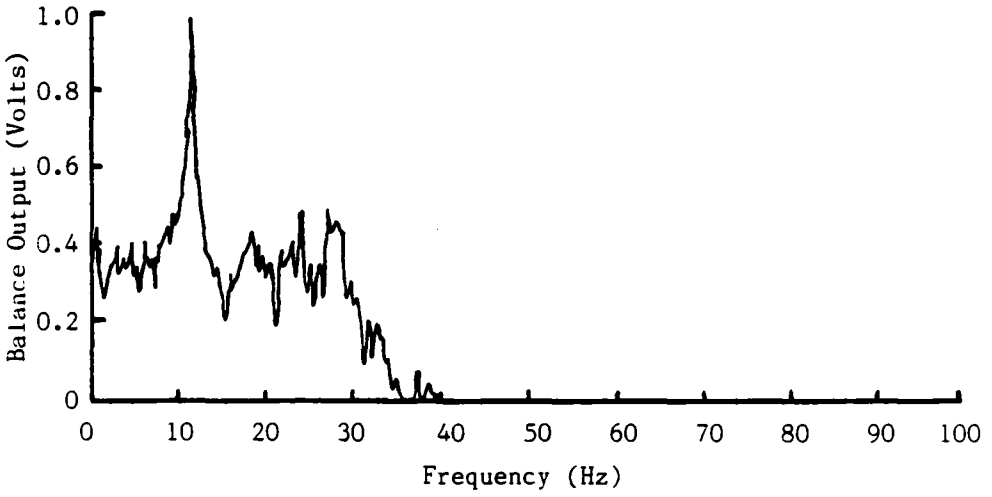

Figure 5. Frequency Spectrum of Side Force Channel at AOA = 50°.

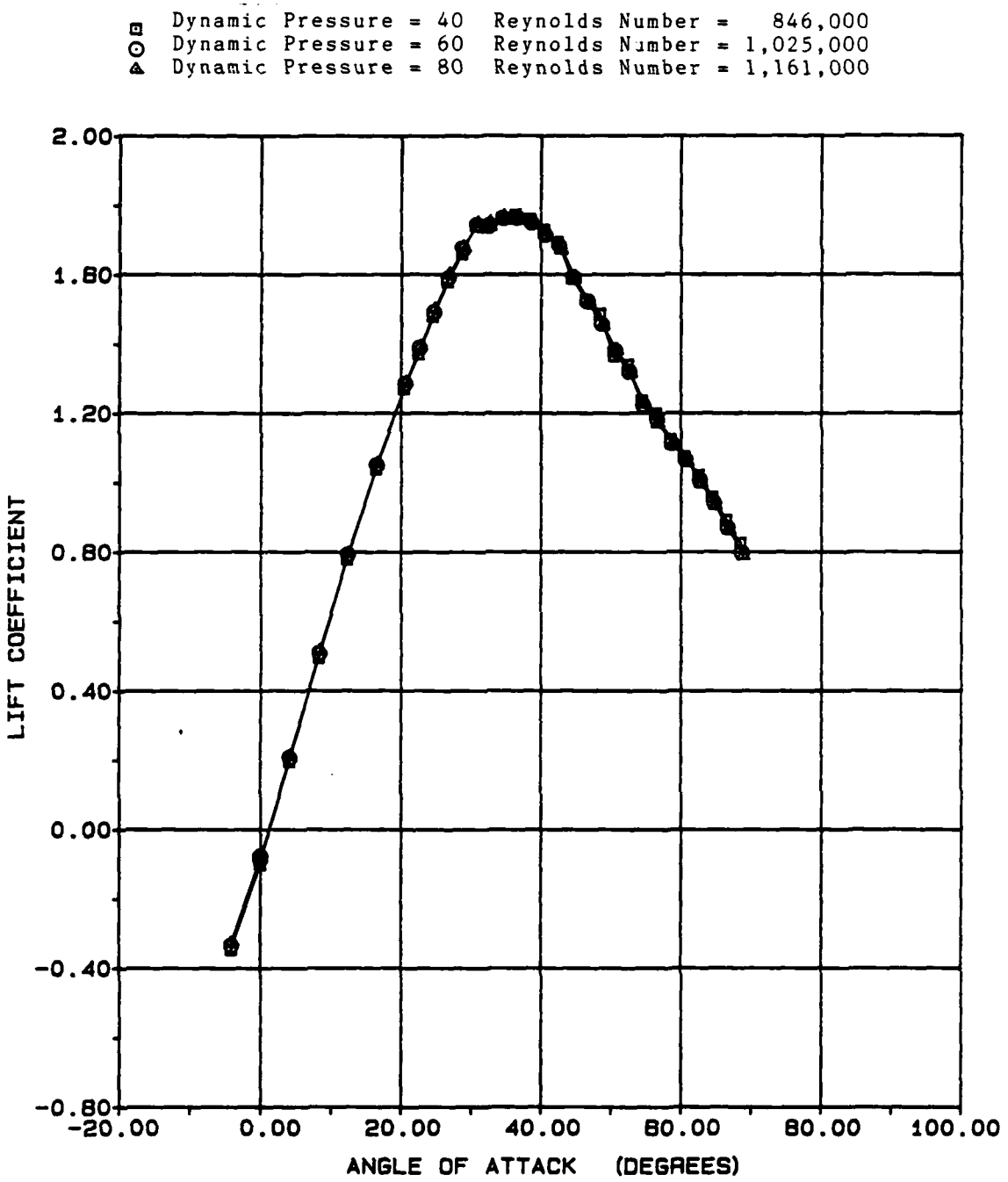

Figure 6. Comparison of Baseline Data at Varying Dynamic Pressures.

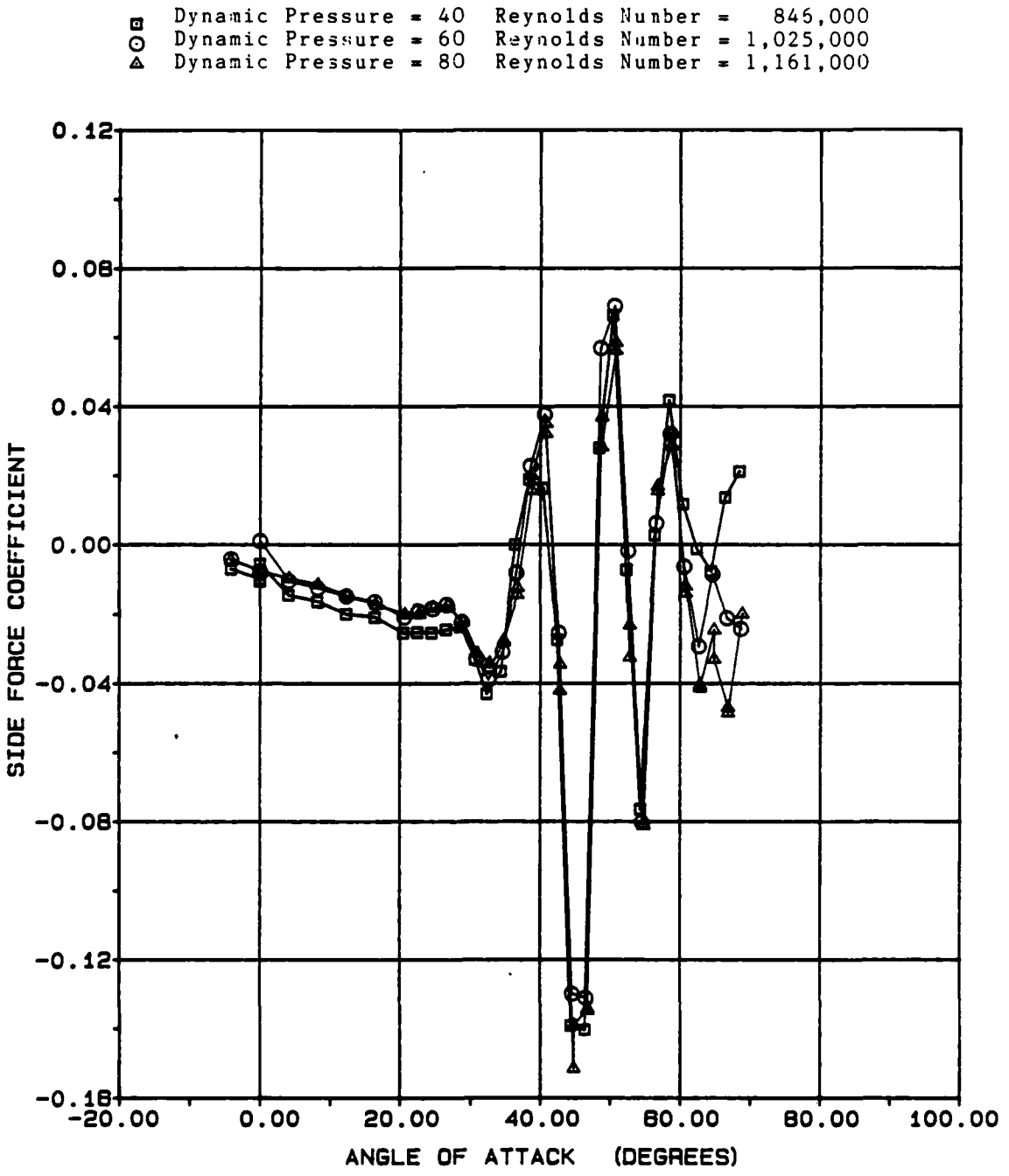

Figure 6. Continued.

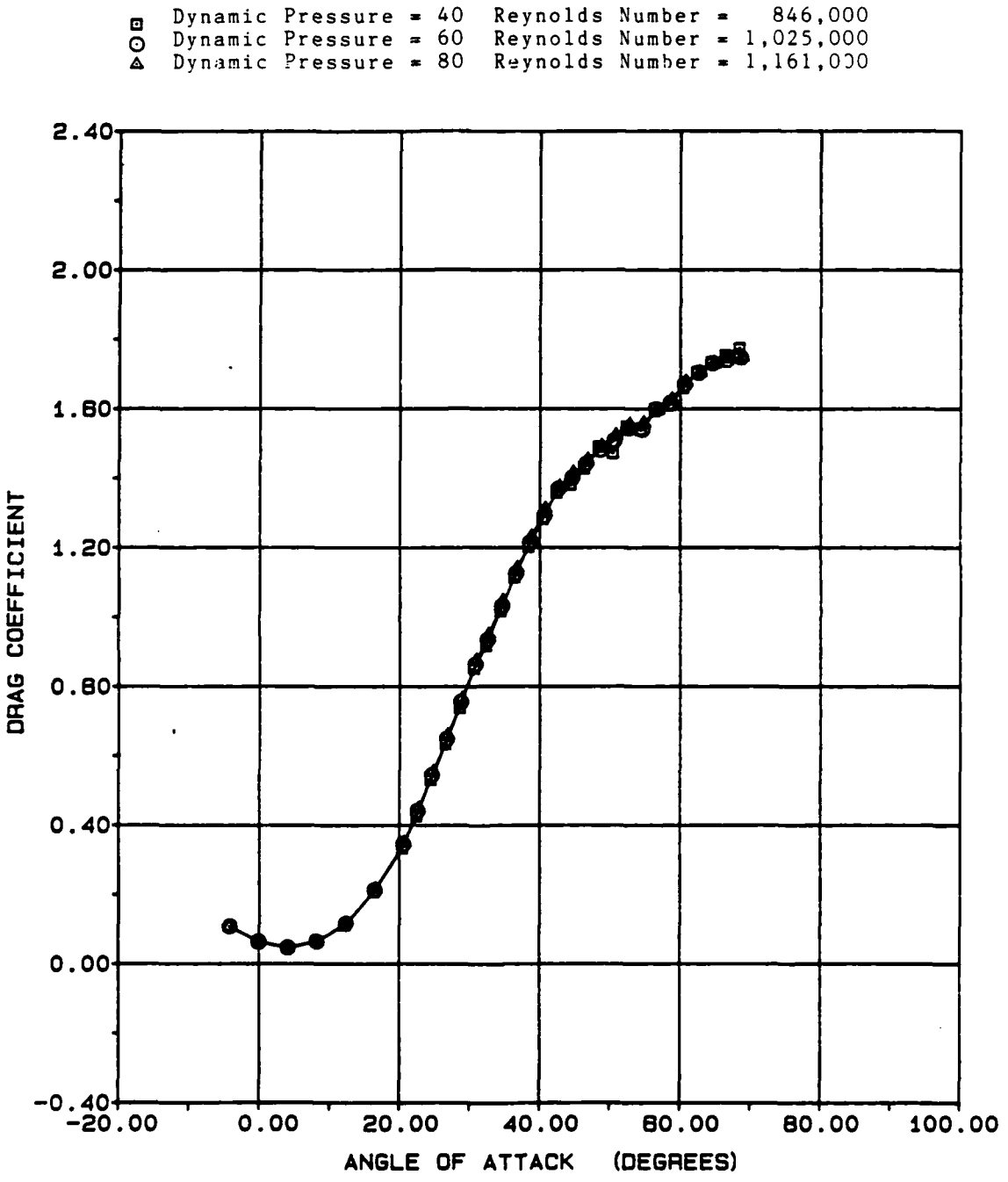

Figure 6. Continued.

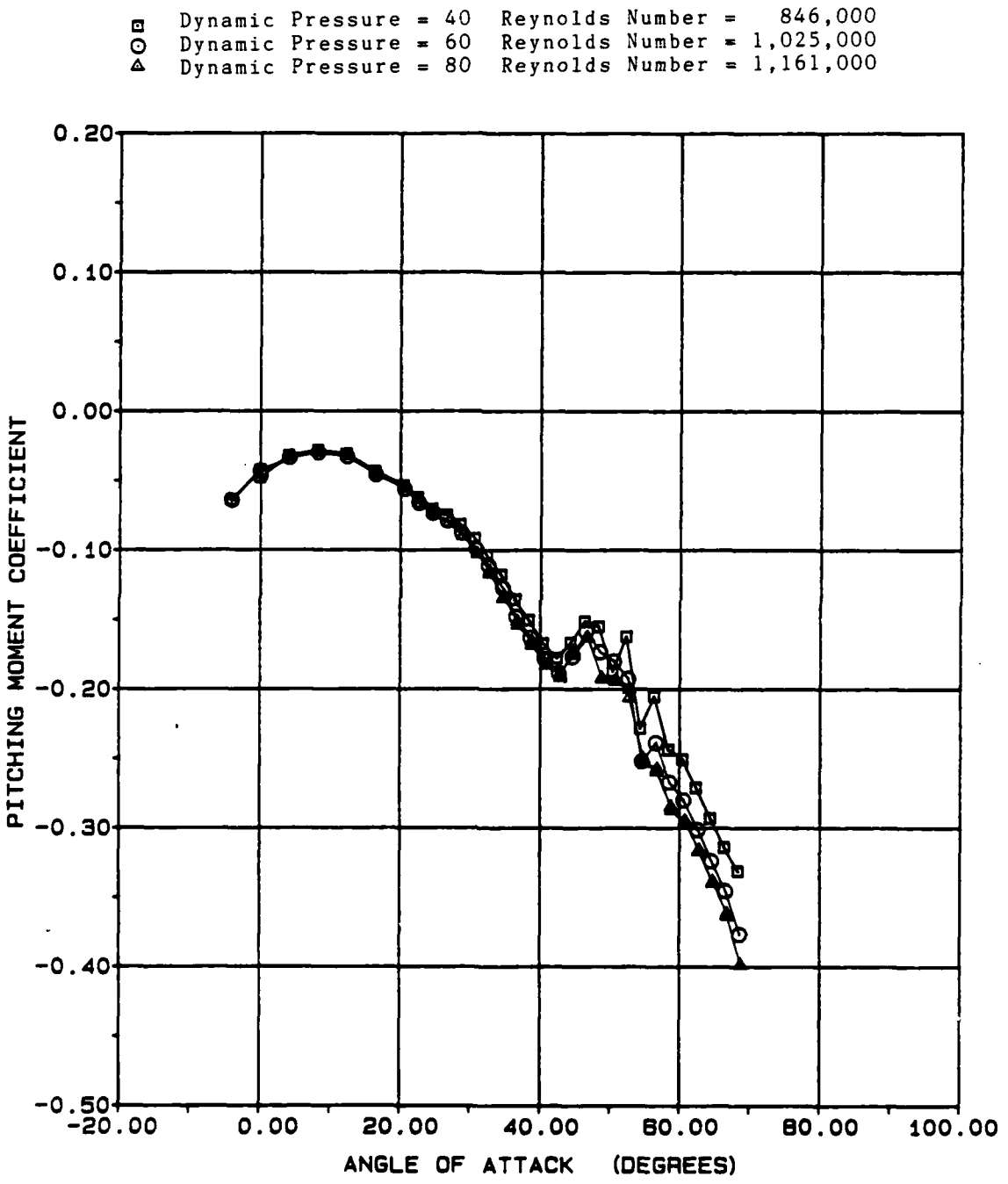

Figure 6. Continued.

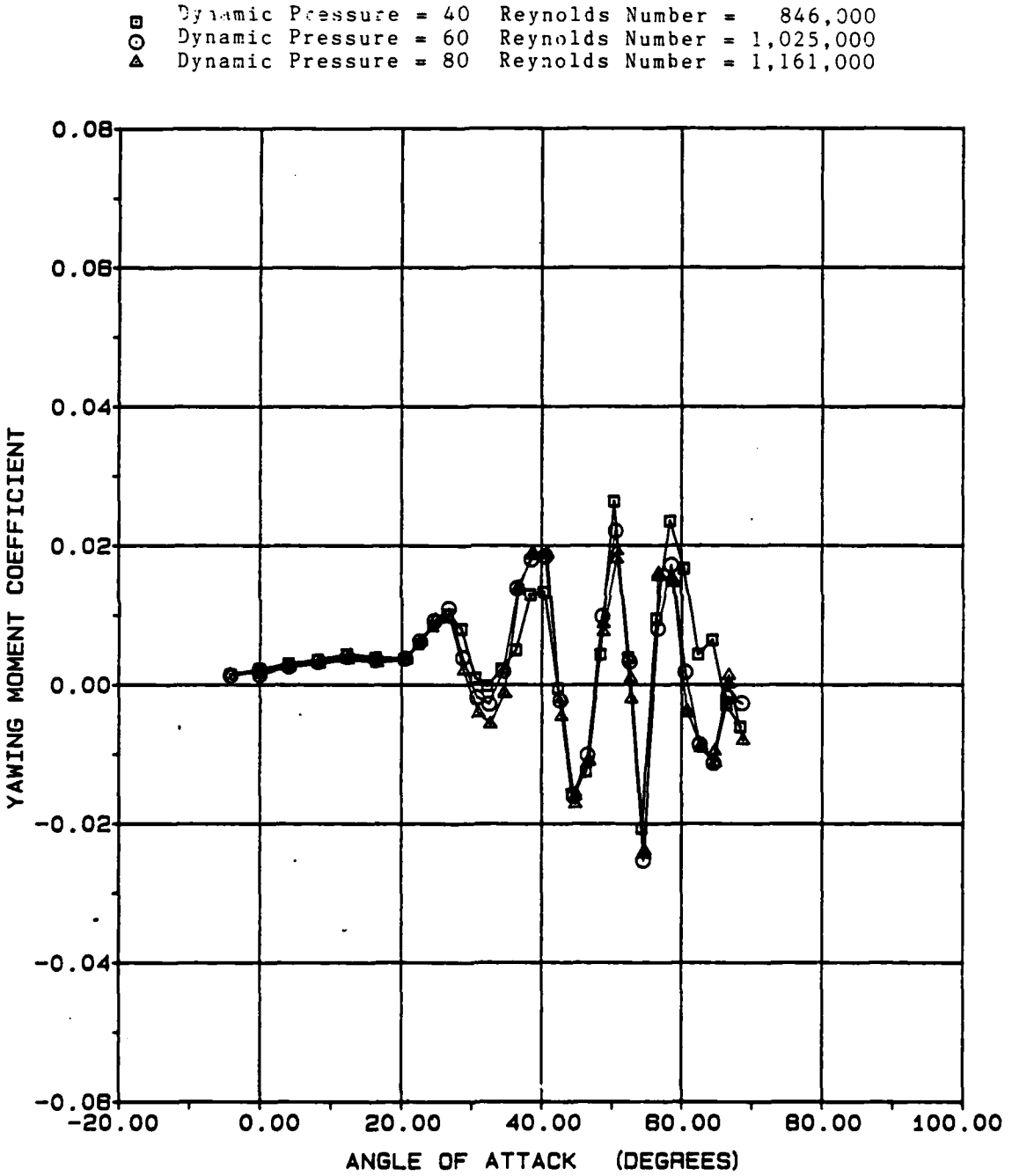

Figure 6. Continued.

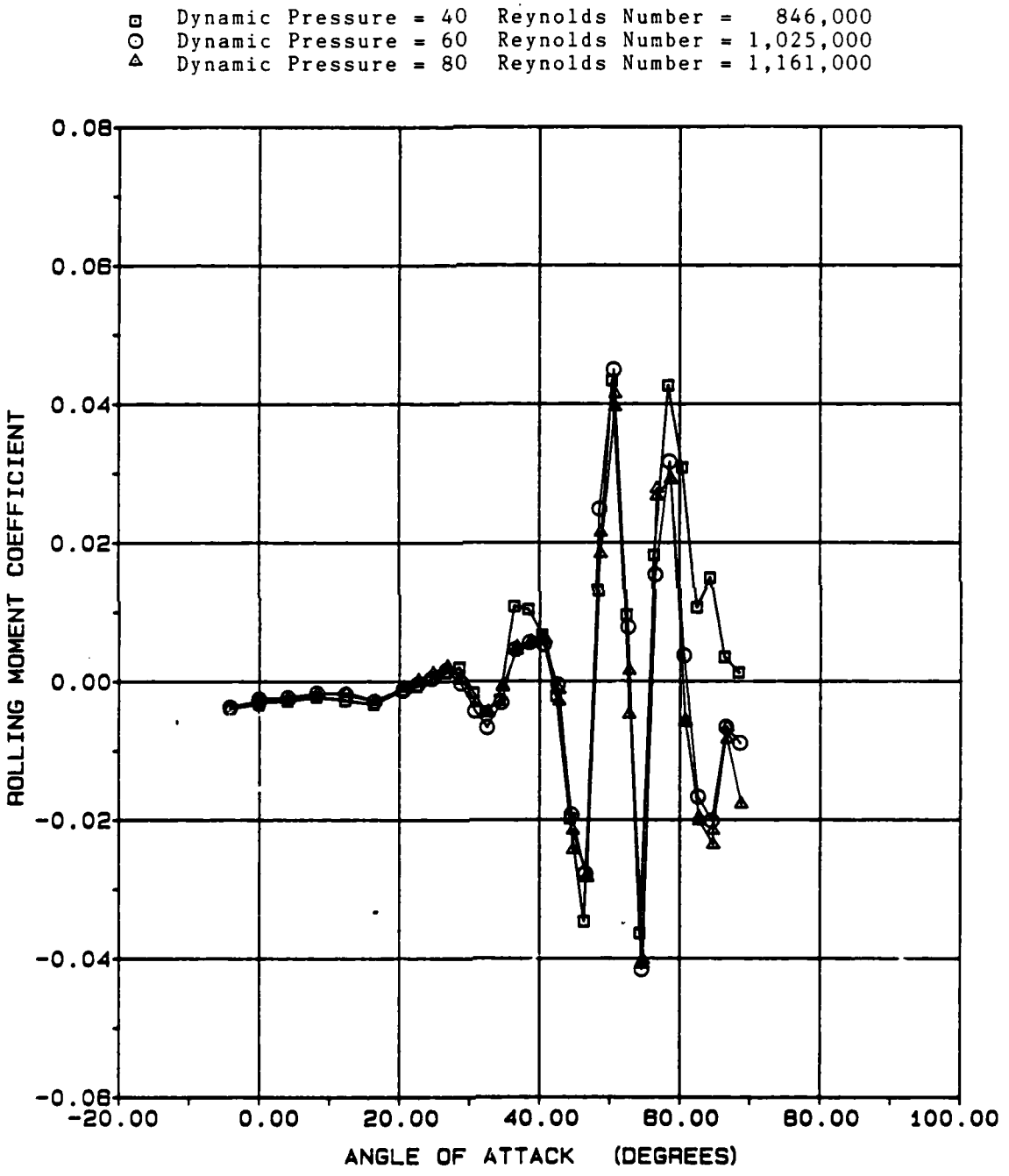

Figure 6. Concluded.

configuration predicted to create the maximum rolling moment to see if the rolling moment would remain within limits. The baseline runs were repeated, and all further runs were made with a dynamic pressure of 60 psf.

Further Reynolds Number effects were seen upon re-entry for the second half of the wind tunnel test. The first runs of this test were used to try to reproduce data from the first half of the test. The rolling moment coefficient was again used as the comparison, since it was the primary parameter of interest. The last two attempts to reproduce Run 2 are shown plotted against Run 2 in Figure 7. Note that Run 46 was conducted without trip strips, which had worn off the model during previous runs. On Run 47, these trip strips were replaced, and were used for the remainder of the test. Note that the trip strips cause a change in rolling moment, especially at the higher angles of attack. Also, the agreement between the first and second entry in the LSWT is not as close as desired in the region of primary interest (AOA = 30^{o} to 40^{o}). In fact, the signs are reversed on the coefficients in some cases between tests. However, since all measurements and parameters that could be changed had been set as close as possible to the conditions of the first half of the test, the test was continued from here. Similar problems with asymmetries have been seen before.[8] It is still not clear if the lack of trip strips and/or asymmetries in the model and airflow are the source of this disagreement. Due to lack of time to run new baseline data, the data from from the second entry were used in conjunction with the data from the first entry. As will be seen later, this would only really affect the results for the $+15^{o}$ and $+30^{o}$ strake deflections, since the anhedral-dihedral data would not be used.

The longitudinal coefficients, C_L, C_D, and C_m, appear to be well behaved across the full angle of attack range, in that they do not change rapidly from one angle of attack to another. Also, C_L and C_D vary insignificantly with sideslip angle, and C_m shows only a slight change at higher angles of attack. See Figures 8-9.

The lateral-directional coefficients, C_Y, C_n, and C_ℓ, show a very different behavior with varying angle of attack. At lower angles

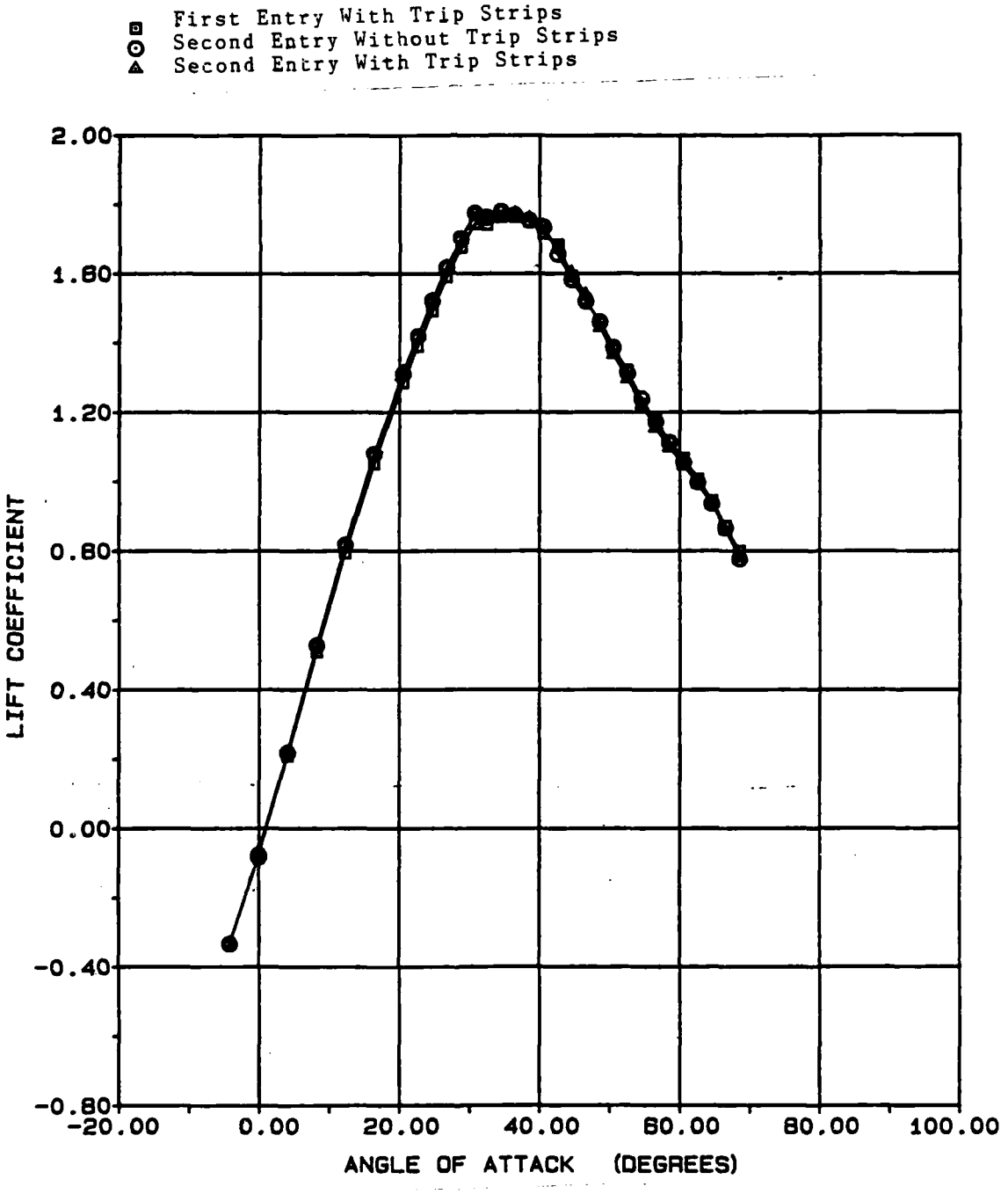

Figure 7. Comparison of Baseline Data Between Tunnel Entries.

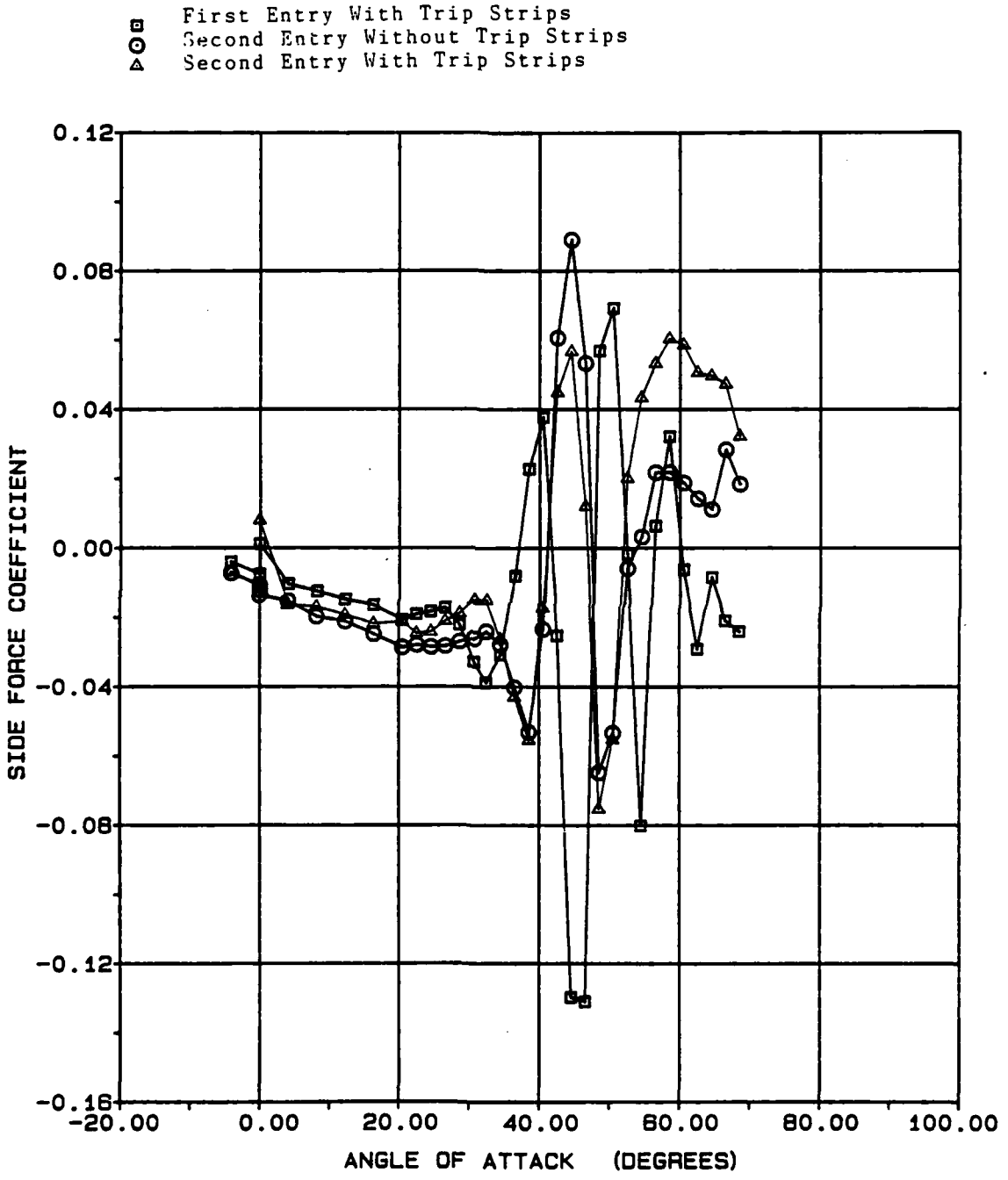

Figure 7. Continued.

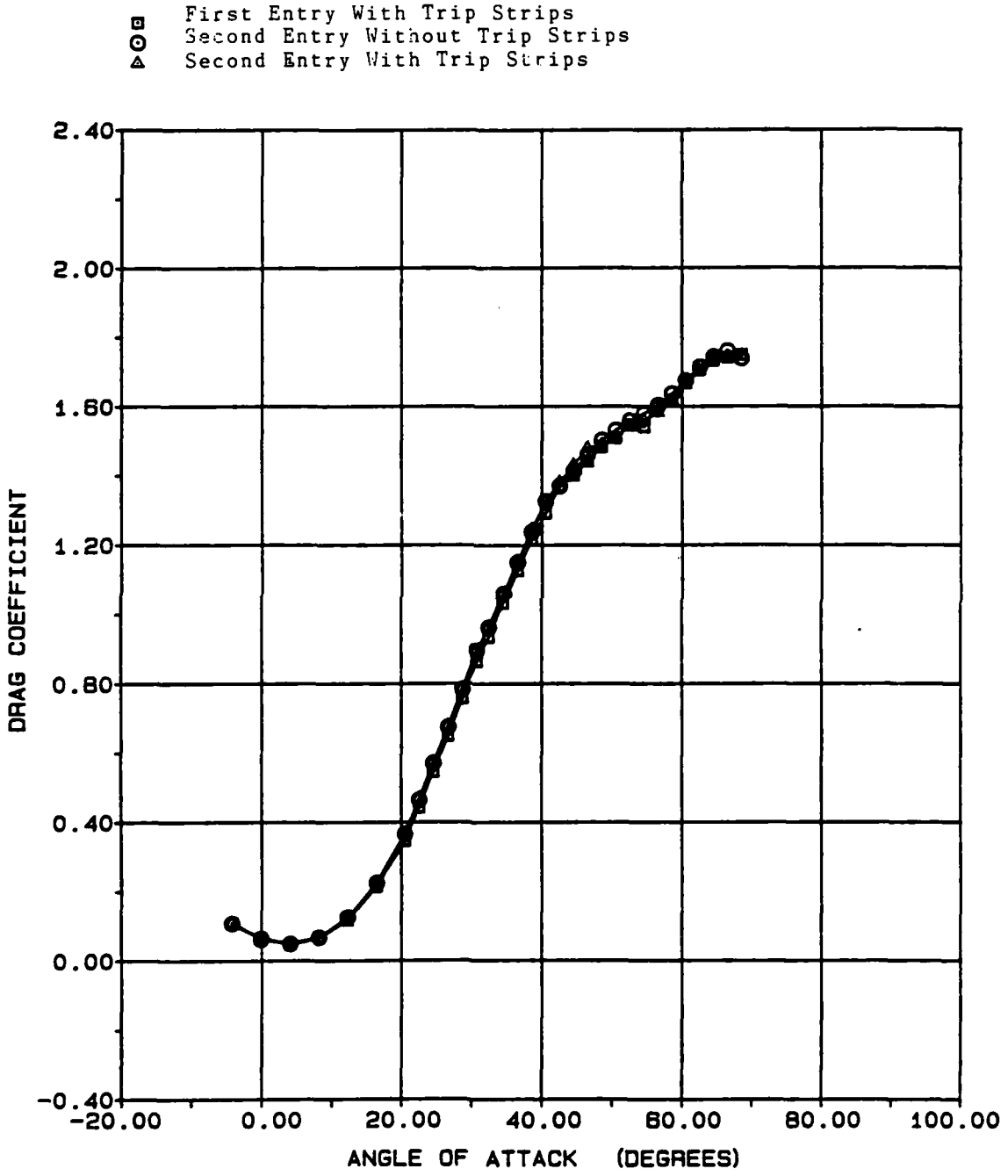

Figure 7. Continued.

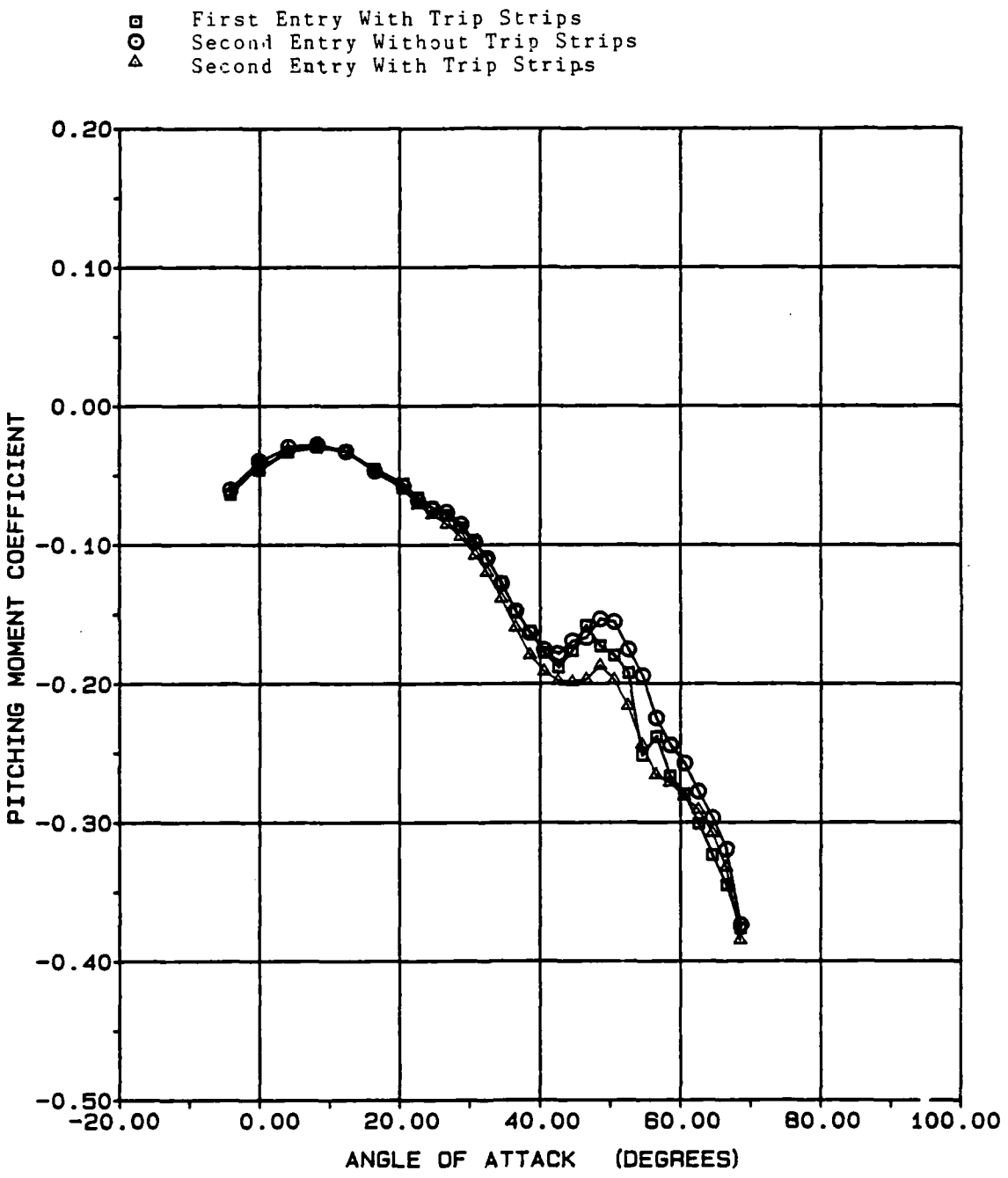

Figure 7. Continued.

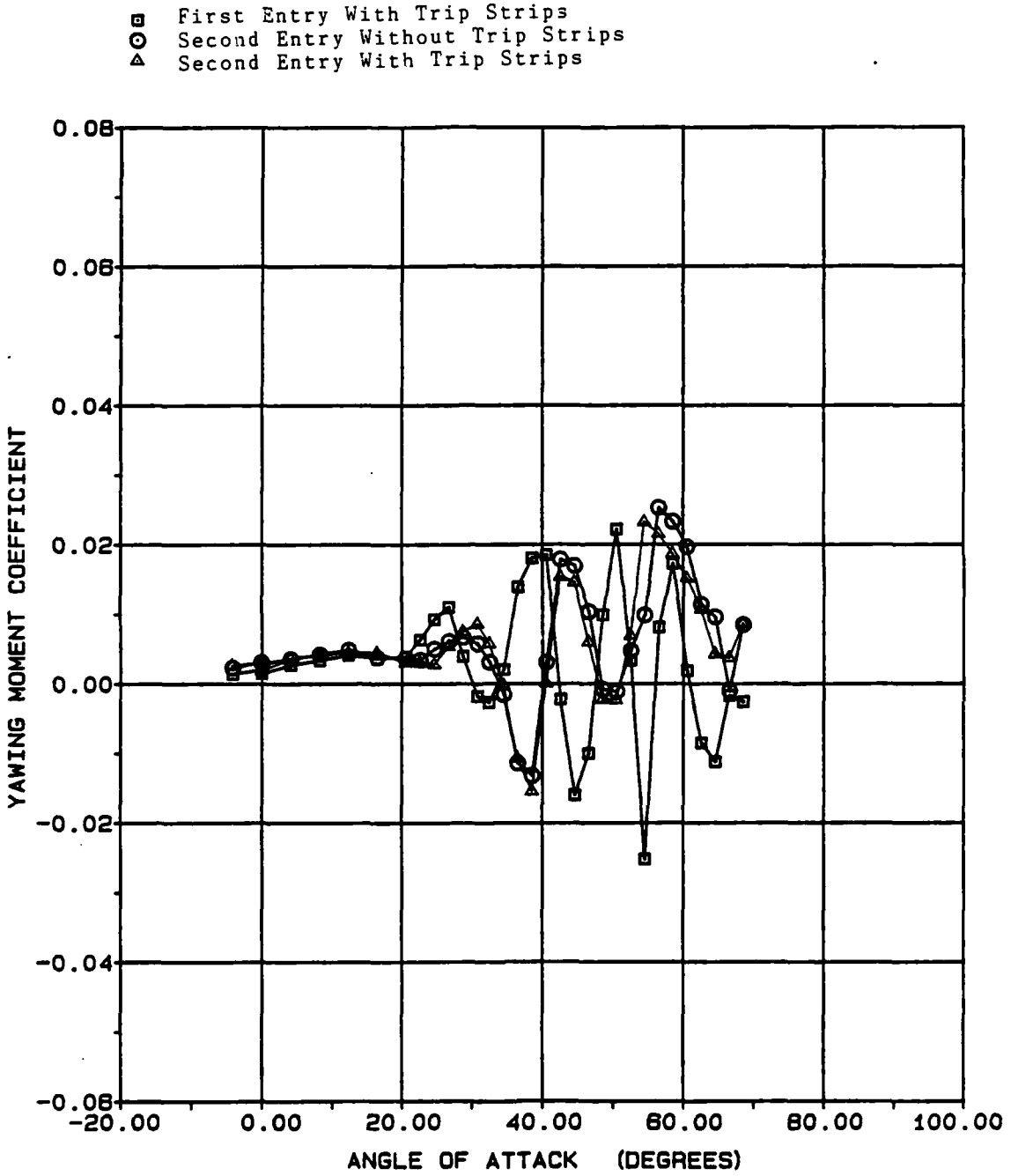

Figure 7. Continued.

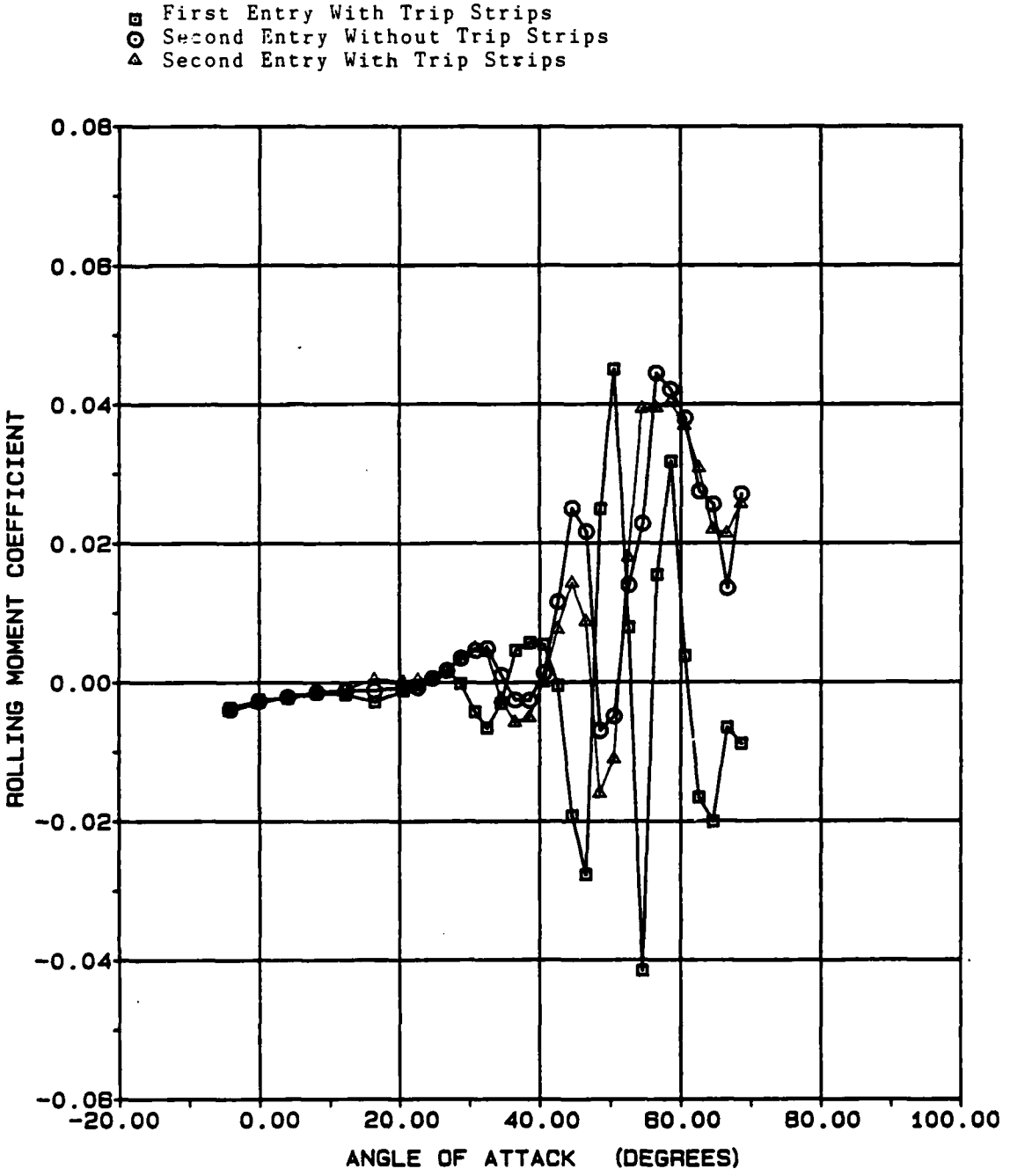

Figure 7. Concluded.

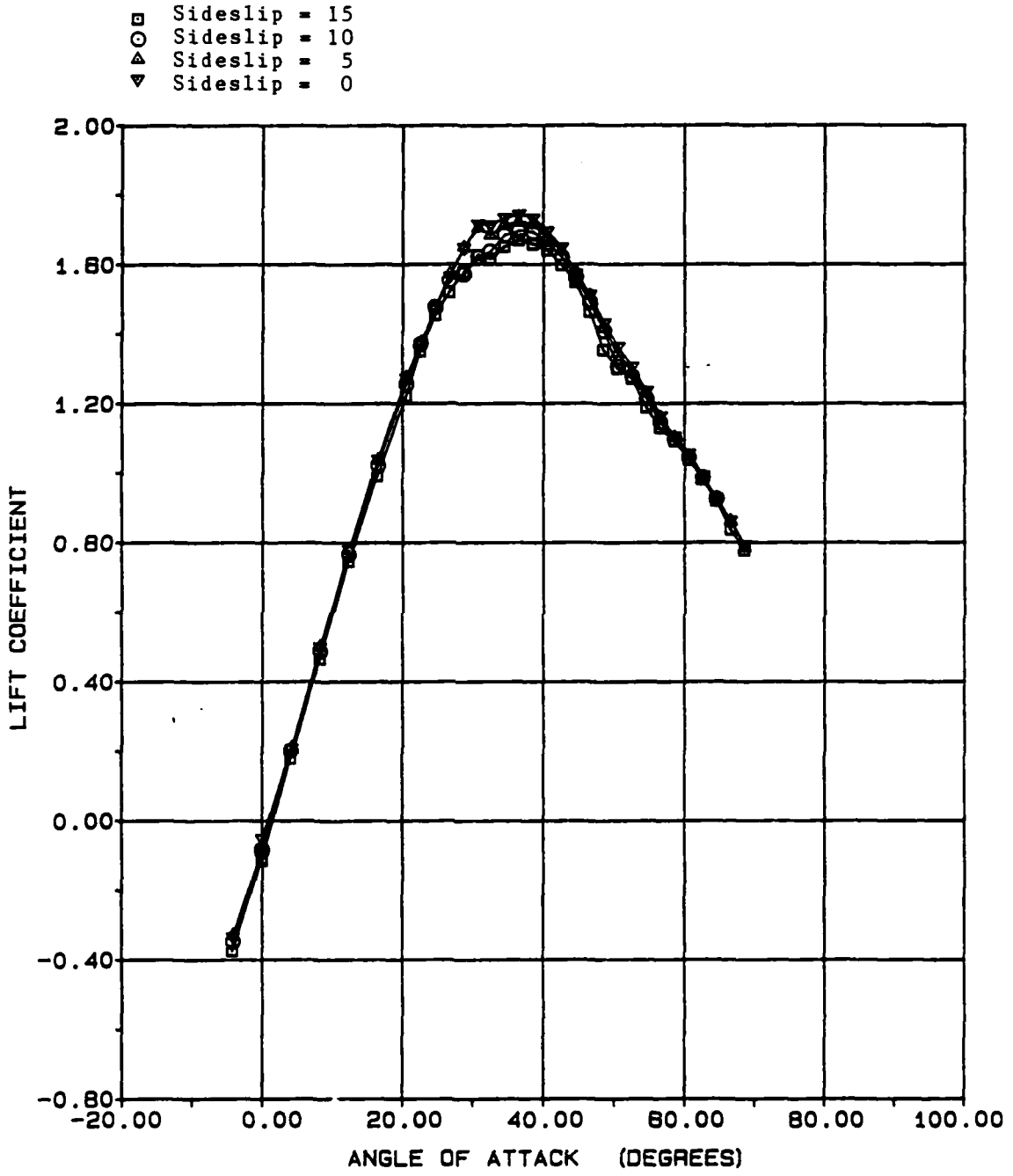

Figure 8. Aerodynamic Coefficients at Strake Deflection = -45.

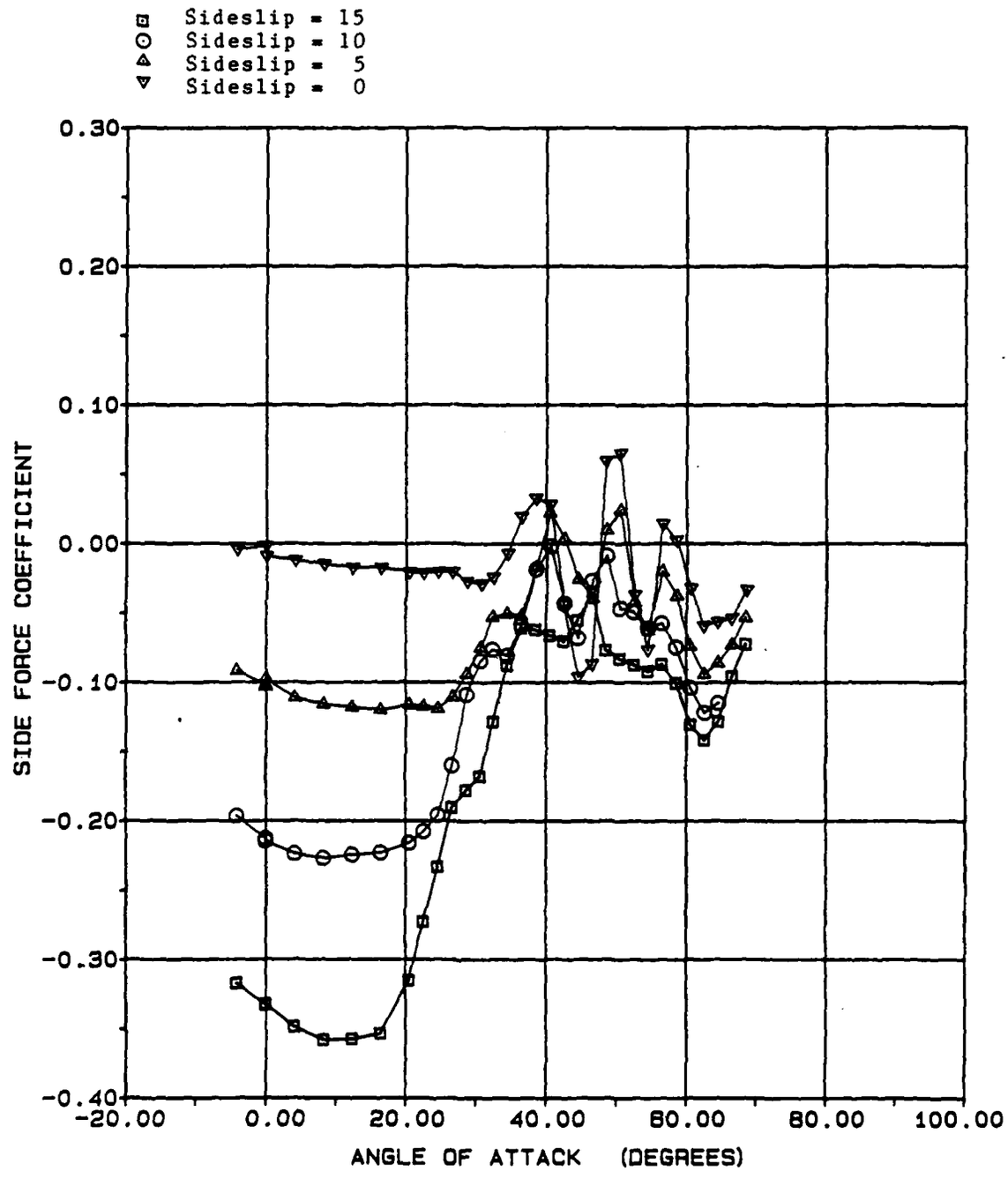

Figure 8. Continued.

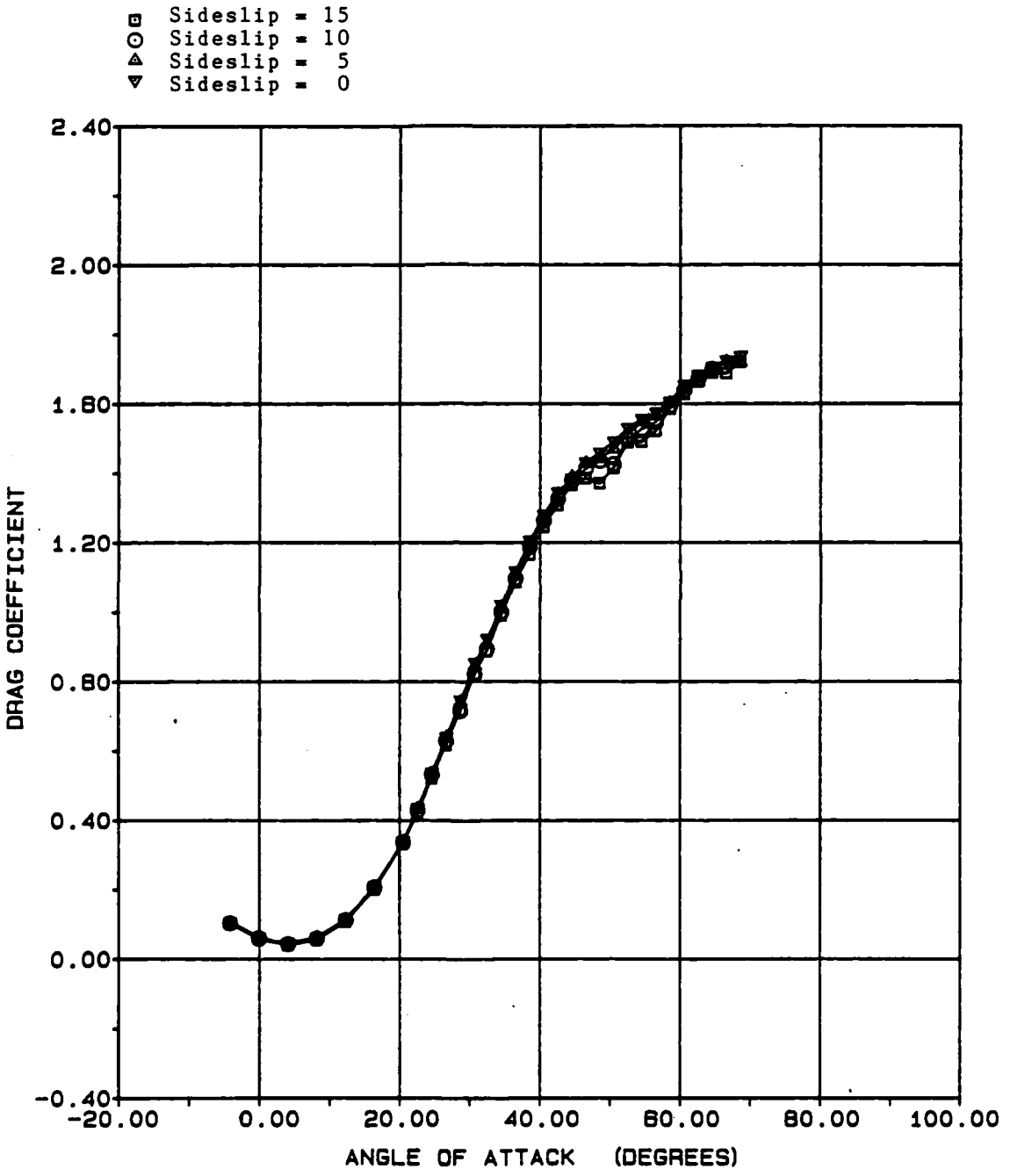

Figure 8. Continued.

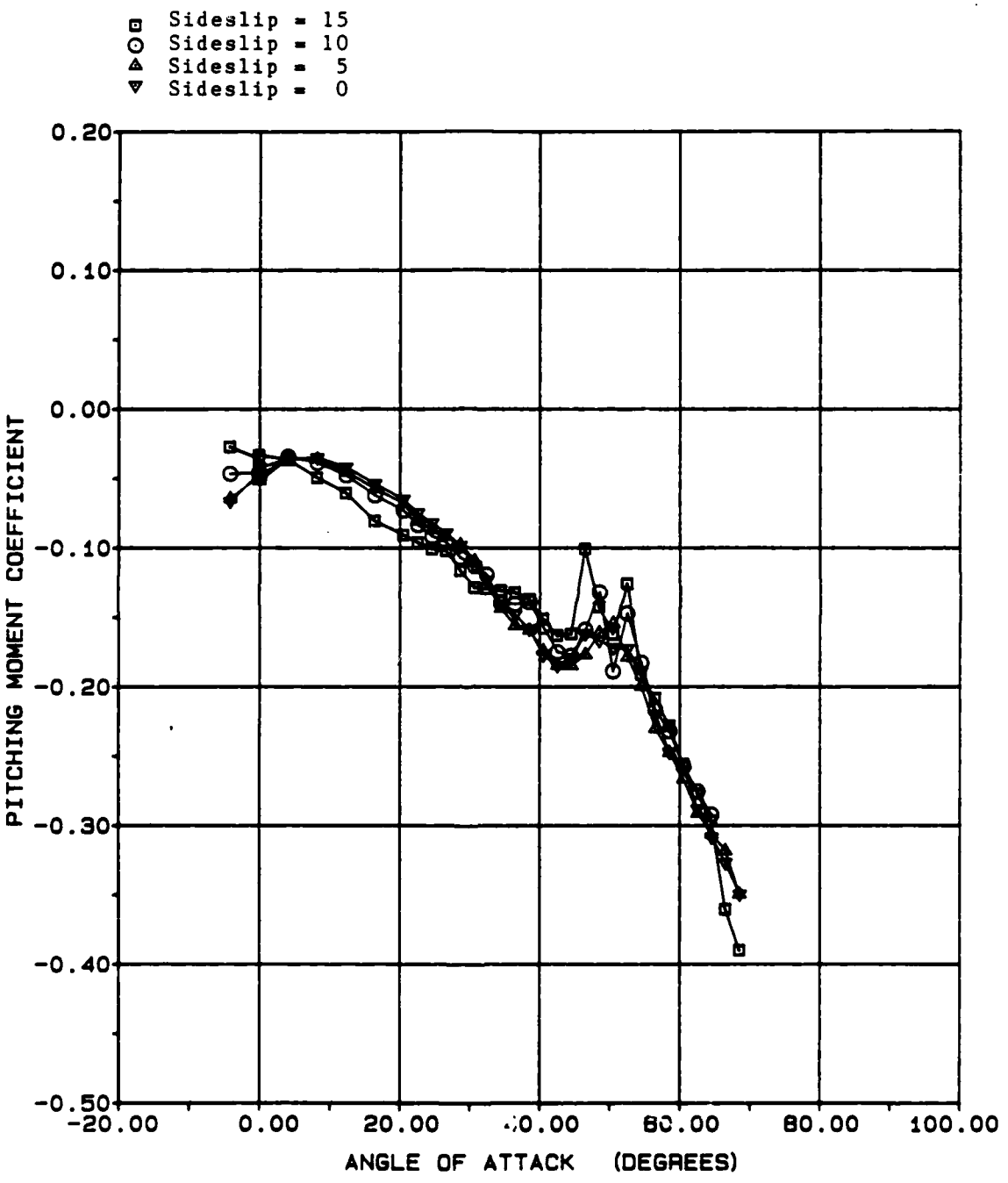

Figure 8. Continued.

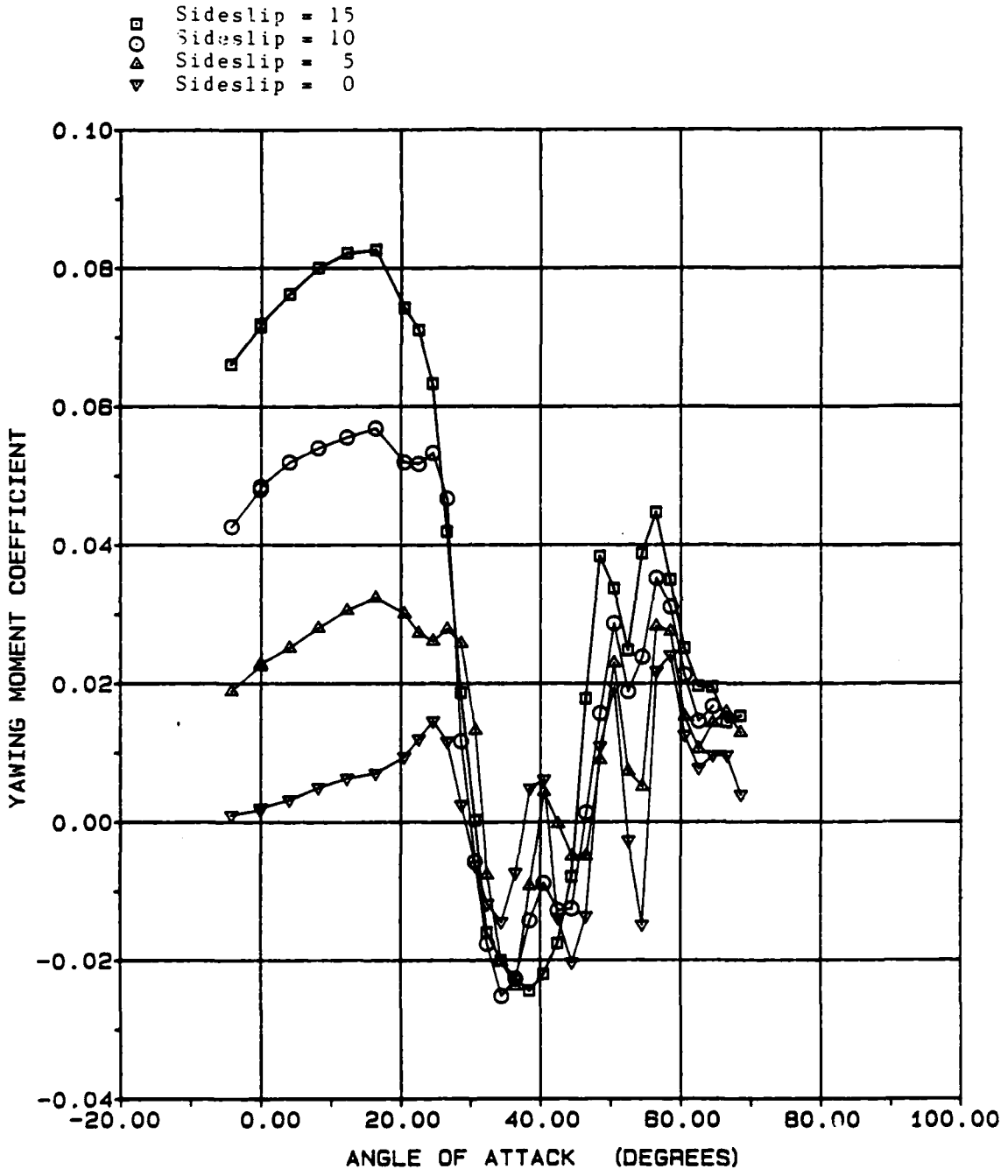

Figure 8. Continued.

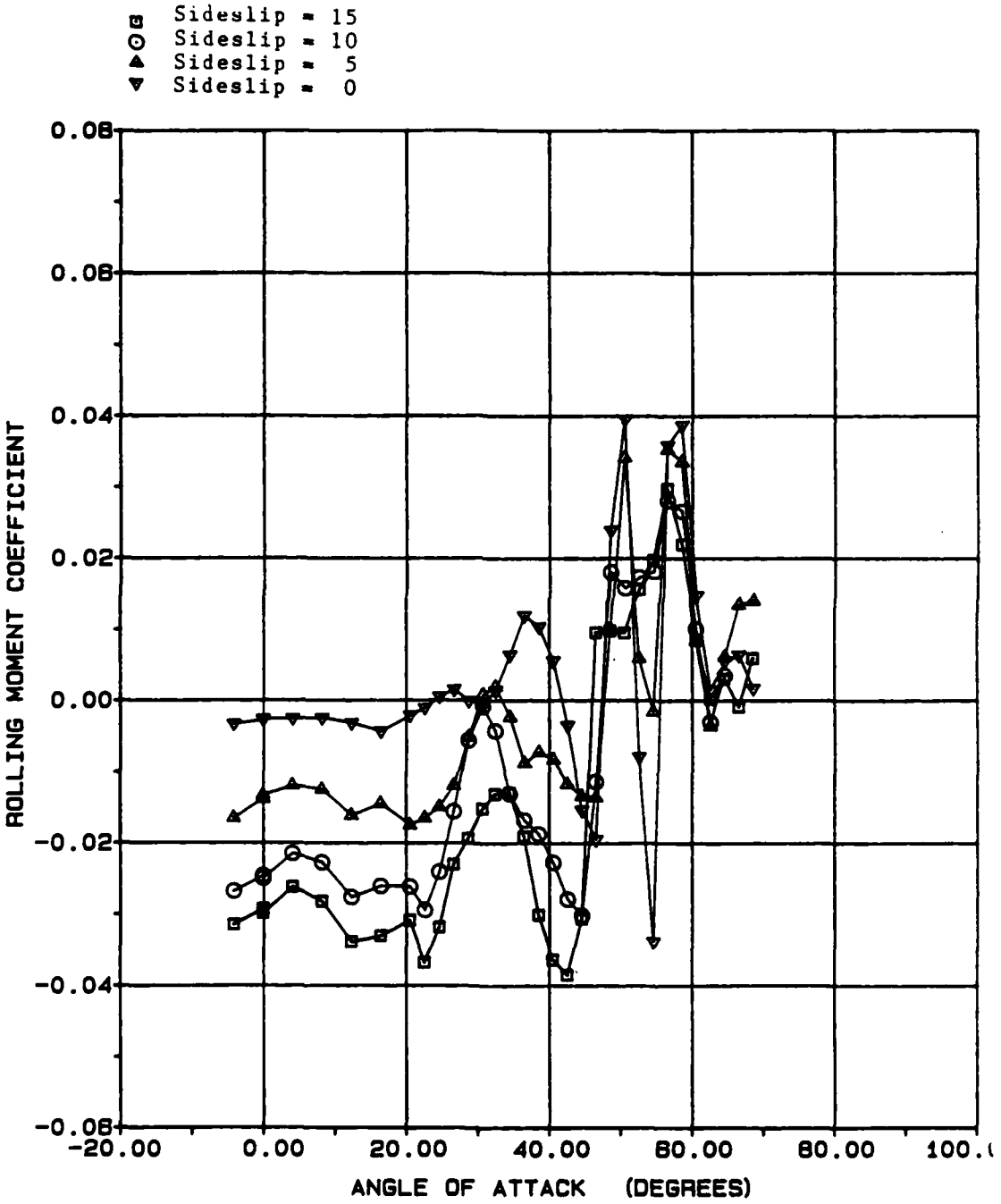

Figure 8. Concluded.

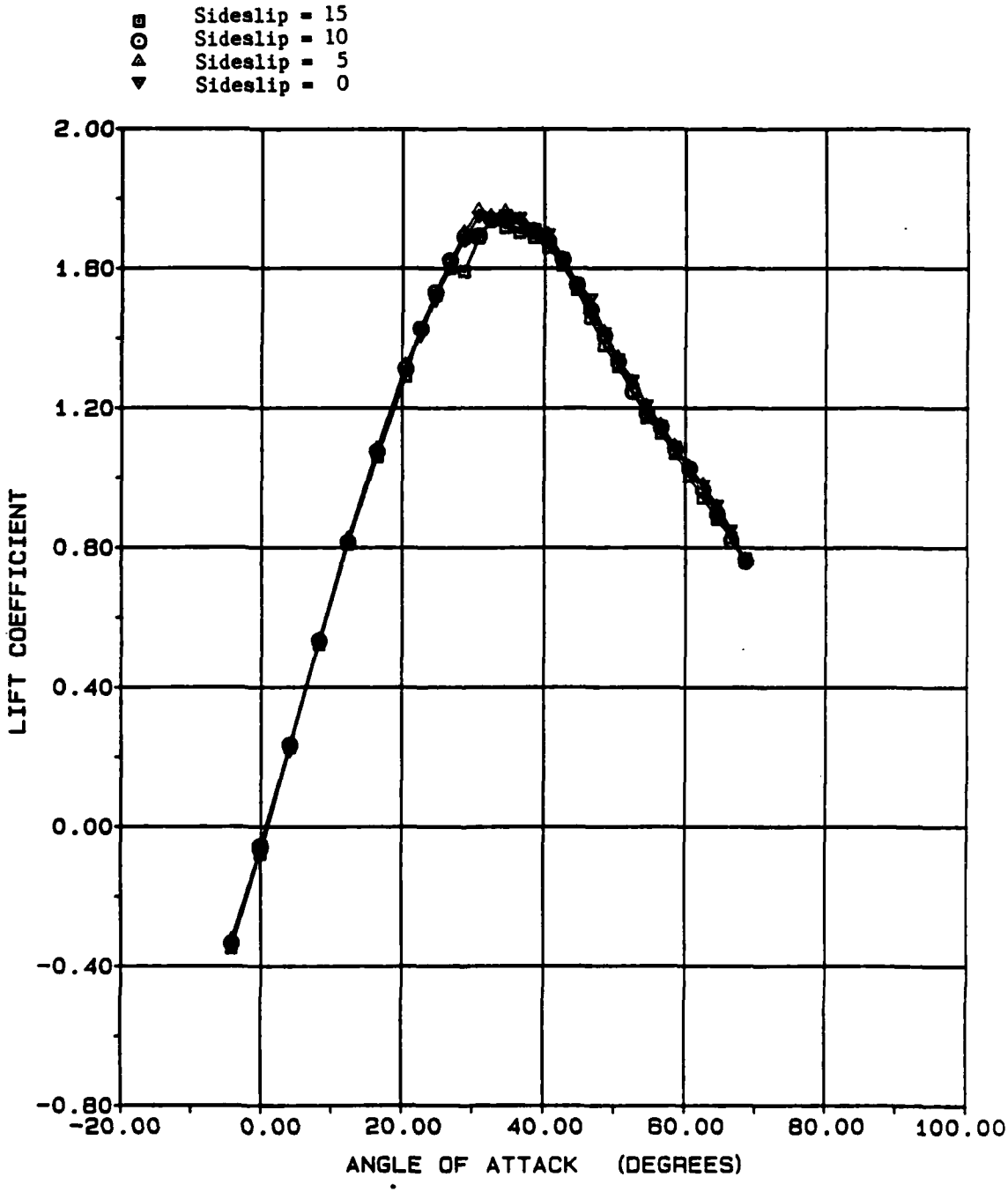

Figure 9. Aerodynamic Coefficients at Strake Deflection = +30.

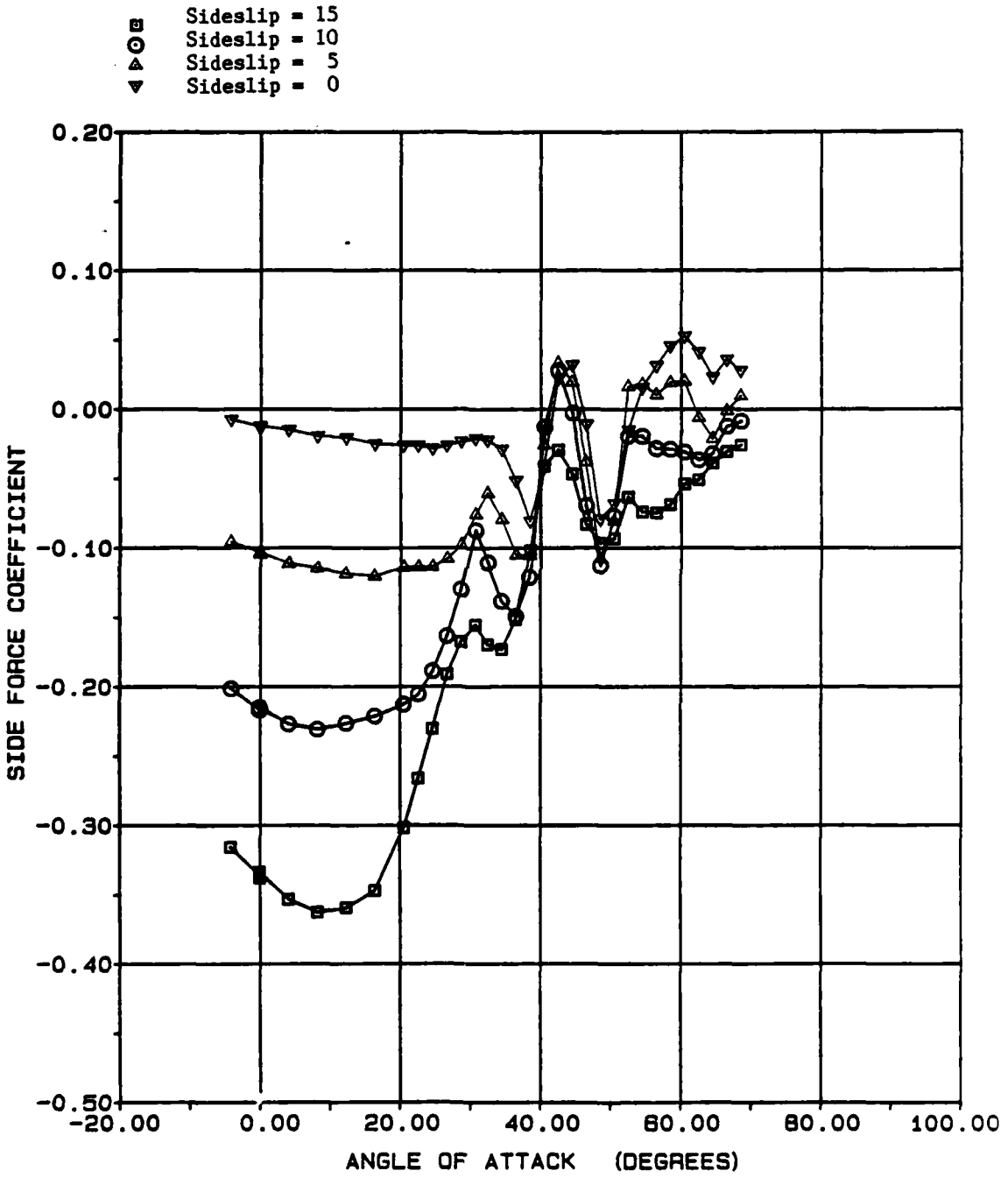

Figure 9. Continued.

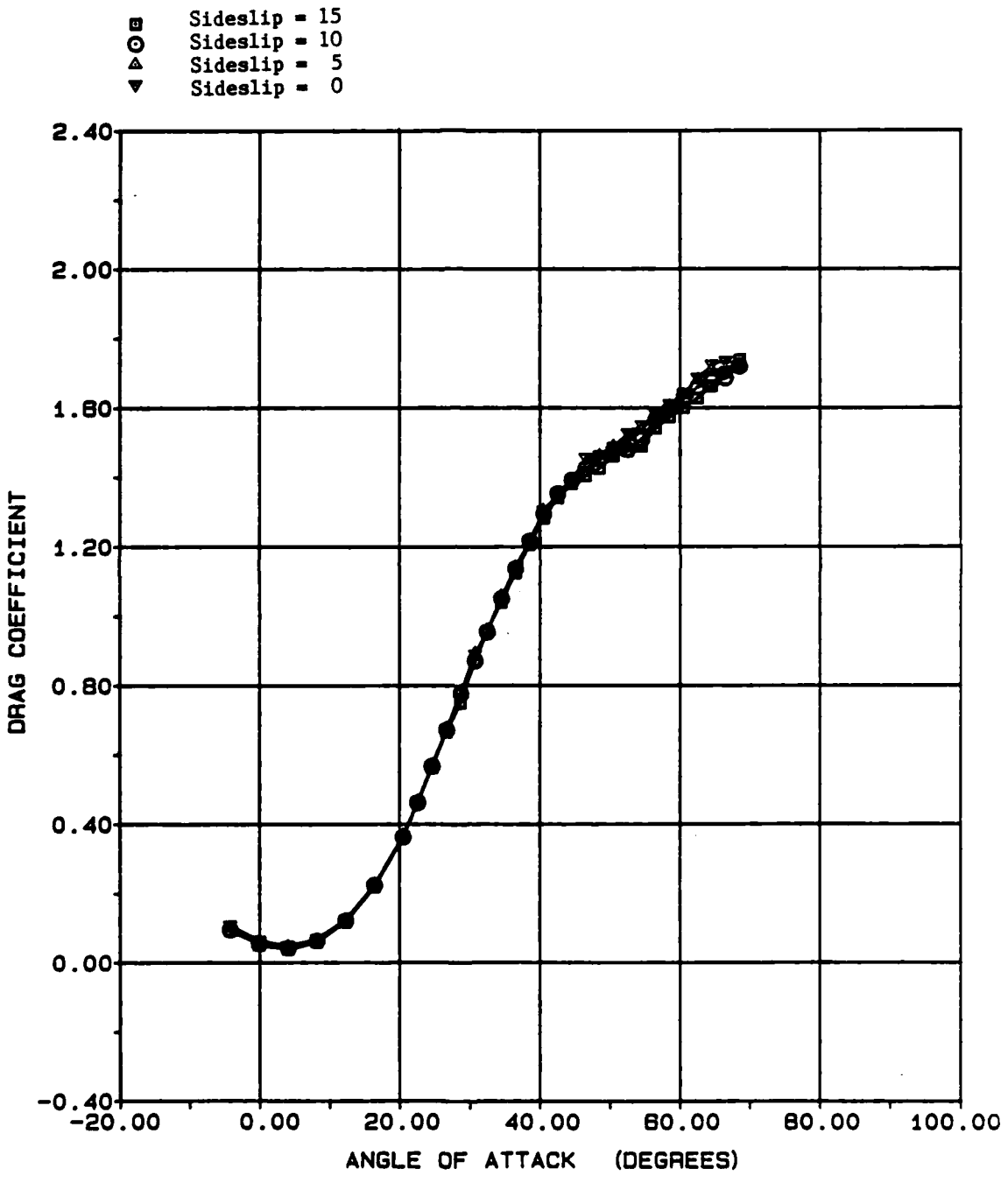

Figure 9. Continued.

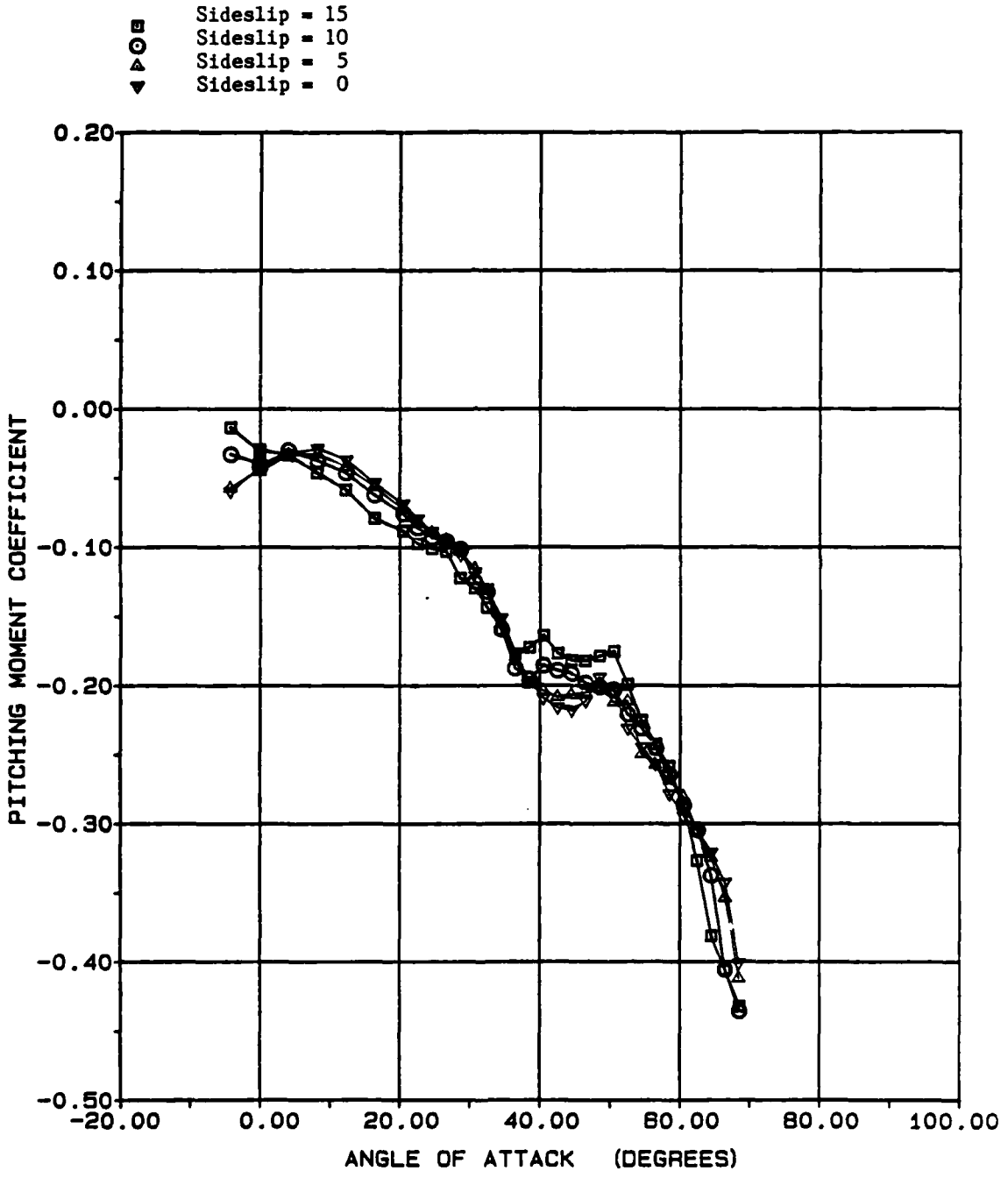

Figure 9. Continued.

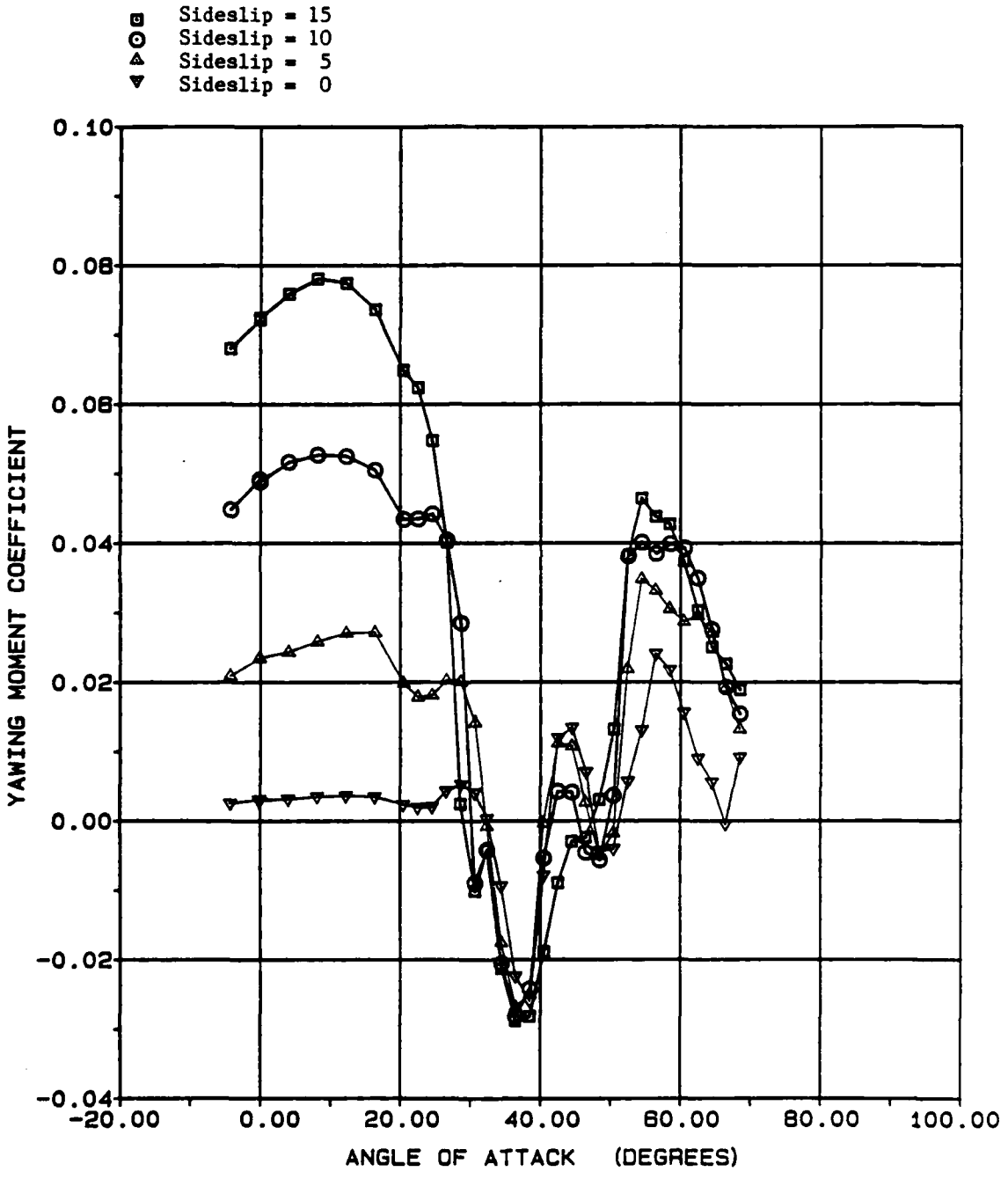

Figure 9. Continued.

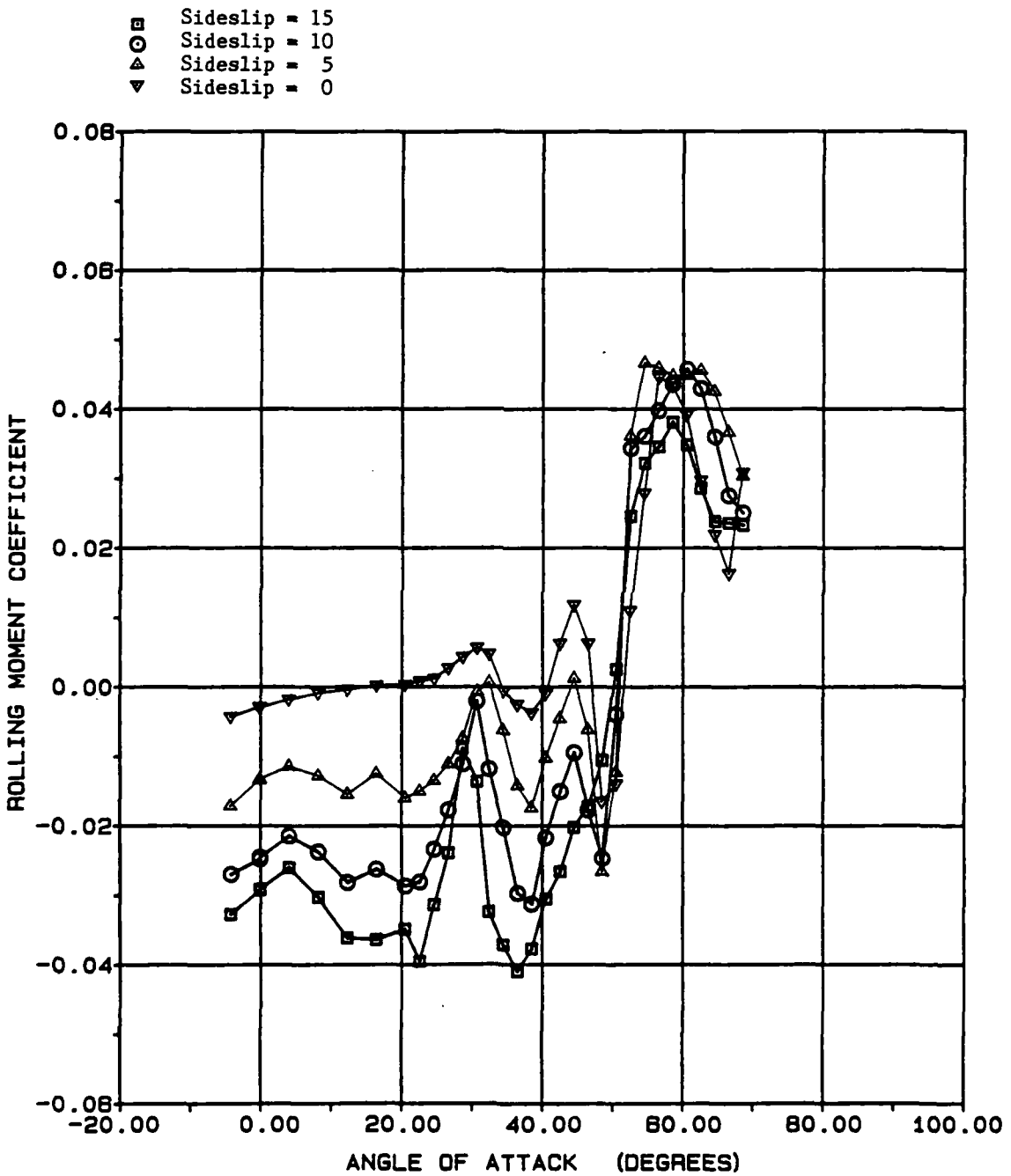

Figure 9. Concluded.

of attack, up to about 30°, these coefficients change very slowly with angle of attack and are almost constant. Above about 30°, they change rapidly, even changing sign with small increments of angle of attack. These plots give the appearance of scatter but the data were repeatable even at the higher angles of attack. Comparing the plots for different sideslip angles, the trends are consistent, that is, the sign of the slope with respect to AOA is the same and changes at approximately same AOA.

One other important point seen in coefficients plotted across angle of attack deals with the anhedral-dihedral (AnDi) cases. Each of these cases was plotted against the corresponding asymmetric case with the same positive strake deflection on the right side. In each case, no noticeable change was seen in Figure 10 due to deflecting the second strake. Consequently, no further consideration was given to the AnDi case.

The major interest in this investigation concerned the control power of the hinged strakes. This control power could be seen in how much a given force or moment changed when the strake was deflected. These changes in the forces and moments would be used in the 6 DOF simulation to simulate the aircraft's response to deflecting the strakes. In order to obtain this change in the coefficients, the coefficients of a baseline run at a given AOA were subtracted from the coefficients at the same AOA for a run with the strake deflected. The baseline run used was the run with the same sideslip angle without either strake deflected. These changes in the coefficients due to deflecting the strakes were plotted. As seen in Figures 11-12, deflecting the strake does cause a change in the lateral-directional coefficients. Like the coefficients themselves, these increments also vary rapidly with angle of attack at the higher angles of attack. The differences and similarities between anhedral and dihedral strake deflections can also be seen in Figures 11-12. While the forces and moments change when the strake is deflected either up or down, in both cases the results are not well behaved, i.e. for both positive and negative deflections, the forces and moments do not follow a smooth curve with increasing AOA. Since the response of the aircraft to a

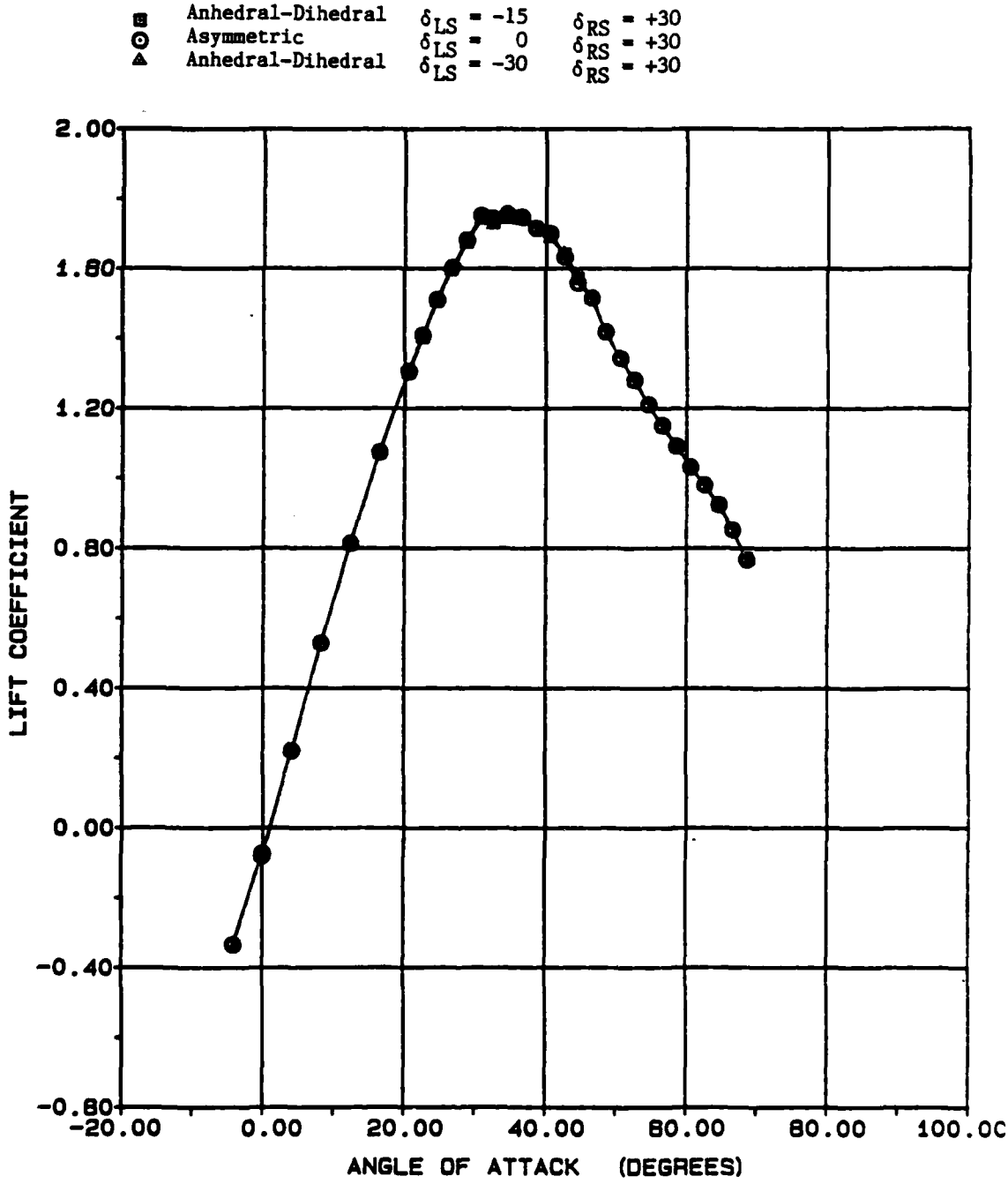

Figure 10. Comparison of Anhedral-Dihedral Configuration to Asymmetric Configuration.

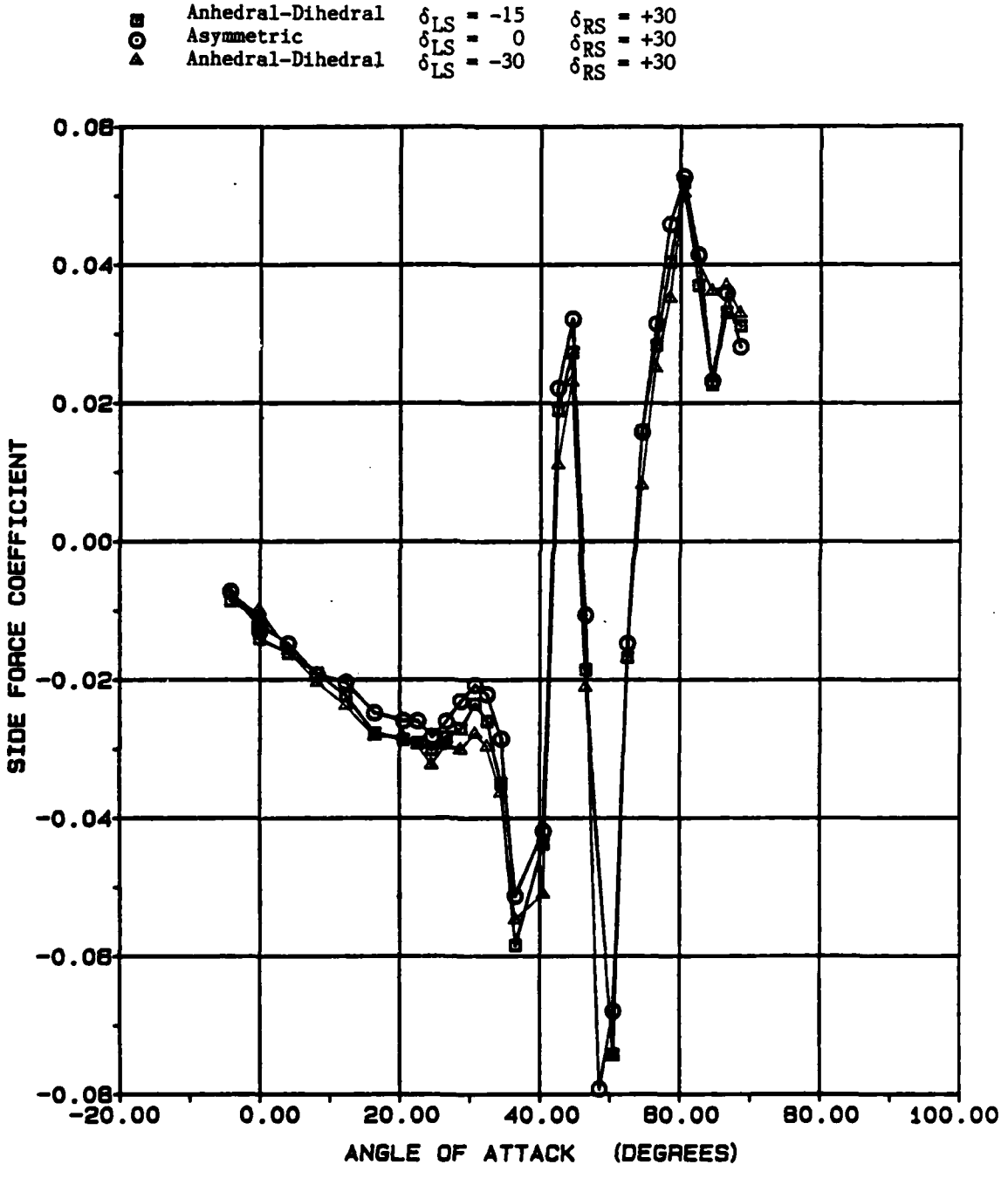

Figure 10. Continued.

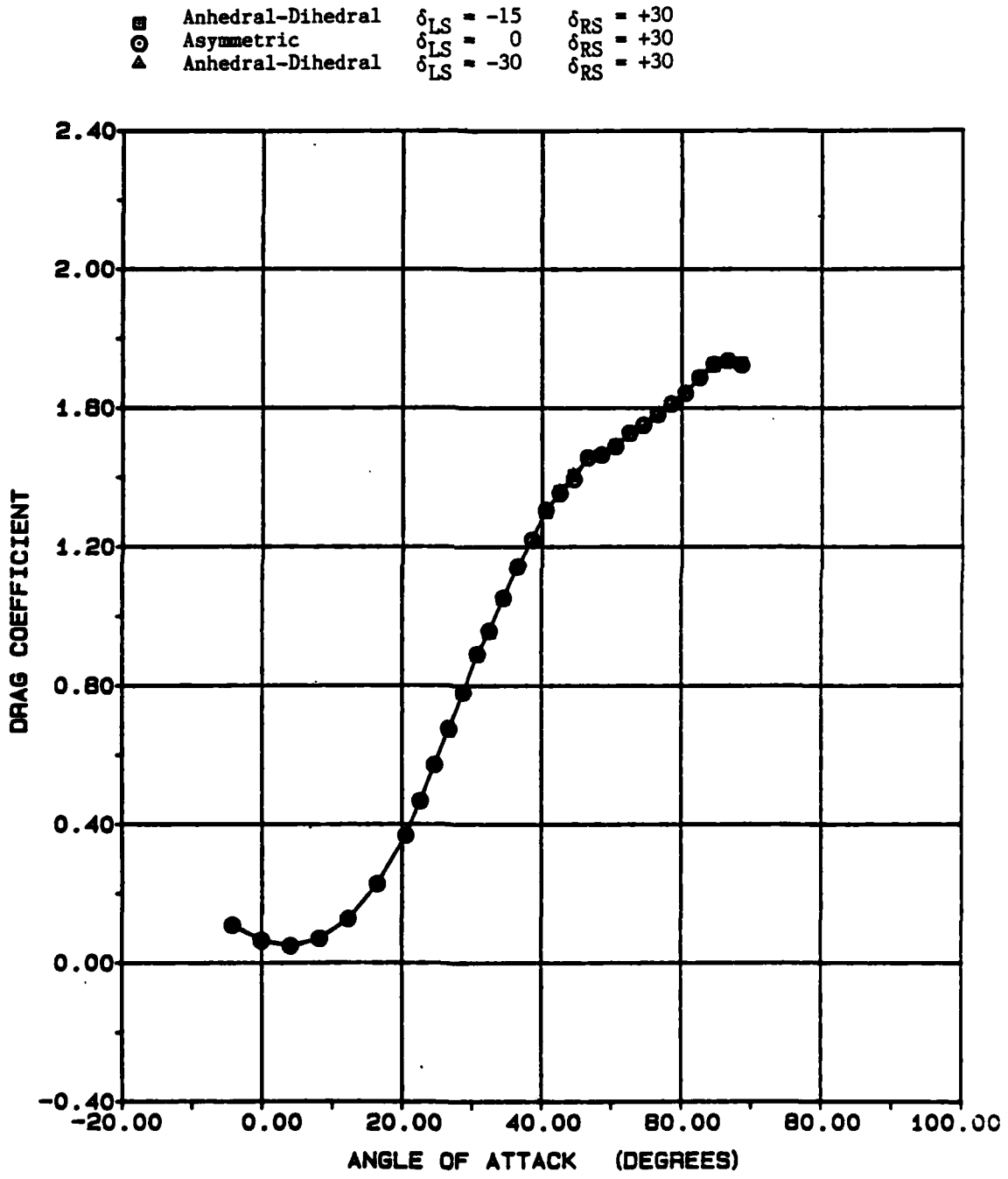

Figure 10. Continued.

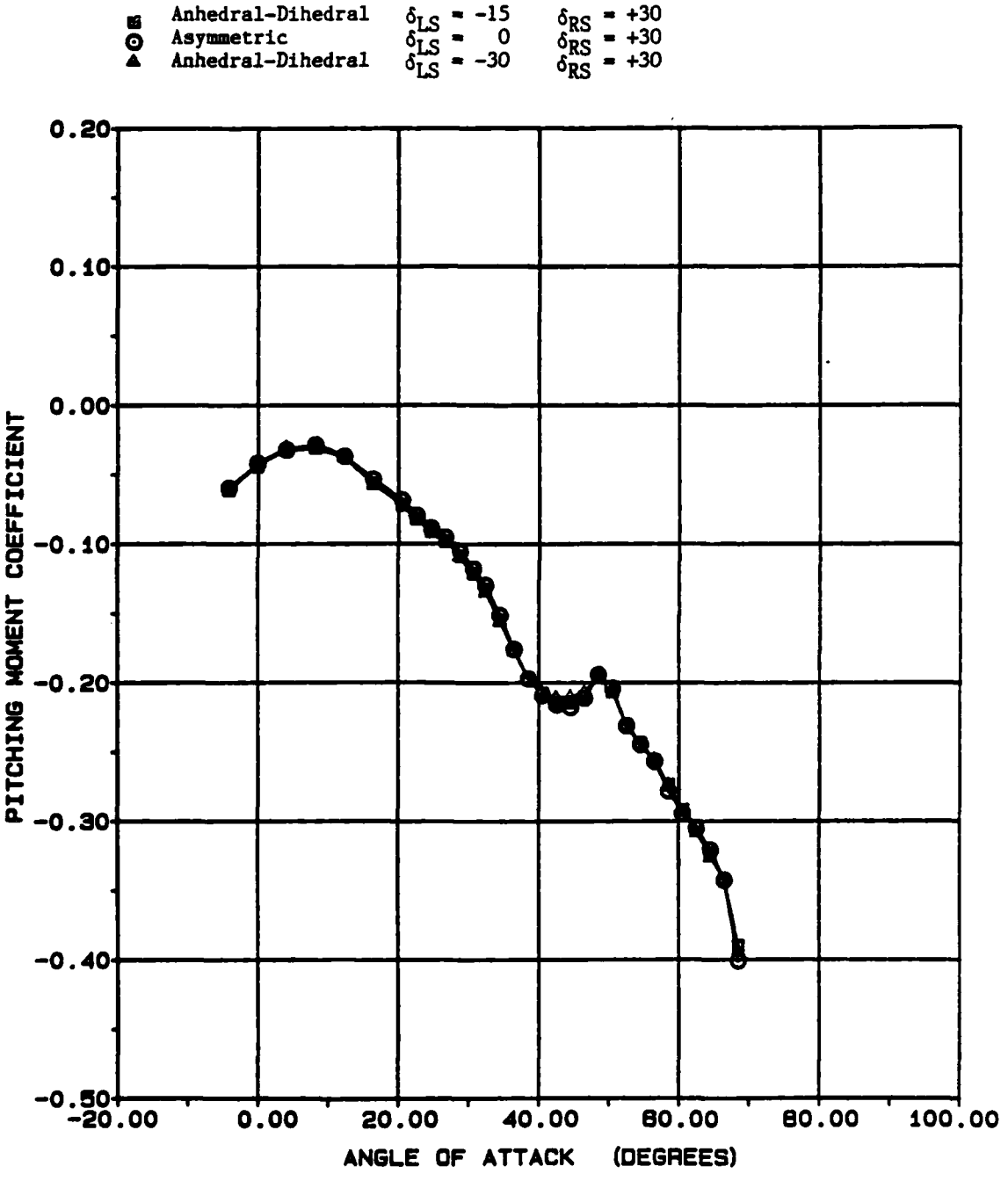

Figure 10. Continued.

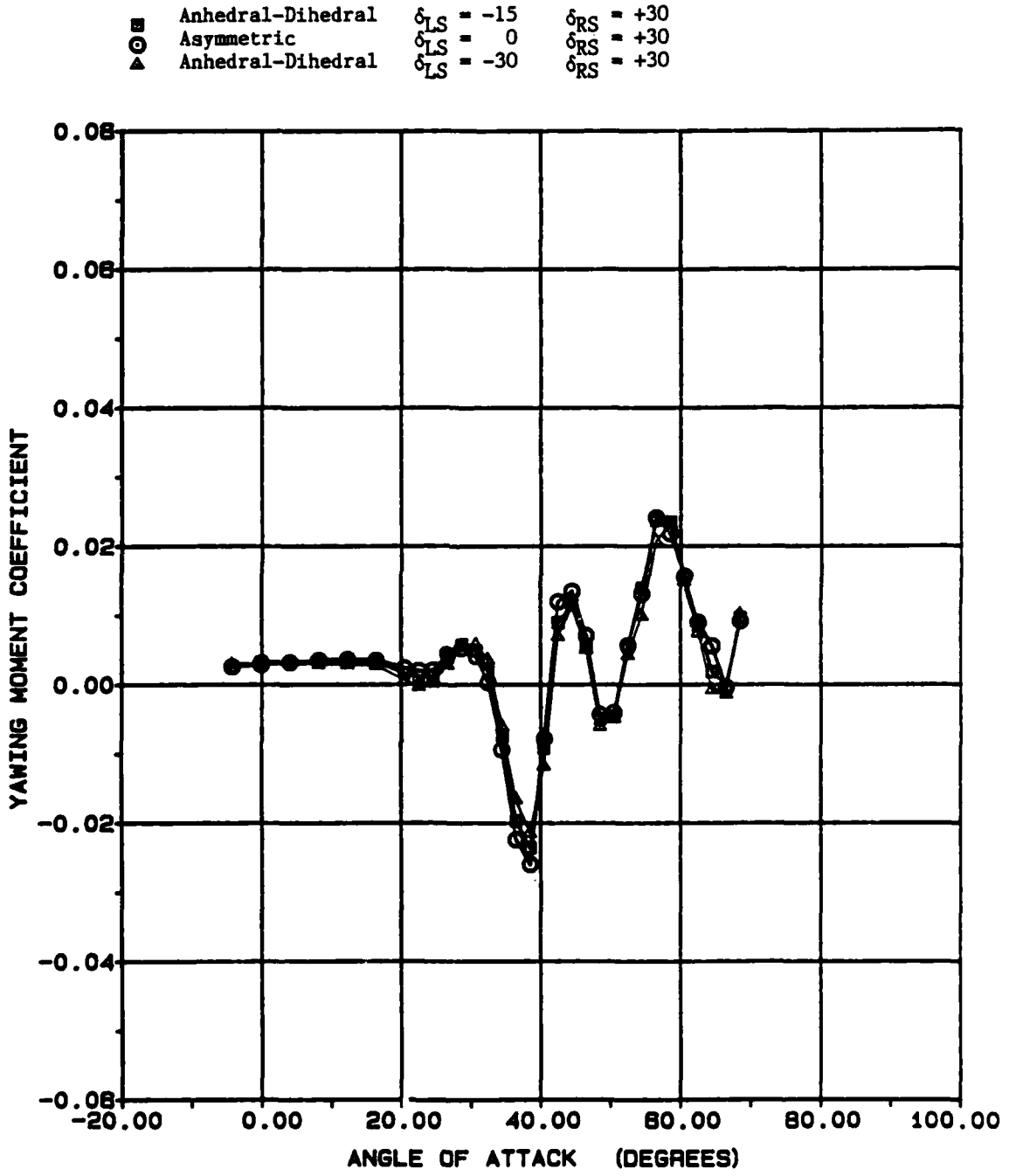

Figure 10. Continued.

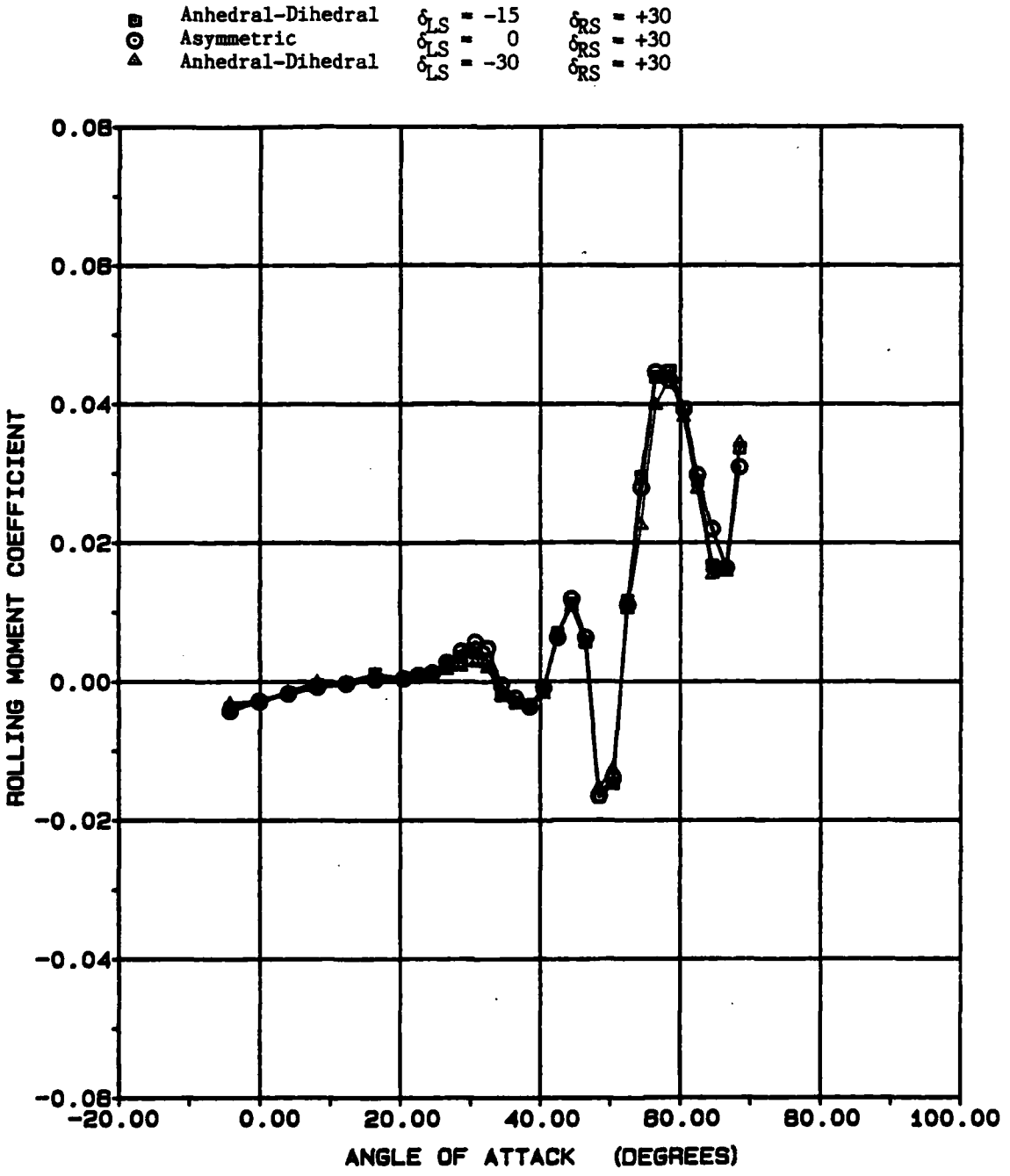

Figure 10. Concluded.

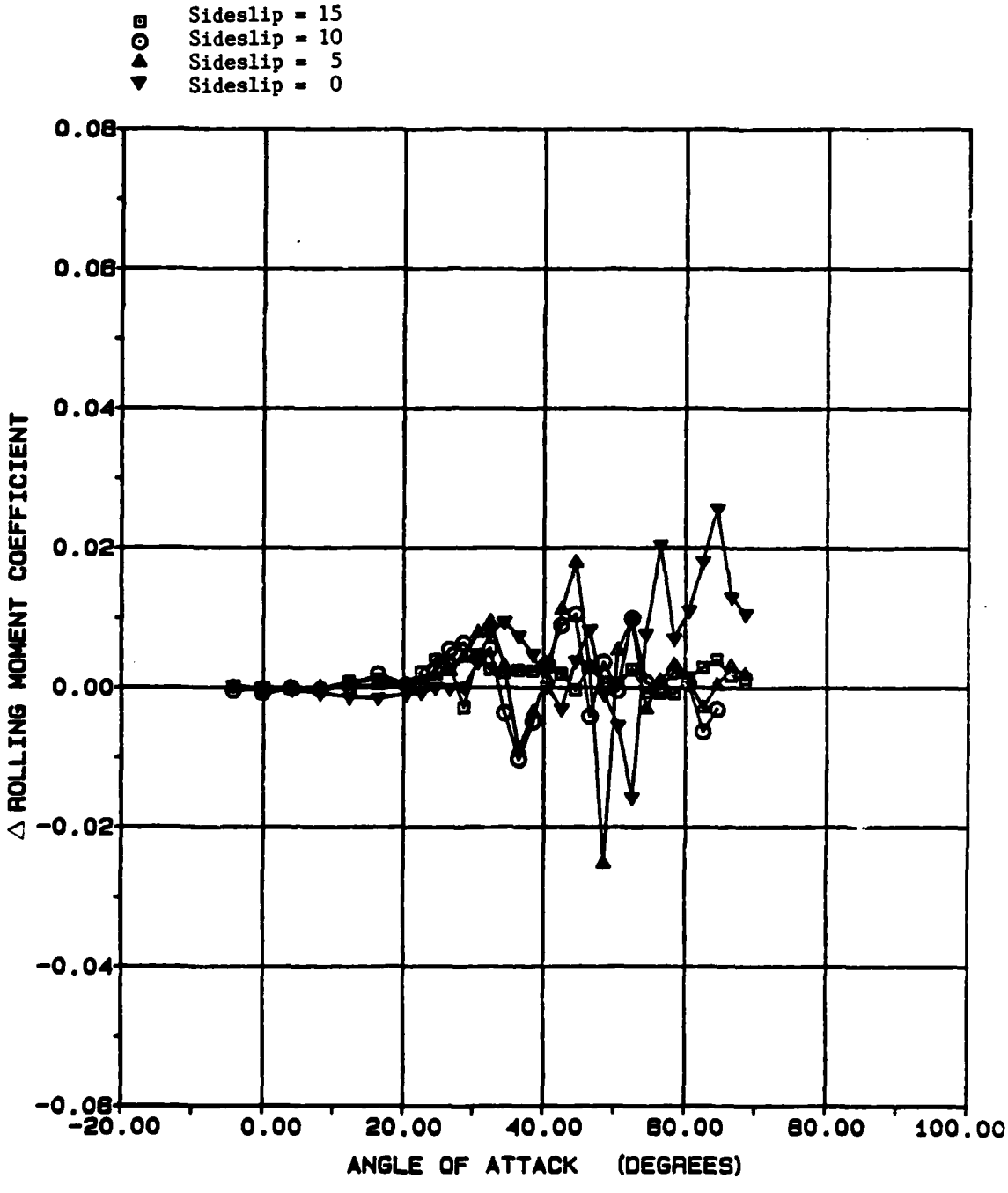

Figure 11. Incremental Aerodynamic Coefficients at Strake Deflection = -45.

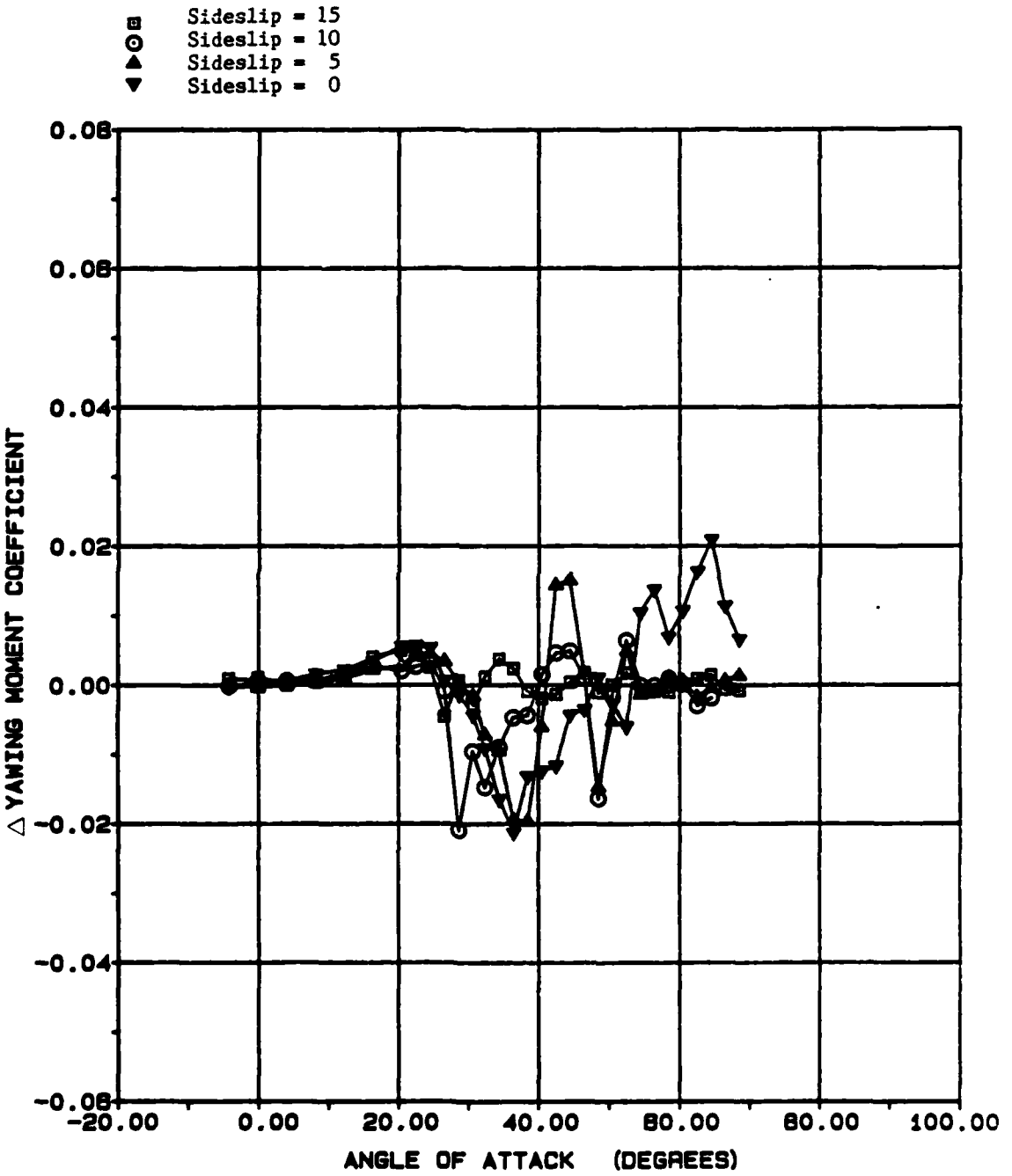

Figure 11. Continued.

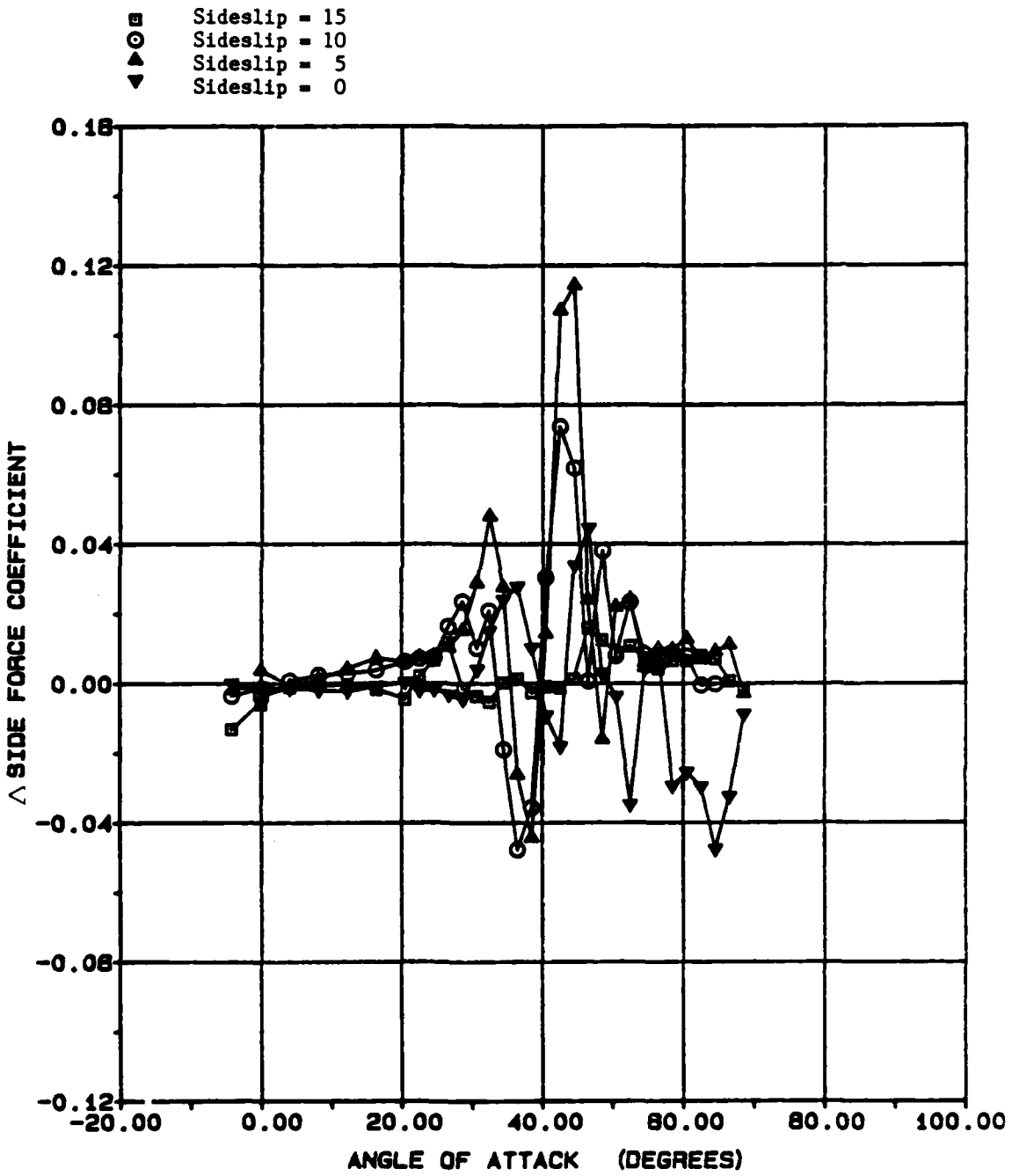

Figure 11. Continued.

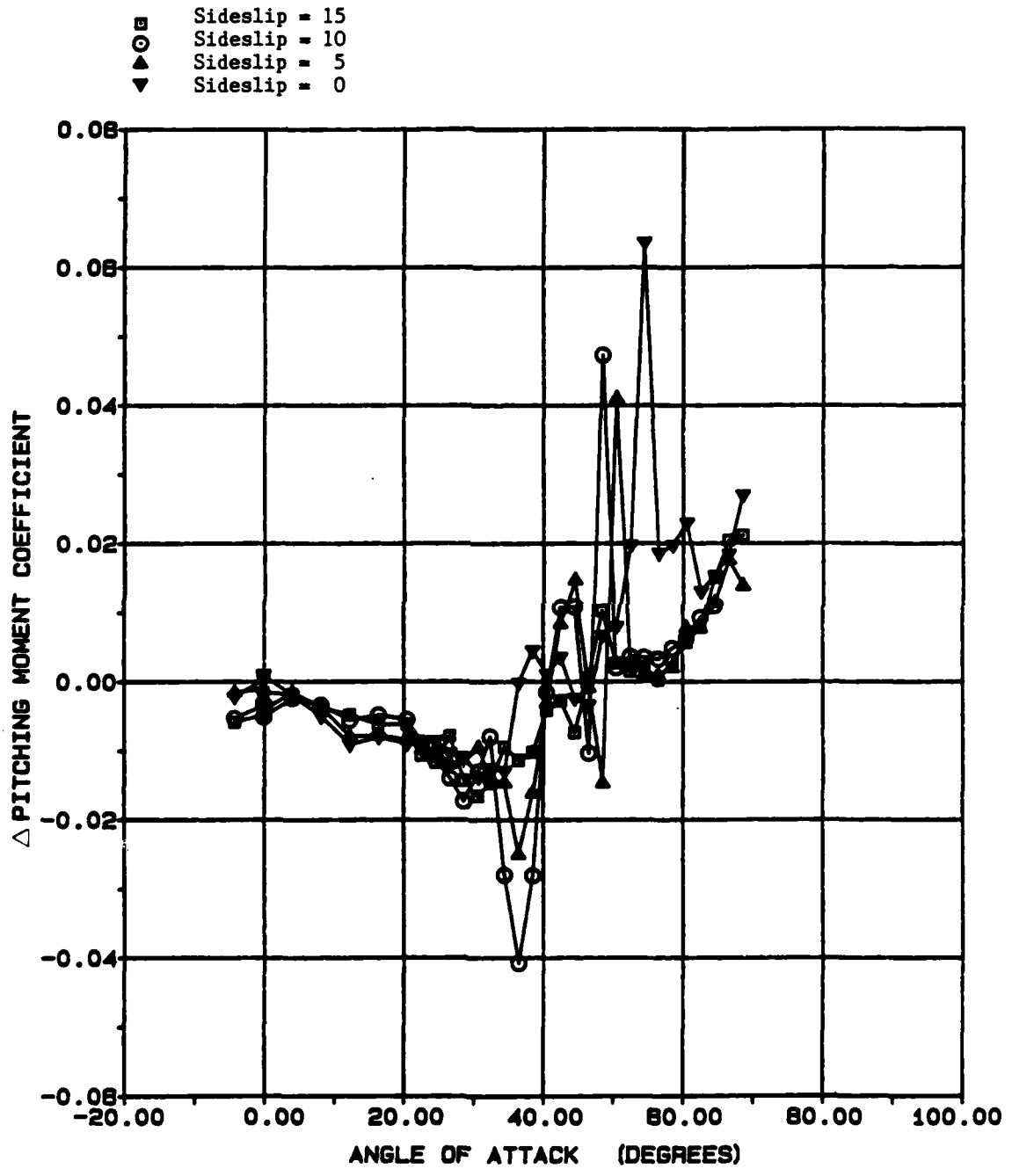

Figure 11. Concluded.

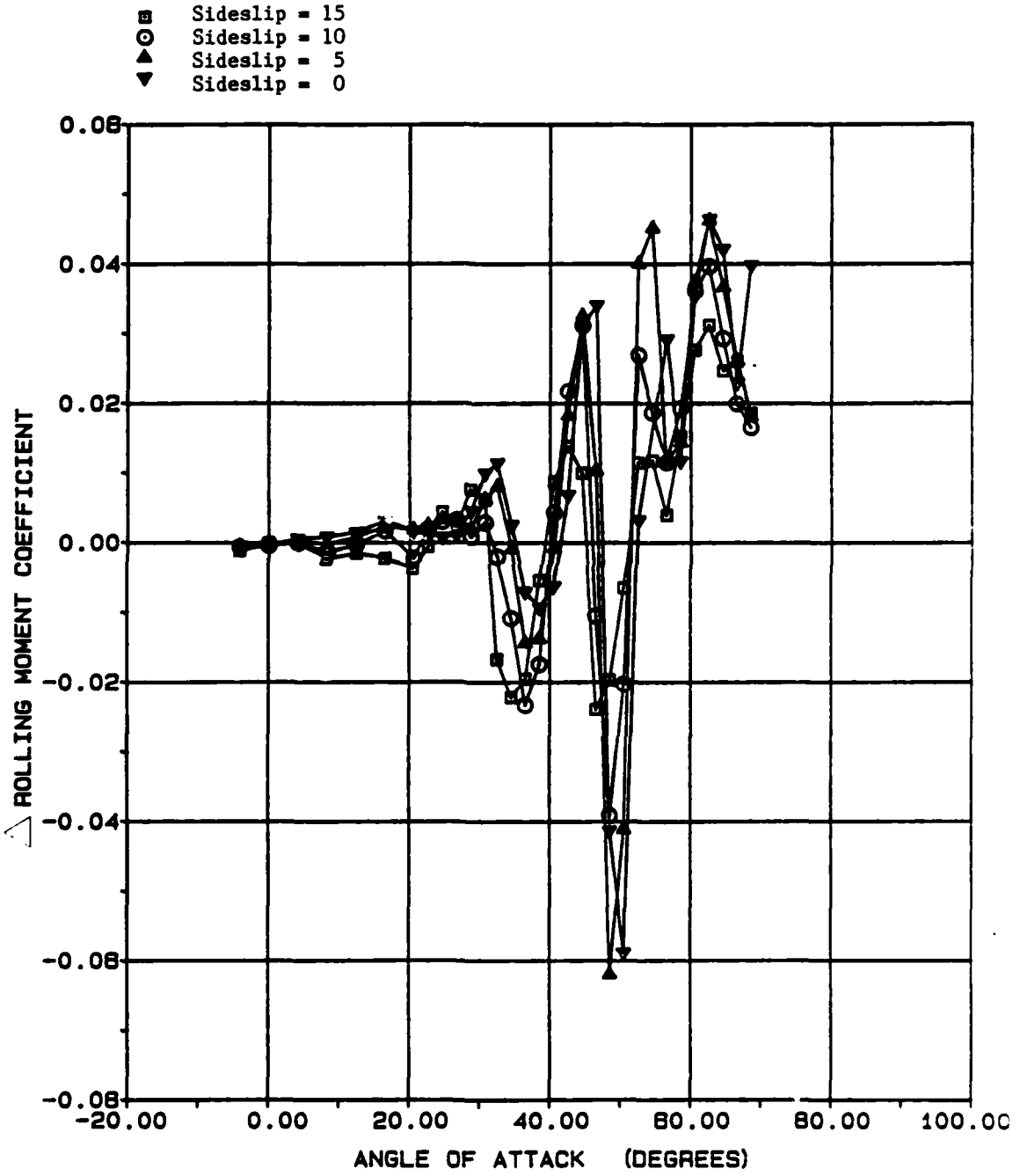

Figure 12. Incremental Aerodynamic Coefficients at Strake Deflection = +30.

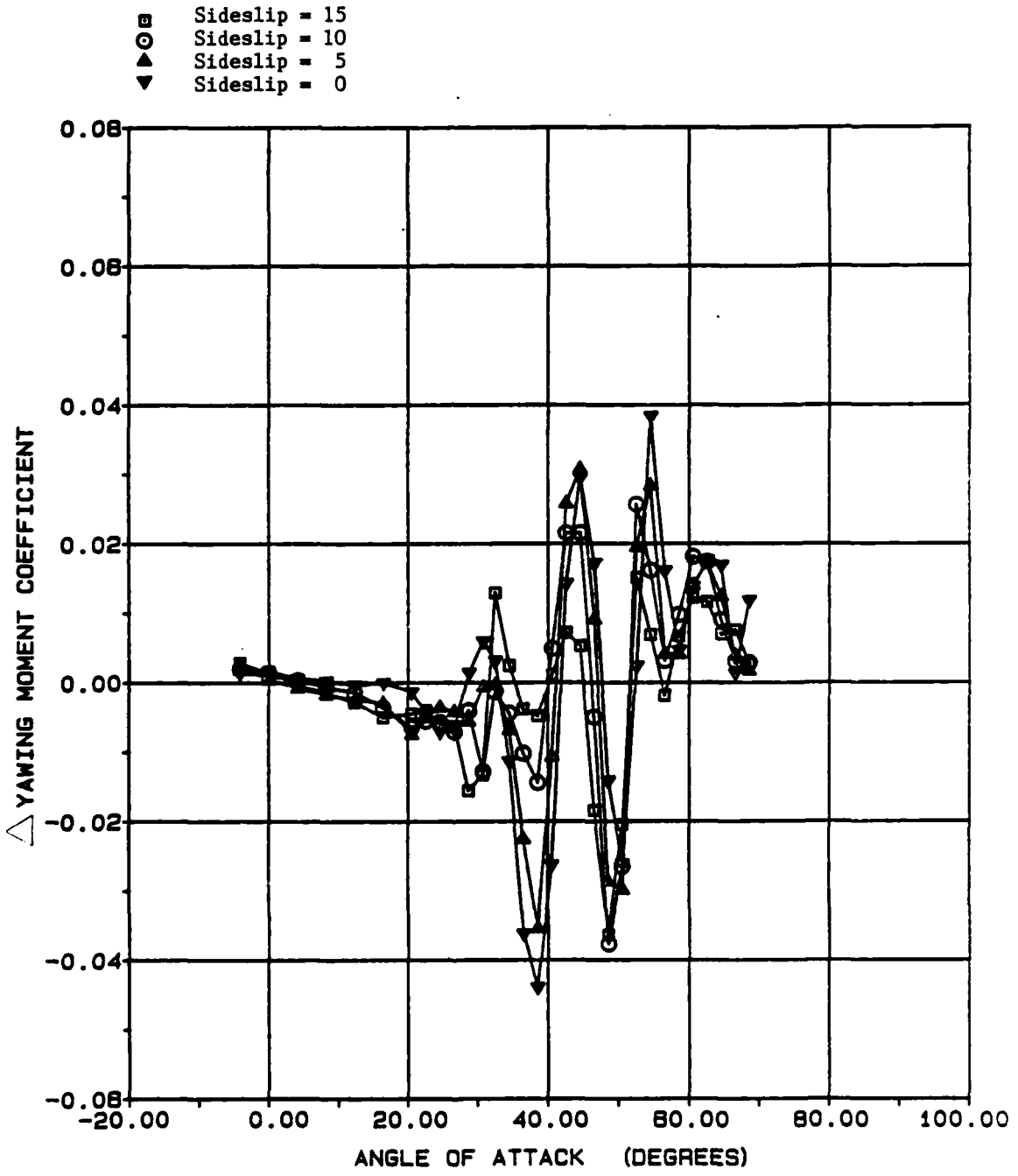

Figure 12. Continued.

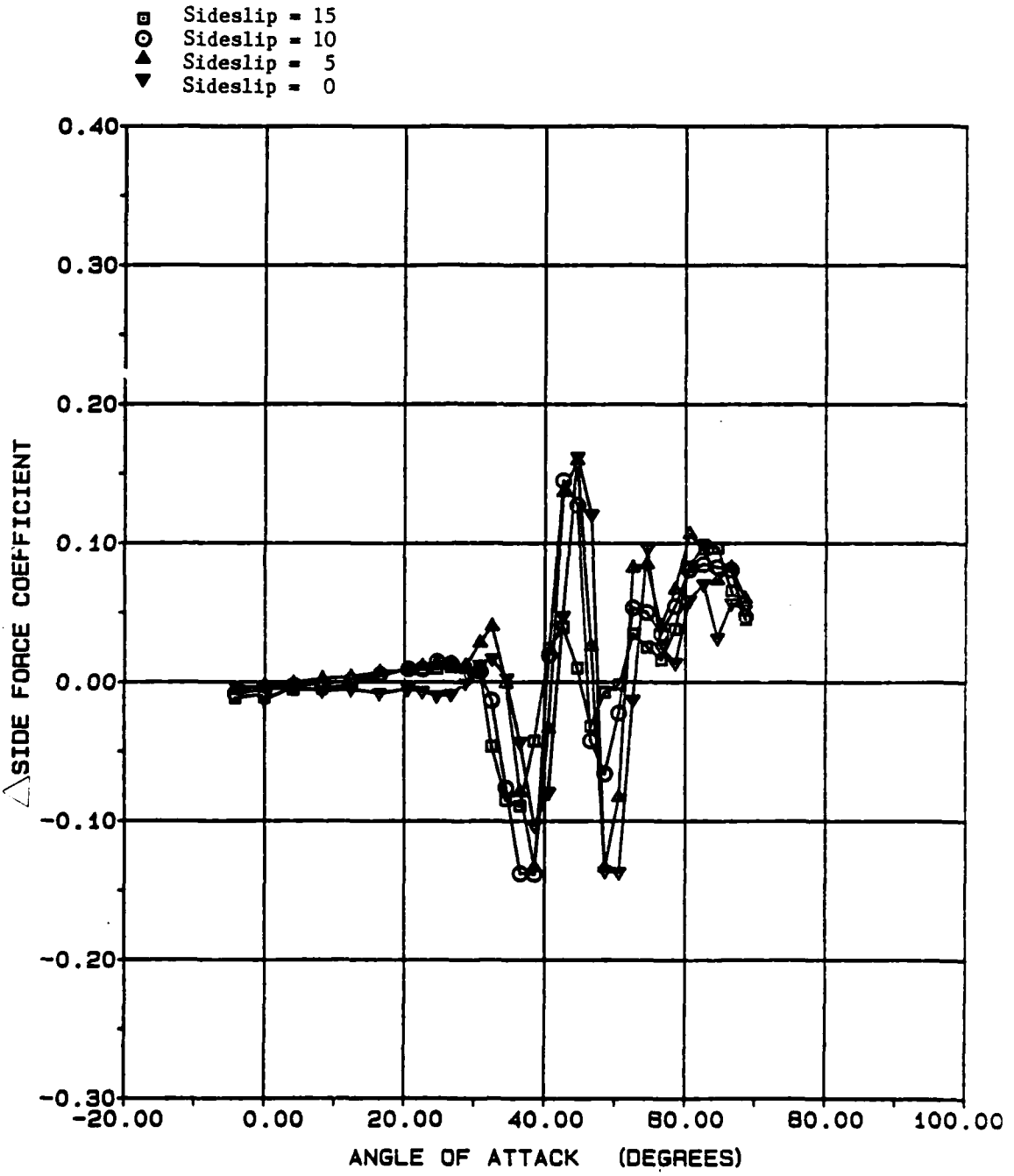

Figure 12. Continued.

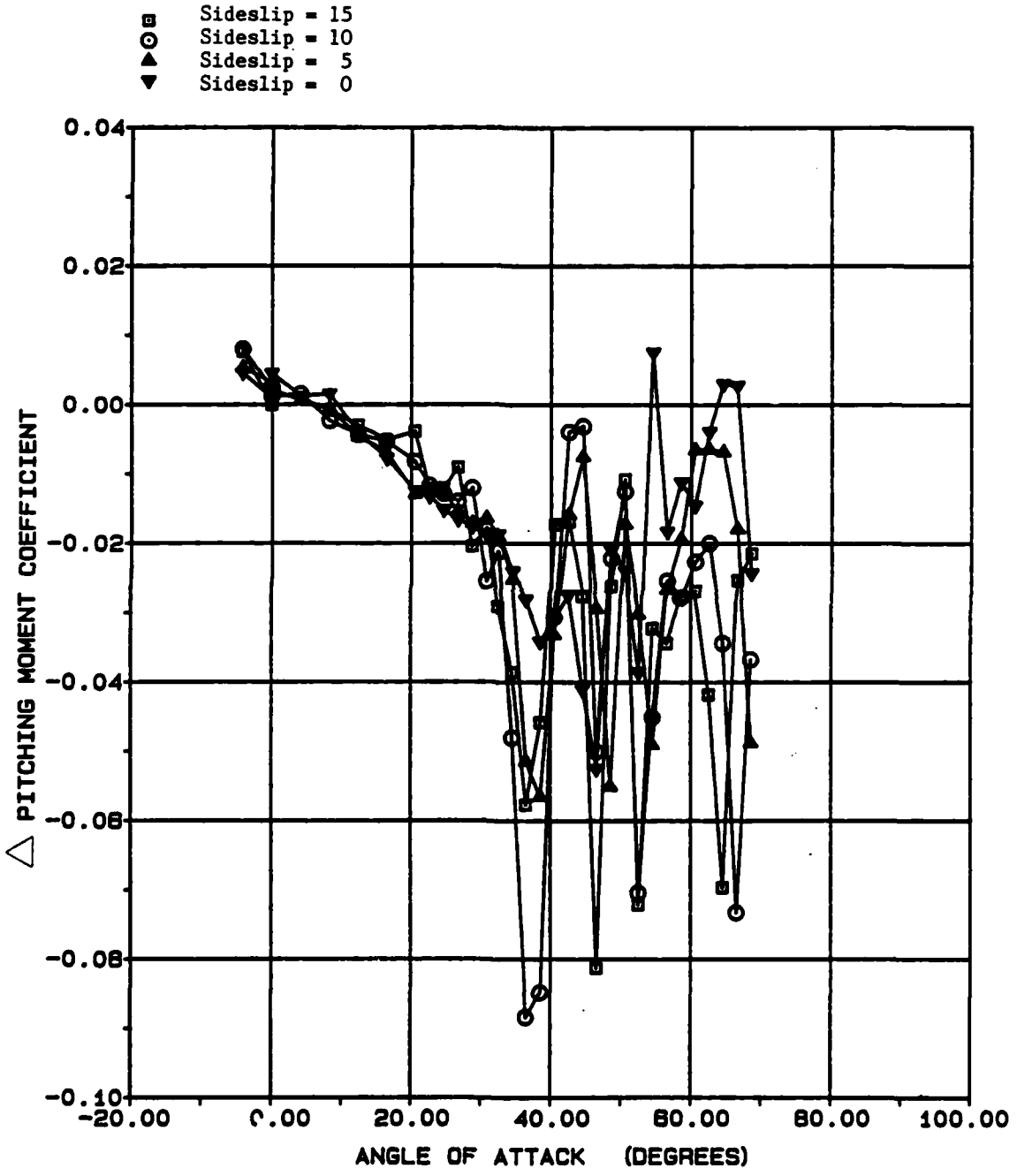

Figure 12. Concluded.

strake deflection is very complex, a 6 DOF simulation must be used to determine which strake deflection (positive or negative) will give the best overall performance.

Figure 13 shows the incremental rolling moment for the -45^{o} strake deflection and the $+30^{o}$ strake deflection at zero sideslip plotted against the incremental rolling moment of 10^{o} aileron deflection[5]. This plot shows that the strakes are virtually ineffective below 28^{o} AOA, while in this region the ailerons are the most effective. Above about 30^{o} AOA, the ailerons begin to lose their effectiveness, while in this same region, the strakes become effective.

These increments were also plotted as a function of sideslip. An example can be seen in Figures 14-15. Two points are emphasized by these plots. First, since the configuration is not symmetric, the coefficients are not symmetric about zero sideslip. Second, the variation of the incremental coefficients is not smooth throughout the high angle of attack region; a given incremental coefficient may even have a larger magnitude at a lower sideslip angle. This nonlinear behavior could be due to factors such as the vortex system from the nose and strake is changing character rapidly with changing sideslip. The current increment in sideslip of roughly 5^{o} is very coarse for this region, and a smaller increment might help explain this behavior.

The coefficients were also plotted across strake deflection, at constant angle of attack and sideslip. See Figure 16. The slope of the line is roughly equivalent to the control power derivative. Again, there is little if any change in the longitudinal derivatives due to the position of the strakes. The variation of the lateral-directional derivatives is not monotonic; the slope of the line often changed sign with increasing strake deflection. For instance, at an AOA = 38^{o}, deflecting the strake from 0^{o} to -15^{o} causes a reduction in rolling moment, while deflecting the strake from -15^{o} to -30^{o} causes an increase in rolling moment. The result of this behavior is that the hinged strakes can not be treated like conventional surfaces such as ailerons, whose forces and moments change smoothly and monotonically with deflection angle. For instance, deflecting an aileron twice as much as a given deflection typically produces twice as much rolling moment. However,

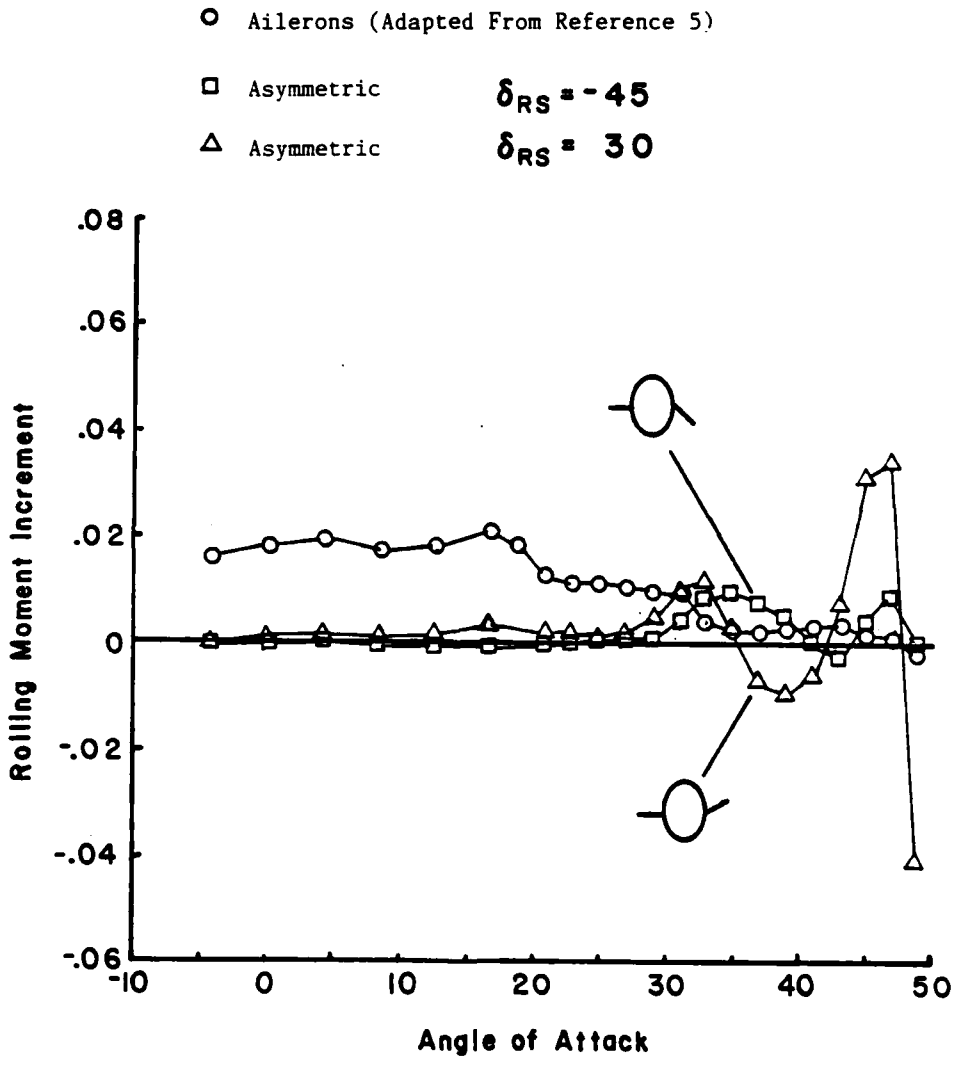

Figure 13. Comparison of Hinged Strakes to Ailerons.

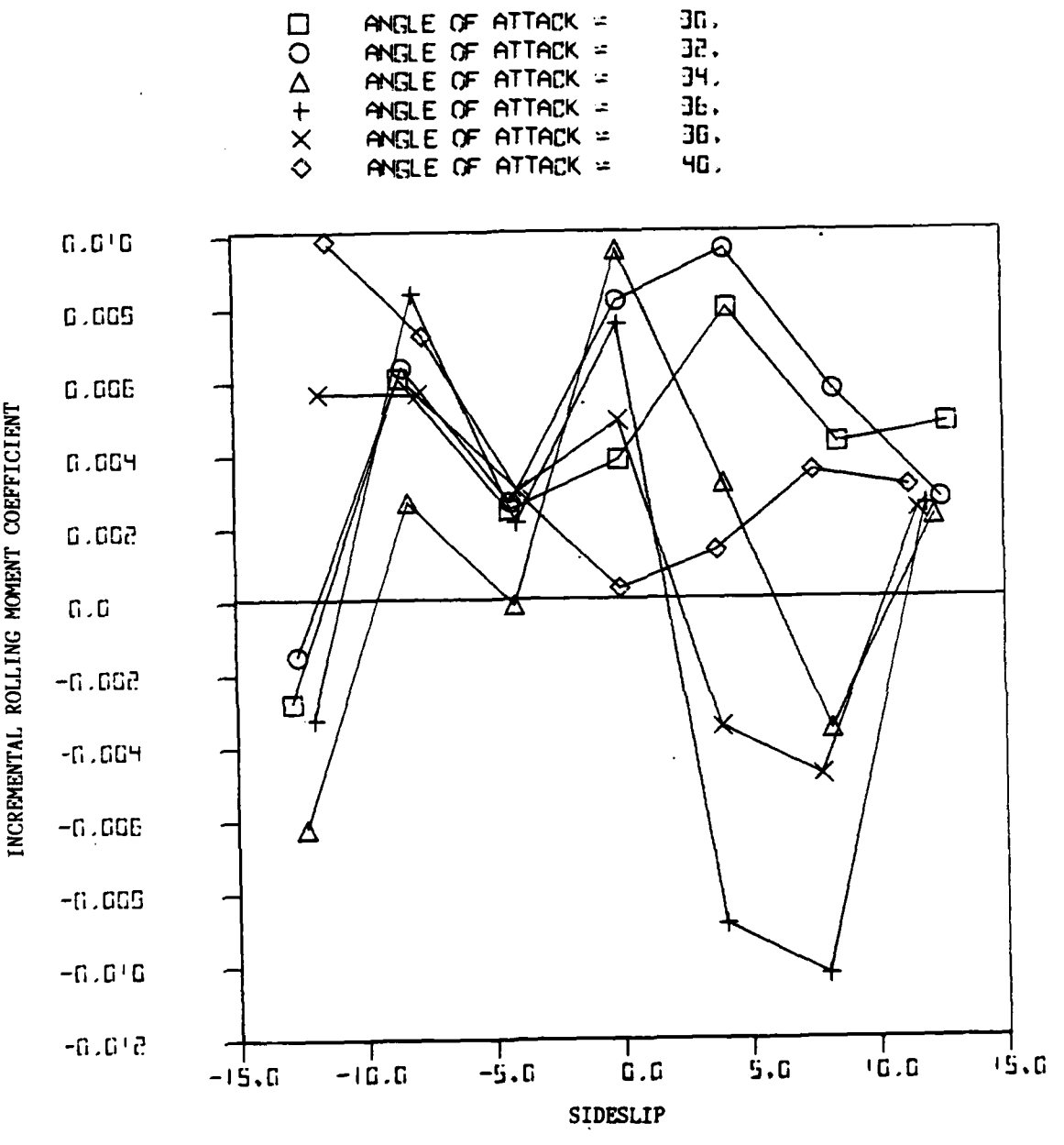

Figure 14. Incremental Aerodynamic Coefficients as a Function of Sideslip (Strake Deflection = -45).

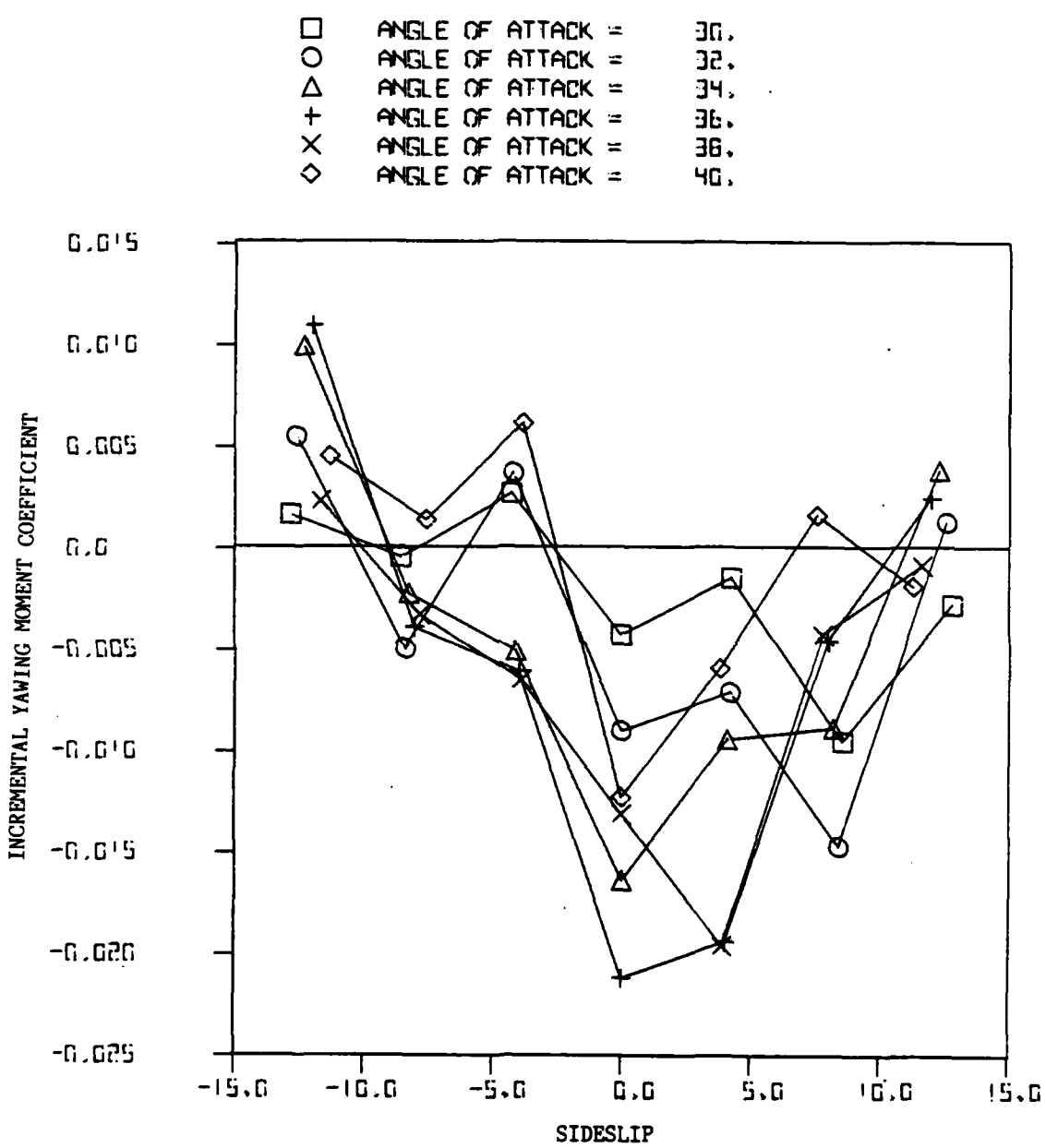

Figure 14. Continued.

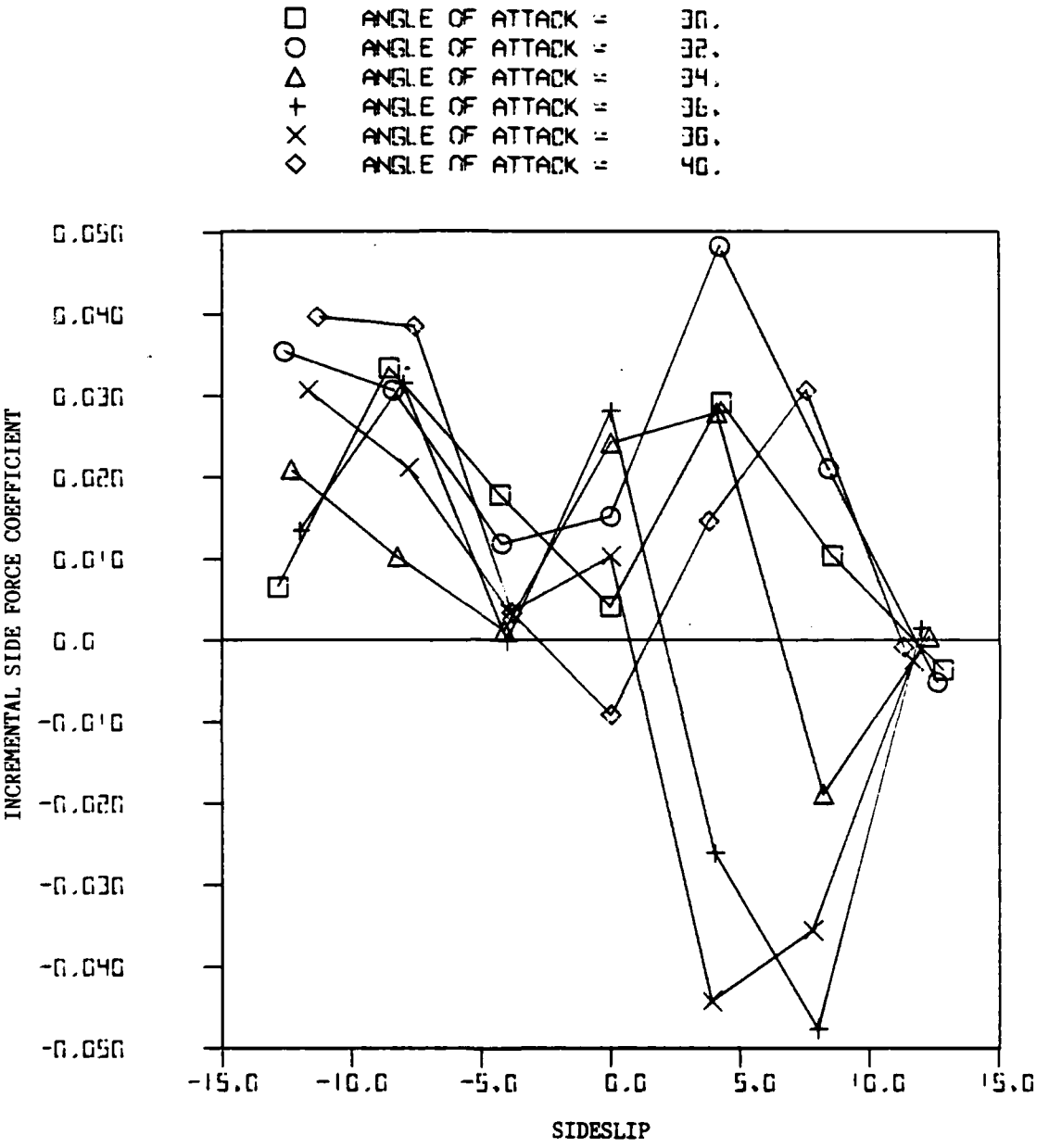

Figure 14. Concluded.

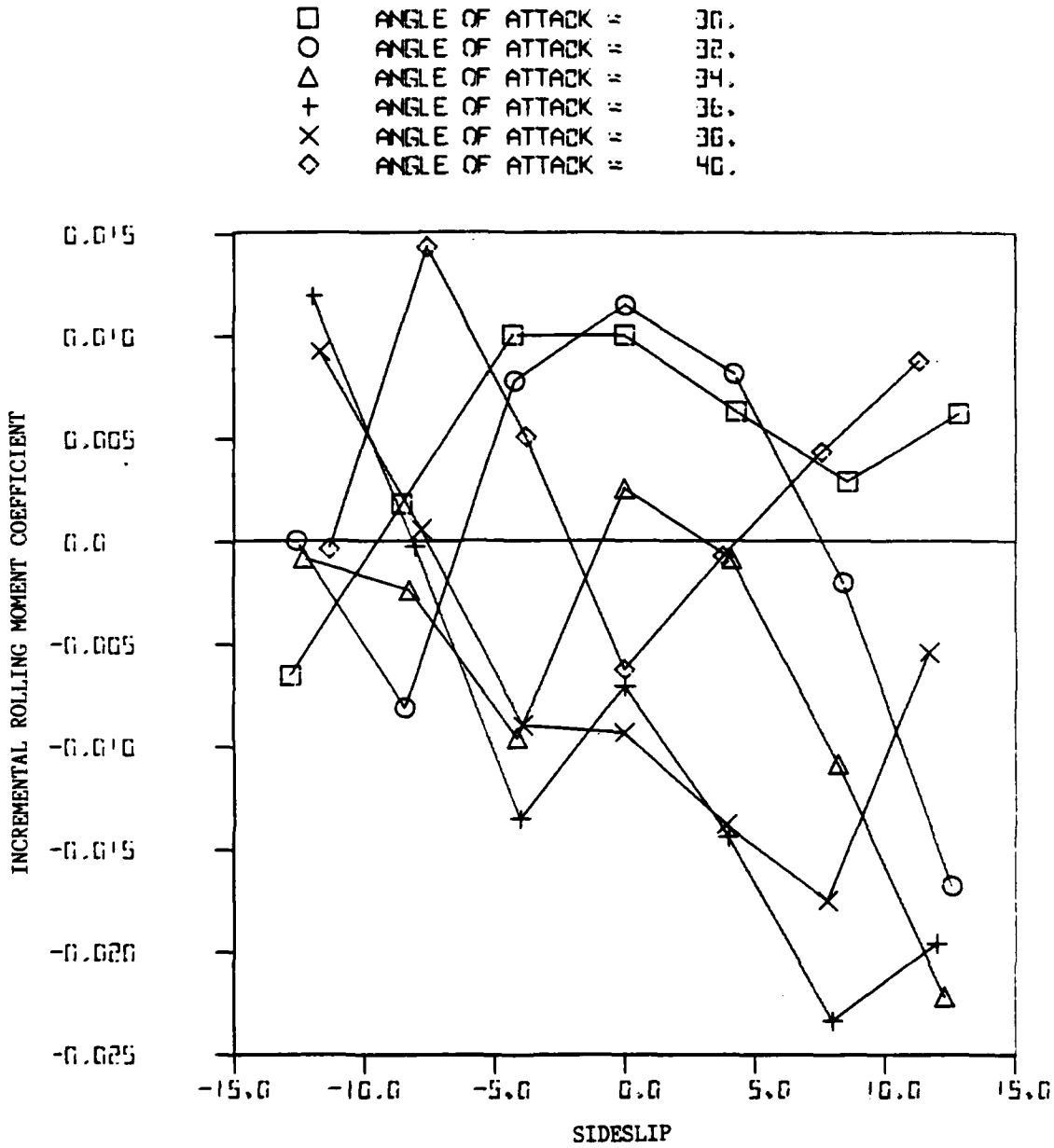

Figure 15. Incremental Aerodynamic Coefficients as a Function of Sideslip (Strake Deflection = +30).

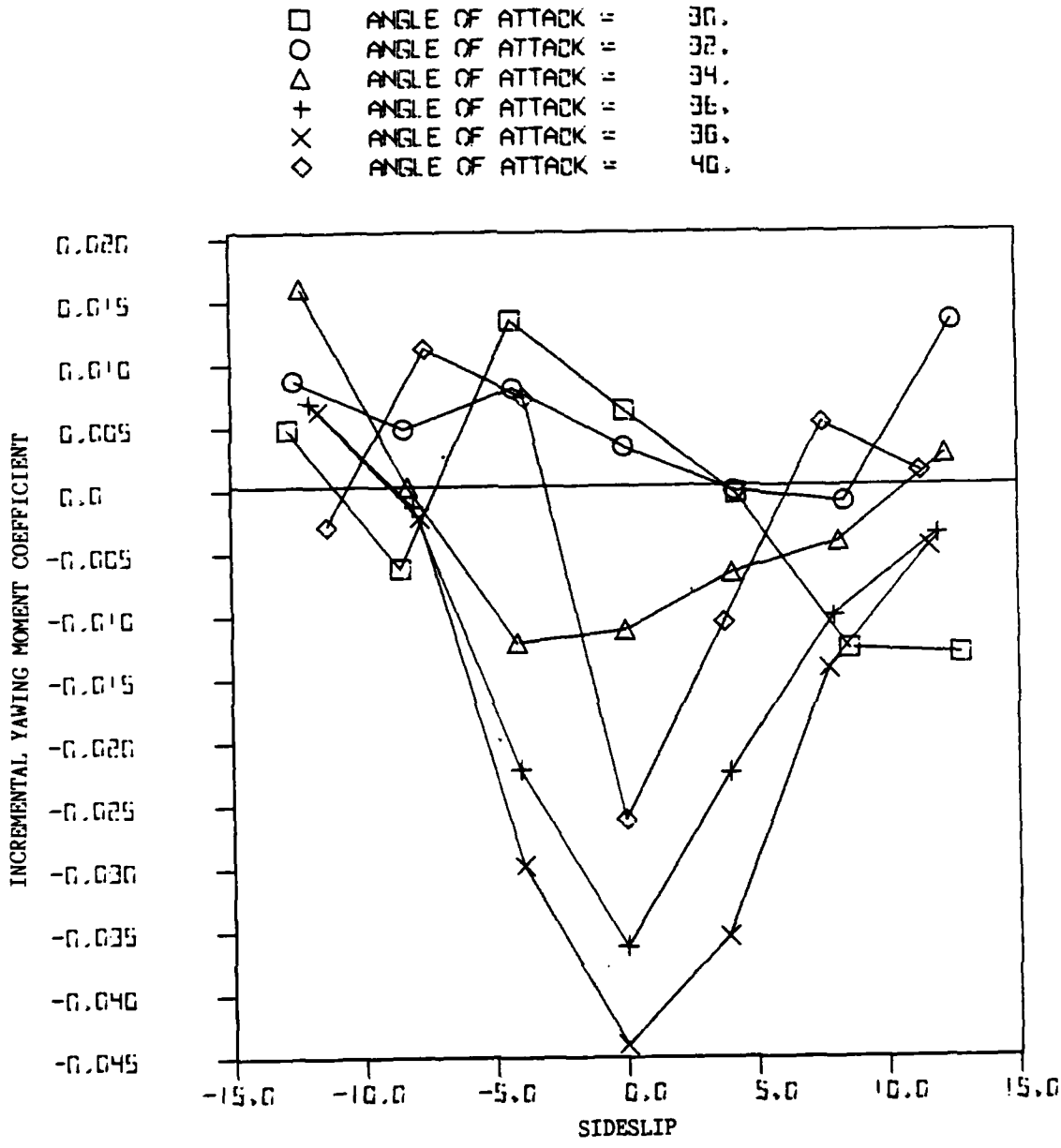

Figure 15. Continued.

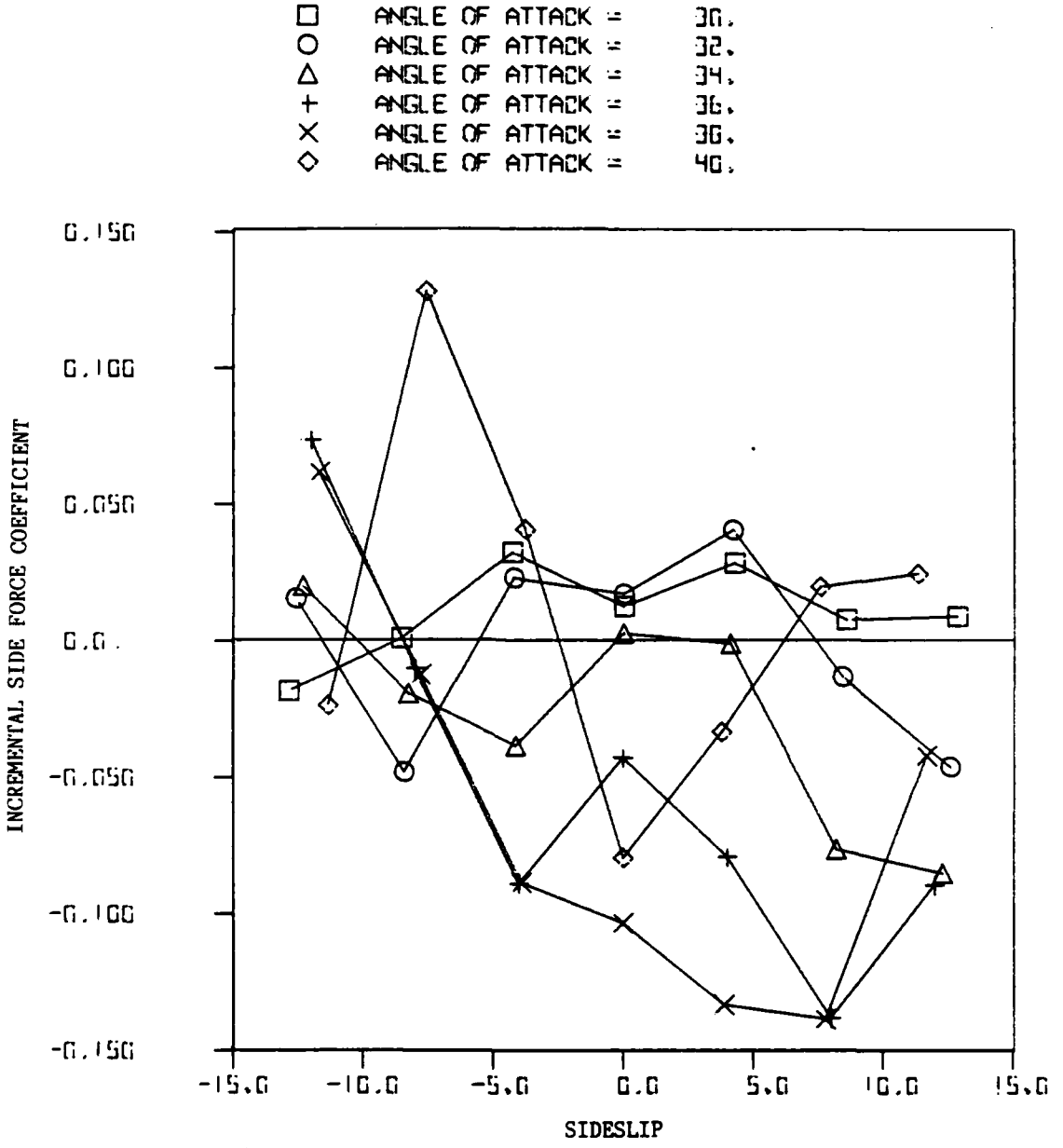

Figure 15. Concluded.

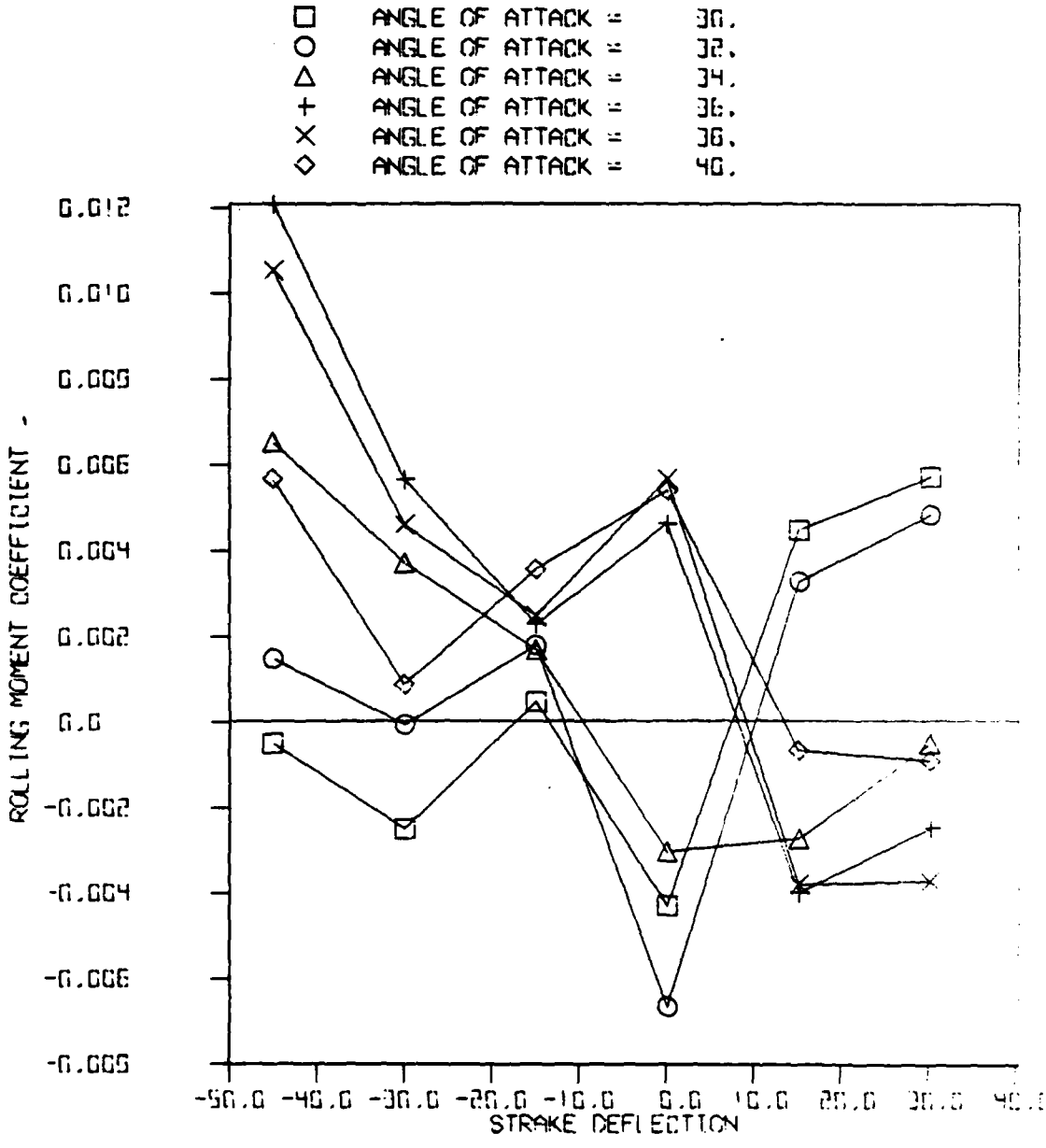

Figure 16. Aerodynamic Coefficients as a Function of Strake Deflection at Zero Sideslip.

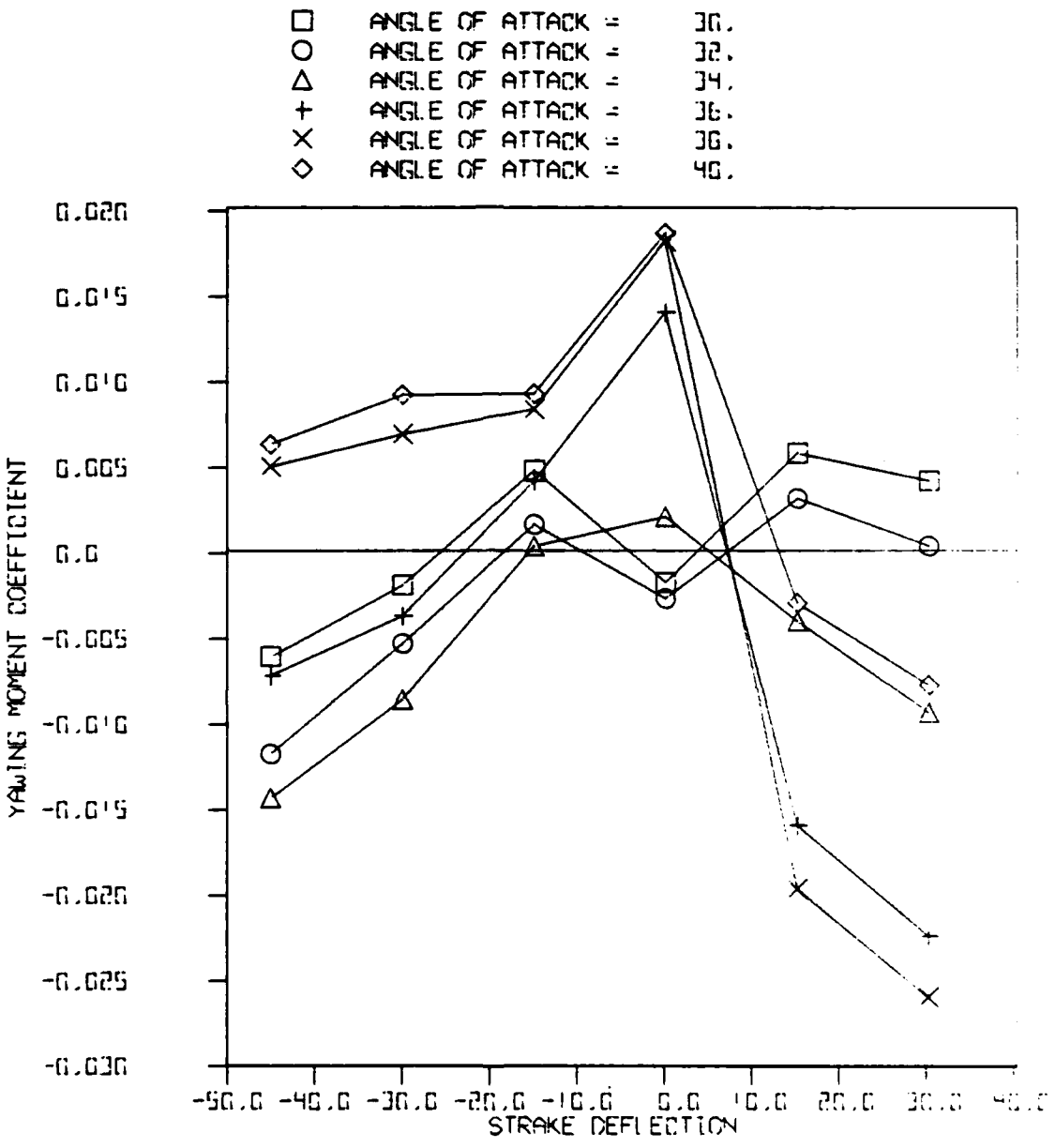

Figure 16. Continued.

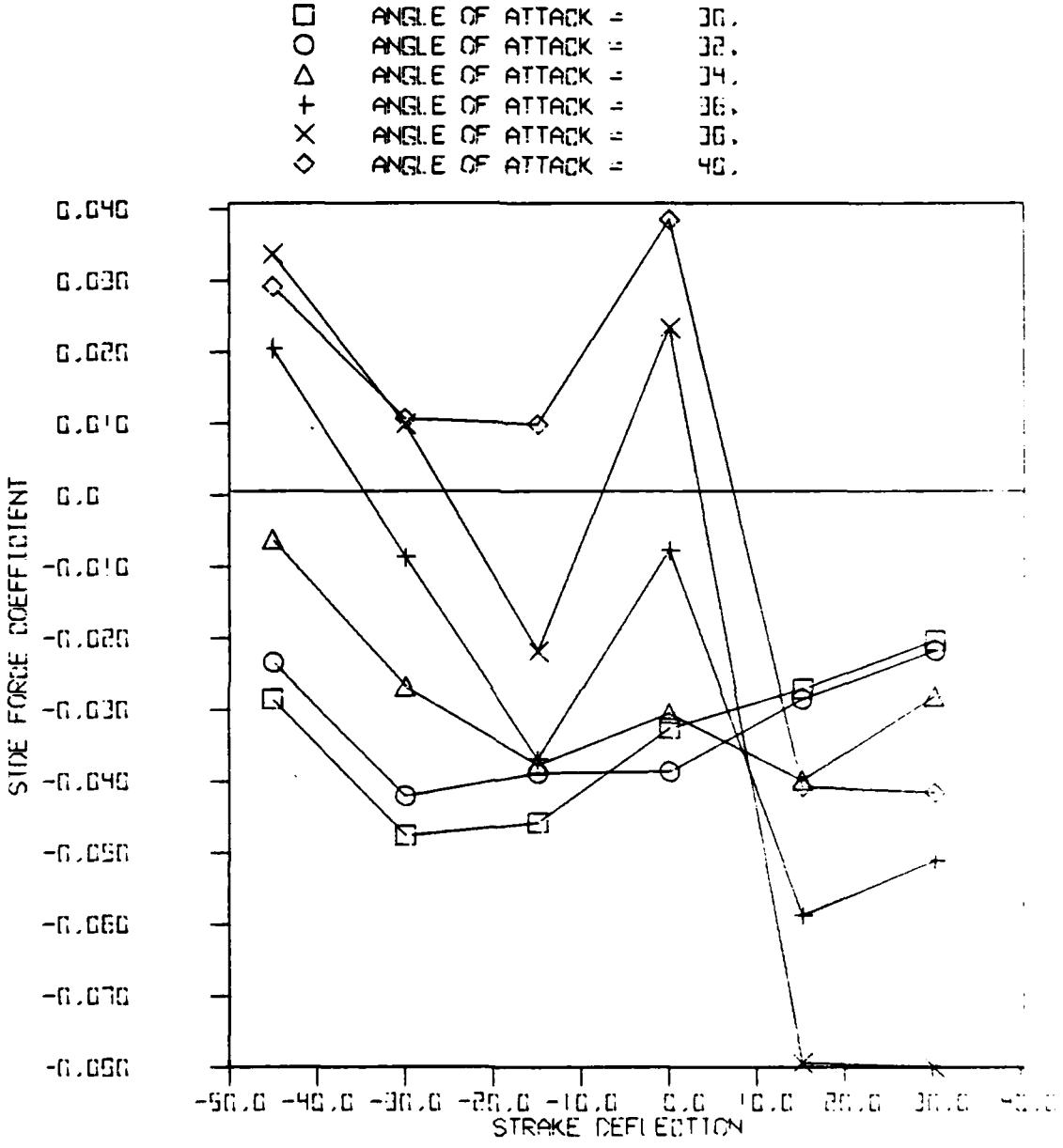

Figure 16. Continued.

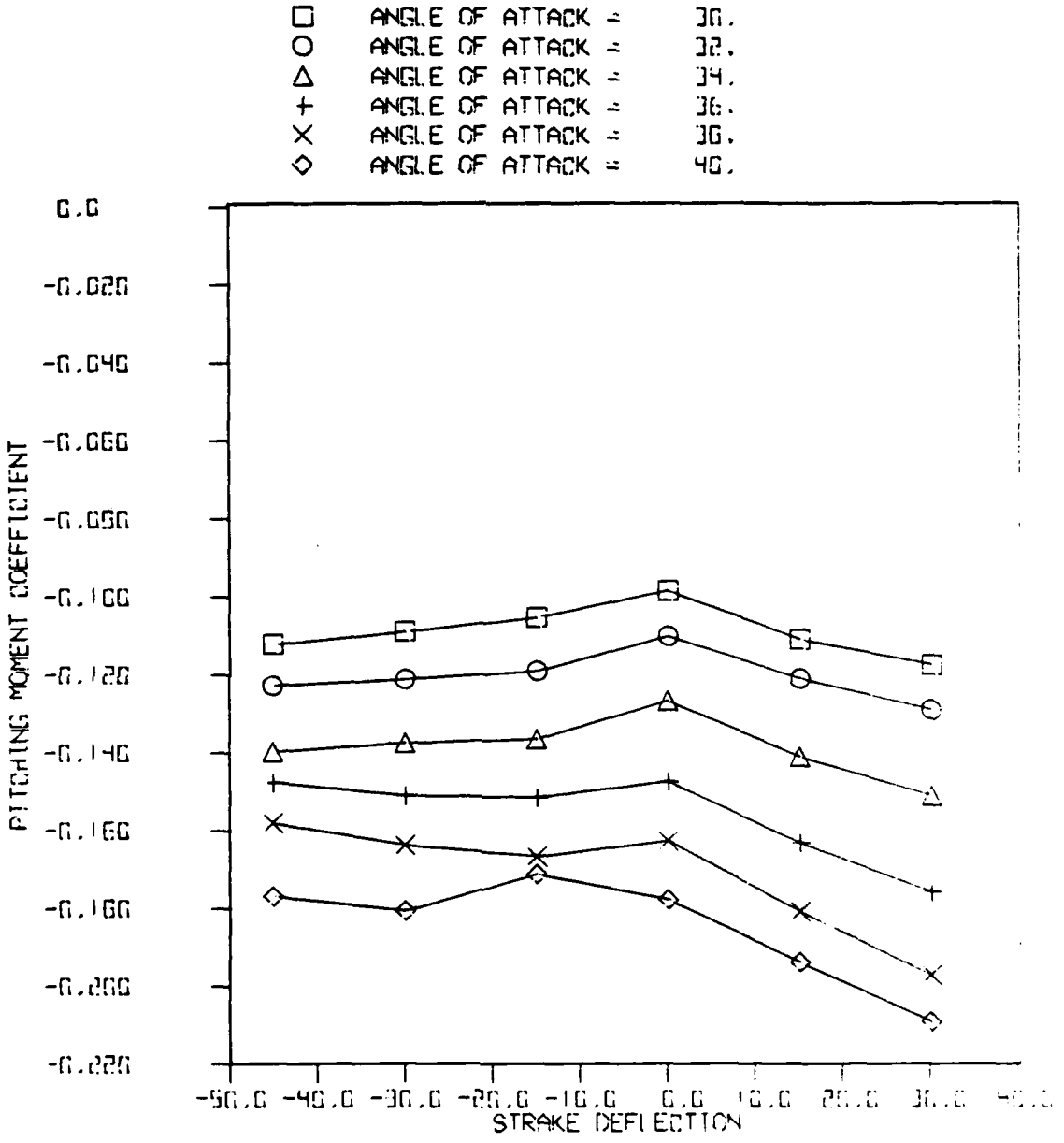

Figure 16. Continued.

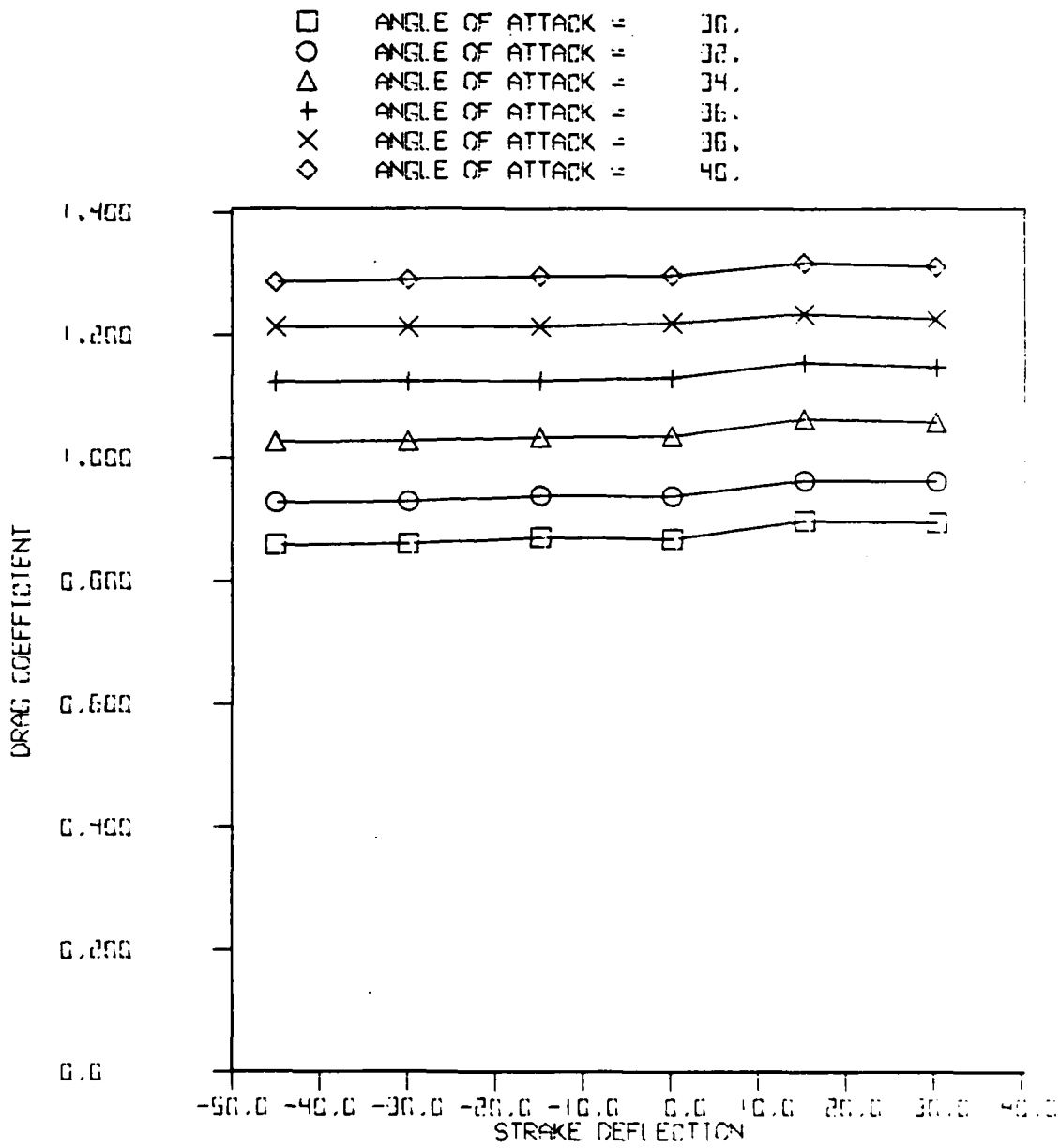

Figure 16. Continued.

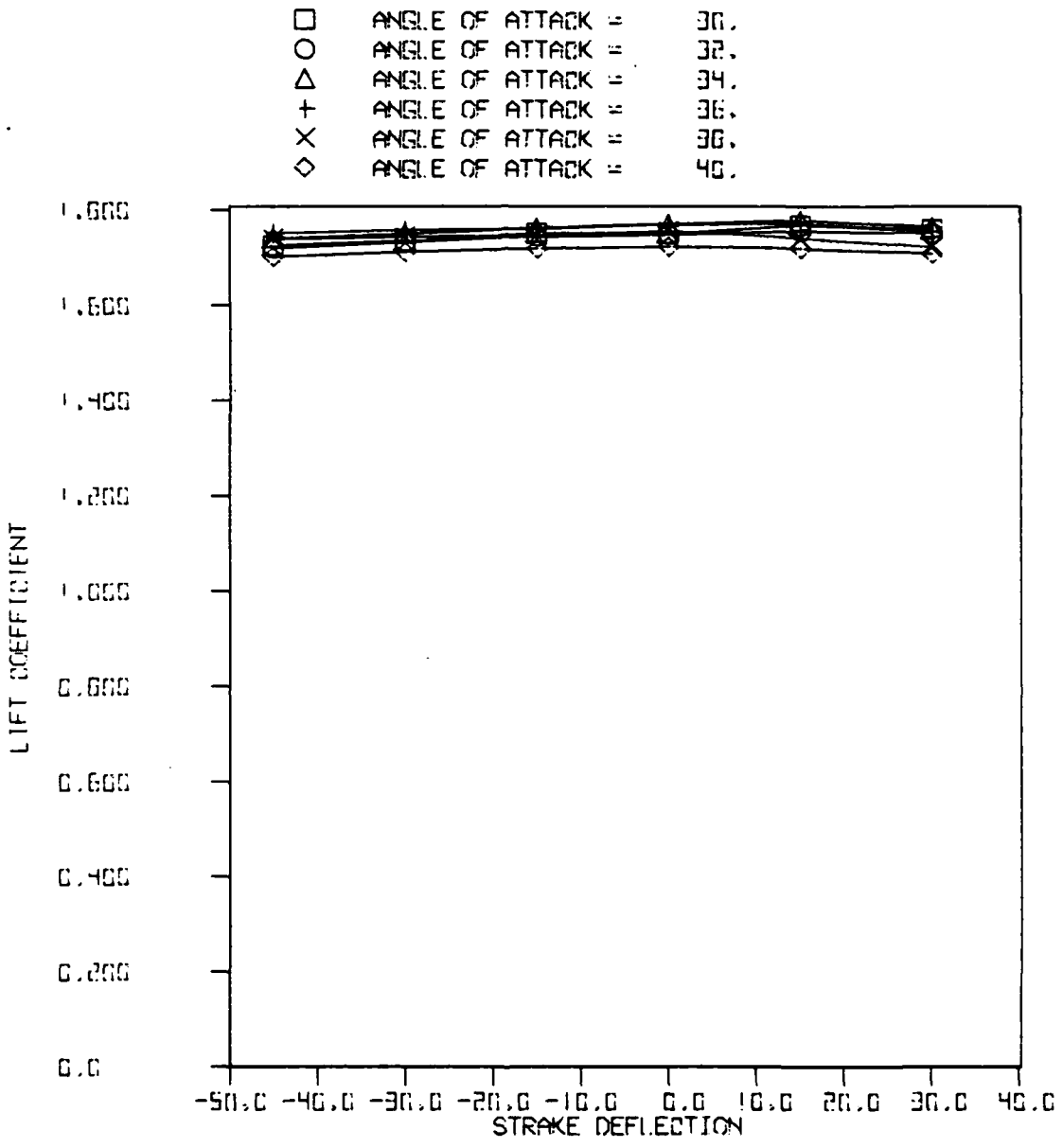

Figure 16. Concluded.

this is not the case with the hinged strakes. Therefore, the strakes were used by moving the approriate strake immediately to a given deflection any time that they are used. This would avoid having an unpredictable reaction caused by deflecting the strake a partial amount.

COMPARISON TO PUBLISHED DATA

To check for consistency with previous tests, the data obtained in this test were compared to that obtained by Rao and Huffman[4]. Both sets of data for incremental rolling and yawing moment are plotted in Figures 17-18. These data are at zero sideslip for -30^{o} and -45^{o} anhedral strake deflection. Note that the data are plotted in body axes.

Many similarities can be seen in the shape of the data between the two tests. Above 20^{o} AOA both cases show a large increase in incremental rolling moment, until about 30^{o} AOA. At this point, there is a sharp decrease in the incremental rolling moment continuing until 40^{o} AOA. This sudden break has been attributed to the bursting of the strake vortex. Both cases also show a higher incremental rolling moment for the -45^{o} case than the -30^{o} case.

The incremental yawing moments are likewise very similar. In the low AOA region up to about 20^{o} AOA each test shows both deflections to cause roughly the same magnitude of incremental yawing moment. At about 20^{o} AOA both tests show the incremental yawing moment decreasing and changing sign until about 30^{o}, where the incremental yawing moment is roughly constant until about 40^{o}. In both cases, the break in the incremental yawing moment corresponds to the same AOA as the break in the incremental rolling moment.

Figures 19-20 compare the data for the two tests with 5^{o} sideslip. Again, many similarities between the data can be seen. The incremental rolling moment for both tests in this case continues to show the same basic shape, rising around 20^{o} angle of attack, reaching a maximum around 30^{o} to 34^{o}, and dropping back down by 40^{o}. The overall magnitude of both incremental rolling moments has also decreased as a result of the introduction of sideslip. The incremental yawing moment curves also show the same basic shape as before. Reference 4 is not clear in stating if the yawing moment contribution of the baseline model was subtracted from the data for the deflected strakes. If it were not, this ommission could account for the negative magnitudes at low AOA where the fighter data of this test shows a positive magnitude.

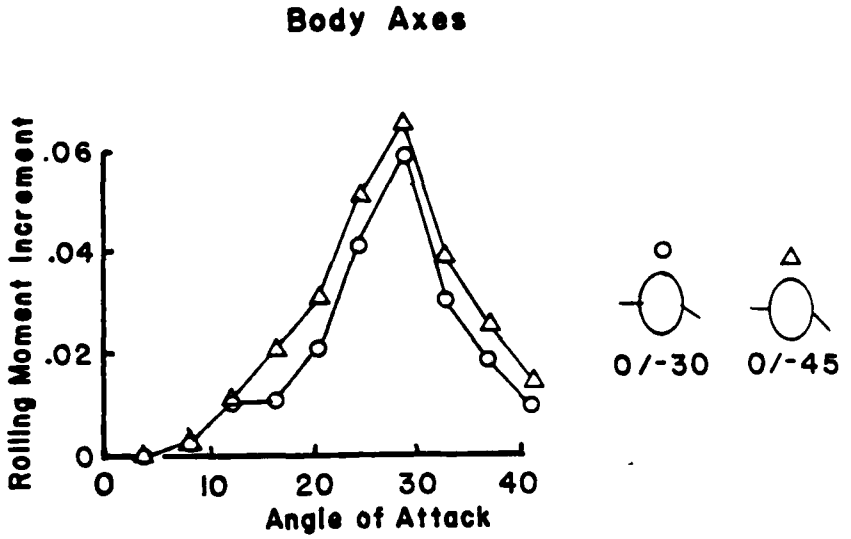

(Adapted From Reference 4)

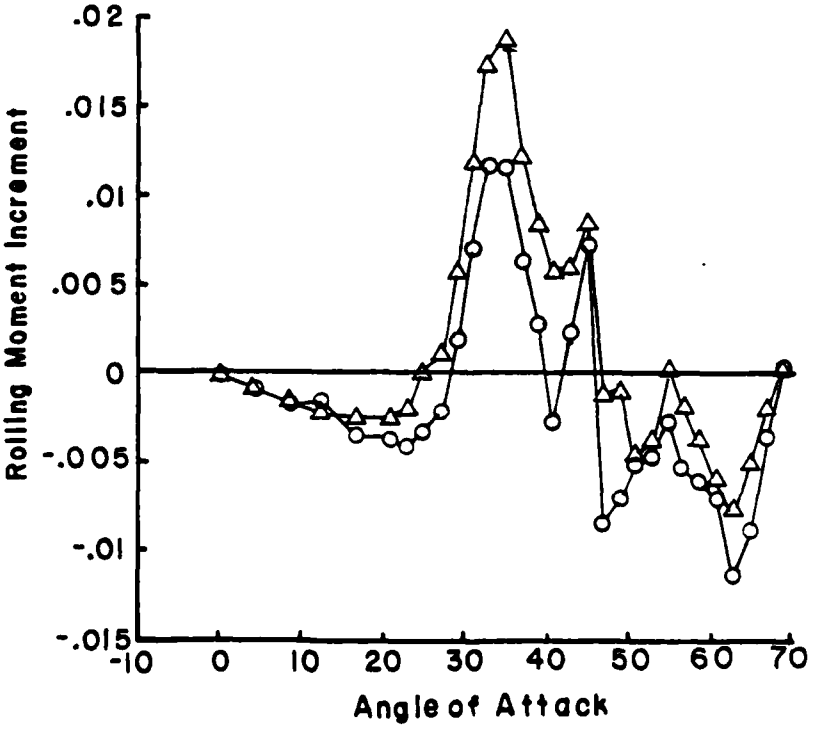

Figure 17. Comparison of Rolling Moment Due to Hinged Strakes at Zero Sideslip With Published Data.

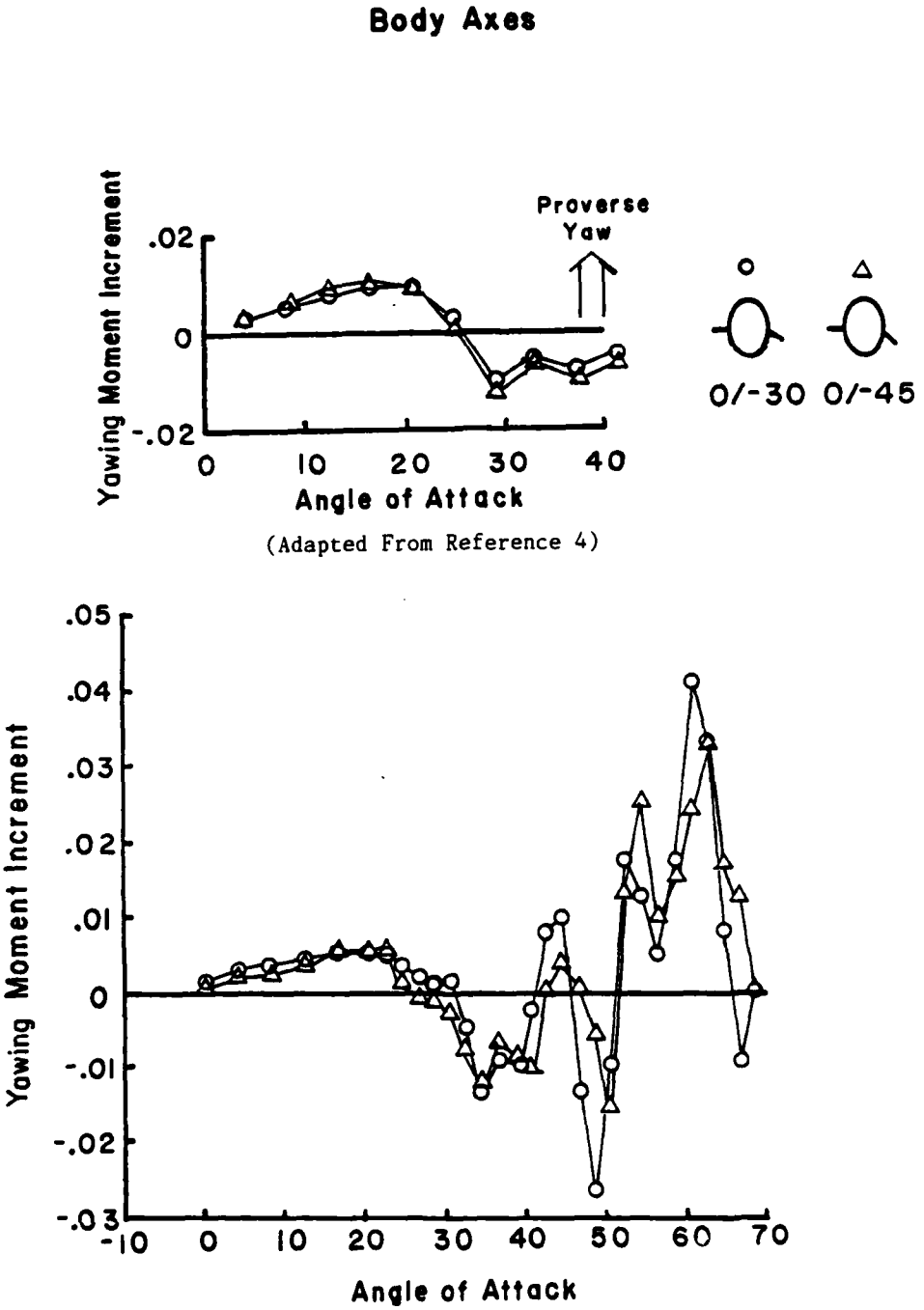

Figure 18. Comparison of Yawing Moment Due to Hinged Strakes at Zero Sideslip With Published Data.

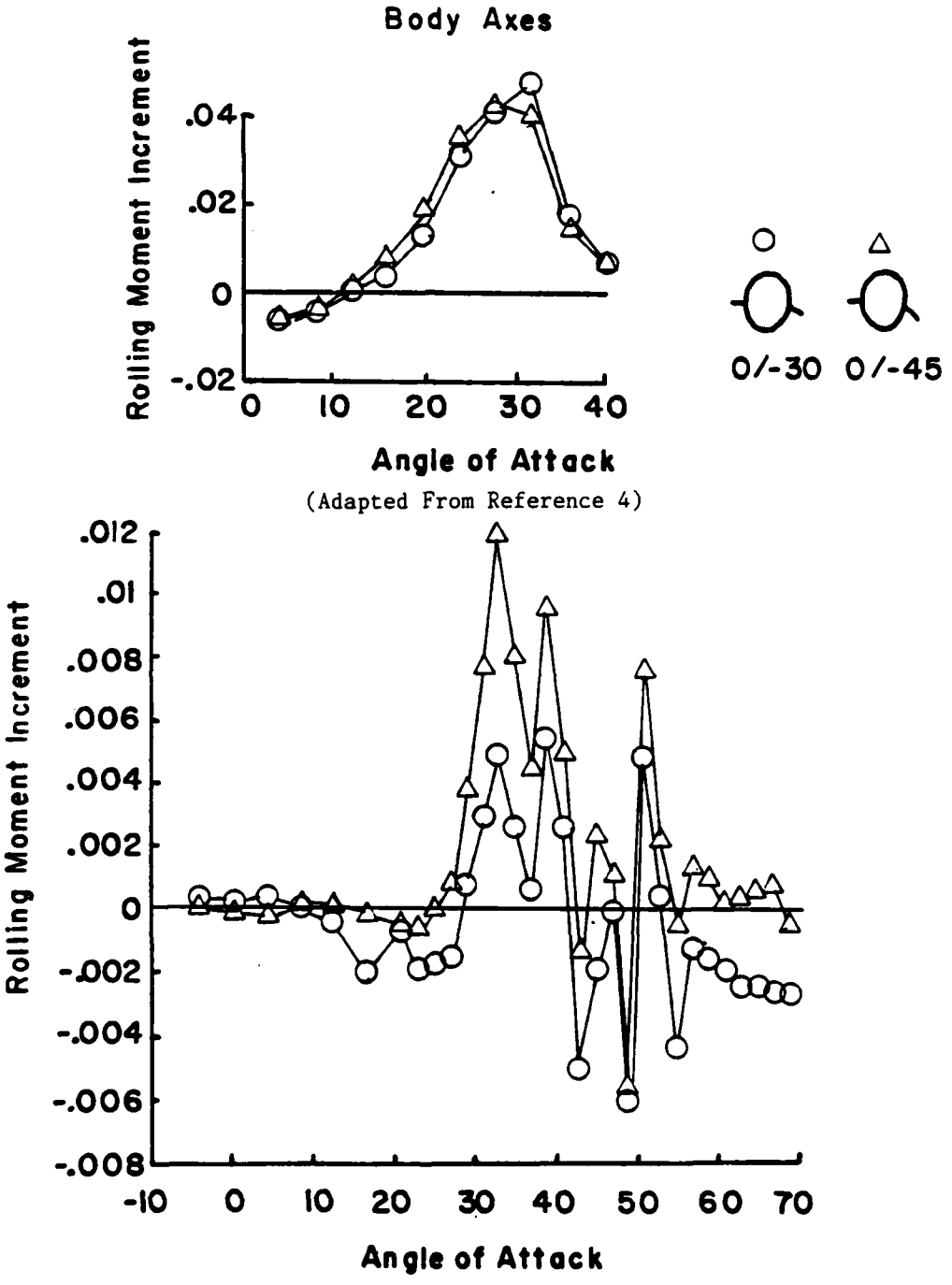

Figure 19. Comparison of Rolling Moment Due to Hinged Strakes at 5° Sideslip With Published Data.

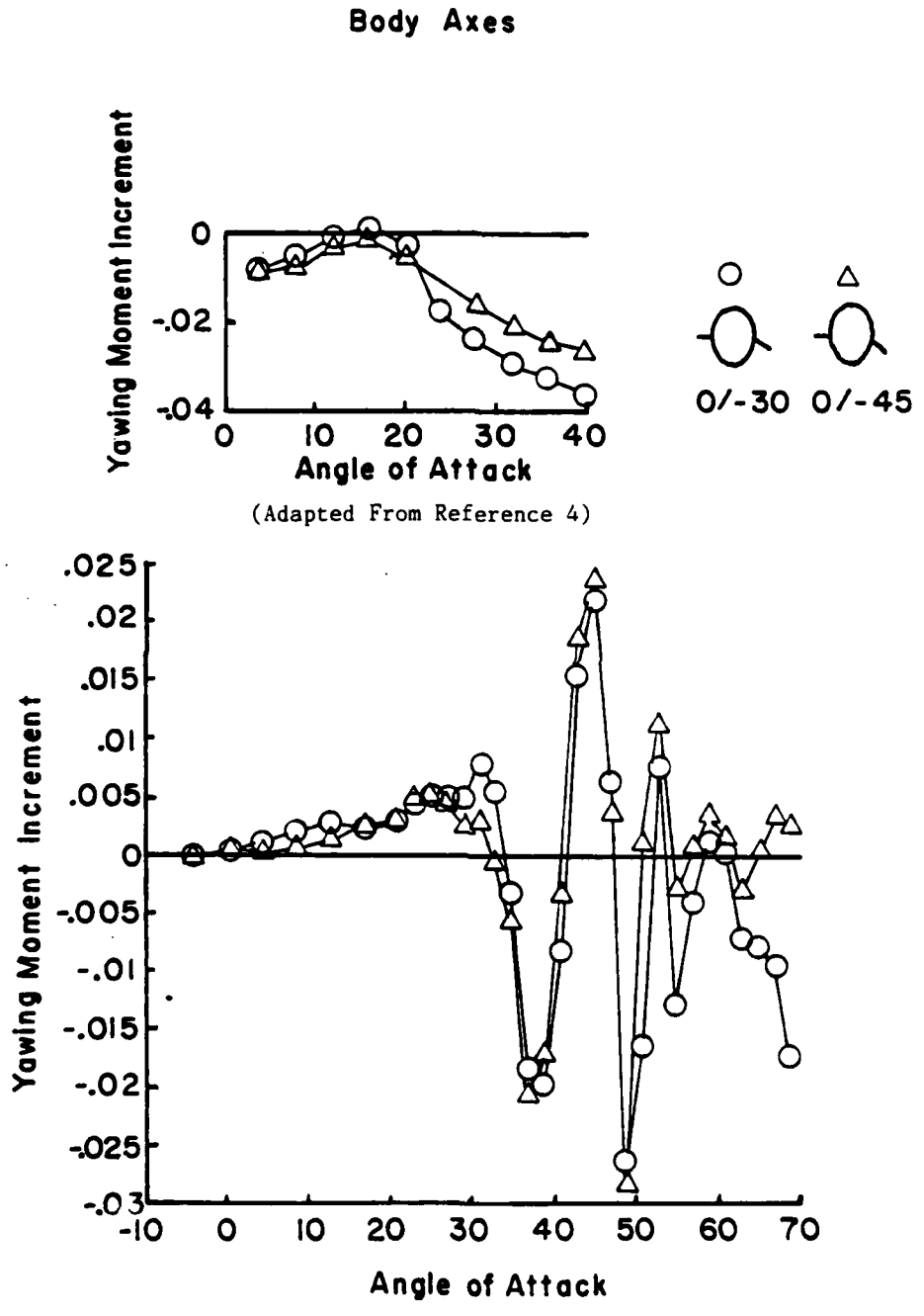

Figure 20. Comparison of Yawing Moment Due to Hinged Strakes at 5° Sideslip With Published Data.

While the behavior of the data in both tests is similar, there is a significant difference in their magnitudes. The most obvious difference between the generic model of Reference 4 and the high performance fighter of this test is the difference in strake area in terms of percentage of wing area. Both models are shown in Figure 21 with equal wing span. The generic model has a 44° leading edge sweep, compared to a 45° sweep on the high performance fighter model. Both wings can be considered roughly the same for purposes of this comparison. The exposed area of the strakes of the generic model equals 26.6% of the wing area, while the area of the strakes of the fighter is only 3.6% of the wing area. If the magnitude of the incremental moments was strictly a function of the area ratio between the strake and the wing, then the ratio of the magnitudes of the incremental moments would be 3.6/26.6 = rolling moment is .29, and the ratio of the magnitudes of the maximum incremental yawing moment is 0.5. Comparing the maximum incremental rolling moment for the case with sideslip, the ratio of the magnitudes is still .29, indicating that the effects of sideslip are similar in both cases. In addition, the generic model shows that with and without sideslip, $\delta_s = -45^o$ and $\delta_s = -30^o$ produce about the same rolling moment both with and without sideslip. The fighter model shows the -45^o case to produce roughly twice the rolling moment as the -30^o case both with and without sideslip. Likewise, both models show each case to produce equal amounts of yawing moment regardless of sideslip. Apparently, the effects of sideslip are similar.

Since the ratio of incremental rolling moment is greater than the ratio of strake/wing area, the source of the rolling moment is not only due to the reduction of the projected area of the strake, but that a major portion arises from the decrease of circulation velocities in the vortex. If strake area were the only factor, then the ratio of the magnitudes of the incremental rolling moments of the two tests would have been equal to .16, the ratio of the strake areas. However, the rolling moment due to deflecting the smaller strakes is greater than would be predicted by such an analysis. Since the strength of the vortex is not only dependent on the are of the strake, this result would

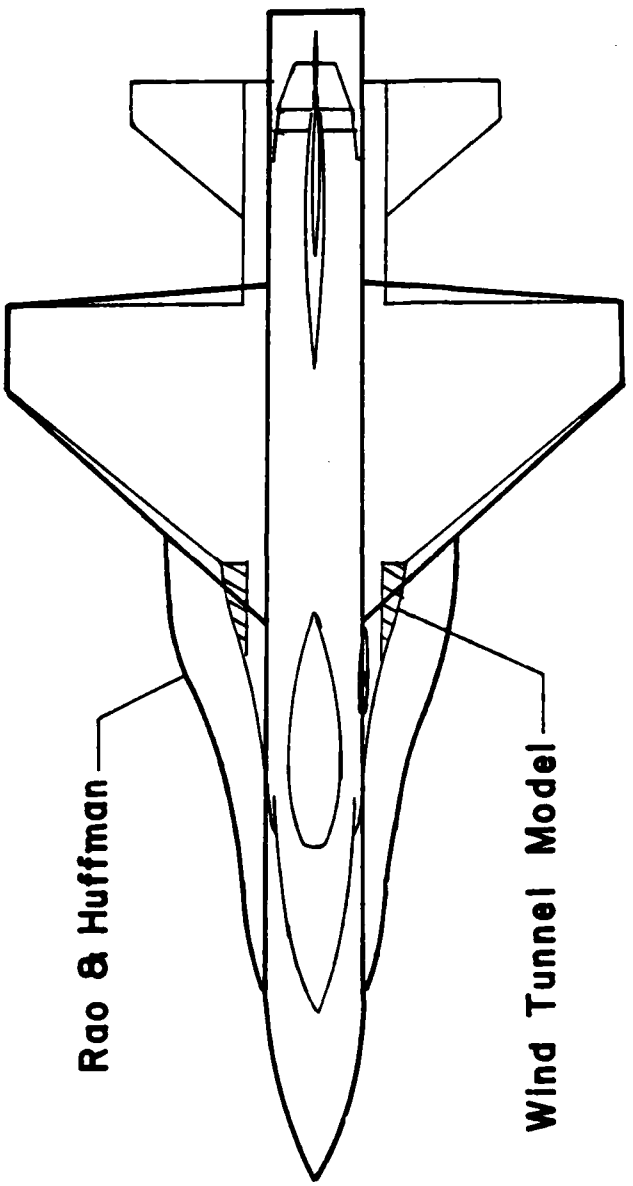

Figure 21. Comparison of Wind Tunnel Model To Model Used by Rao & Huffman.

indicate that the weakening of the vortex one of the causes of the rolling moment.

Since the yawing moment coefficient of the smaller strake is closer to the yawing moment coefficient of the large strake than the rolling moment coefficient of the small strake is to that of the large strake, it seems that the incremental rolling moment coefficient is more sensitive to the size of the hinged strake. Although insufficient data are available to reach a conclusion at this point, it is possible that larger strakes would create a change in available rolling moment without as large a change in yawing moment.

In spite of these differences, a consistency in basic trends can be seen between the data of this test and thet data shown by Rao and Huffman[4]. Rao and Huffman had recommended that the hinged strake concept be tested on more realistic configurations, and this test shows that many of their basic concepts are still valid even with a different configuration.

SIMULATION ANALYSIS

Since an aircraft flying at high AOA has highly coupled behavior between the longitudinal and lateral-directional modes, it is difficult to obtain any sense of the response to control inputs just by examining the static aerodynamic data. Therefore, the bulk of the analysis in this study was done using a six DOF computer simulation model.

The mathematical model used was a modification of the model developed by Stout[5] at Texas A&M. This model was set up to run using the EASY4 Dynamic Analysis Program[9] on a CDC Cyber 825. This program simulates the behavior of the aircraft using a state variable approach, integrating the states of the aircraft while stepping through time. Through the use of tabular input data, the program can simulate the nonlinear behavior of the aircraft at these high AOAs. Since dynamic derivatives for the strakes were not available, only the static data for the strakes are considered in the analysis.

The original simulation had a trim routine which calculated the states for the Flight Control System (FCS) for 1 g, straight and level flight. This routine not only calculated the airspeed for 1 g flight at the given angle of attack, but also calculated the states at the given operating point such that none of the states would have an initial transient. At the angles of attack investigated, this trim approach yielded a dynamic pressure of about 25 psf and possibly led to unrealistically low roll rates in the previous study. If the dynamic pressure were increased, it was postualated that these roll rates could be increased. Since the angle of attack was fixed, increased dynamic pressure would yield a higher load factor. With this in mind, the trim routine was rewritten to allow commanded normal acceleration to be input through the pitch stick channel. For conditions other than level flight, this results in a steady pullup. An initial roll angle is allowed, but the iritial roll and yaw rates must be zero. This steady pullup more accurately modeled conditions under which high angle of attack flight would be encountered.

Several points should be noted about the relationship between the commanded g and the resulting normal acceleration at the CG. First, the

stick commands incremental g's in the body normal direction. Since the aircraft is at an angle of attack, the body load factor is related to the stability axes load factor by

$$n = n_{SA}\cos\alpha$$

Thus, for straight and level flight, a normal acceleration of $\cos\alpha$ must be commanded, or since the stick commands incremental g's, for level flight a load factor of $\cos\alpha - 1$ must be commanded. At high angles of attack, the angle of attack limiter reduces the amount of load factor commanded such that the resulting load factor is less than that commanded. As a result, in order to command a desired load factor, the stick input must be calculated by the following equations:

For $\alpha < 29.9^{o}$:

$$n_{com} = n_{desired}\cos\alpha - 1$$

For $\alpha > 29.9^{o}$:

$$n_{com} = n_{desired}\cos\alpha + 0.322(\alpha - 29.9) - 1$$

Note that if $n_{com} > 8.0$, the AOA limiter will not allow the aircraft to trim at the desired load factor.

The nonlinear data for the simulation was obtained from several sources. A majority of the aerodynamic data was obtained from the open literature.[10] These data gave various coefficients of the aircraft as functions of angle of attack and mach number. Additional nonlinear lateral-directional data for the baseline aircraft as functions of angle of attack and sideslip were obtained from the wind tunnel test. Due to slight asymmetries in the model, the baseline data for C_{ℓ}, C_n, and C_Y did not equal zero at zero sideslip. These data were mathematically shifted to pass through zero to eliminate effects on the simulation at zero sideslip. Since all of the analysis is calculated in body axes, all of these data were entered into the model in this format.

The data for the effects of the strakes were entered into the model as the increments in the coefficients between the run with the strake deflected and the baseline run. As seen earlier, deflecting strakes of

this size had virtually no effect on the longitudinal characteristics of the aircraft, so no longitudinal data from the strakes were included in the analysis. The data from the strakes for C_ℓ, C_n, and C_Y were entered as tabular functions of angle of attack and sideslip for each measured strake deflection from -45^o to $+30^o$. These data were entered in stability axes to prevent confusion between these data and the data analyzed earlier. In order to calculate the effect of the strake, its effect was calculated as a function of AOA and sideslip in the tables for both the strake deflection above and below the current deflection. These two values were then interpolated based on the current strake deflection. The resulting coefficients were then converted to body axes before being used in the analysis. As a result of this scheme, the effects of the strakes could be modeled as functions of angle of attack, sideslip, and strake deflection as shown in the previous analysis of the aerodynamic data. The strake data tables ranged in AOA from 26^o to 42^o and in sideslip from -15^o to 15^o. For points outside this data range, the values of the coefficients are treated as constant from the last data point. For instance, at an AOA of 34^o and a sideslip of 20^o, the value of the coefficient at an AOA of 34^o and a sideslip of 15^o was used.

Due to the nonlinear aerodynamics of the hinged strakes, the strakes could not simply be connected to the roll channel. Since the aerodynamic moments were not monotonic with strake deflection, a "bang-bang" control system was installed. When a roll command is received, the appropriate strake is deflected to full deflection until the desired roll rate is achieved, then the strake returns to the undeflected position. The actuators are modeled with a transfer function of

$$\frac{10}{s + 10}$$

with a rate limit of 120 degrees/second. This rate limit was based on the rudder's rate limit of 120 degrees/second, and should be reasonable since the strake is a smaller surface. The initial implementation of the Hinged Strake Flight Control System is shown in Figure 22. Only one strake is commanded to be deflected at any given time, since the

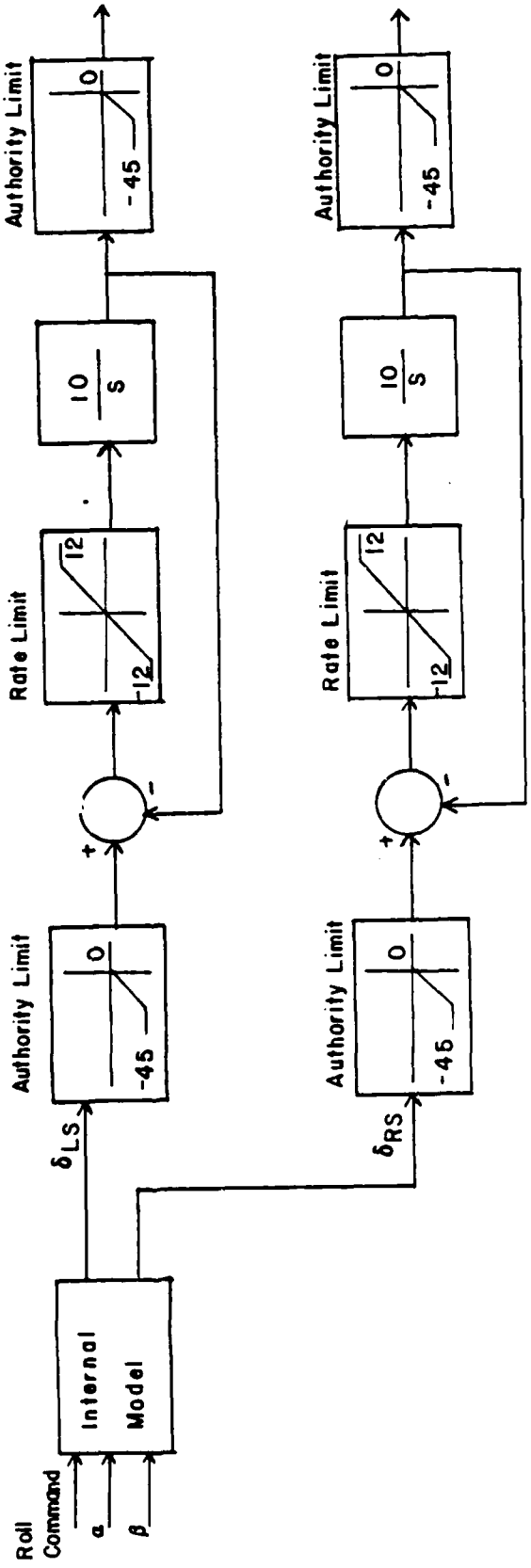

Figure 22. Initial Implementation of Hinged Strake Flight Control System.

AD-A158 005 USE OF HINGED STRAKES FOR LATERAL CONTROL AT HIGH ANGLES OF ATTACK(U) AIR FORCE INST OF TECH WRIGHT-PATTERSON AFB OH R E ERB MAY 85 2/2

UNCLASSIFIED AFIT/CI/NR-85-61T F/G 20/4 NL

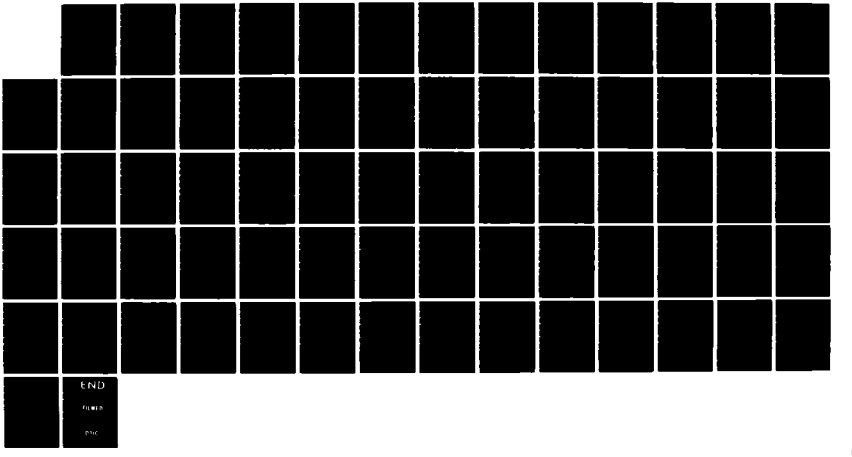

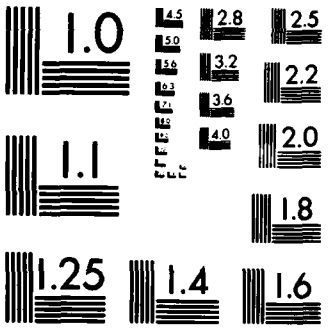

MICROCOPY RESOLUTION TEST CHART
NATIONAL BUREAU OF STANDARDS-1963-A

Anhedral-Dihedral case showed no noticeable change from the Asymmetric case.

The block labeled Internal Model in Figure 22 defines logic for choosing the appropriate strake to deflect. Several factors are considered to produce the command signals to the strake actuators. Since the strakes have virtually no effect below 28°, the strakes return to the undeflected position anytime the angle of attack falls below 28°. Another major consideration is a "unidirectional" region. This region is an area where deflecting either strake produces a rolling moment in the same direction.

Since the asymmetric strake deflections tested only considered deflecting the right strake, symmetry was assumed to calculate the effect of deflecting the left strake. The coefficients due to the left strake are calculated by the equation

$$C_{\ell}{}_{left}(\alpha,\beta) = -C_{\ell}{}_{right}(\alpha,-\beta)$$

See Figure 23. The other force and moment coefficients are calculated in a similar fashion.

The unidirectional region arises from a condition shown in Figure 24. At an angle of attack of 30° and a sideslip of 12.5°, a right strake deflection produces a right rolling moment. In order to find the rolling moment for a left strake deflection, first find the rolling moment for a right strake deflection at an angle of attack of 30° and a sideslip of -12.5°. In this case, the right strake deflection produces a left rolling moment. After converting to the corresponding left strake deflection at an angle of attack of 30° and a sideslip of -12.5°, the left strake deflection produces a right rolling moment. Therefore, at this angle of attack and sideslip both right and left strake deflections produce a right rolling moment. This angle of attack and sideslip is in a unidirectional region. These regions can be identified on the plots of incremental rolling moment versus sideslip, as shown in Figure 25. If two points on the incremental rolling moment plot for a given

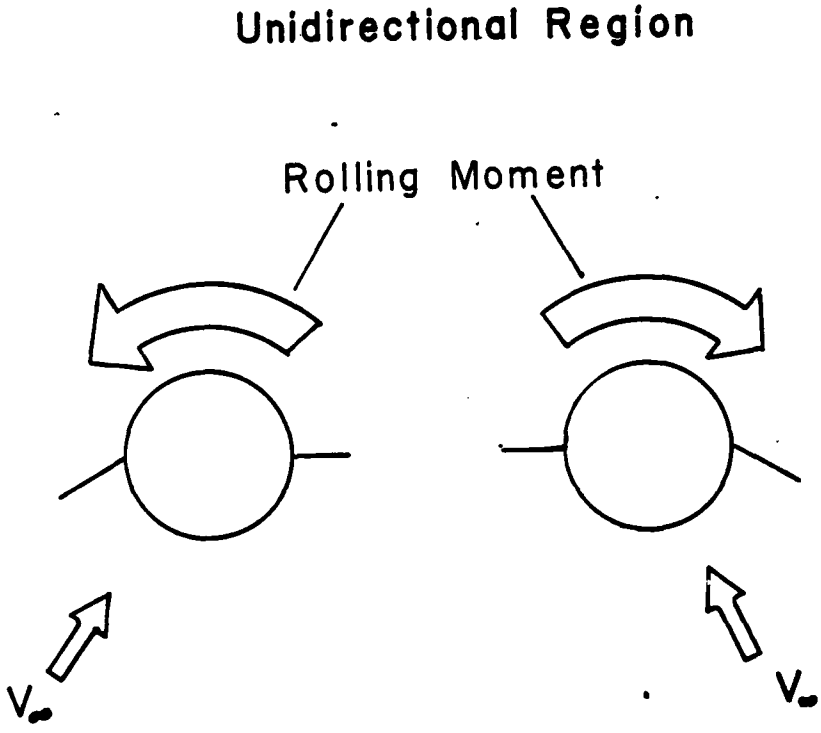

$$C_{\ell_{left}}(\alpha,\beta) = -C_{\ell_{right}}(\alpha,-\beta)$$

Figure 23. Calculation of Coefficients For Left Strake Deflection.

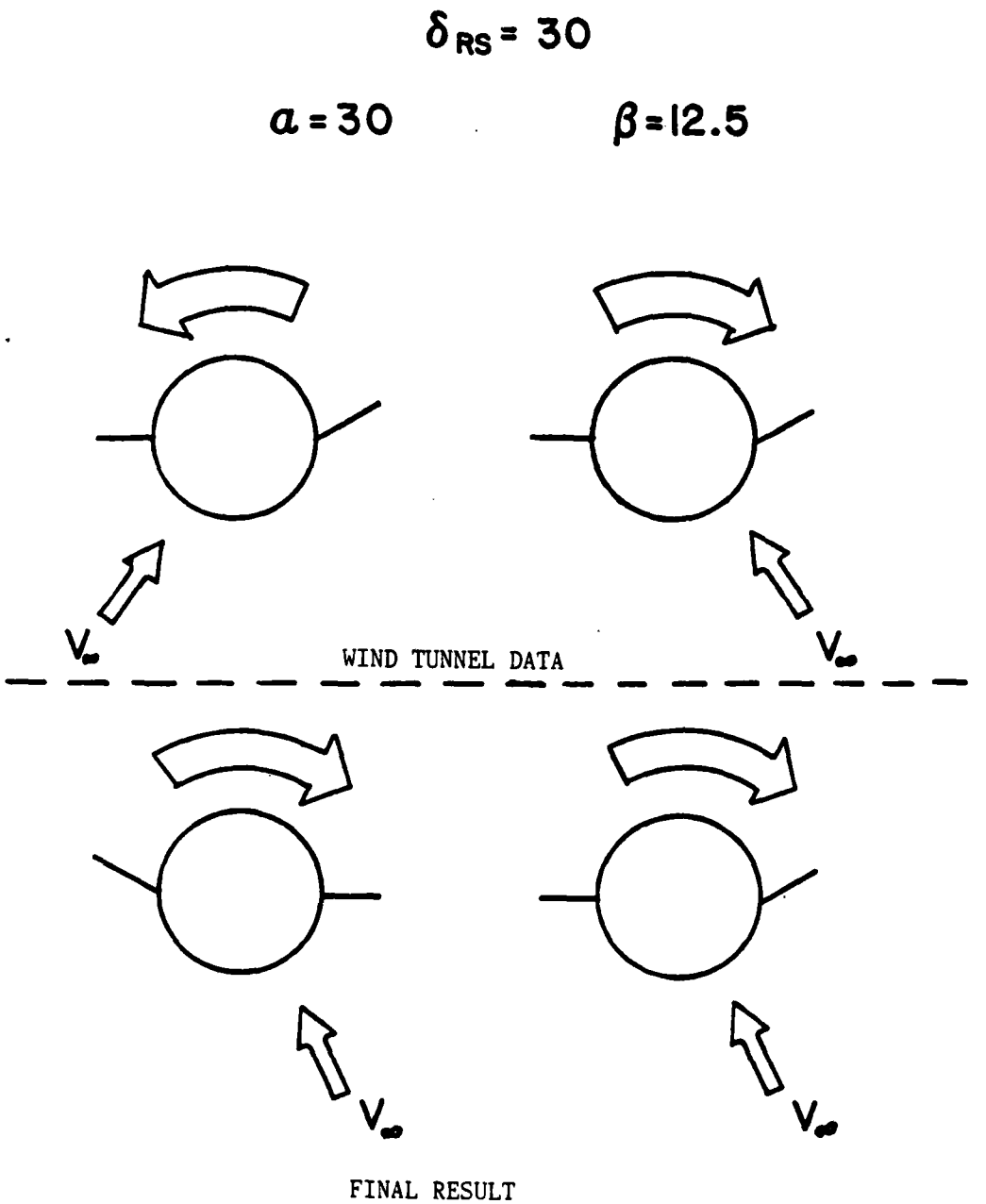

Figure 24. Description of Unidirectional Region.

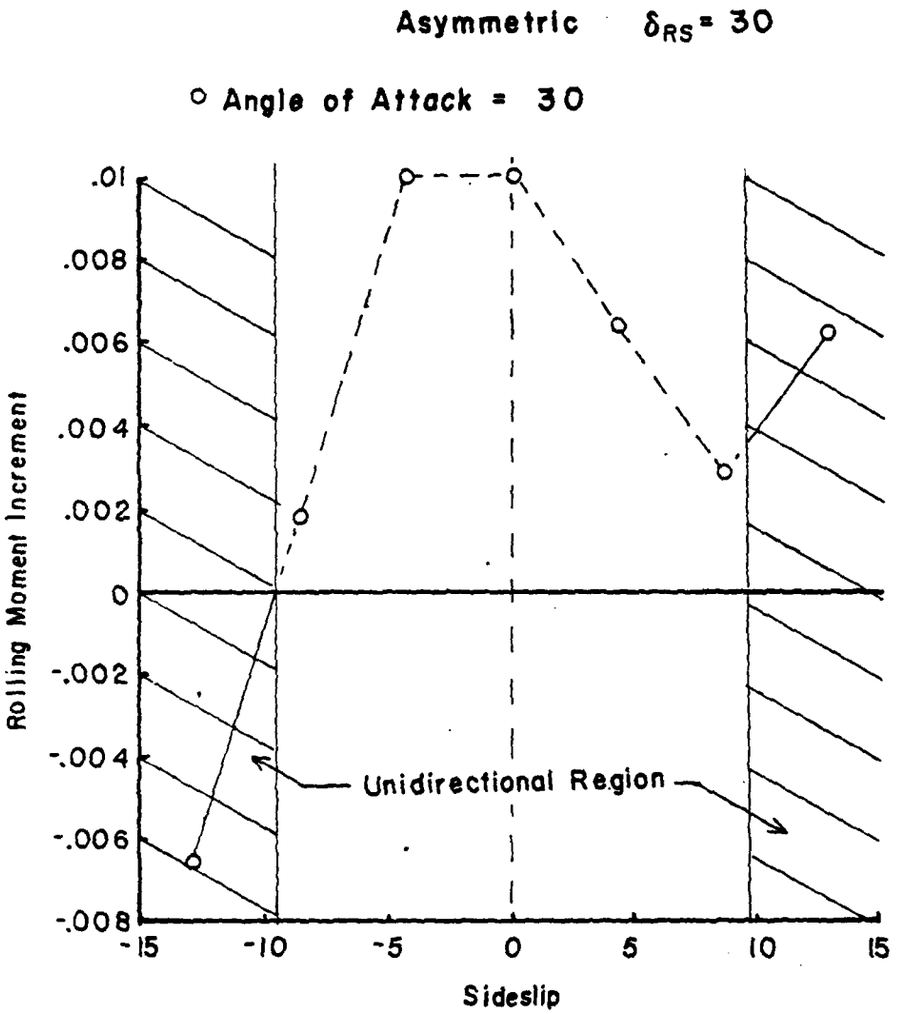

Figure 25. Unidirectional Region With Respect to Sideslip.

angle of attack at equal and opposite sideslip angles have opposite signs, then those points are contained in a unidirectional region.

A flowchart of the logic used in the internal model is shown in Figure 26. If the angle of attack is less than 28^{o} or no roll is commanded, both strakes are commanded to zero deflection. If a roll is commanded, then the roll coefficient for maximum deflection of each strake is calculated. If these coefficients have the different signs, then the strake producing roll in the commanded direction is deflected. If both roll coefficients have the same sign, then the aircraft is in a unidirectional region. If both strakes will roll the aircraft in the commanded direction, then the strake producing the most rolling moment is deflected. If neither strake will produce the desired roll direction, then both strakes are returned to zero deflection.

One should note that two major assumptions are inherent in the design of the strake flight control system. One assumption is that the sideslip angle is available for the logic choices. Presently, no satisfactory sideslip indicators for use at these AOA exist on operational aircraft. The second assumption is that a good model of the strake aerodynamics is available. Creating such a model could be difficult, since it is likely that different store configurations, or even irregularities between aircraft could have a major effect on the strake aerodynamics. This effect of slight irregularities is suspected since a change in the data was seen even when reinstalling the same model in the same wind tunnel. This assumption could be investigated by further wind tunnel tests using different store configurations and different models of the same type of aircraft.

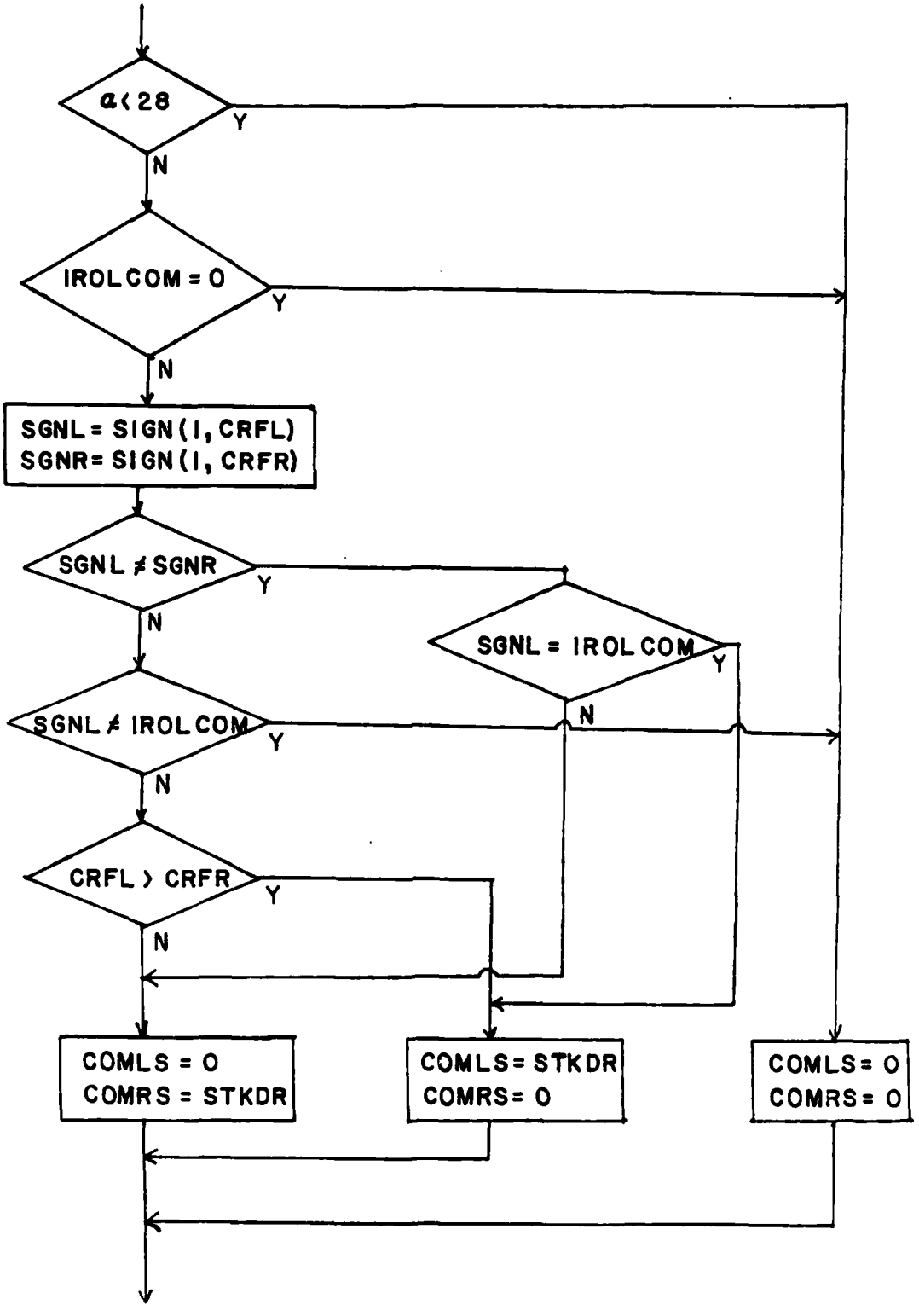

Figure 26. Internal Model Flowchart.

ROLL PERFORMANCE OF STRAKES

The first simulations done used strakes alone as a roll control device. These simulations used the initial implementation of the strake flight control system, in which the strakes were commanded separately from the ailerons. The remainder of the aircraft FCS was unaltered, except that the ailerons were disabled, so that the roll rate feedback to the ailerons would not oppose the roll caused by the strakes. In the yaw axis, only the standard feedback channels were active, namely the stability axis yaw damper and the lateral acceleration. These simulations were initially started in 1 g straight and level flight at 32° AOA with the maximum upward strake deflection of +30°. This condition was chosen because it gave the maximum rolling moment available, and the data at this AOA and strake deflection were the most symmetric about zero sideslip, presumably giving the most consistent behavior. An important additional point was that these simulations used linear derivatives (C_{ℓ_β}, C_{n_β}, C_{Y_β})[10]

The results for the +30° strake deflection can be seen in Figure 27. The control input commands maximum right roll from 0 to 6 seconds, and then no roll from 6 to 8 seconds. At the end of the 6 second period, the aircraft has only rolled 40°. The stability axis roll rate shows an initial increase until about 2 seconds, where it starts oscillating. This roll rate never increased above 10 deg/sec, which is not high enough to truly be useful. This rolling moment was the highest available in simulations at other AOAs between 30° and 40°.

A key to the reason for this low performance is the sideslip produced by this maneuver. The strakes produced a fair amount of adverse yaw, causing a positive sideslip of up to 4°. As a result, the dihedral effect of the aircraft produced a significant left rolling moment, which degraded the rolling performance. A clue to solving this problem is seen in the fact that only 1.5 degrees of rudder was used in this maneuver, while 30° of rudder throw is available.

For purposes of comparison, the same maneuver was performed using the maximum negative deflection of -45° on the strakes. See Figure 28. The dihedral effect was even more evident. This strake deflection

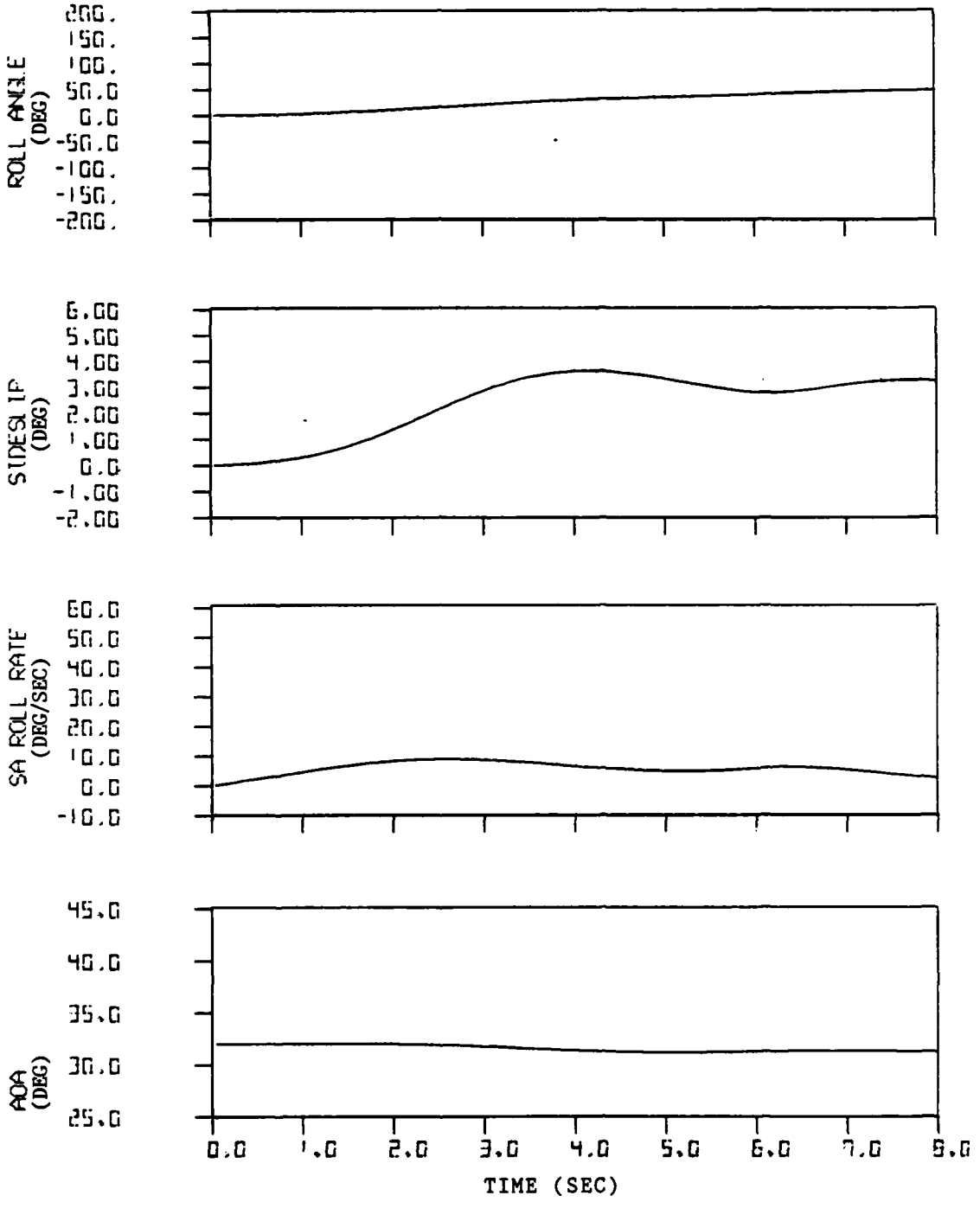

Figure 27. Maximum Roll at 1 g Using Hinged Strakes Only (AOA = 32°, Strake Deflection = +30).

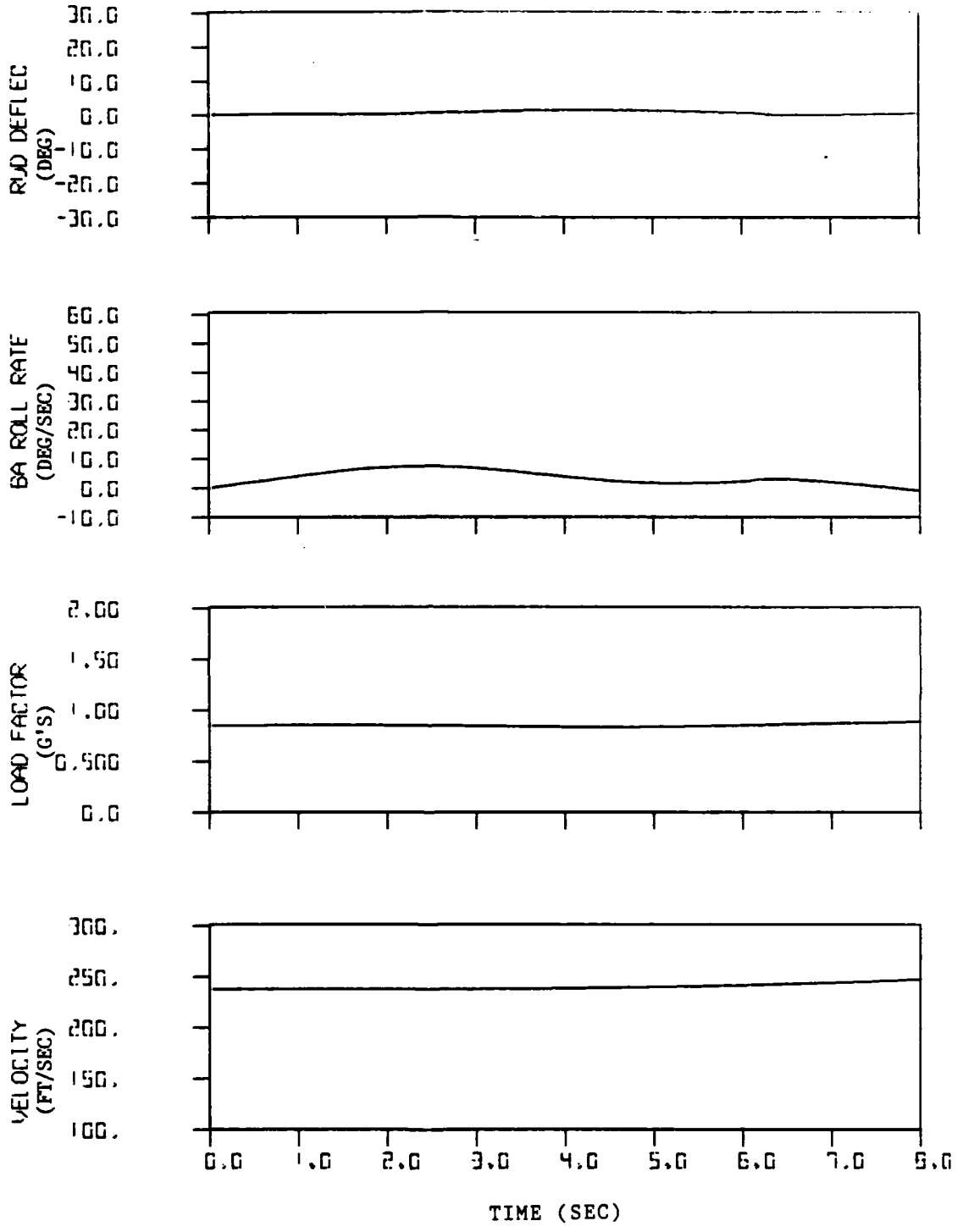

Figure 27. Concluded.

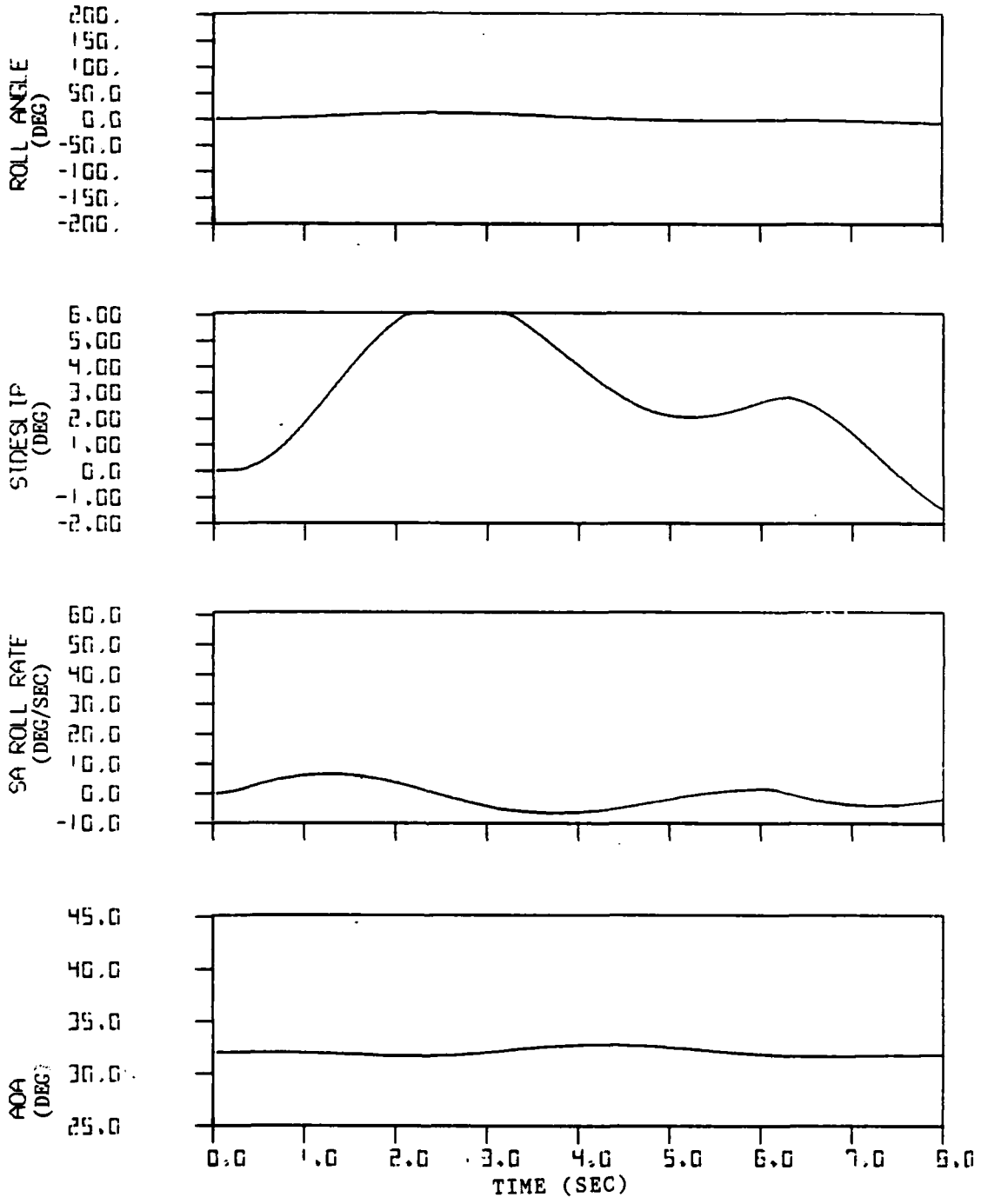

Figure 28. Maximum Roll at 1 g Using Hinged Strakes Only (AOA = 32°, Strake Deflection = -45).

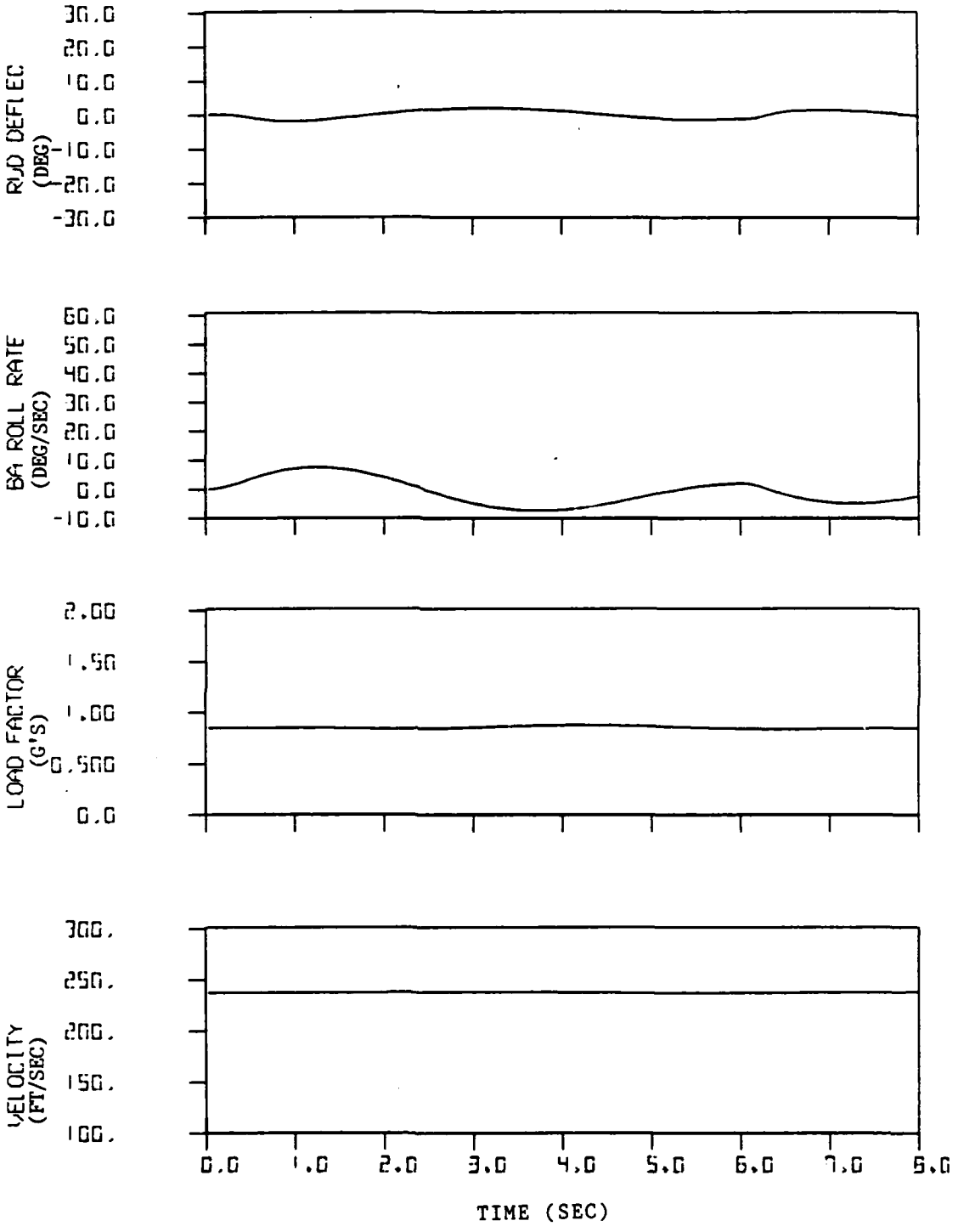

Figure 28. Concluded.

produces more adverse yaw, and up to 7 degrees of sideslip is produced. The sideslip is so severe that the aircraft stops rolling to the right, and actually rolls to the left. Again, only 2^{o} of the available rudder deflection has been used.

After the nonlinear sideslip derivatives obtained from the wind tunnel test were inserted into the simulation, the performance for these cases was degraded even further. Figure 29 shows a roll using the $+30^{o}$ strake deflection with the nonlinear derivatives. The maximum sideslip is now greater than 6^{o}, and the dihedral effect results in no net roll. Again, rudder deflection was minimal. In order to produce any roll, the sideslip angle must be controlled. If the sideslip is not controlled, the dihedral effect will either degrade or will totally prevent the desired roll.

Roll Performance Using Sideslip Feedback

The next step was to see if the rudder could be used to control the sideslip and therefore improve the roll performance. Since sideslip had already been assumed to be available for the internal model, it was decided to try using sideslip feedback to control the rudder.

The sideslip feedback was inserted in the yaw channel immediately after the stability axis yaw damper, as shown in Figure 30. Sideslip was fed back in terms of degrees, and feedback gains of 2, 4, 10, 20, 25, 30, 35, 40, and 50 were tested. Again, these tests were made at an AOA of 32^{o} since the data were well behaved there. All rolls were made to the right. Three quantitative factors were used in evaluating the appropriate feedback gain. These factors were maximum roll angle, maximum sideslip, and maximum roll rate (stability axes) in the six seconds that roll was commanded. A summary of these data are shown in Figure 31.

This analysis narrowed the choice of feedback gain down to 25, 30, or 35. Gains above 35 showed an increase in maximum sideslip, along with an increase of oscillations in sideslip. In addition, when the control input was removed at six seconds, these cases continued to oscillate in sideslip. Gains below 25 did not produce as much roll angle or roll rate. Large sideslip angles were still present, and the

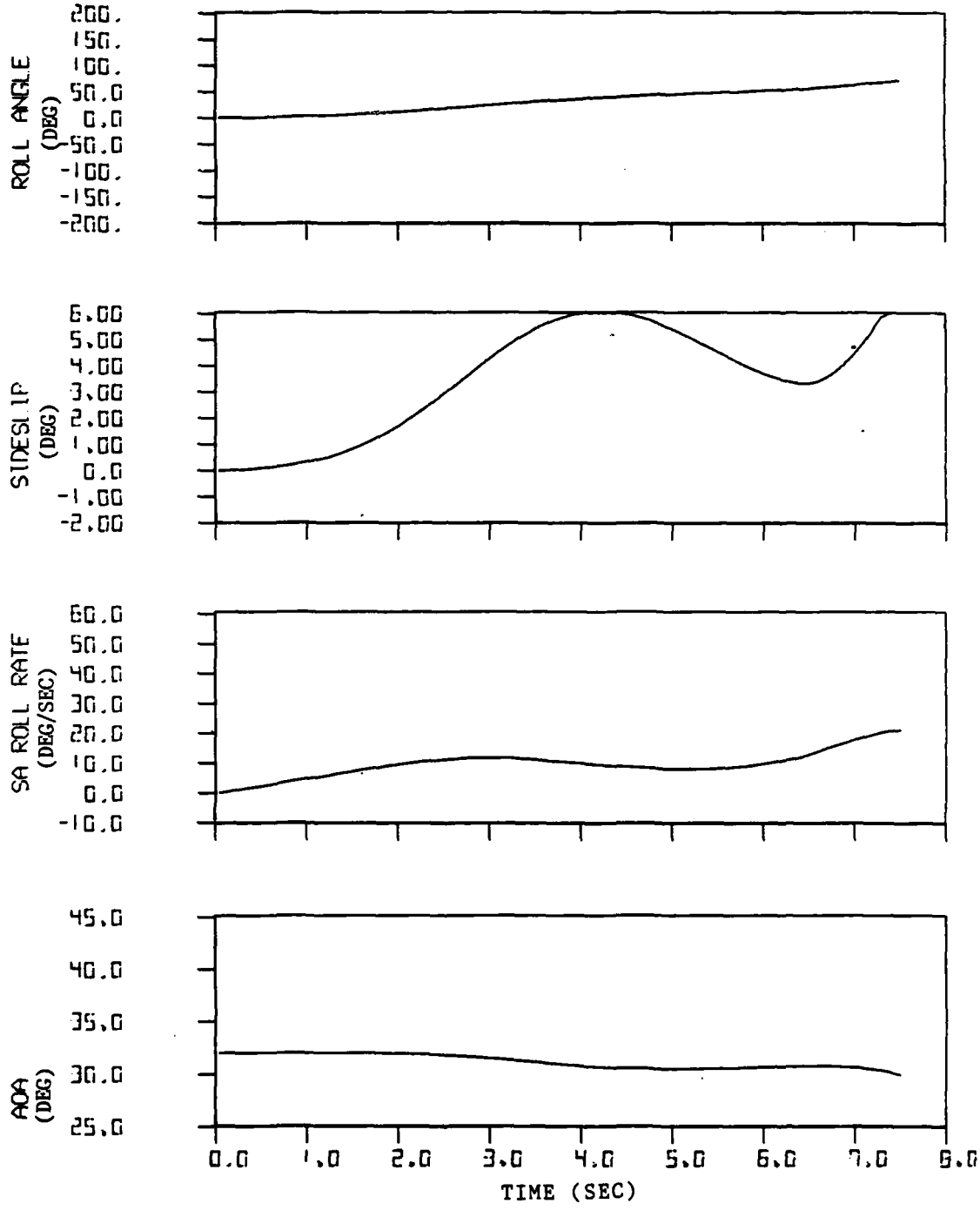

Figure 29. Maximum Roll at 1 g Using Hinged Strakes Only With Nonlinear Derivatives (AOA = 32°, Strake Deflection = +30).

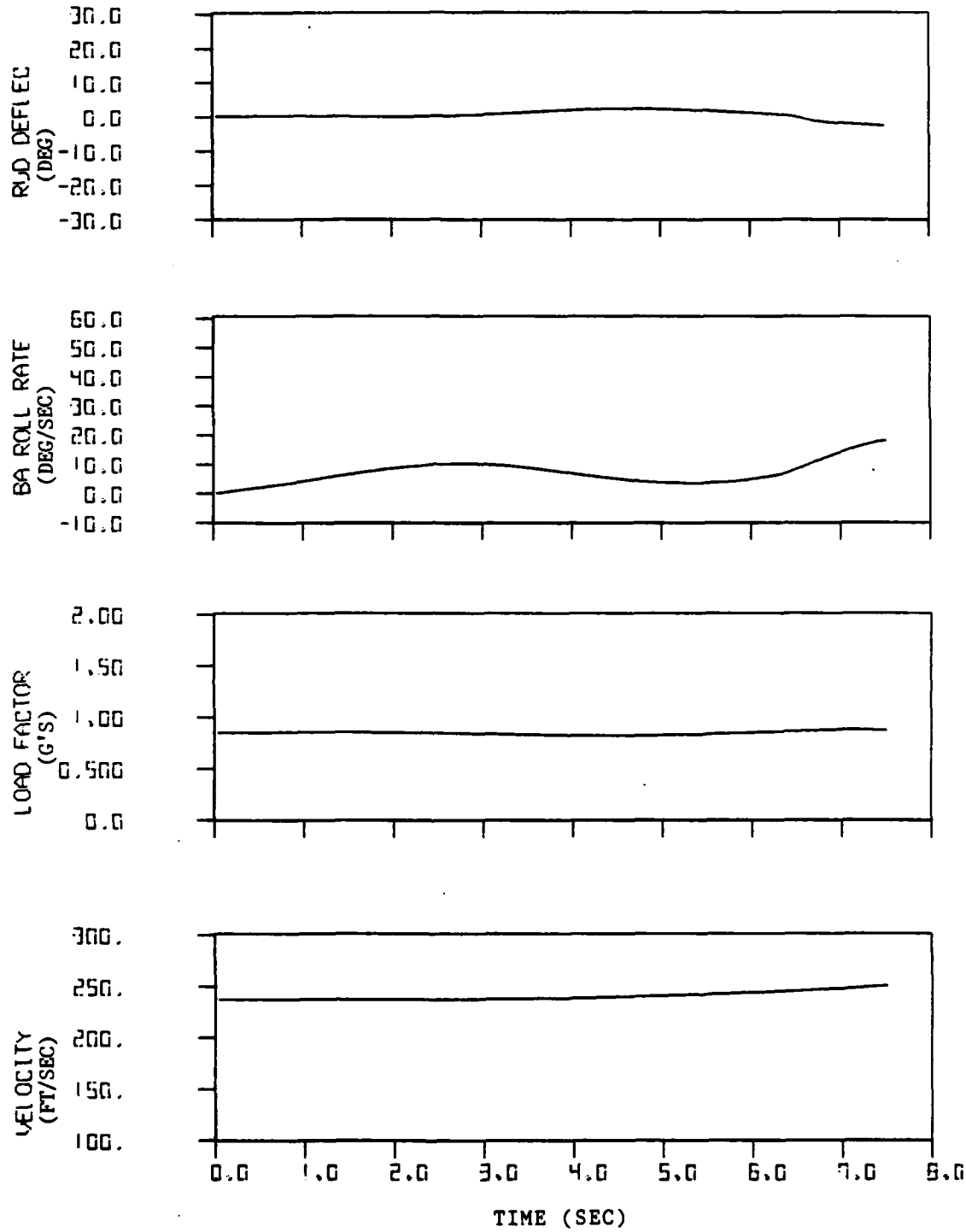

Figure 29. Concluded.

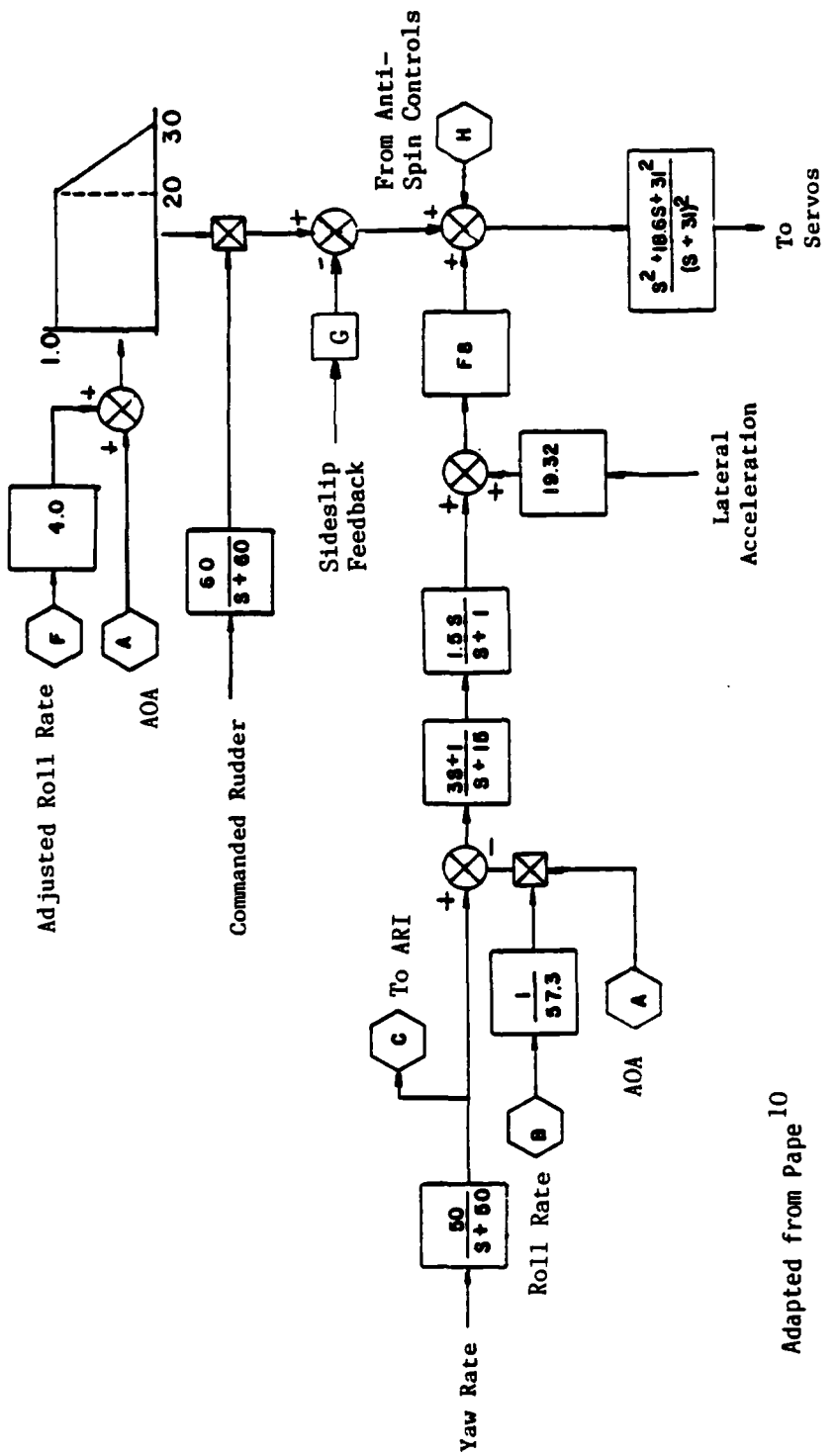

Adapted from Pape[10]

Figure 30. Yaw Channel Modifications For Direct Sideslip Feedback.

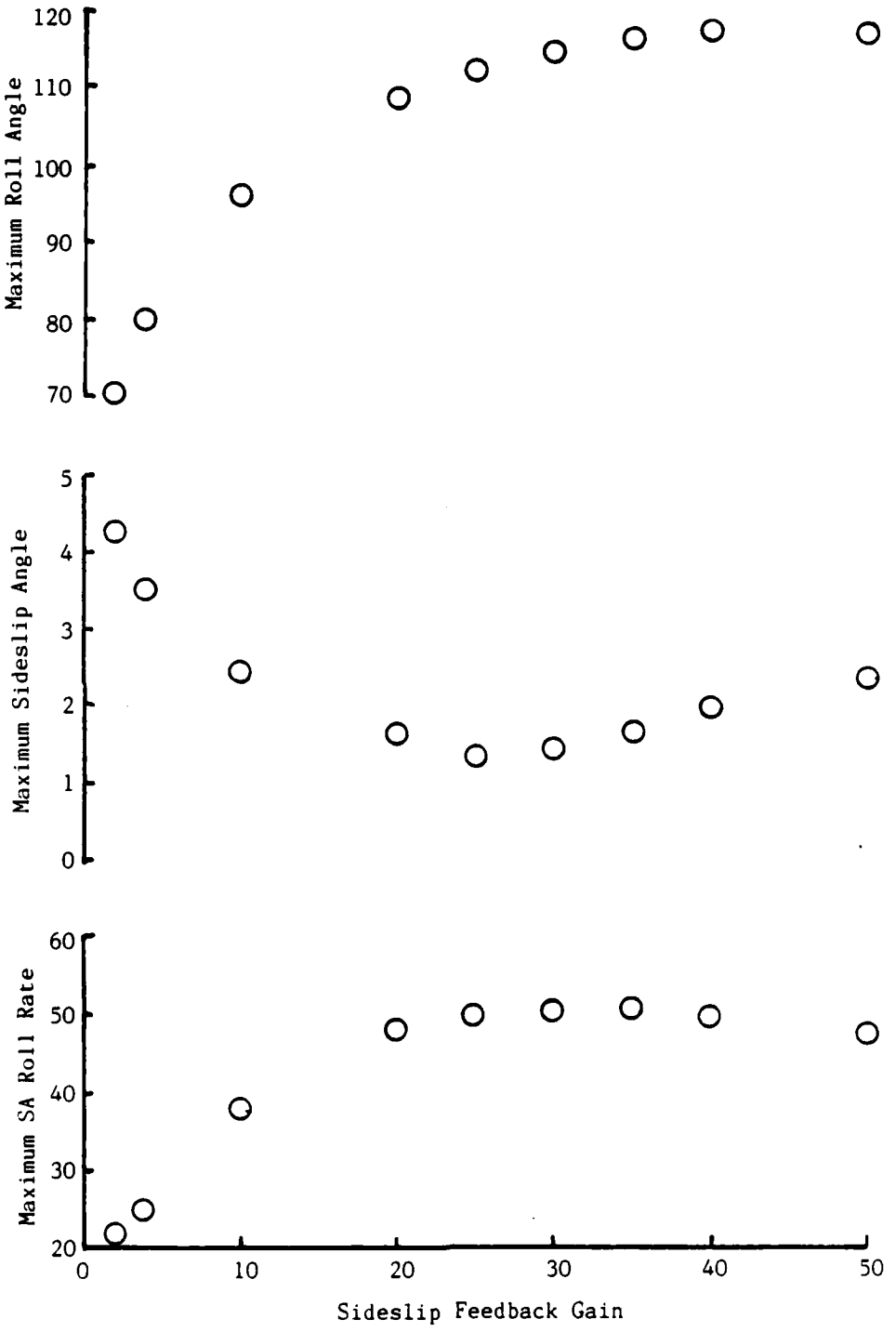

Figure 31. Summary of Response at 1 g to Direct Sideslip Feedback Gain (AOA = 32°, Strake Deflection = +30).

rudder was not saturated.

Gains of 25, 30, and 35 all produced roughly the same roll angle, with a gain of 35 only producing about 4 degrees more than a gain of 25, or an increase of only 3%. Likewise, there is little difference in maximum sideslip or maximum roll rate. However, there is a noticeable difference between the gains shown in the time histories (Figures 32-34). Gains of 30 and 35 show noticeable oscillations in sideslip once the control input is removed. Such oscillations are highly undesirable for a tracking condition. A gain of 25 had a much smoother recovery once the control input was removed, with only minor oscillations in sideslip. This was also the lowest gain tested which would saturate the rudder, thereby using all of its capability. Unlike the higher gains, a gain of 25 used all of the rudder with out excessive saturation. For these reasons, a sideslip feedback gain of 25 was used in subsequent simulations.

After choosing this gain, simulations were run in 1 g straight and level flight at AOAs from 30^{o} to 40^{o} in 2^{o} increments. These simulations were run using the initial implementation of the strake FCS with the separate control on the strakes and the ailerons disabled. The standard feedback paths in the yaw channel, the stability axis yaw damper and the lateral acceleration, remained active in addition to sideslip feedback. The control input commanded maximum roll for 6 seconds, and was removed from 6 to 8 seconds.

The rudder was effective in controlling the sideslip angle throughout the AOA range from 30^{o} to 40^{o}. In each case the sideslip was held to less than $\pm 2^{o}$. From 30^{o} to 40^{o} AOA the maximum roll angle follows the same trend with AOA as do the roll coefficients at zero sideslip (Figure 13), that is, the maximum roll angle occurs at 32^{o} AOA decreasing to 34^{o} and then increasing again to 36^{o}. At 32^{o} AOA, the roll angle after 6 seconds is 114^{o}, as compared to 40 degrees after 6 seconds without beta feedback. See Figure 35.

The stability axis roll rate increases fairly constantly with time. An evidence of roll oscillations can be seen at AOAs of 38^{o} and above, as evidenced by oscillations in the roll rate time history. The 38^{o} case is shown in Figure 36.

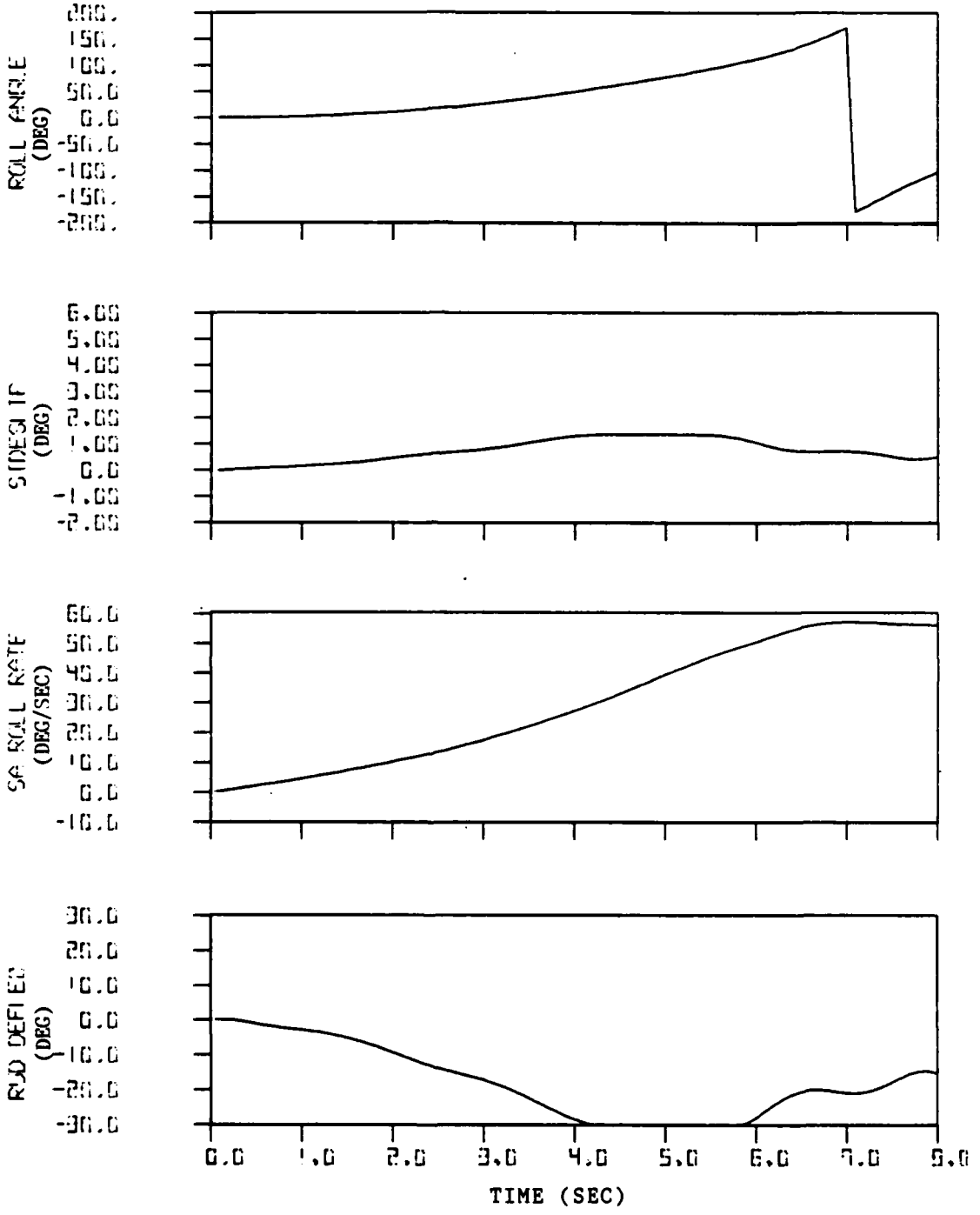

Figure 32. Maximum Roll at 1 g Using Hinged Strakes Only With Sideslip Feedback (AOA = 32°, Strake Deflection = +30, Sideslip Feedback Gain = 25).

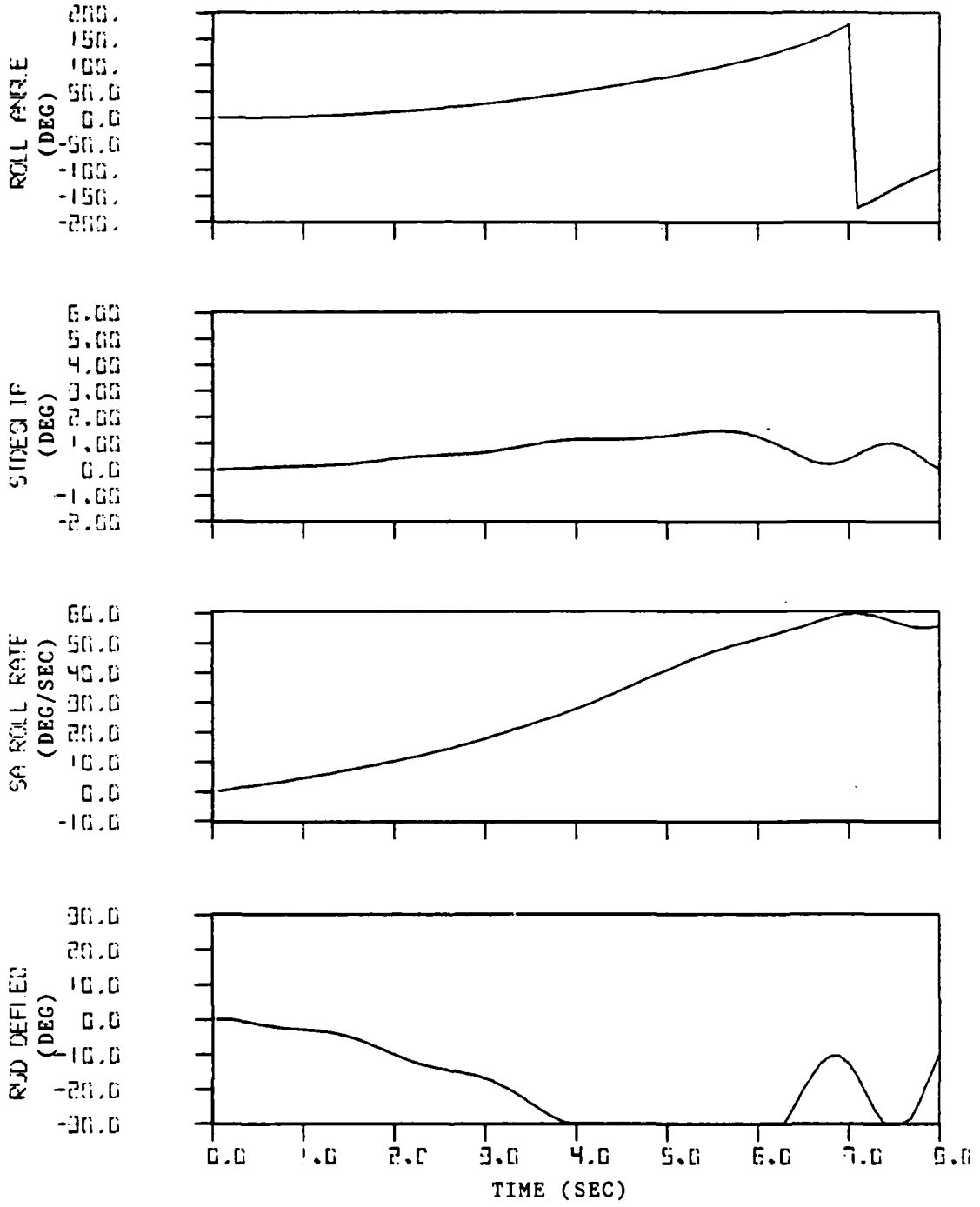

Figure 33. Maximum Roll at 1 g Using Hinged Strakes Only With Sideslip Feedback (AOA = 32°, Strake Deflection = +30, Sideslip Feedback Gain = 30).

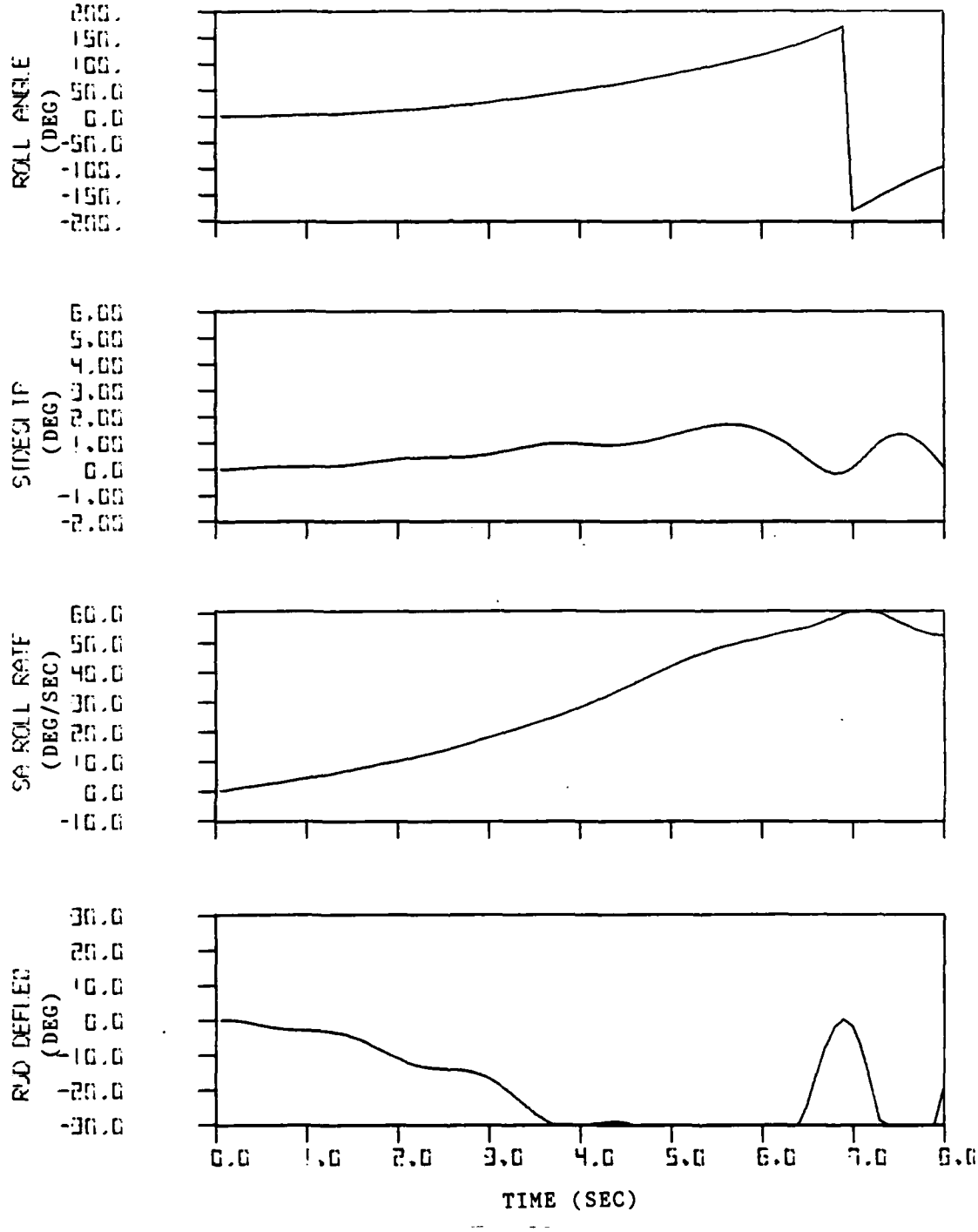

Figure 34. Maximum Roll at 1 g Using Hinged Strakes Only With Sideslip Feedback (AOA = 32°, Strake Deflection = +30, Sideslip Feedback Gain = 35).

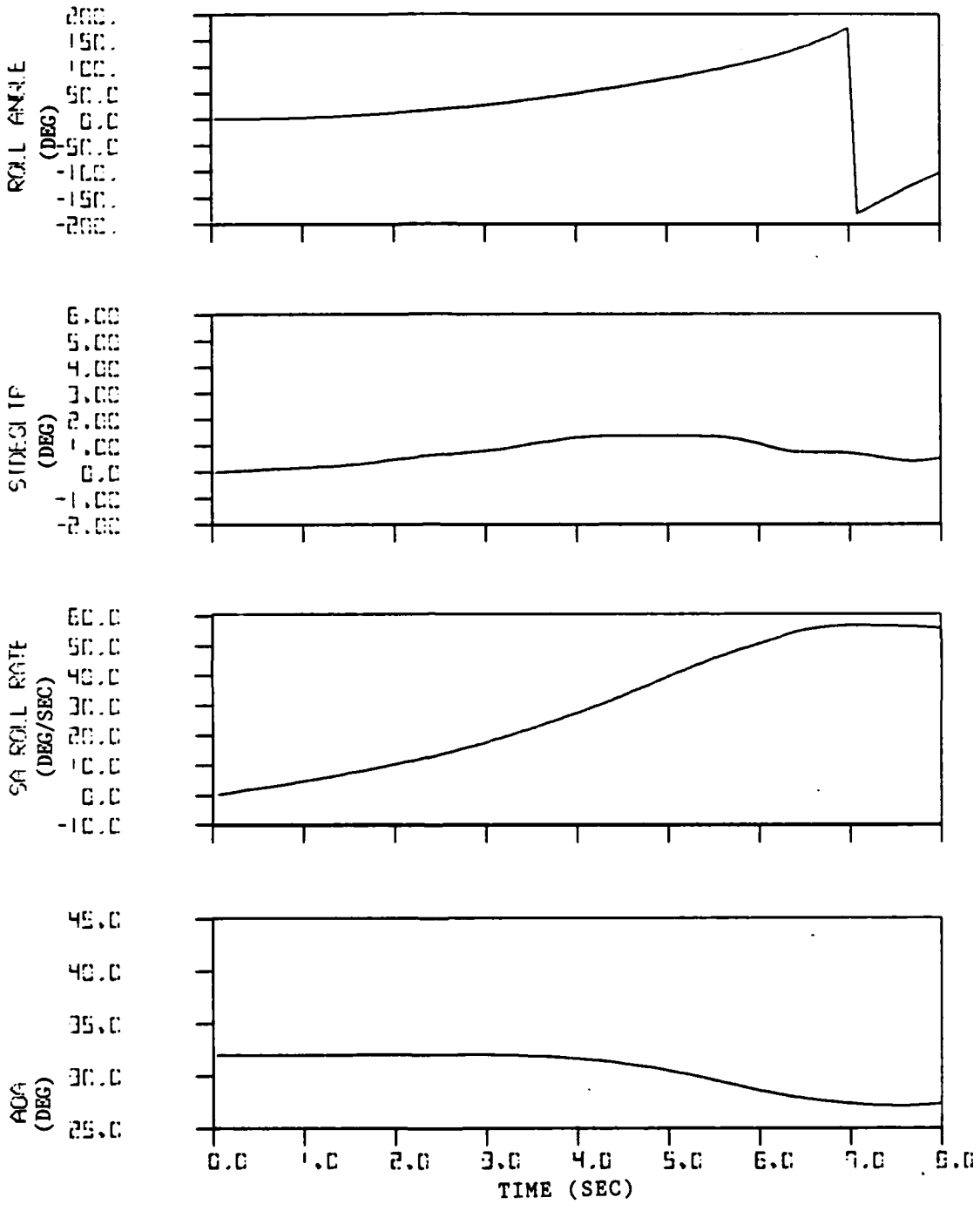

Figure 35. Maximum Roll at 1 g Using Hinged Strakes Only With Sideslip Feedback (AOA = 32°, Strake Deflection = +30).

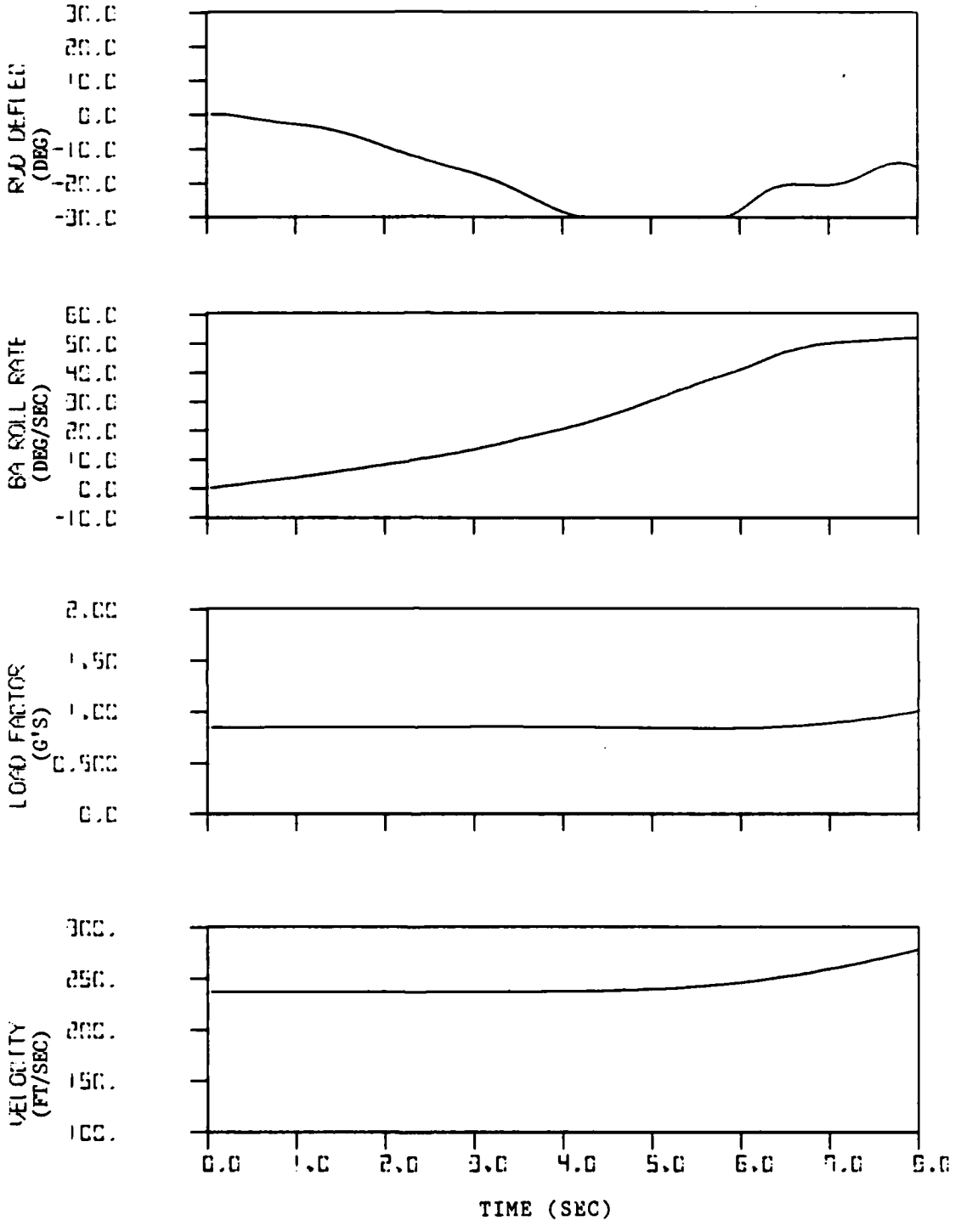

Figure 35. Concluded.

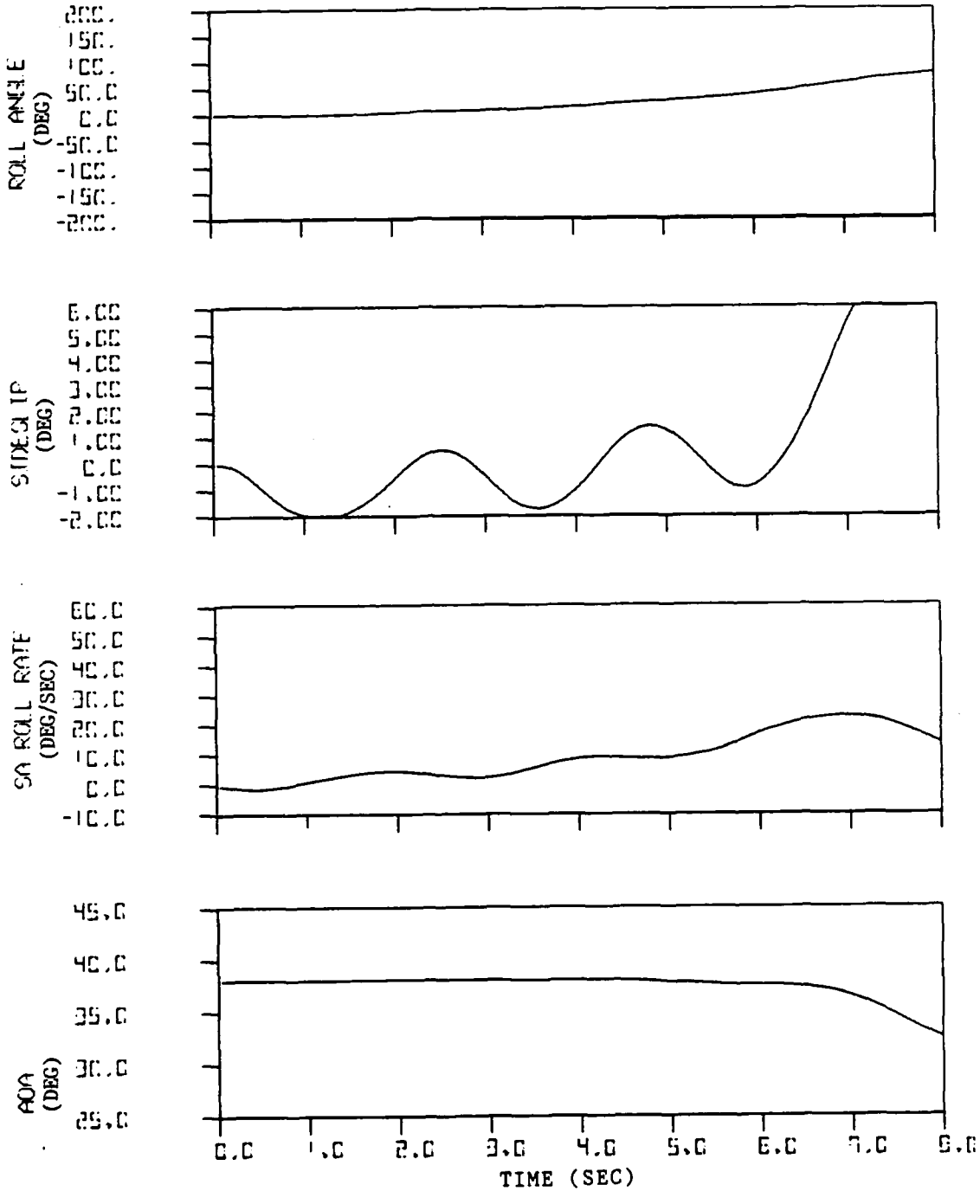

Figure 36. Maximum Roll at 1 g Using Hinged Strakes Only With Sideslip Feedback (AOA = 38°, Strake Deflection = +30).

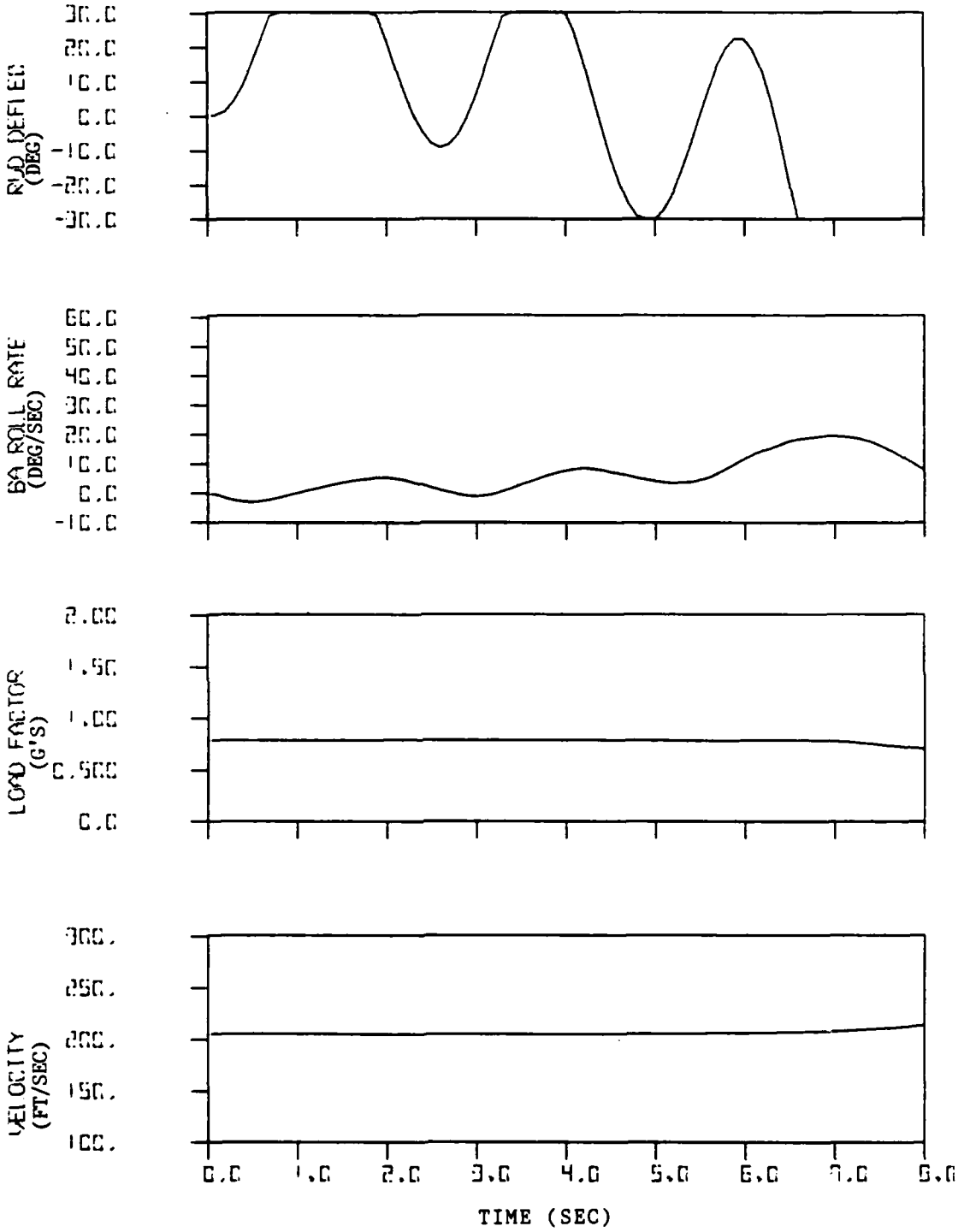

Figure 36. Concluded.

In general, the AOA is virtually constant for at least 4 seconds, and then decreases. The constant behavior in the first 4 seconds is largely due to the fact that the longitudinal forces and moments were essentially unchanged by stake deflection. The eventual decrease in AOA was due to another factor. As the aircraft rolls, the lift vector, unchanged in magnitude, is no longer pointing upward. As the aircraft begins to dive, it picks up speed and the lift is increased. This lift increases the normal acceleration, which is fed back to the pitch channel, causing a decrease in angle of attack in order to maintain the commanded normal acceleration.

The reactions of the aircraft after the control input is removed are equally important. In all cases, the roll angle continues to increase due to the angular momentum of the aircraft. At 30^{o} and 32^{o} AOA the sideslip angle decreased after the control input was removed. However, at 36^{o} to 40^{o} AOA the sideslip shows a very different behavior. Above 34^{o} AOA, the $C_{n_{\beta}}$ of the aircraft becomes negative (unstable). At approximately this same point, the strakes begin to produce proverse yaw. This proverse yaw offsets the effects of the unstable $C_{n_{\beta}}$, but when it is removed, the aircraft reacts to this instability, which shows up as increasing sideslip.

One case was run using the -45^{o} strake deflection at 32^{o} AOA for comparison purposes, shown in Figure 37. After the 6 second control input, the aircraft had rolled virtually the same amount (114^{o}), but the sideslip variations were larger, about 6^{o} compared to 1.4^{o} maximum. This behavior was comparable to the earlier findings for negative strake deflections.

A set of simulations was run for the positive strake deflection commanding left rolls. With the very small sideslip angles, the results were essentially the same as for the right rolls.

The simulations seemed to indicate that the faster the rudder was deflected, the less sideslip would be allowed to build up. To investigate this possibility, a simulation was run at 32^{o} commanding a maximum roll with the strakes and maximum rudder deflection simultaneously. See Figure 38. The result of this combined input was that the sideslip went negative initially, and no roll was produced for the first two seconds.

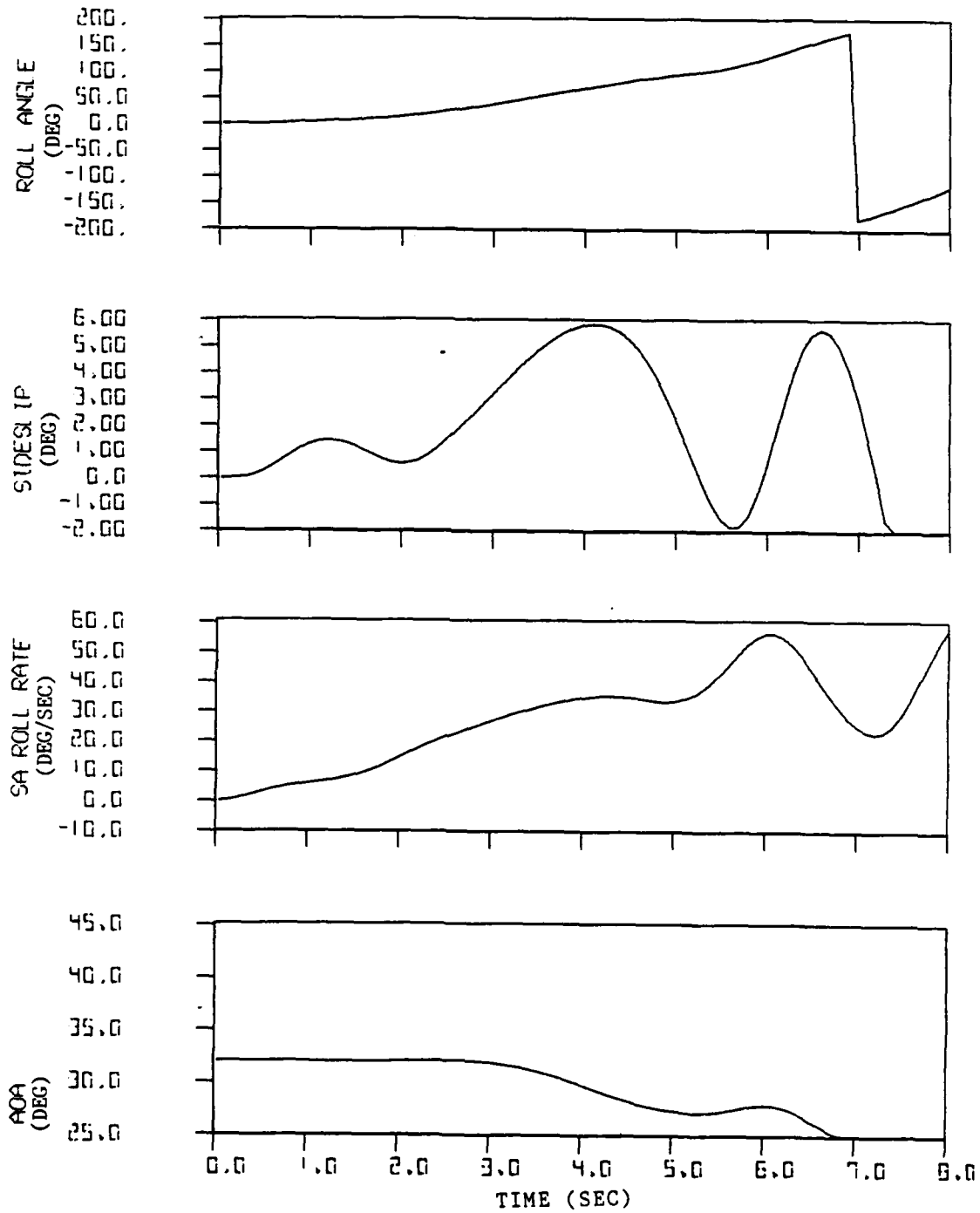

Figure 37. Maximum Roll at 1 g Using Hinged Strakes Only With Sideslip Feedback (AOA = 32°, Strake Deflection = -45).

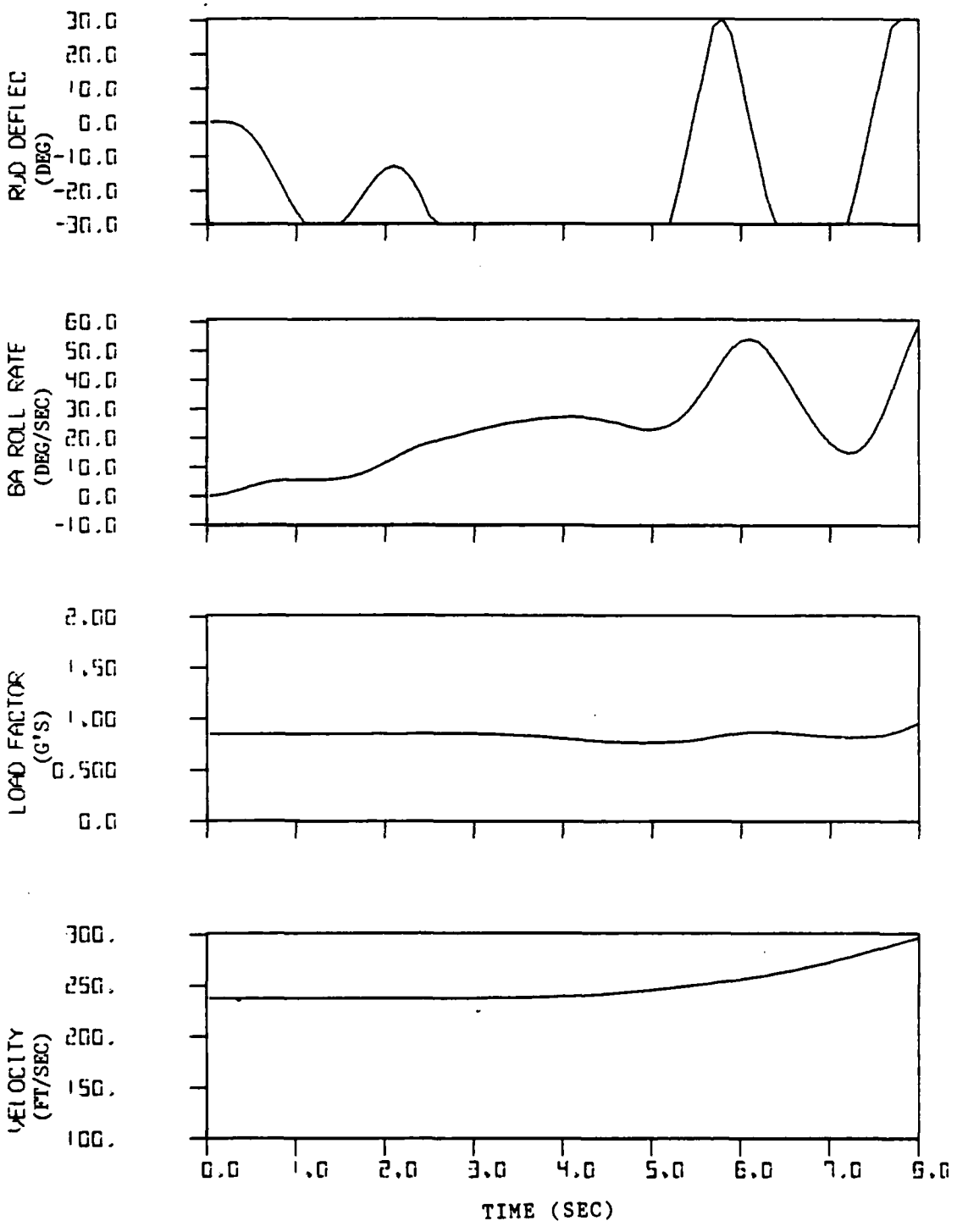

Figure 37. Concluded.

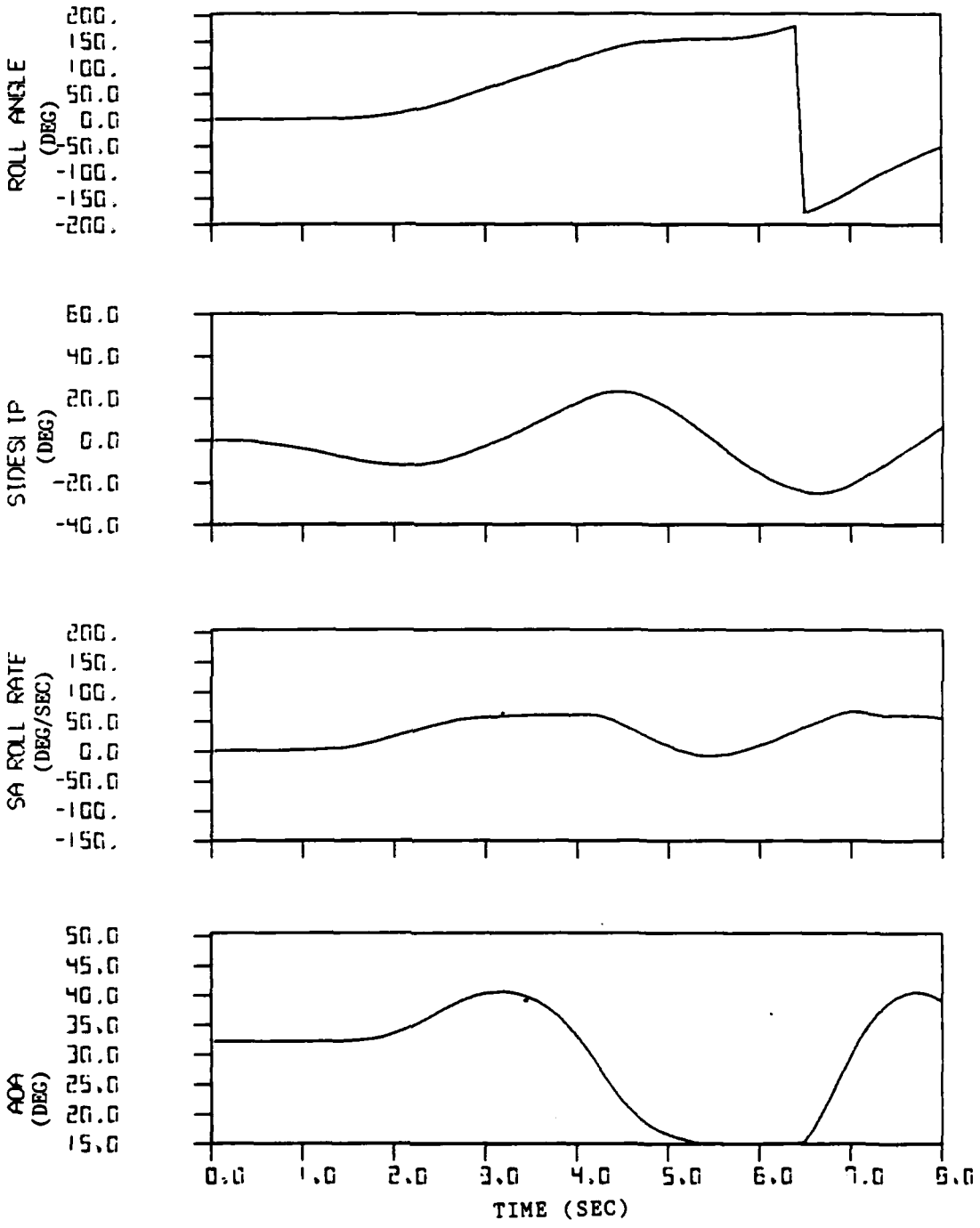

Figure 38. Maximum Roll at 1 g Using Hinged Strakes and Full Rudder Command With Sideslip Feedback (AOA = 32°, Strake Deflection = +30).

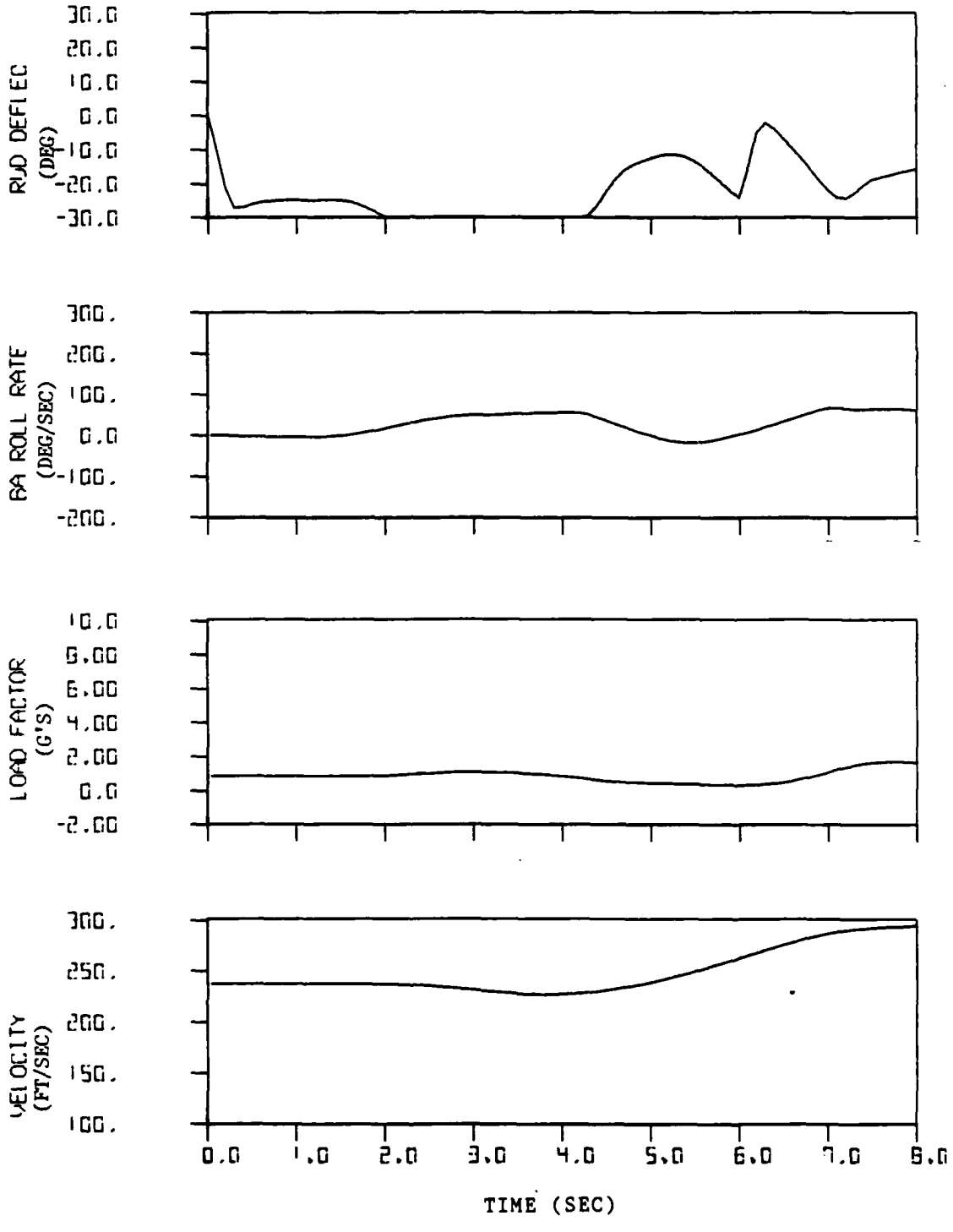

Figure 38. Concluded.

The sideslip had much larger oscillations, reaching over 20°, and the AOA varied from 15° to 40°. These oscillations were undesirable, so this case was not pursued any farther. Additionally, some of these sideslip angles were outside the data limits of the simulation.

Roll Performance at Higher Load Factors

As mentioned earlier, the previous simulations were done at a dynamic pressure of about 25 psf in order to achieve straight and level flight. At this low dynamic pressure, none of the control surfaces were very effective. If a certain angle of attack is maintained as the dynamic pressure is increased, the load factor will necessarily increase. Additionally, this condition would be a more realistic high AOA case. After the modifications to the initial conditions were made, a simulation was run for a left roll at 32° AOA with increment of 5 g's commanded and with a positive strake deflection of +30°. See Figure 39. The initial dynamic pressure for this simulation was 200 psf. After 6 seconds, the aircraft had rolled approximately 540°, achieving a stability axis roll rate of -150 degrees per second.

This high roll rate raised concern about roll coupling and divergence due to reduced stability caused by decreased control authority, which could be seen in this simulation. After the control was removed, the aircraft pitched up to 50° AOA and subsequently departed. It was now necessary to limit the roll rate. In order to do this, the strake FCS was modified slightly. Instead of having a separate input, the strake FCS was connected to the aileron input command. The strakes then commanded a maximum roll based on the sign of the aileron input command. This change is shown in Figure 40. With this setup, if the roll rate became too high, the sign on the aileron roll signal would change, and the strakes would command an opposite roll to decrease the roll rate.

After this change was made, a set of simulations was run to compare the performance of the strakes alone, the ailerons alone, and the strakes and ailerons combined. Strake deflections included +30° and -45°. Two major trends were seen in these simulations. These trends were divided below and above 38° AOA. Below 38° the response is typified by the simulation at 32° AOA. Figure 41 shows this trajectory,

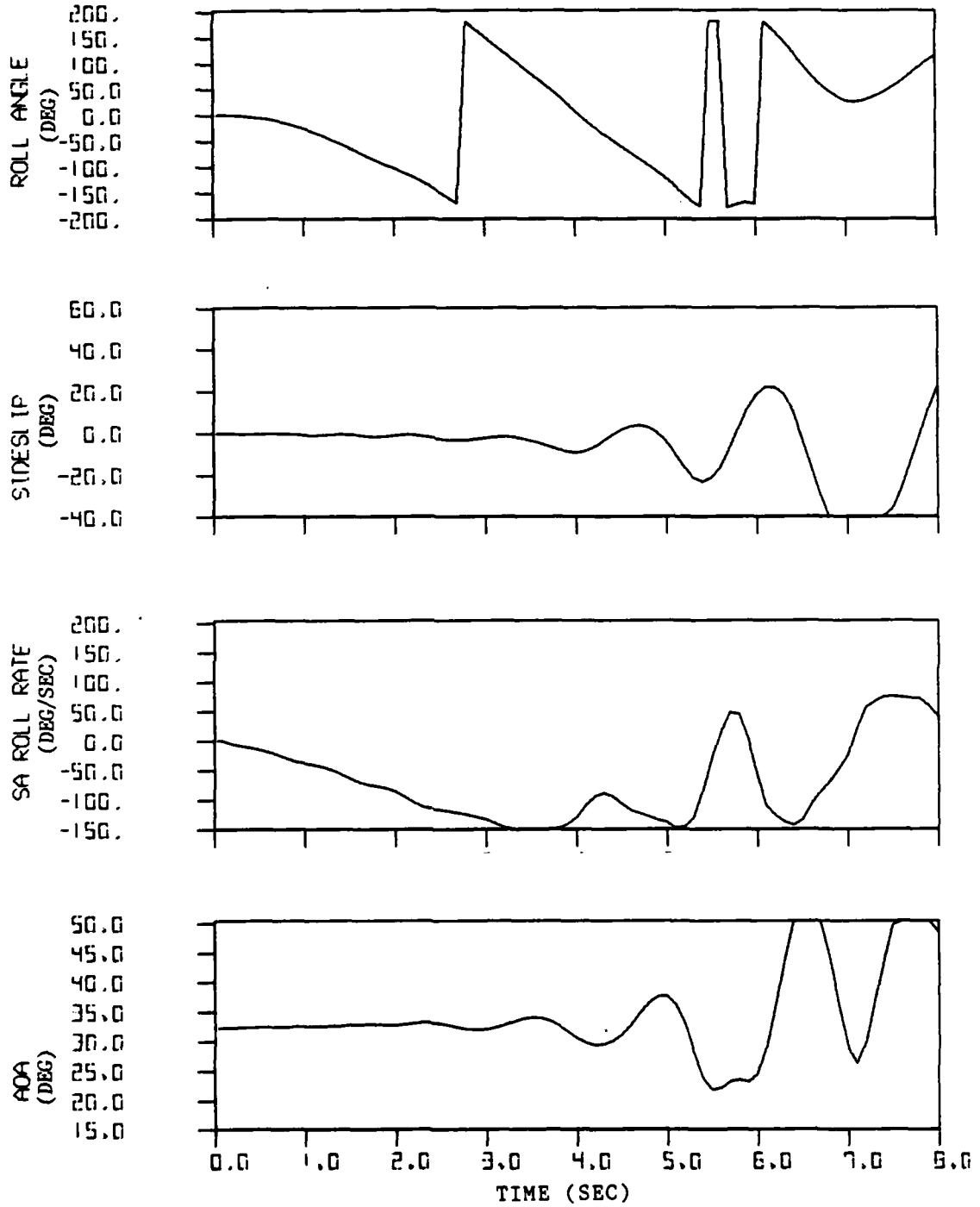

Figure 39. Maximum Left Roll at 5 g's Using Hinged Strakes Only With Sideslip Feedback (AOA = 32°, Strake Deflection = +30).

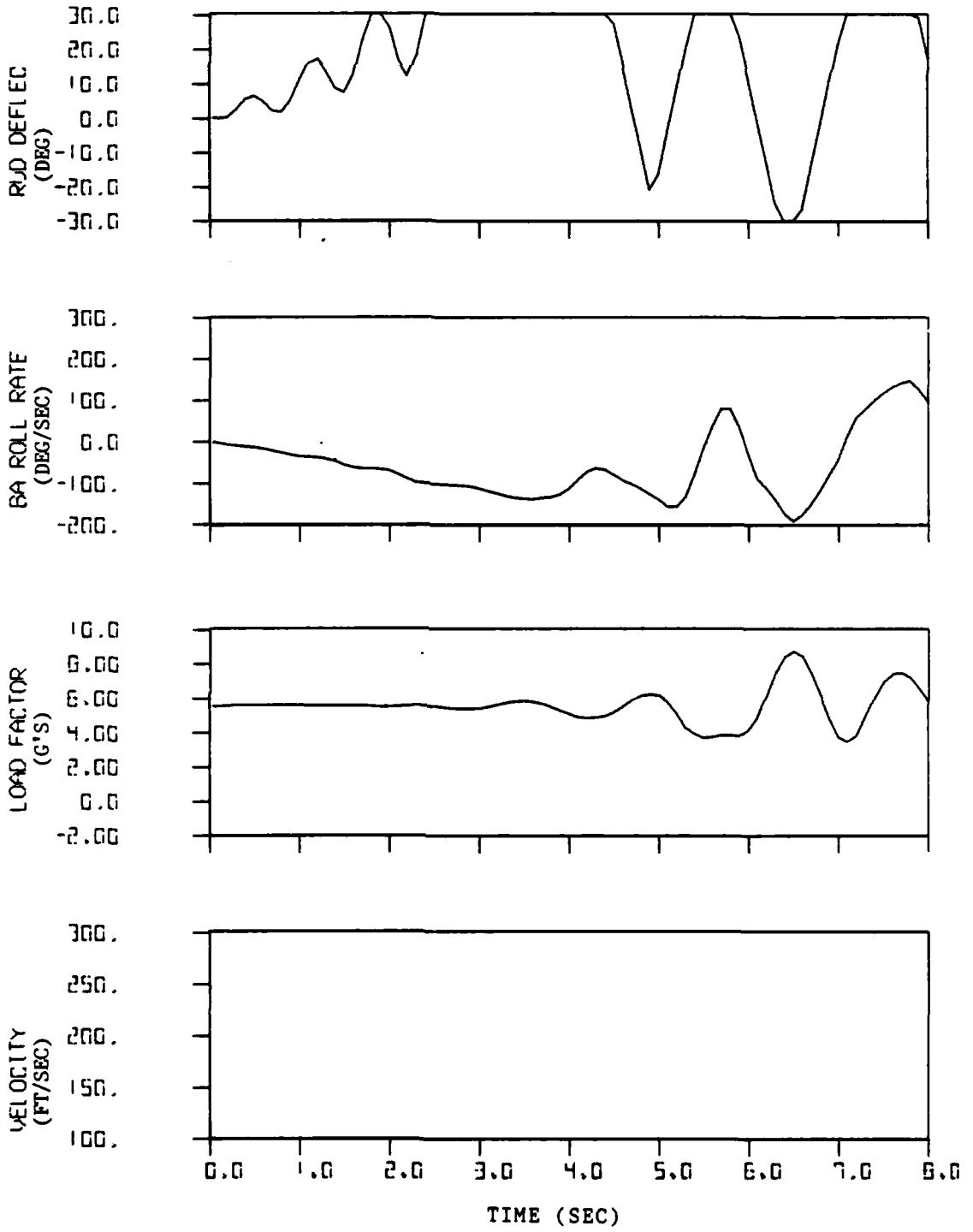

Figure 39. Concluded.

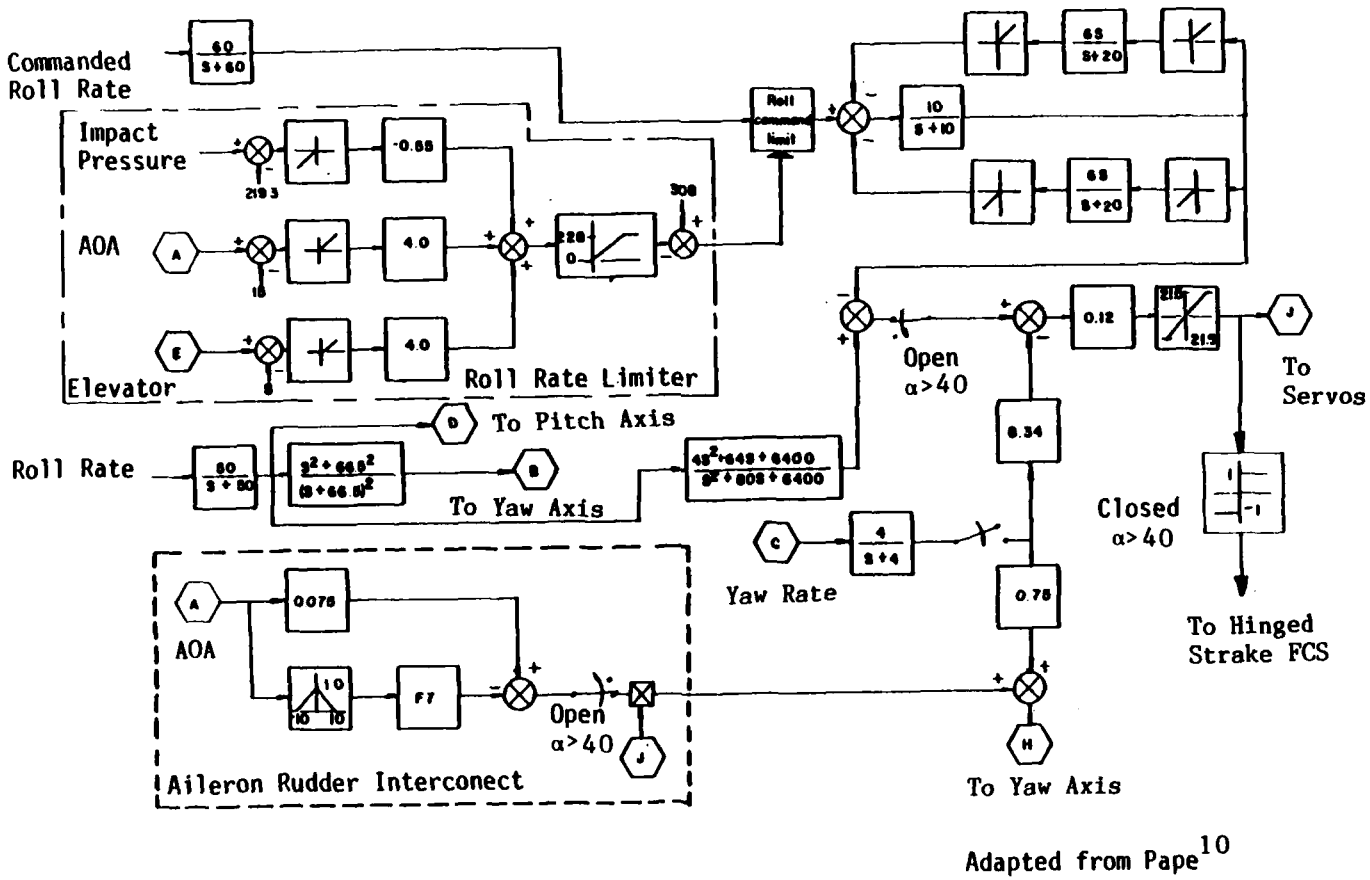

Figure 40. Roll Channel Modifications for Connecting Strake FCS Into Aileron Input Command.

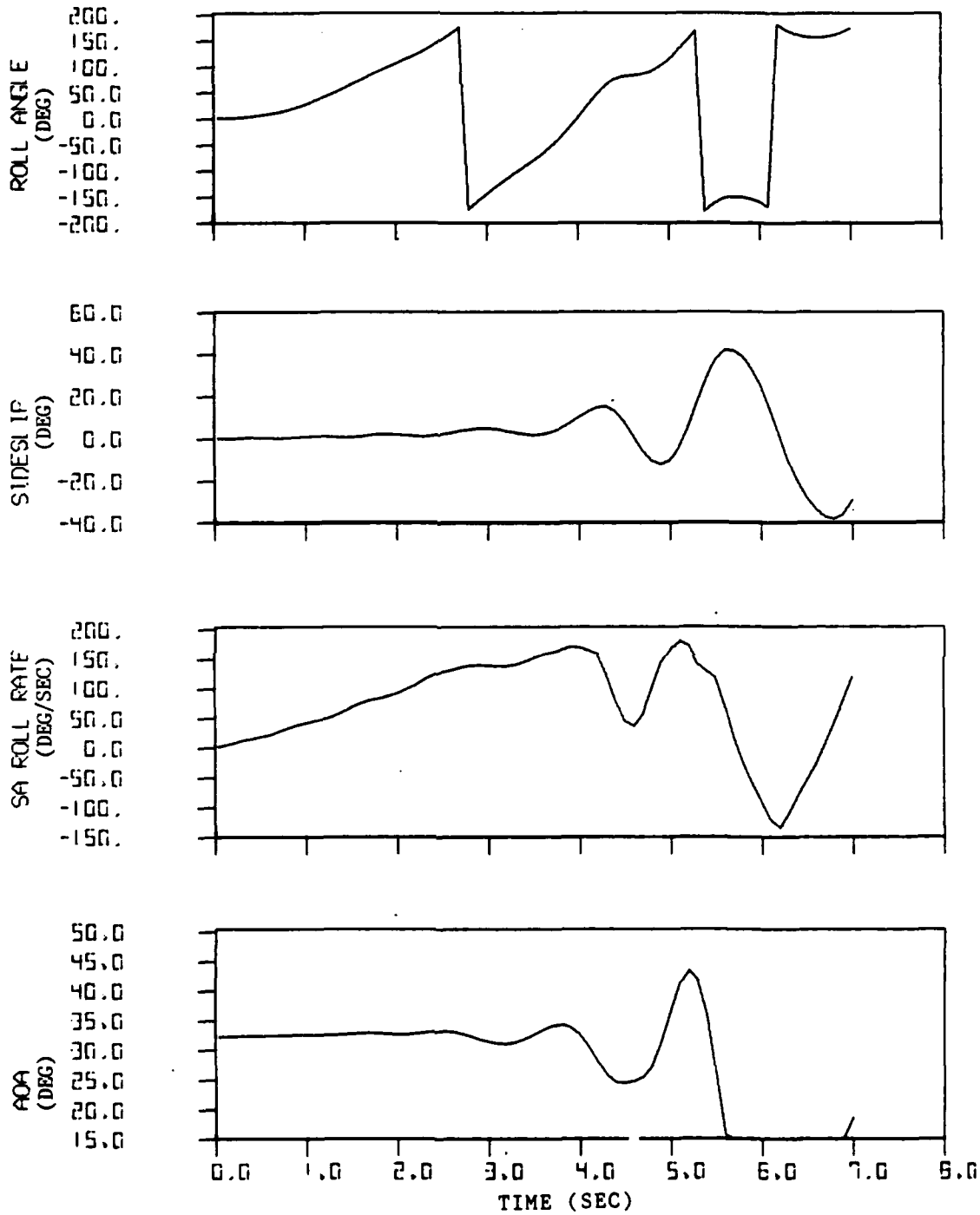

Figure 41. Maximum Roll at 5 g's Using Hinged Strakes Only With Sideslip Feedback (AOA = 32°, Strake Deflection = +30).

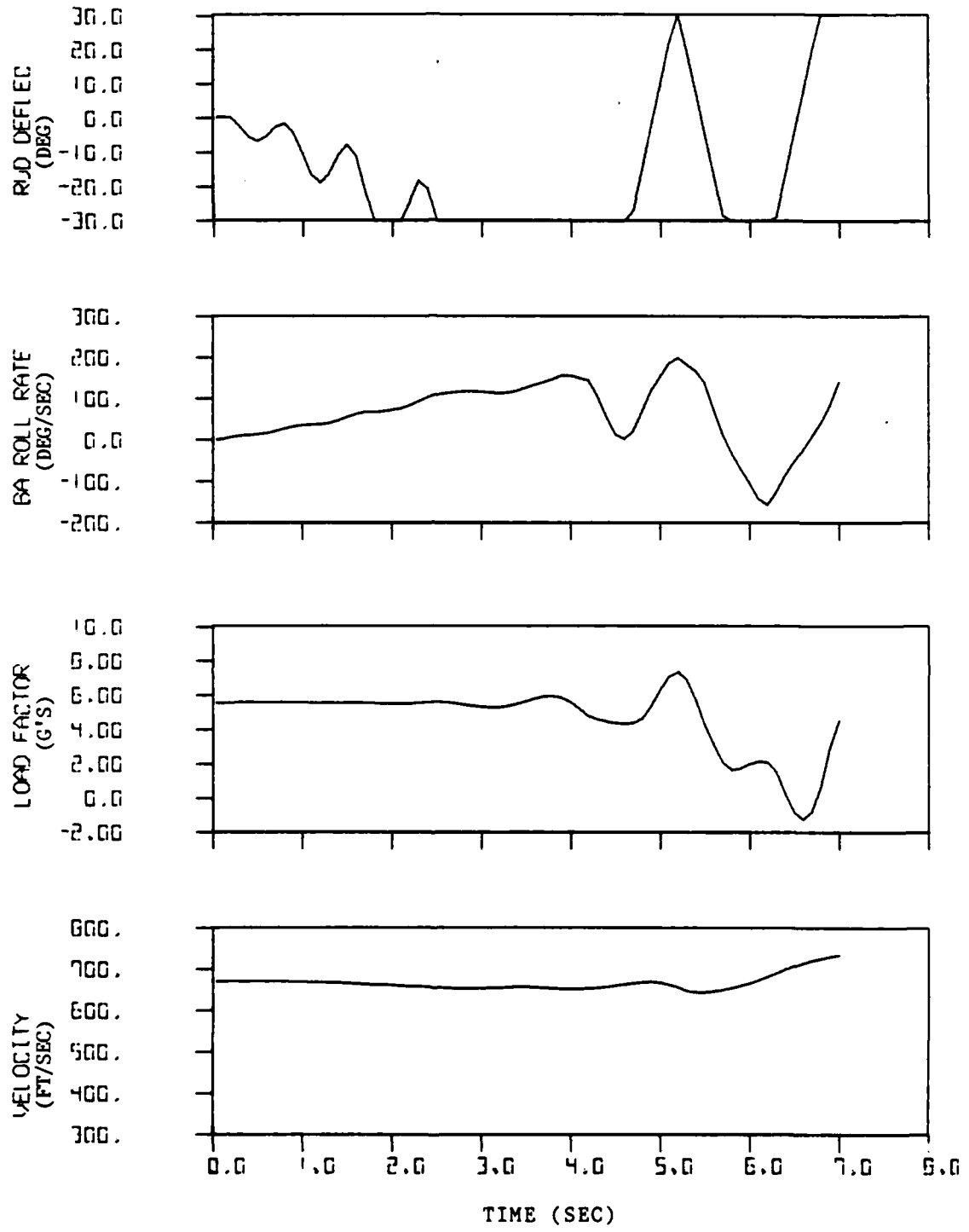

Figure 41. Concluded.

using a 30° strake deflection alone to roll the aircraft. The aircraft rolls to 180° in under three seconds, but as the roll continues, the sideslip and AOA begin to oscillate, and the aircraft departs after the control input is removed. In Figure 42, the strake is deflected to -45°. Again, the aircraft rolls well for a short time, until the sideslip and AOA begin to oscillate. As seen in the 1 g simulations, the -45° case has larger oscillations in sideslip.

Figure 43 shows a roll using ailerons only. While the sideslip and AOA oscillations are not as severe in this case, there is a noticeable roll oscillation with a period of about 1.3 seconds.

The effects of combining the strakes and ailerons are shown in Figures 44-45. In Figure 44, a strake deflection of +30° is used with the ailerons. Here the aircraft not only reaches 180° faster than in any of the previous cases, but there is also less roll oscillation and less variation in sideslip and AOA. Figure 45 shows the combination of a strake deflection of -45° with the ailerons. Again, this strake deflection causes more sideslip variations due to a stronger yawing moment, and the roll oscillation is as bad as in the ailerons only case. In all these cases, the aircraft was likely to depart after the control input was removed. This condition could be due to the length of roll causing the aircraft to move to an unstable region, or possibly the controls used for rolling have a stabilizing effect on the entire airplane which is lost when the control input is removed.

At and above 38° AOA the ailerons have lost most of their effectiveness and the strakes alone become more effective. Figure 46 shows the effects of a strake deflection of +30, and Figure 47 shows the effects of the ailerons only. While the strakes alone take 4.5 seconds to reach 180° of roll, the ailerons take 5.2 seconds to reach 180°. The effect of combining them, shown in Figure 48, does not improve on the performance of the strakes alone.

Based on these simulations, the best roll performance can be attained by combining the +30° strake deflection with the ailerons up to an AOA of about 38°, at which time better performance can be attained with +30° strake deflection alone. At 40° AOA, neither control surface produces satisfactory results.

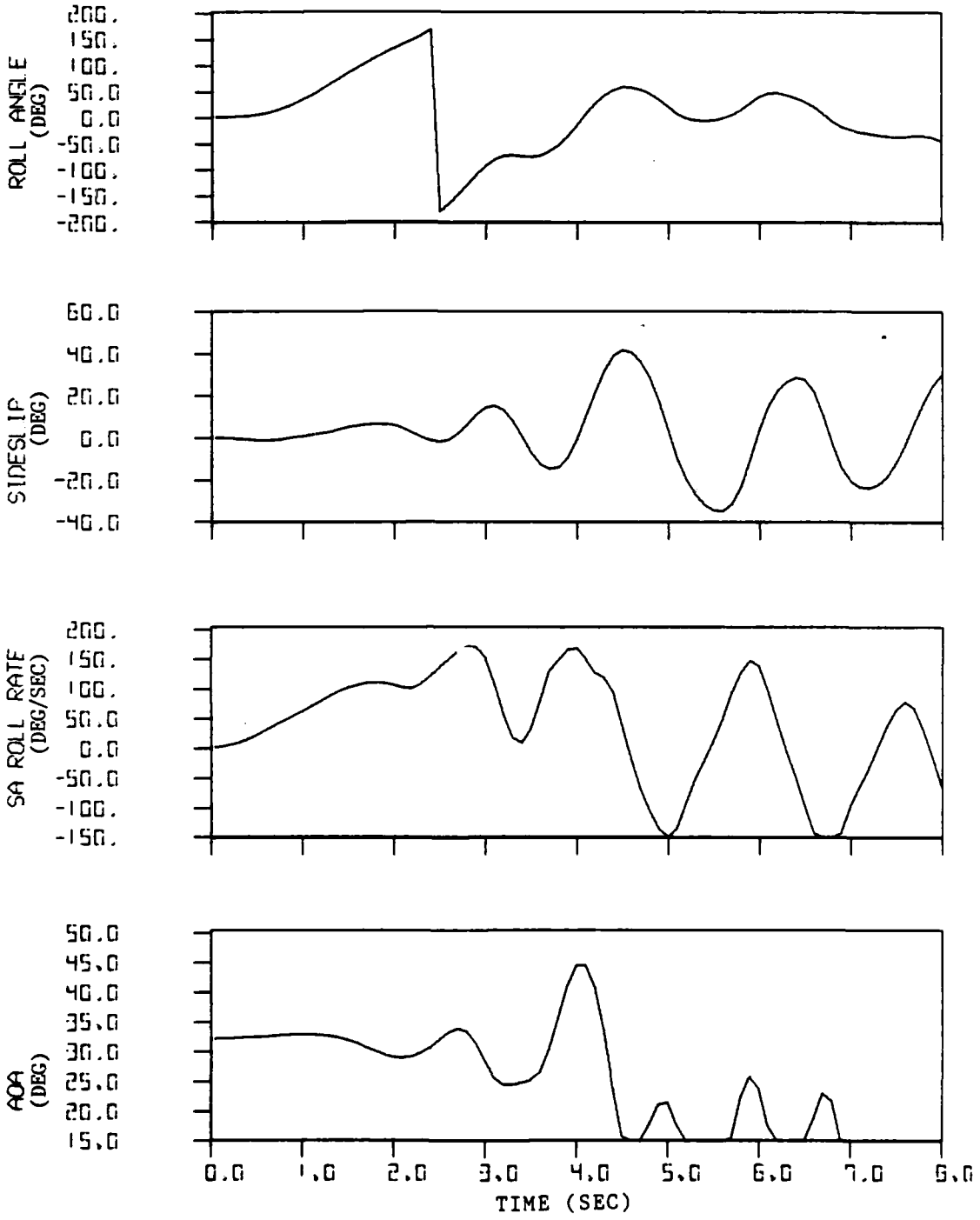

Figure 42. Maximum Roll at 5 g's Using Hinged Strakes Only With Sideslip Feedback (AOA = 32°, Strake Deflection = -45).

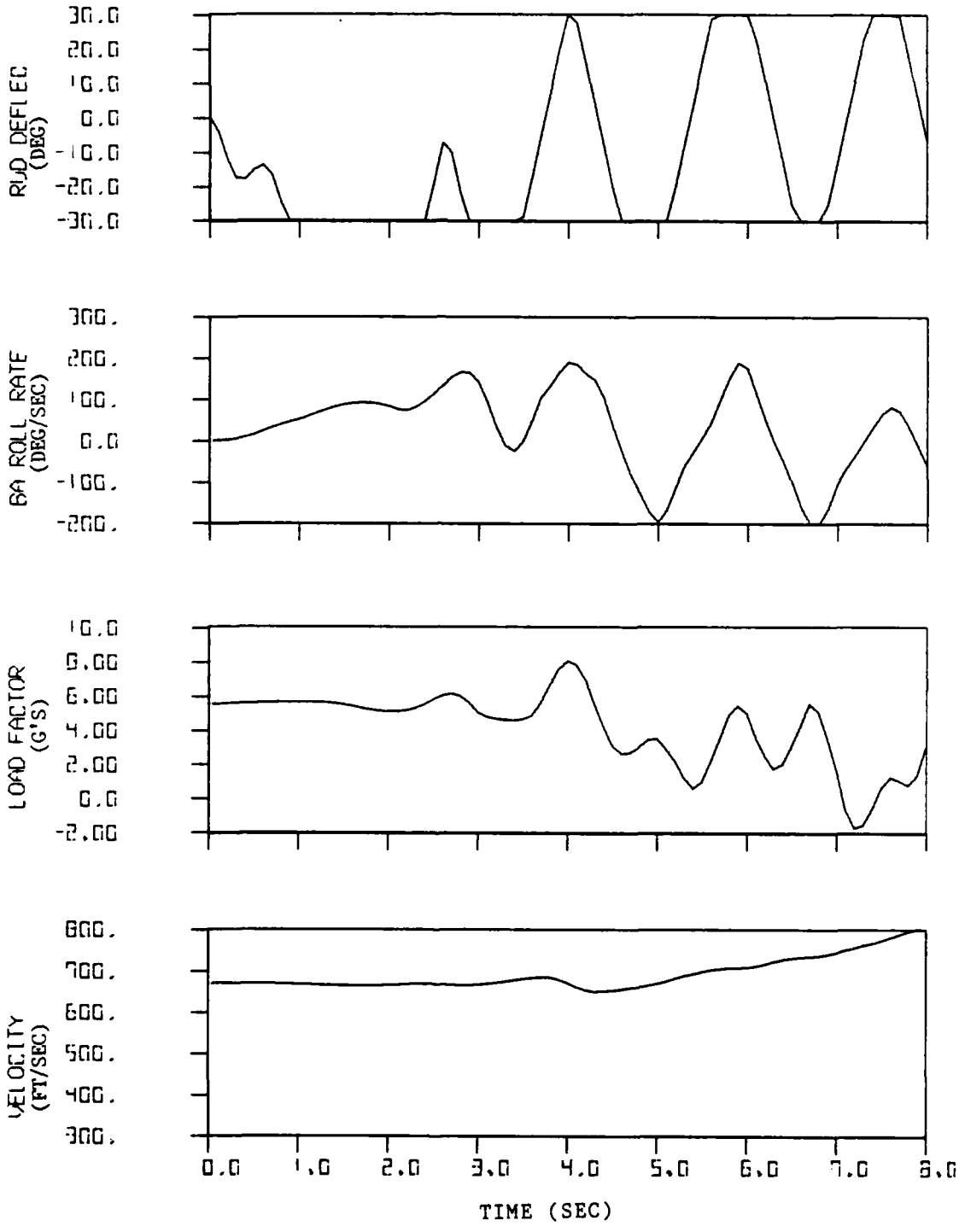

Figure 42. Concluded.

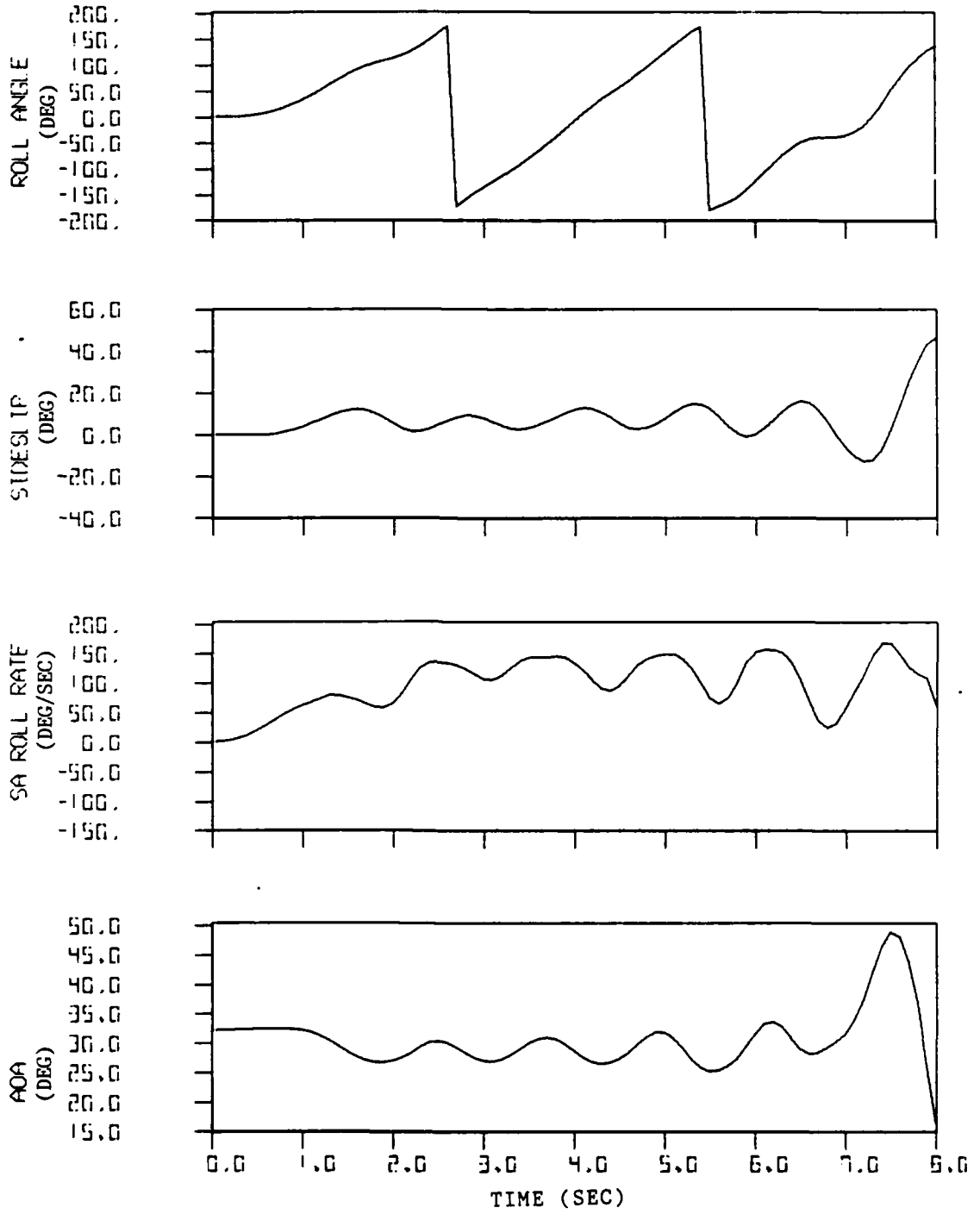

Figure 43. Maximum Roll at 5 g's Using Ailerons Only With Sideslip Feedback (AOA = 32°).

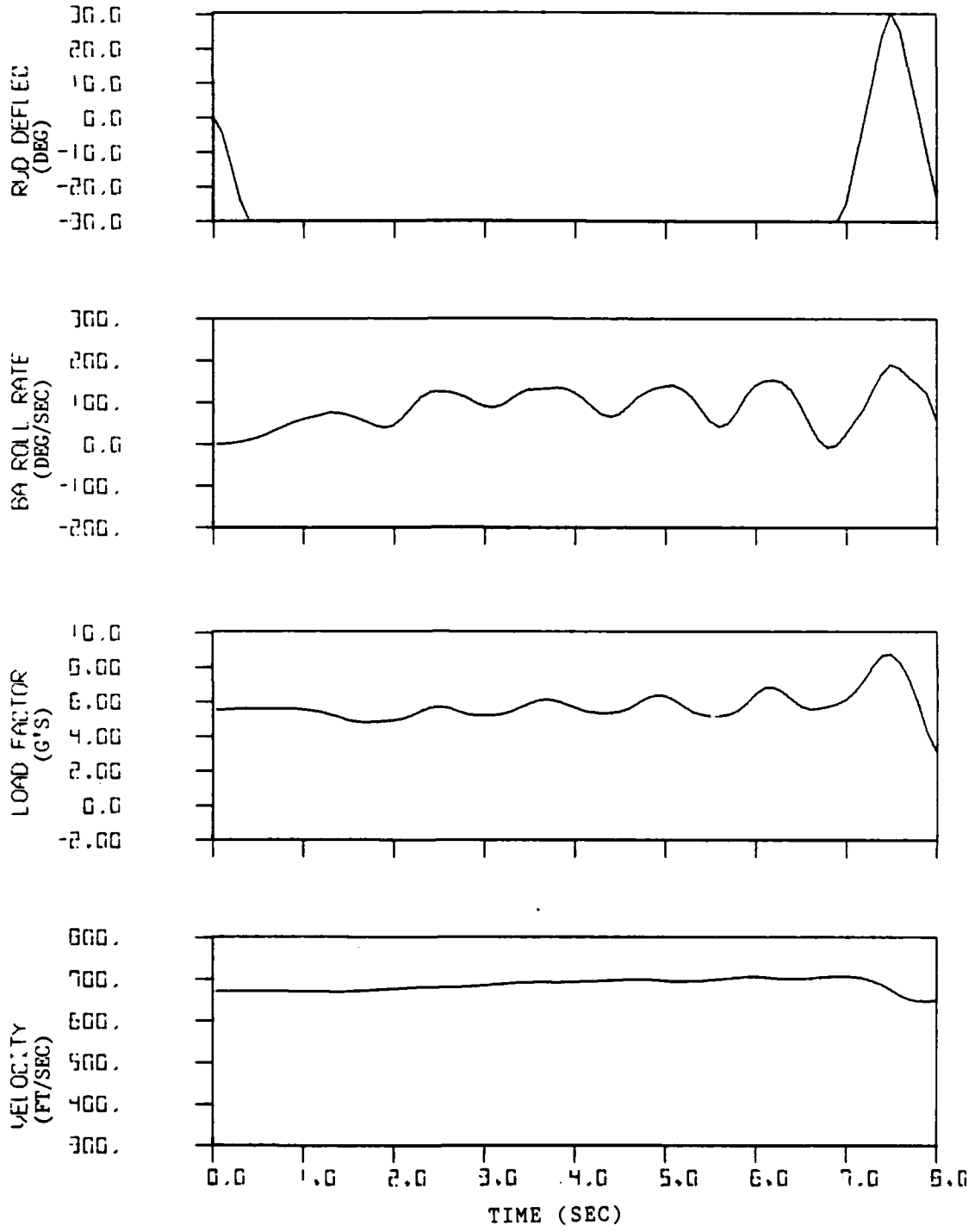

Figure 43. Concluded.

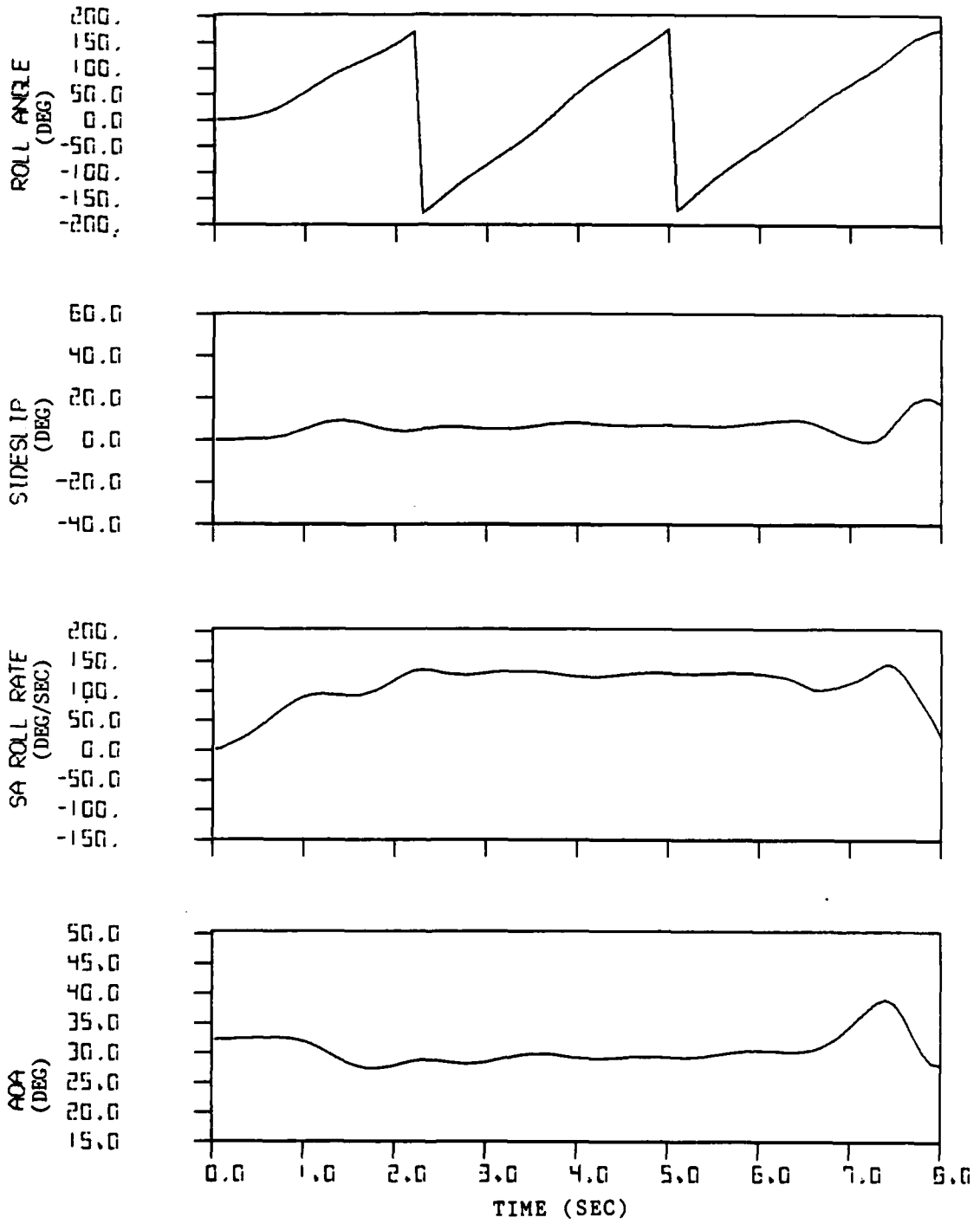

Figure 44. Maximum Roll at 5 g's Using Hinged Strakes and Ailerons With Sideslip Feedback (AOA = 32°, Strake Deflection = +30).

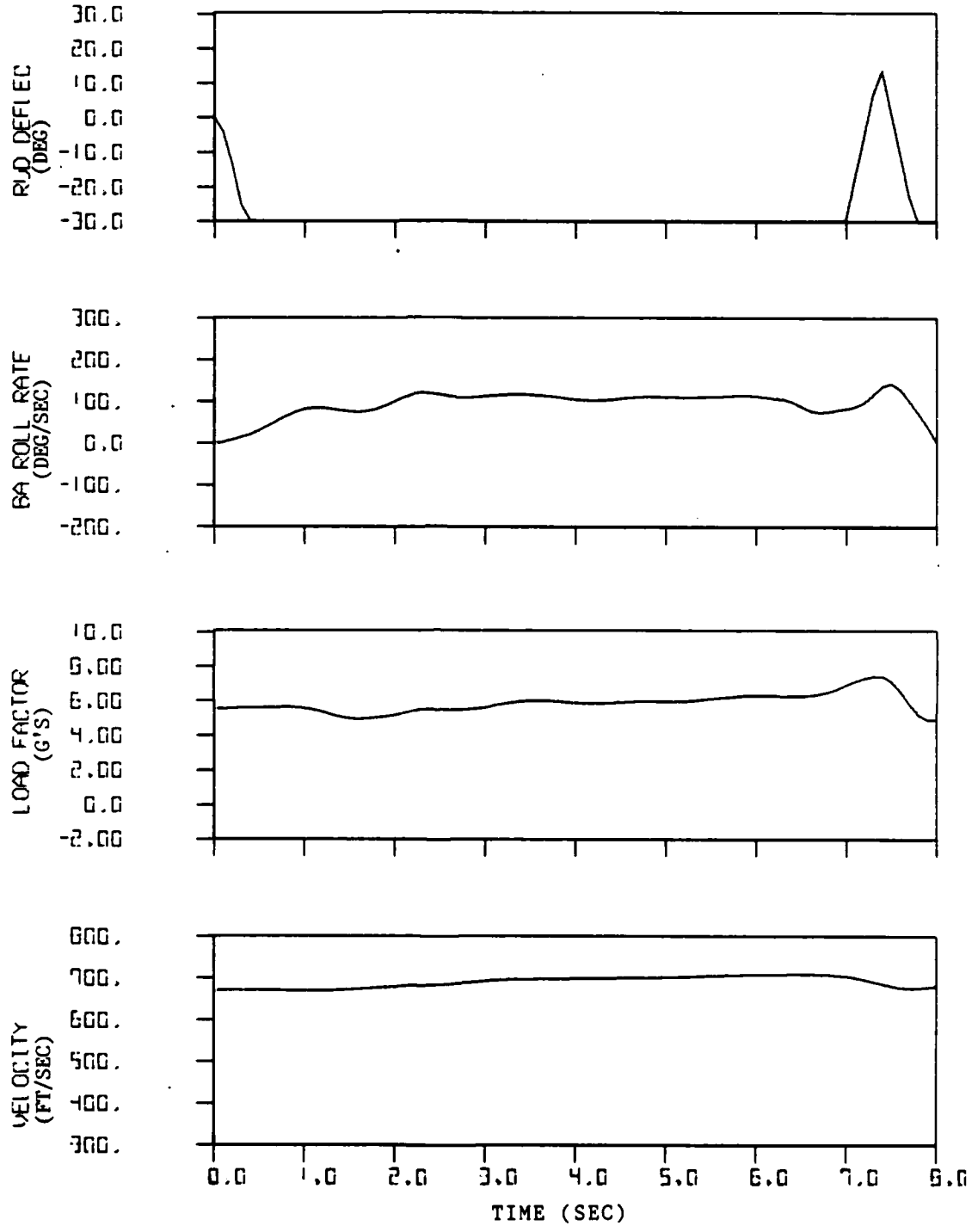

Figure 44. Concluded.

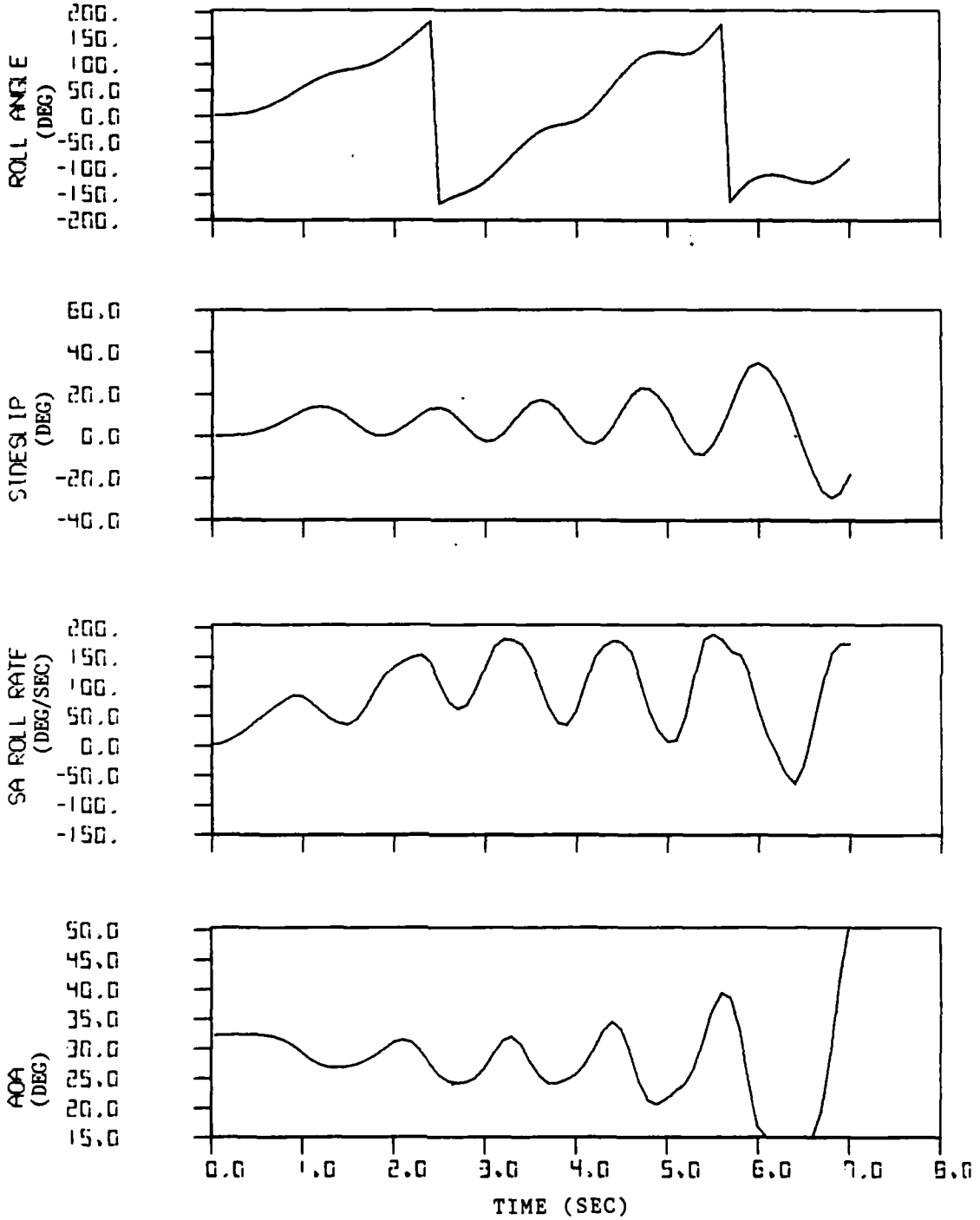

Figure 45. Maximum Roll at 5 g's Using Hinged Strakes and Ailerons With Sideslip Feedback (AOA = 32°, Strake Deflection = -45).

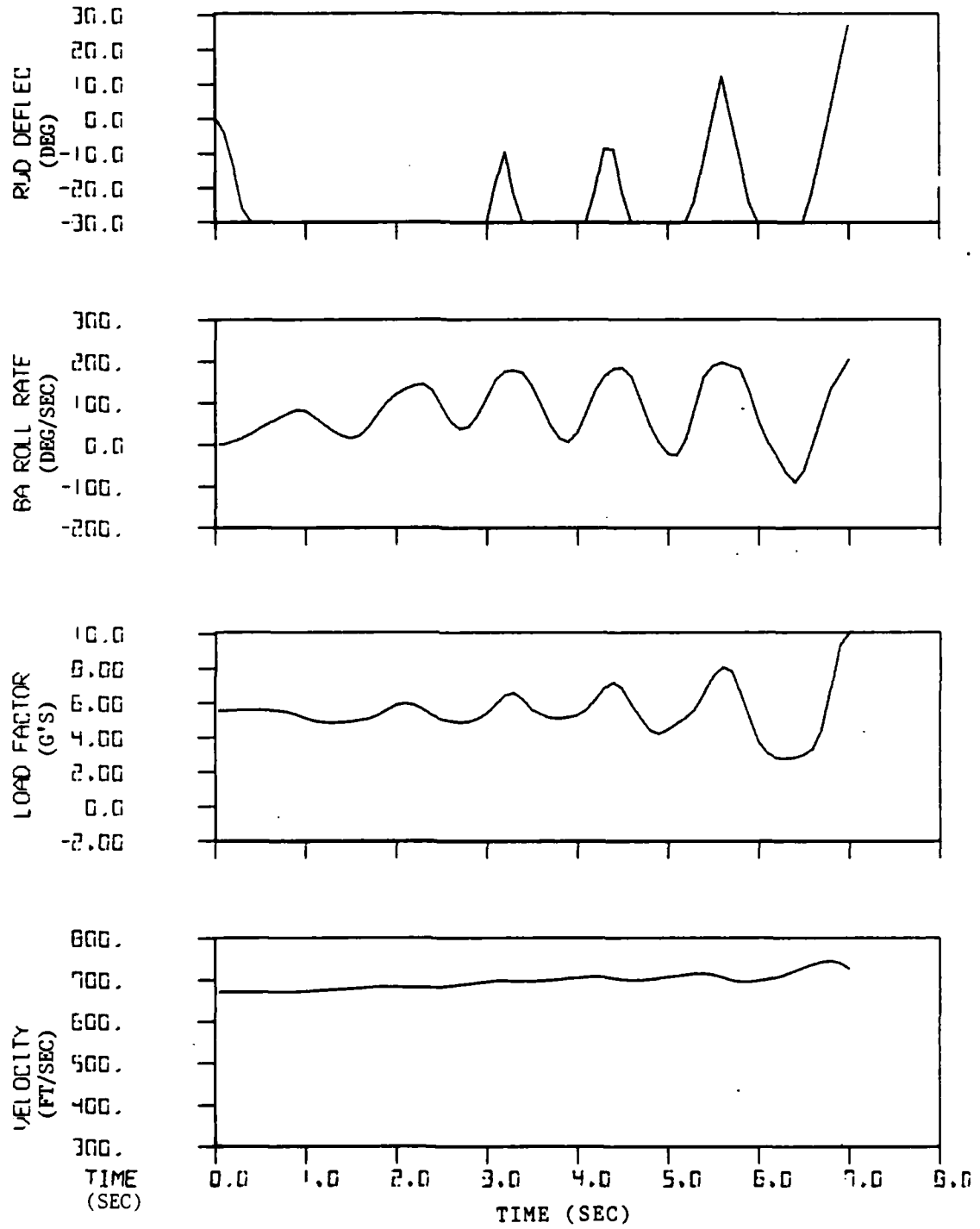

Figure 45. Concluded.

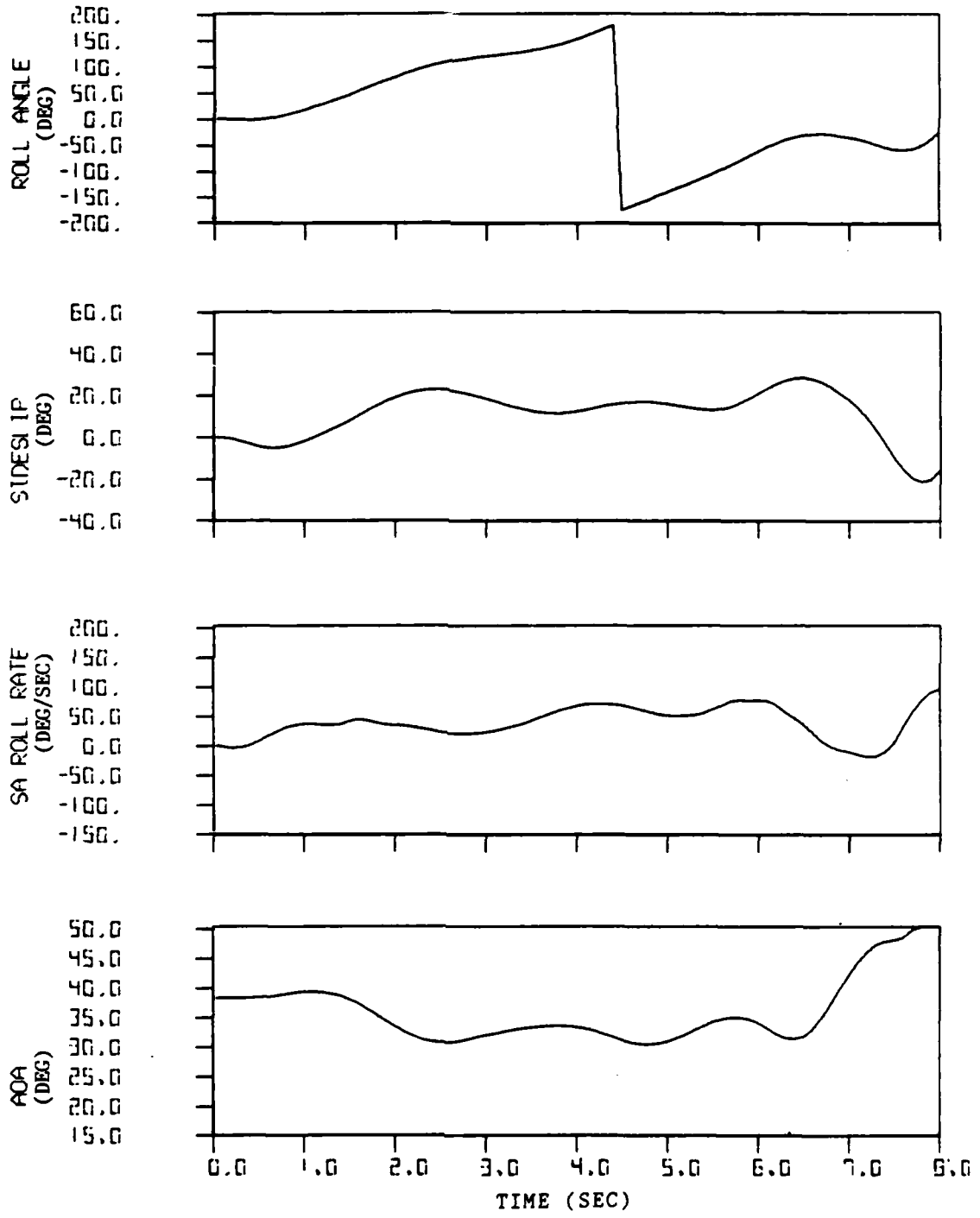

Figure 46. Maximum Roll at 5 g's Using Hinged Strakes Only With Sideslip Feedback (AOA = 38°, Strake Deflection = +30).

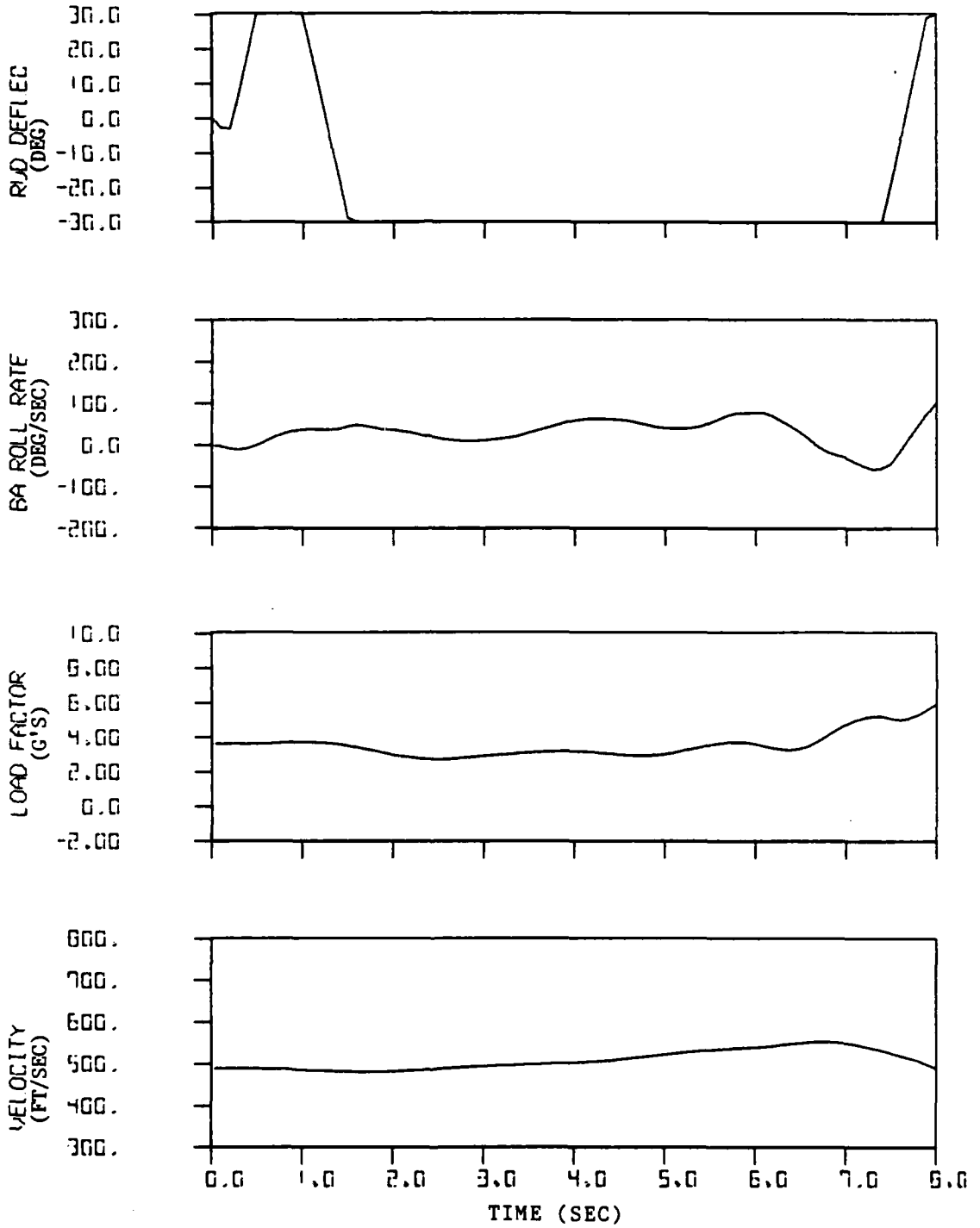

Figure 46. Concluded.

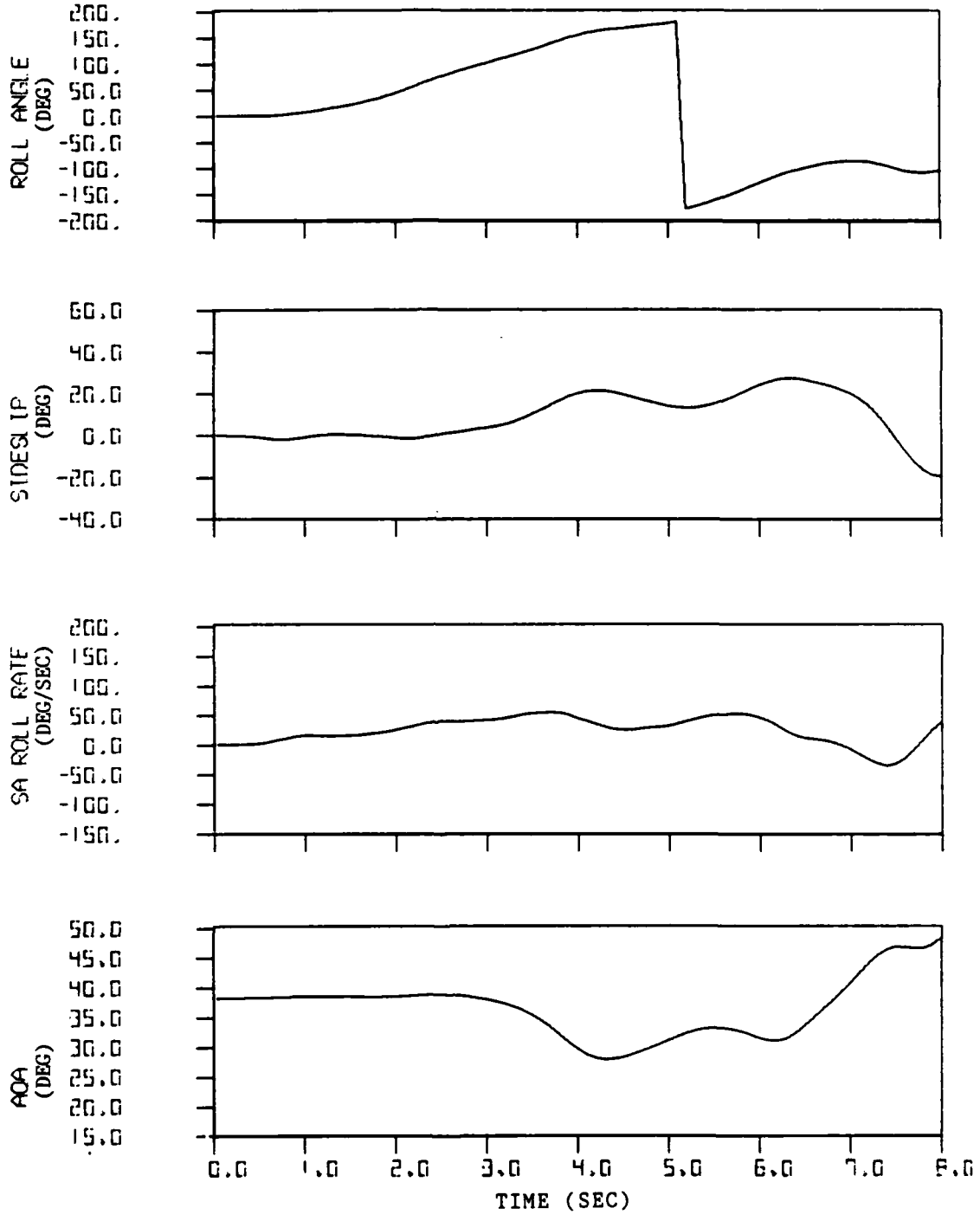

Figure 47. Maximum Roll at 5 g's Using Ailerons Only With Sideslip Feedback (AOA = 38°).

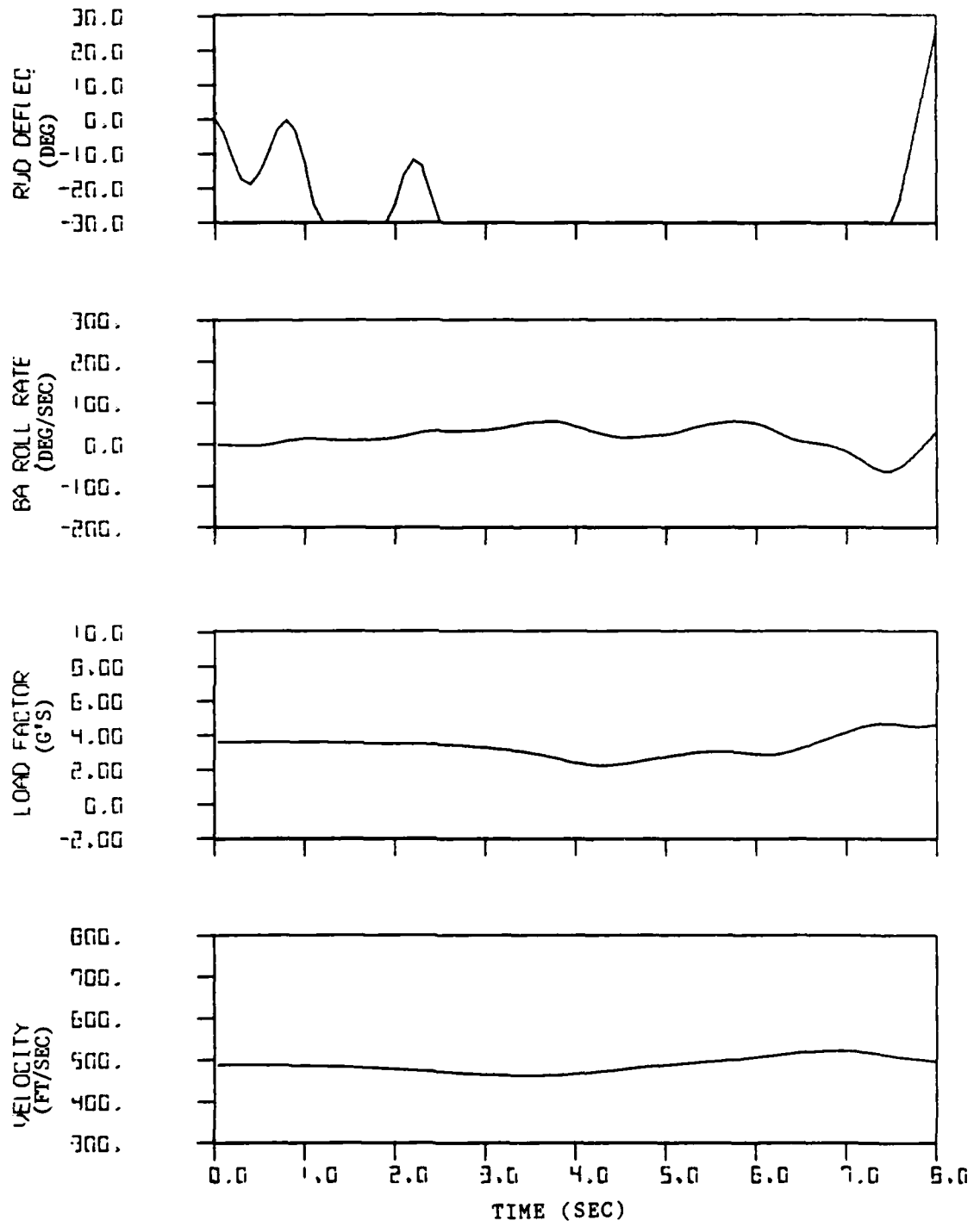

Figure 47. Concluded.

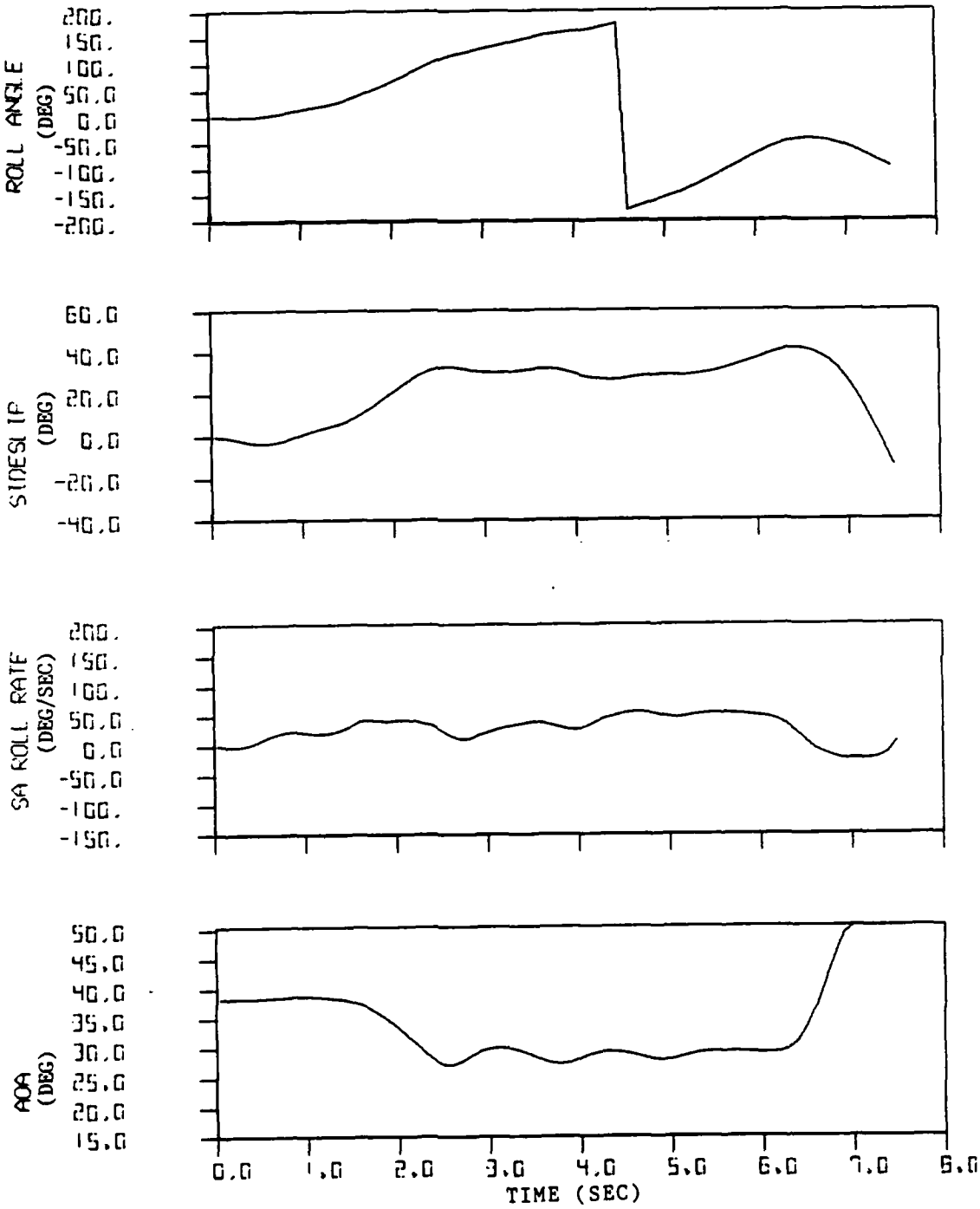

Figure 48. Maximum Roll at 5 g's Using Hinged Strakes and Ailerons With Sideslip Feedback (AOA = 38°, Strake Deflection = +30).

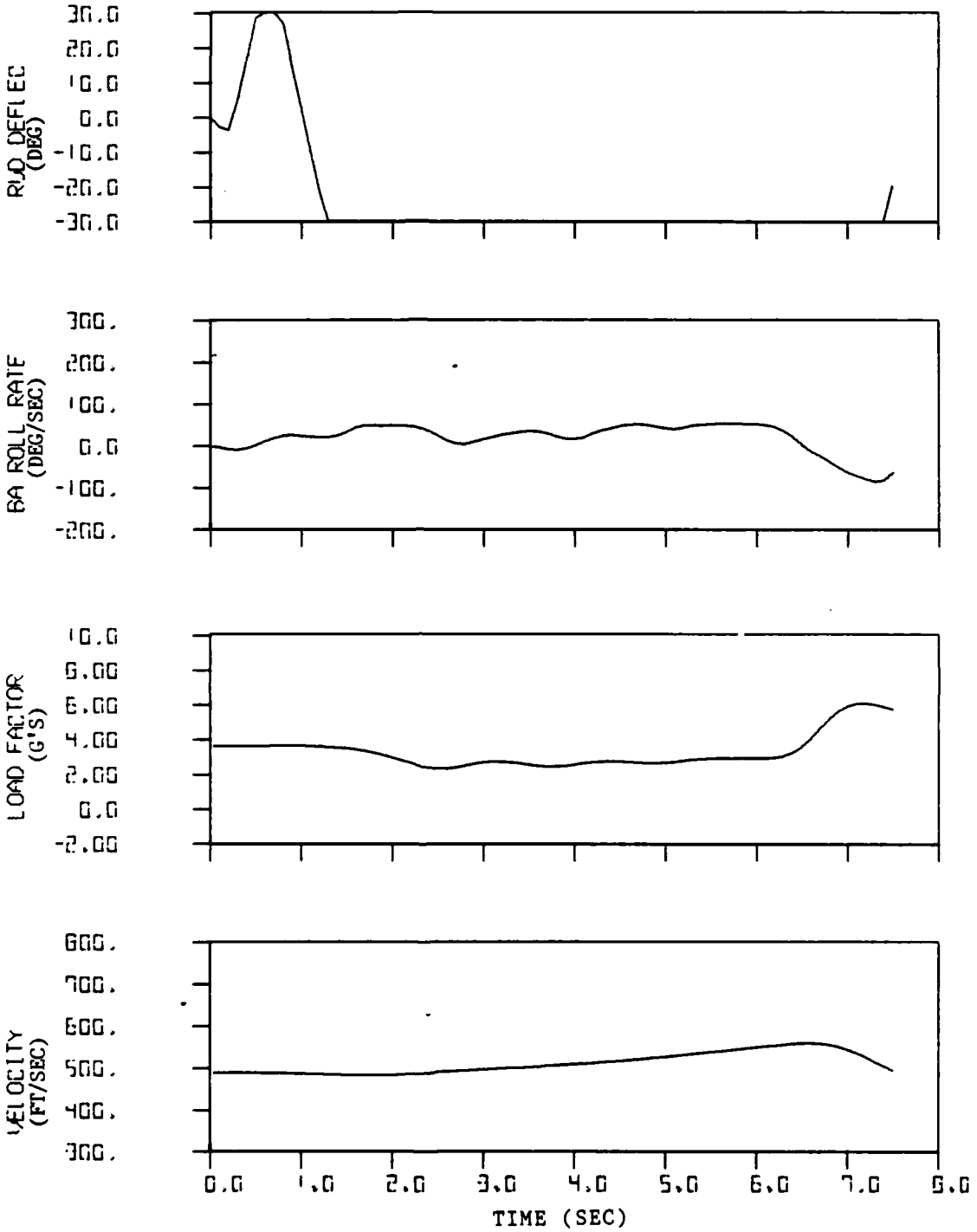

Figure 48. Concluded.

It should be noted that the effects of the strake and the ailerons have been added together linearly. The deflection of the strake will probably affect the aileron effectiveness, since the flow field over the wing is changed when the strake is deflected. This effect would probably change the results when the two controls are used together.

A common problem throughout the AOA range is a need for better regulation of sideslip and AOA. This difficulty suggests greater rudder and elevator authority. While the rudder authority would be harder to resolve, it should be noted that these simulations were done using data for a smaller elevator than is now in use. The larger elevator has improved high AOA flying qualities, and might reduce some of the AOA variations seen in these simulations. Short of a way to more closely control sideslip, a short term solution to the departure problem could be to limit the maximum angle of roll to something small, such as 130°.

Effects of Thrust Limiting

All of the previous simulations were run setting the initial thrust level to equal the thrust required. This thrust level usually resulted in a thrust level that was higher than was actually available. Using published curves[11] for thrust available for an installed F100 engine, the thrust was set to the maximum available as a function of Mach number and altitude. The thrust curve used was defined for flight at low AOA, so the thrust available could be further degraded by factors such as inlet stall. The results are shown in Figure 49. Rolling with both a +30° strake deflection and full ailerons at 32° AOA, the time required to roll to 180° is about the same as the case with no thrust limiting (Figure 44), but as the airspeed decreases, the FCS attempts to maintain the same load factor by increasing AOA, and the roll stops after 5 seconds as the AOA diverges.

Effects of Increased Yaw Damper Gain

The yaw channel contains a feedback path which feeds back $(r - p\alpha)$, which is an approximation of $\dot{\beta}$. This path is known as the stability axes yaw damper, and its purpose is to cause the aircraft to roll about the velocity vector instead of the longitudinal body axis. Since the

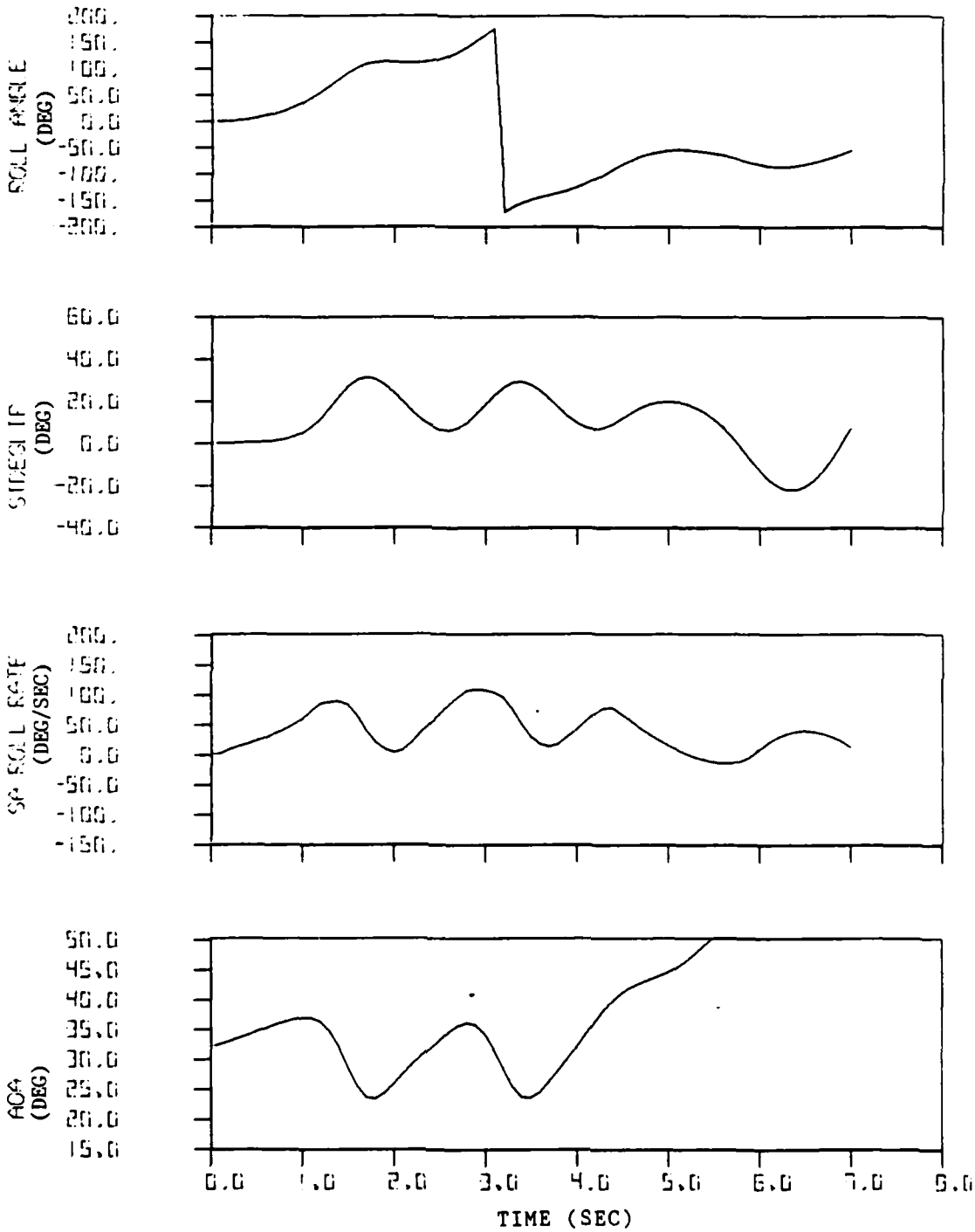

Figure 49. Maximum Roll at 5 g's Using Hinged Strakes and Ailerons With Sideslip Feedback and Thrust Limiting (AOA = 32°, Strake Deflection = +30).

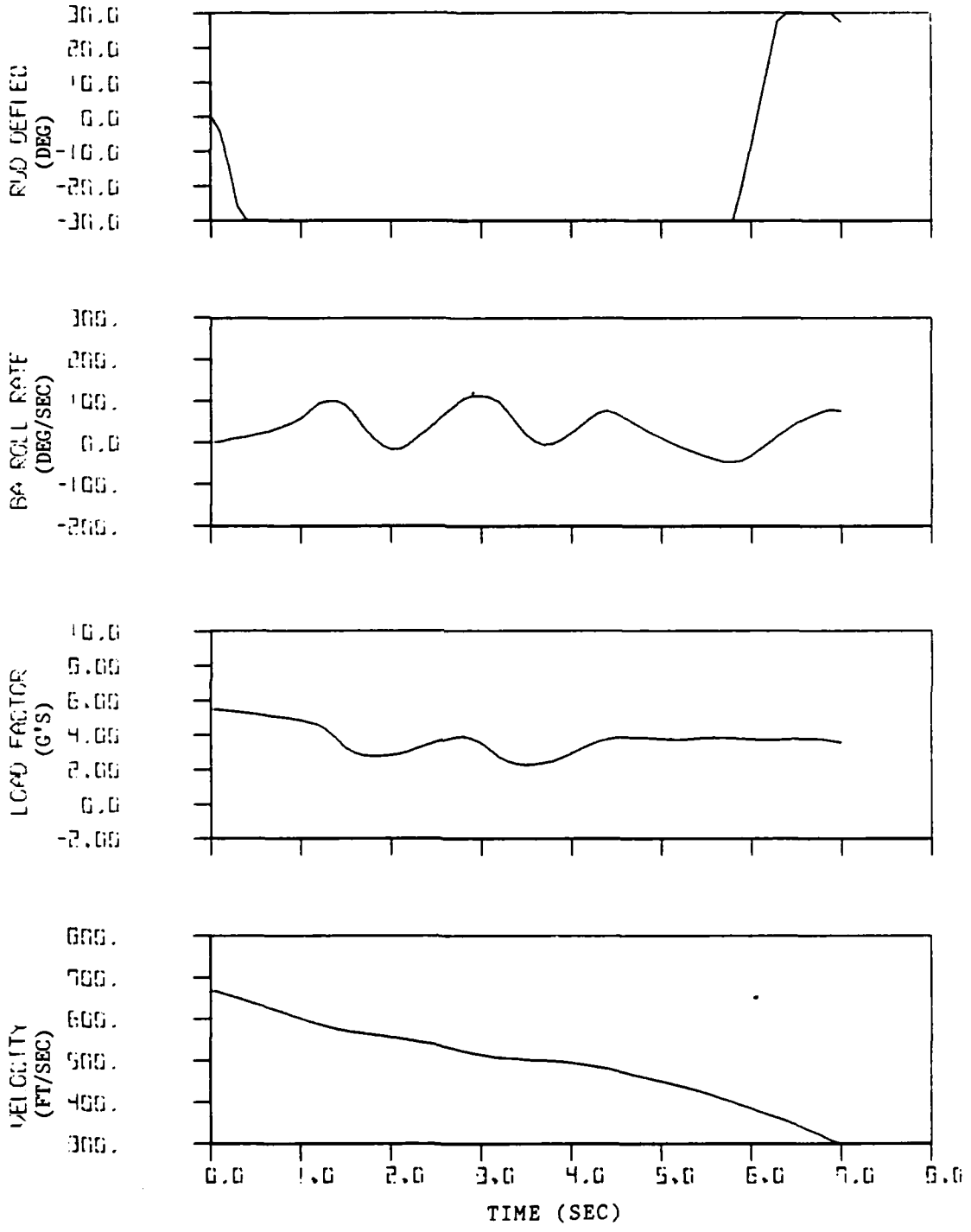

Figure 49. Concluded.

sideslip feedback used in the previous analysis is not currently available, another candidate solution to solving the problem of excessive sideslip was to increase the gain on the output of the stability axes yaw damper. It was hoped that by damping out the change in sideslip, the overall sideslip angle could be reduced.

Simulations were run using feedback gains of 15 and 30 at an AOA of 32° and load factors of 1 g and 5 g's commanded. The simulations at 1 g showed essentially no change from the cases using the strakes alone with no feedback modifications to the FCS, as seen previously in Figures 27-28. At 5 g's commanded load factor, both feedback gains tested gave essentially the same results. The case for the gain of 15 is shown in Figure 50. Using strakes alone, the aircraft takes over 4.5 seconds to roll to 180°. As seen in Figure 43, the ailerons alone rolled the aircraft to 180° in just over 2.5 seconds at this AOA. The roll shown in Figure 43 was done using beta feedback to the rudder, but since the yaw characteristics of the ailerons are well defined, the same result could be obtained by driving the rudder through the Aileron-Rudder Interconnect (ARI). Thus, the strakes in this case do not show an improvement over the performance available with the current ailerons. In addition, the rudder oscillates excessively, causing a disconcerting roll oscillation.

The combination of the positive strake deflection and ailerons was also run at both feedback gains. The case for the feedback gain of 15 is shown in Figure 51. Again, no significant improvement over the use of ailerons was seen, and a roll oscillation was still present. A major reason for no improvement is that AOA drops below 28° after about 1.5 seconds and the strake deflection is removed by the internal model. Therefore, the remainder of this roll was done with ailerons only.

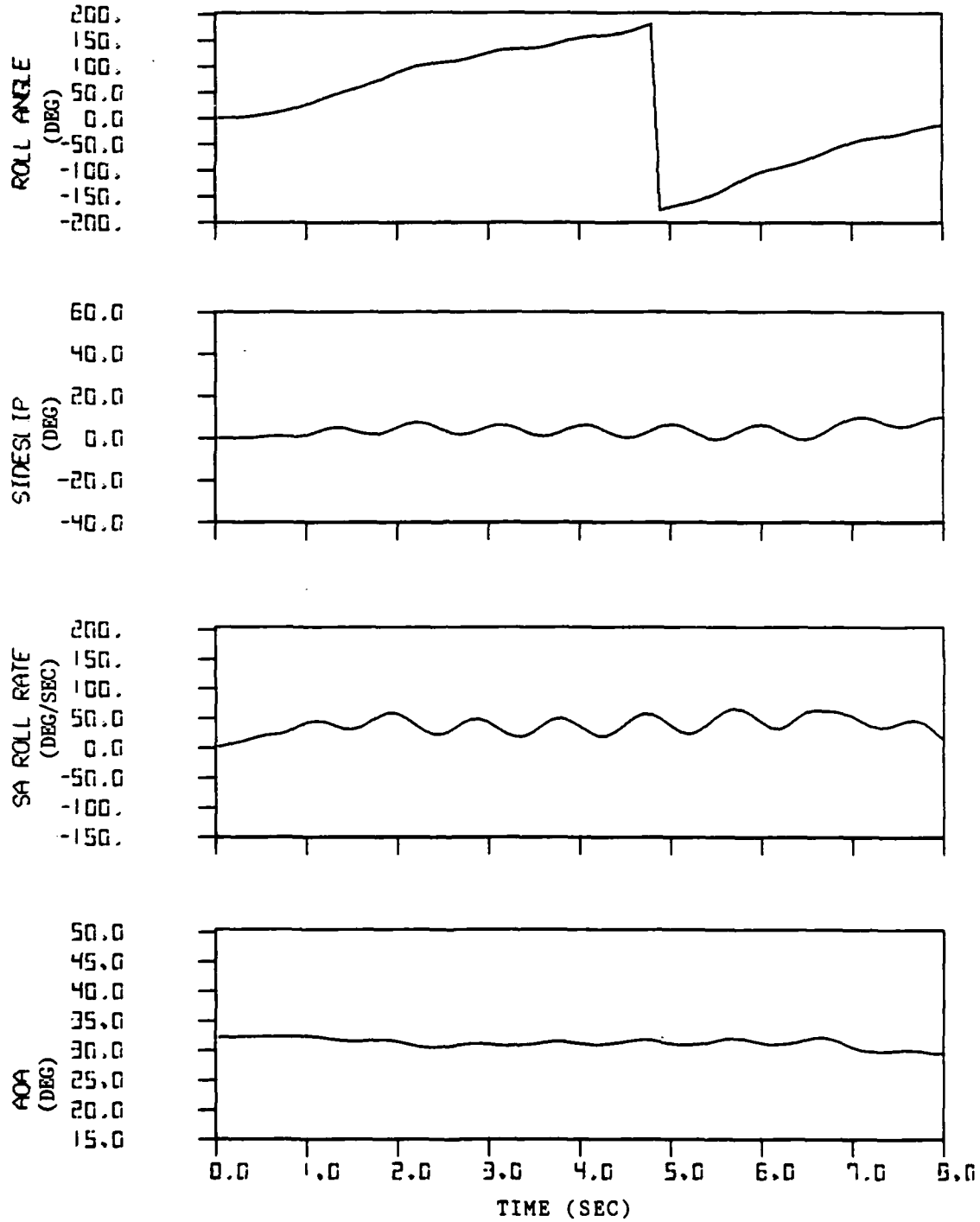

Figure 50. Maximum Roll at 5 G's Using Hinged Strakes Only With Increased Yaw Damper Gain (AOA = 32°, Strake Deflection = +30, Yaw Dampe- Gain = 15).

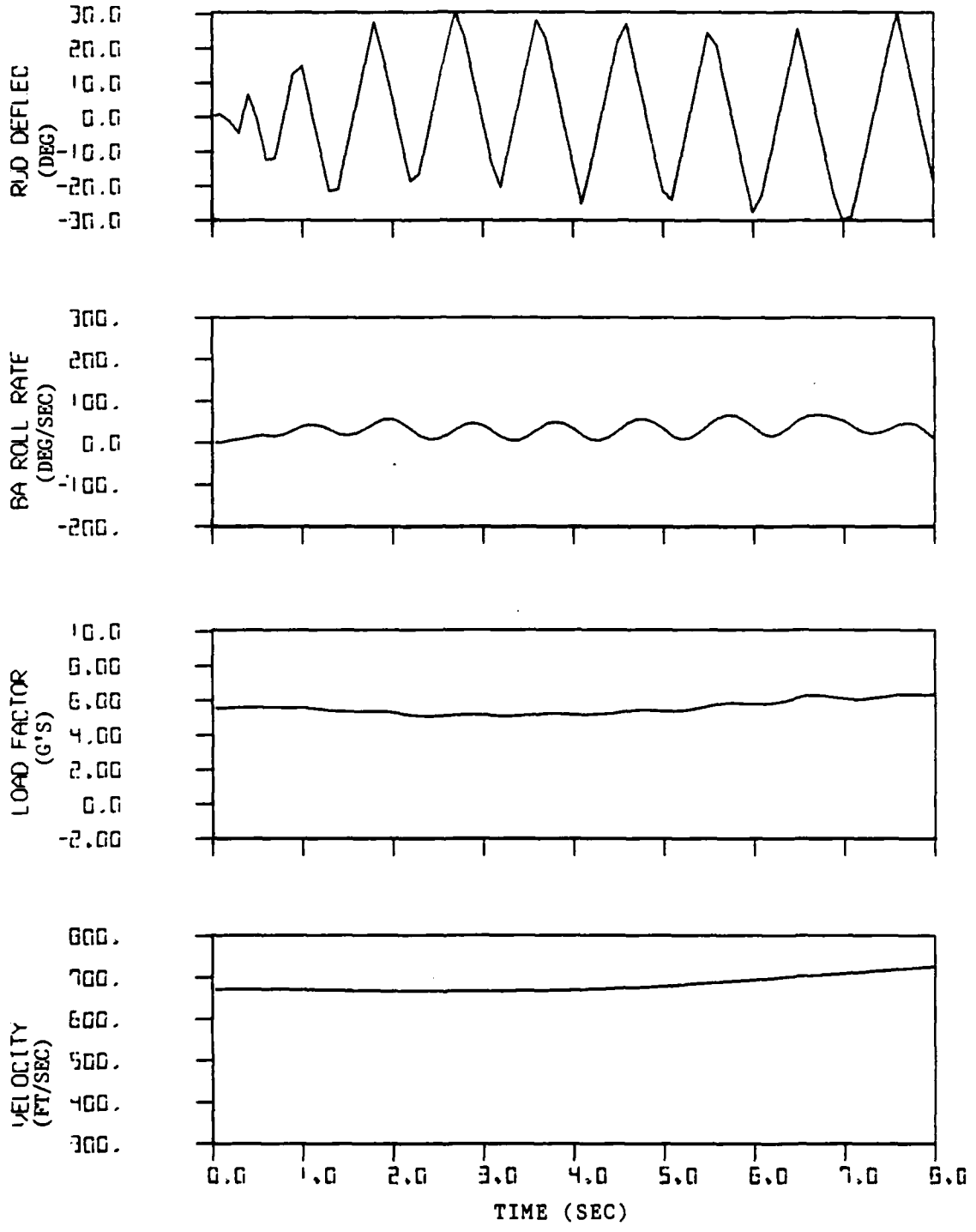

Figure 50. Concluded.

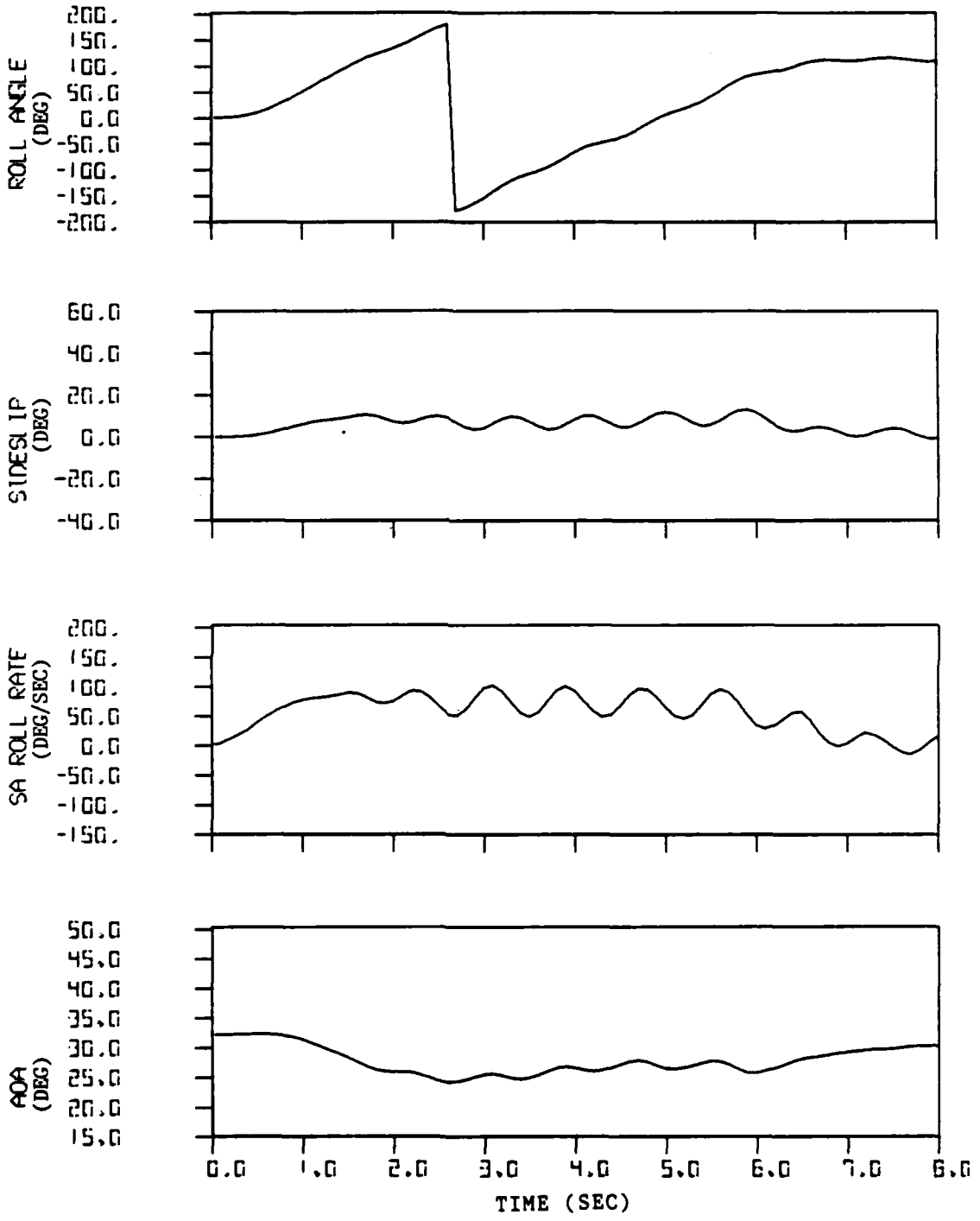

Figure 51. Maximum Roll at 5 G's Using Hinged Strakes And Ailerons With Increased Yaw Damper Gain (AOA = 32°, Strake Deflection = +30, Yaw Damper Gain = 15).

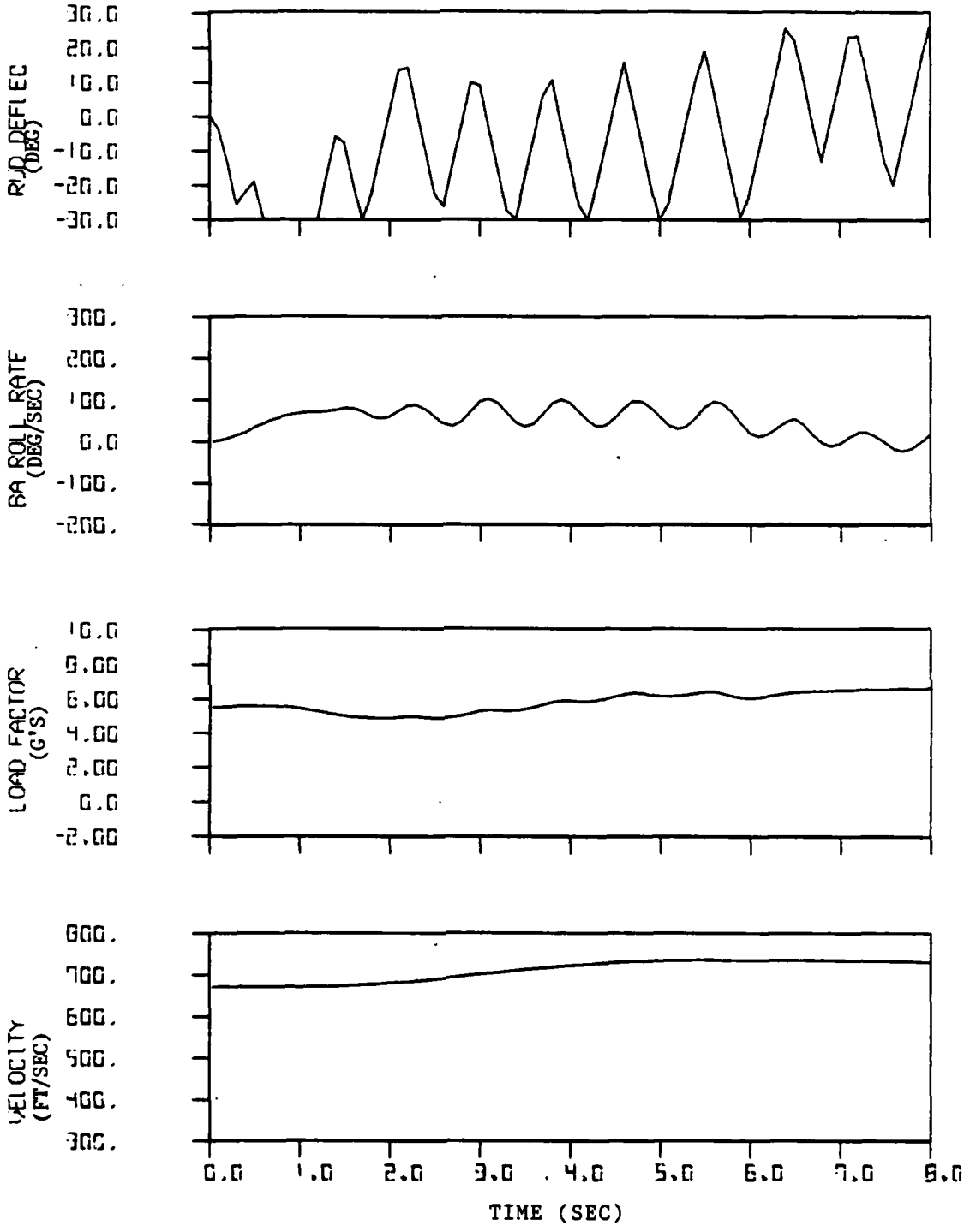

Figure 51. Concluded.

COMPARISON TO DIFFERENTIAL LEADING EDGE FLAPS

In order to gain a better appreciation for the usefulness of the hinged strakes, they were briefly compared against differential leading edge flap (DLEF) deflections for roll control as studied by Stout[5]. For this comparison, the model used in Reference 5 was upgraded to allow simulations at higher load factors. Two simulations were ran at AOAs of 32^{o} and 34^{o} for a 5 g commanded load factor. The results for 32^{o} AOA are shown in Figure 52.

Comparing Figures 52 and 44, the DLEFs gave a comparable roll, having roughly the same roll rates. The DLEFs currently show four advantages over the hinged strakes. First, the rudder is not saturated. Second, roll oscillations are minimal. Third, the recovery at the end of the roll is smoother, showing no tendencies toward departure. Fourth, the rudder is connected directly through the ARI, and does not require any beta feedback. These advantages of the DLEFs are not reasons to abandon the hinged strake concept altogether. The current data base for DLEFs is much smaller than that for hinged strakes, particularly with regards to behavior as a function of sideslip (all of the current DLEF data was taken at zero sideslip). Further investigation should be done into possible combined effects of various combinations of hinged strakes, DLEFs, and ailerons.

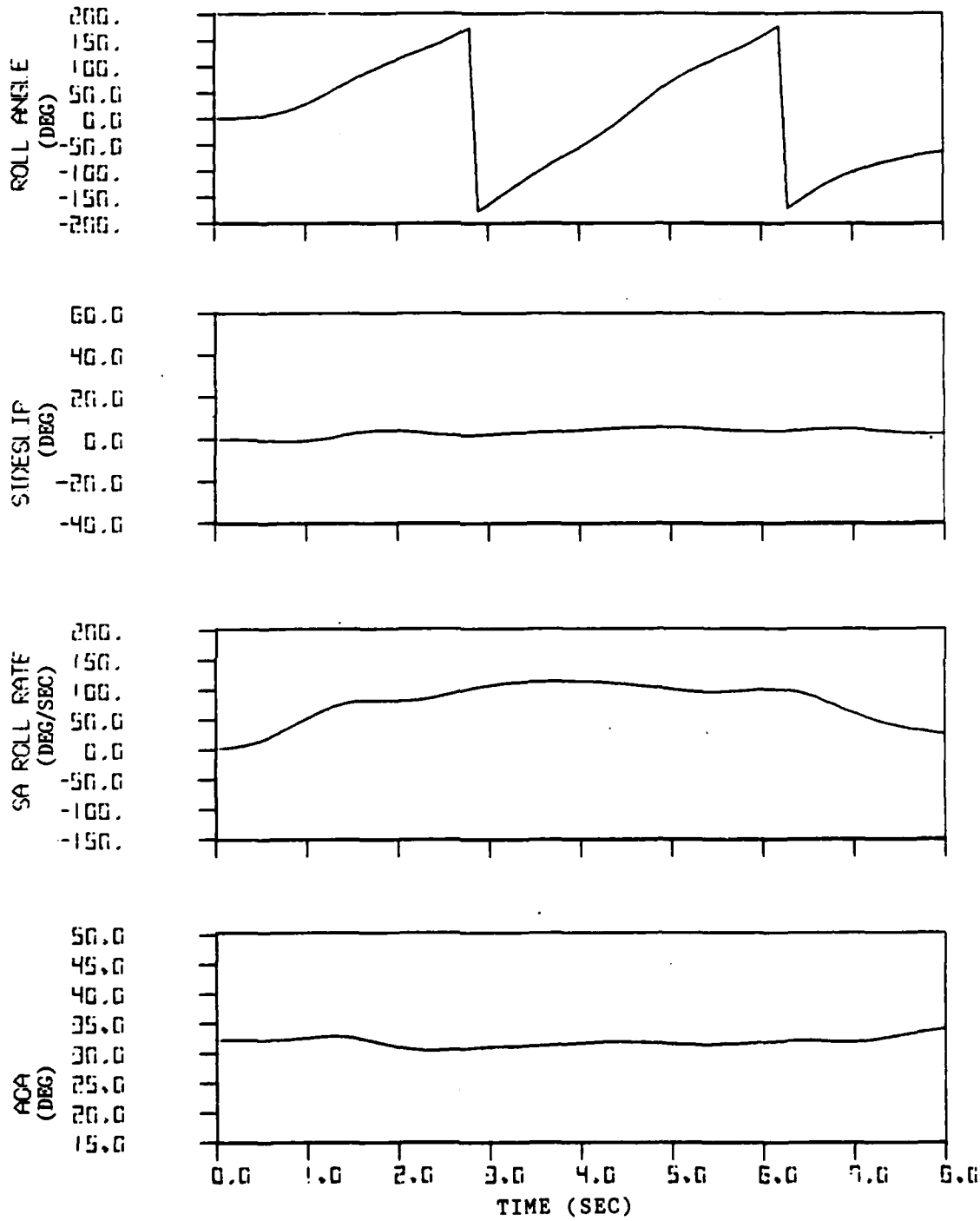

Figure 52, Maximum Roll at 5 G's Using Differential Leading Edge Flaps (AOA = 32°, Flap Deflection = 10)

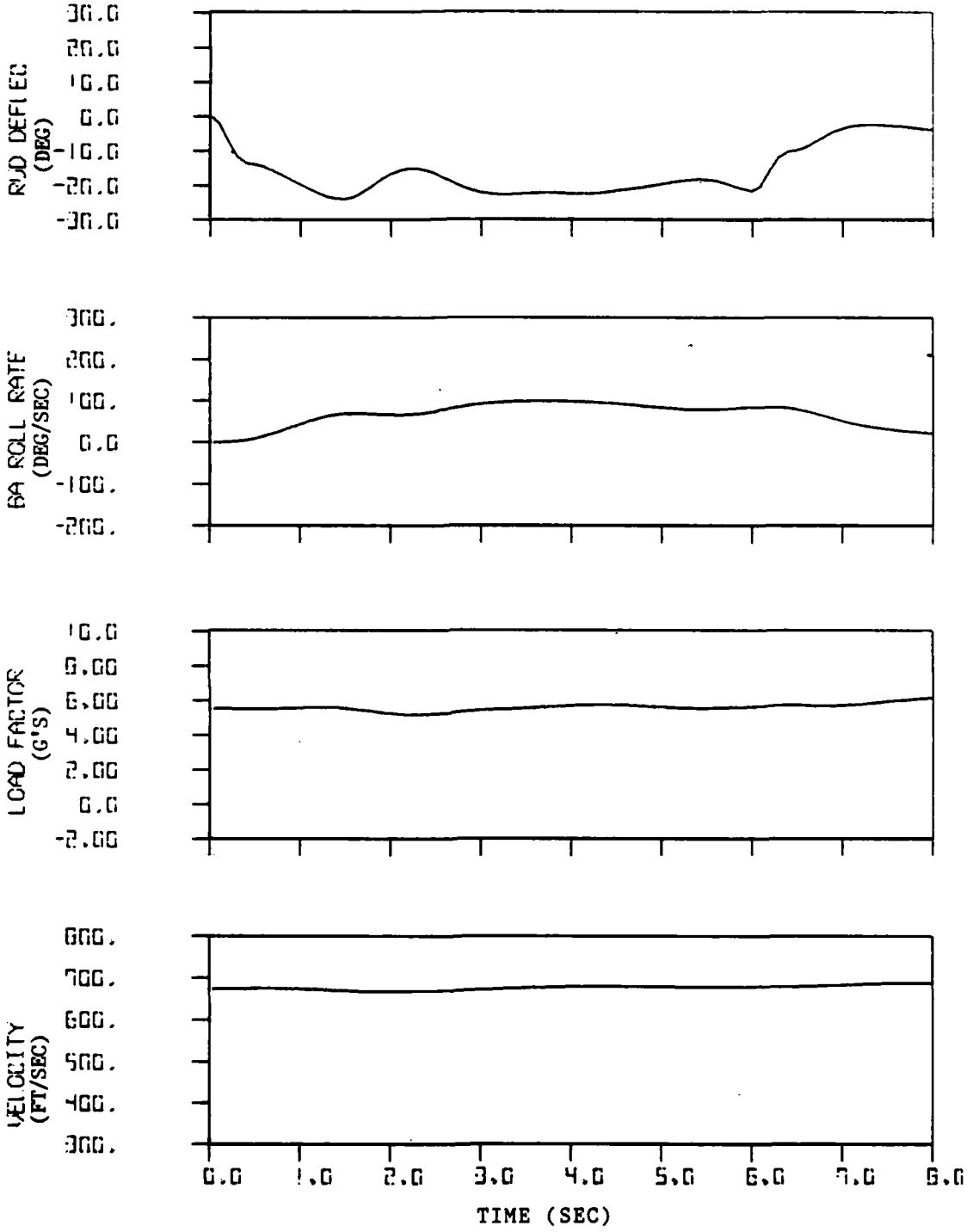

Figure 52. Concluded

CONCLUSIONS AND RECOMMENDATIONS

Conclusions

1. Based on comparisons with published data, the results of this test were consistent with previous tests.
2. The changes in the forces and moments due to dihedral strake deflection are different from the changes due to anhedral strake deflection. In both cases, the changes in the forces and moments are complex, nonlinear functions of AOA, sideslip, and strake deflection.
3. The anhedral-dihedral configuration, deflecting one strake upward and the other strake downward, showed no noticeable improvement over the asymmetric case of deflecting one strake upward.
4. In order to maximize rolling performance at high AOA, the sideslip must be kept small to prevent dihedral effect (C_{ℓ_β}) from inhibiting the roll rate.
5. Using direct sideslip feedback to control the sideslip angle, a gain of 25 was chosen based on maximum roll angle, minimum sideslip, and maximum roll rate, and roll recovery in 1 g flight. However, a direct reading of sideslip at high AOAs is not currently available.
6. The best roll performance was seen using $+30^{\circ}$ strakes combined with the ailerons at AOAs less than 38°, and using $+30^{\circ}$ strakes only above 38°. Both of these cases were using beta feedback to control sideslip.
7. The -45° strake deflection produced more yawing moment than the $+30^{\circ}$ strake deflection, causing larger sideslip excursions.
8. In all cases, the aircraft was very prone to departure when the control input was removed. This was due to large variations in sideslip and AOA resulting from degraded stability at high AOA. If the sideslip and AOA cannot be more closely controlled, a possible solution to this problem is to limit the amount of roll allowed.
9. Limiting the thrust level to thrust available while commanding a constant load factor causes the aircraft to decelerate during the maneuver and results in a loss of rudder and elevator effectiveness. The end result is early departure.

10. Increasing the gain on the stability axes yaw damper does not improve the roll performance over that which is currently available, and serves to increase roll oscillations.
11. Based on the current data base, differential leading edge flaps alone appear to give better performance as a roll control device than the hinged strakes alone.

Recommendations

Further tests should be conducted to investigate the following areas:

1. Investigate the effects of strake area to see if a larger strake will produce an increase in rolling moment without a large increase in yawing moment.
2. Investigate the effects of different configurations, such as store loadings, on the reactions due to the strakes.
3. Investigate the possible combined effects of combining hinged strakes, differential leading edge flaps, and/or ailerons as roll control devices.
4. Conduct tests to fill in the current hinged strake data base. The primary areas of concern would be data for smaller increments in sideslip and testing for dynamic derivatives.
5. Investigate other possible FCS mechanizations for using the hinged strakes.
6. Conduct tests at other dynamic pressures to check for further Reynold's Number effects.
7. Investige possibilities for sideslip sensors, such as the Inertial Navigation System, vanes, or multi-holed probes.

REFERENCES

1. Polhamus, E. C., "Application of the Leading-Edge-Suction Analogy of Vortex Lift to the Drag Due to Lift of Sharp-Edge Delta Wings," NASA TN D-4739, August 1968.

2. Luckring, J. M., "Aerodynamics of Strake-Wing Interactions," Journal of Aircraft, Vol. 16, Nov. 1979, pp. 756-762.

3. Frink, N. T. and Lamar, J. E., "Analysis of Strake Vortex Breakdown Characteristics in Relation to Design Features," Journal of Aircraft, Vol. 18, Apr. 1981, pp. 252-258.

4. Rao, D. M. and Huffman, J. K., "Hinged Strakes for Enhanced Maneuverablity at High Angles of Attack," Journal of Aircraft, Vol. 19, Apr. 1982, pp. 278-282.

5. Stout, L. J., "Control Authority of Unconventional Control Surface Deflections on a Fighter Aircraft," Masters Thesis, Texas A&M University, May 1985.

6. Low Speed Wind Tunnel Facility Handbook, Aerospace Engineering Division, Texas Engineering Experiment Station, The Texas A&M University System, College Station, TX., Jan. 1982.

7. Pope, A., and Harper, J. J., Low Speed Wind Tunnel Testing, John Wiley and Sons, Inc., New York, 1966.

8. Ward, D. T. and Stout, L. J., "Wind Tunnel Test of Fighter Aircraft Control Authority at High Angles of Attack," TEES Report No. TR-8321, Feb. 1984.

9. "Application of the EASY Dynamic Analysis Program to Aircraft Environmental Control Systems Reference Guide," AFFDL-TR-77-102, Oct. 1977.

10. Pape, J. K., and Garland, M. P., "F-16A/B Flying Qualities Full Scale Development Test And Evaluation," AFFTC-TR-79-10, Sep. 1979.

11. Nicolai, L. M., Fundamentals of Aircraft Design, METS, Inc., San Jose, CA, 1975.

APPENDIX A

SUMMARY OF CONSTANTS

Duct Exit Area ($M \leq 1.20$)	A_e =	3.0000 in^2
Fuselage Cavity Area (M = 1.20 windshield)	A_c =	3.0089 in^2
Reference Wing Span	b =	23.1862 in.
Reference Wing Mean Aerodynamic Chord	$\bar{c}$ =	8.7490 in.
Reference Wing Area (280.0 ft , full scale)	S =	1.2444 ft^2
Balance Incidence Angle	i_b =	-0^o 57'
Reference Inlet Area	A_i =	3.6311 in^2
Moment Reference Center (.35$\bar{c}$) Fuselage Sta.		20.773 in.
Waterline		6.067 in.
Planform Area (Model)		2.263 ft^2
Frontal Area (including inlet)		.187 ft^2
Body Volume		.214 ft^3
Lifting Surface Volume		.015 ft^3
Horizontal Tail Area (movable, 2 panels)		.189 ft^2
0.25$\bar{c}$ (wing) to 0.25$\bar{c}$ (h. tail)		1.044 ft
Horizontal effectiveness, $\frac{dC_m}{di_t}$ (per degree)		-.0113/deg
Moment Transfer Distances $\bar{u}$		-.1172 ft.
$\bar{h}$		.023 ft.
$\bar{v}$		.000 ft.

APPENDIX B

RUN SCHEDULE

RUN	CONFIGURATION	Q	α	β	δ_{LS}	δ_{RS}	COMMENTS
1	BASELINE	40	A	0	0	0	A=-4 -> 20 Delta= 4
2	I	60	A	0	0	0	20 -> 68 Delta= 2
3	I	80	B	0	0	0	B=-4 -> 20 Delta= 4
4	I	80	A	5	0	0	20 -> 68 Delta= 2
5	I	80	A	10	0	0	68 -> 20 Delta=-2
6	I	80	A	15	0	0	
7	I	80	A	-15	0	0	
8	I	80	A	-10	0	0	
9	ASYMMETRIC	60	A	-15	45	-45	
10	BASELINE	60	A	-15	0	0	
11	I	60	A	-10	0	0	
12	I	60	A	-5	0	0	
13	I	60	A	-0	0	0	
14	I	60	A	5	0	0	
15	I	60	A	10	0	0	
16	I	60	A	15	0	0	
17	ASYMMETRIC	60	A	15	0	-45	
18	I	60	A	10	0	-45	
19	I	60	A	5	0	-45	
20	I	60	A	0	0	-45	
21	I	60	A	-5	0	-45	
22	I	60	A	-10	0	-45	
23	I	60	A	-15	0	-45	
24	I	60	A	-15	0	-30	
25	I	60	A	-10	0	-30	
26	I	60	A	-5	0	-30	
27	I	60	A	0	0	-30	
28	I	60	A	5	0	-30	
29	I	60	A	10	0	-30	
30	I	60	A	15	0	-30	
31	I	60	A	15	0	-15	
32	I	60	A	10	0	-15	
33	I	60	A	5	0	-15	
34	I	60	A	0	0	-15	
35	I	60	A	-5	0	-15	
36	I	60	A	-10	0	-15	
37	I	60	A	-15	0	-15	
38	I	60	A	-15	0	15	
39	I	60	A	-10	0	15	
40	I	60	A	-5	0	15	
							TEST 8430
41	I	60	A	0	0	-15	Rpt #34,correct by 0.2
42	I	60	A	0	0	-15	correct possible foul
43	I	60	A	0	0	-15	correct alpha by .19°
44	I	60	A	0	0	-15	
45	I	60	A	0	0	-15	rpt #44 for repeatability
46	BASELINE	60	A	0	0	0	Baseline repeat #2

47	I	60	A	0	0	0	add trips
48	ASYMMETRIC	60	A	0	0	15	
49	I	60	A	5	0	15	
50	I	60	A	10	0	15	
51	I	60	A	15	0	15	
52	I	60	A	15	0	30	
53	ASYMMETRIC	60	A	10	0	30	
54	I	60	A	5	0	30	
55	I	60	A	0	0	30	
56	AnDi	60	A	0	-15	30	
57	I	60	A	5	-15	30	
58	I	60	A	10	-15	30	
59	I	60	A	10	-30	30	
60	I	60	A	5	-30	30	
61	I	60	A	0	-30	30	
62	I	60	A	0	-30	15	
63	I	60	A	5	-30	15	
64	I	60	A	10	-30	15	
65	I	60	A	-10	-30	15	
66	I	60	A	-5	-30	15	
67	I	60	A	-0	-30	15	clay missing left strake
68	I	60	A	-0	-30	30	
69	I	60	A	-5	-30	30	
70	I	60	A	-10	-30	30	
71	ASYMMETRIC	60	A	-0	0	30	
72	I	60	A	-5	0	30	
73	I	60	A	-10	0	30	
74	I	60	A	-15	0	30	
75	AnDi	60	A	-0	-15	30	
76	I	60	A	-5	-15	30	
77	I	60	A	-10	-15	30	

----EOT----

APPENDIX C
DERIVATION OF ACTUAL SIDESLIP ANGLE

The geometric angles available from the Wind Tunnel were the angle of attack, α, and the sting angle, β_s. The actual Sideslip, β_{actual}, is given by

$$\sin(\beta_{actual}) = \frac{v}{V_\infty} \tag{1}$$

To solve for v, find the component of V_∞ in the x-y plane.

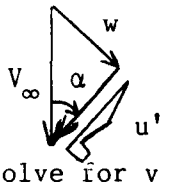

$$u' = V_\infty \cos\alpha \tag{2}$$

Now solve for v in the x-y plane.

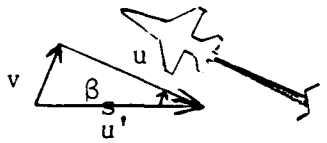

$$v = u' \sin\beta_s \tag{3}$$

$$v = V_\infty \cos\alpha \sin\beta_s \tag{4}$$

$$\frac{v}{V_\infty} = \cos\alpha \sin\beta_s \tag{5}$$

Substituting (1) in (5)

$$\sin(\beta_{actual}) = \cos\alpha \sin\beta_s$$

$$\beta_{actual} = \sin^{-1}(\cos\alpha \sin\beta_s)$$

VITA

Russell Earl Erb was born in Arlington, Texas on 3 August 1961, and graduated from Arlington High School on 31 May 1979. He went to the United States Air Force Academy in the summer of the same year. At the Air Force Academy, he majored in Aeronautical Engineering in the Flight Mechanics track. During the summer of 1982, he spent six weeks at Edwards Air Force Base working at the Air Force Flight Test Center in the F-16XL Combined Test Force. During his senior year at the Academy, he applied for and was awarded a National Science Foundation Graduate Fellowship. On 1 June 1983 he was awarded the degree of Bachelor of Science in Aeronautical Engineering. After graduation, he returned to the Air Force Flight Test Center for six weeks before reporting to Texas A&M University. While at Texas A&M University, he worked under Dr. Donald T. Ward of the Aerospace Engineering Department in the field of stability and control, specifically control of aircraft at high angles of attack. Following successful completion of his degree program, he will be stationed at Eglin Air Force Base with the 3246th Test Wing. He maintains his permanent address at 832 S. Collins, Arlington, TX 76010.

END

FILMED

10-85

DTIC